E-733-65-2

FINAL REPORT
VOLUME II
FOR
MILLIMETER COMMUNICATION PROPAGATION PROGRAM
(1 NOV., 1964 – 1 NOV., 1965)

Contract No. NAS 5-9523

Prepared by
RAYTHEON COMPANY
SPACE & INFORMATION SYSTEMS DIVISION
Sudbury, Massachusetts

Raytheon Report No. FR-65-334-2

for

GODDARD SPACE FLIGHT CENTER
SYSTEMS DIVISION
OMMUNICATIONS RESEARCH BRANCH
CODE 733
Greenbelt, Maryland

E-733-65-2

FINAL REPORT
VOLUME II
FOR
MILLIMETER COMMUNICATION PROPAGATION PROGRAM
(1 NOV., 1964 - 1 NOV., 1965)

Contract No. NAS 5-9523

Prepared by
RAYTHEON COMPANY
SPACE & INFORMATION SYSTEMS DIVISION
Sudbury, Massachusetts
Raytheon Report No. FR-65-334-2

for

GODDARD SPACE FLIGHT CENTER
SYSTEMS DIVISION
COMMUNICATIONS RESEARCH BRANCH
CODE 733
Greenbelt, Maryland

RAYTHEON COMPANY
SPACE AND INFORMATION SYSTEMS DIVISION
RAYTHEON

SUMMARY

This document is Volume II of the final report for the Millimeter Communication Progagation Program being performed under NASA Contract No. NAS5-9523 by Raytheon's Space and Information Systems Division for Goddard Space Flight Center. This program is a study to design experiments which will determine the effects of the propagating medium on millimeter-wave space-earth communications.

The First Quarterly Report discussed the effects of the propagating medium as they are known today and recommended a one-year space-earth experiment to be performed in 1968 with a 6000 nautical mile medium altitude satellite. The Second Quarterly Report described a one-year space-earth experiment using a synchronous stationary satellite. It also described in detail the ground and satellite equipment to be used in an experiment, most of which is compatible with either the medium altitude or synchronous altitude Applications Technology Satellites.

The Final Report for this experiment design study consists of three volumes with Volume I being the summary of the experiment design study. Volume III contains a descriptive biliography of related reports and a recommended outline for a propagation data handbook. This report, Volume II, describes how the raw data, which is collected during the propagation experiments, should be processed and evaluated. Volume II includes a preliminary discussion on the design of communication and progagation experiments for low altitude and synchronous altitude manned spacecraft. Among other subjects, Volume II gives the effects of refraction on pointing millimeter-wave antennas and discusses the usefulness of radiometric data, weather radar data and aircraft-ground propagation tests.

Existing computer facilities are equipped to handle the data processing required for the propagation data collection program. Special computer programs can be generated to provide estimates of the channel parameters. Little computation will be required to infer, from these basic parameters, the effects of propagation on commonly used waveforms and modulation systems since this information is available in existing literature.

Data to be used in the final description of the propagating medium will come from three principal sources: amplitude and phase data from the transmitted waveform, meteorological and radiometric data from correlative sensors, and spacecraft position data from the satellite tracking facility. Proper emphasis must be placed upon correlative data processing in order to classify the atmospheric conditions existing during each measurement period and determine the probability of each class of conditions during the annual cycle.

Each ground facility receiver should be equipped with identical signal processors and analog magnetic tape recorders to minimize data processing expense. Since each ground receiver shares its RF head with a radiometer, sky temperature measurements are recorded on the same tape in synchronism with the signal phase and amplitude. Short term and long term variations of antenna azimuth and elevation are also recorded on the same tape. Real-time analog strip line recorder presentations of the same data which was recorded on magnetic tape would be made at each site for calibration check-out and operational monitoring; and to provide the cooperating agencies with immediate access to the raw data. The taped analog data from satellites and ground facilities would be converted to digital form at a central data processing facility. An extensive quantity of data will result from the experimental program, and, of course, it is not necessary to statistically process all of the data collected. However, it is necessary to look at the analog presentations for the occurrence of unusual propagation effects to

insure that the data which is processed adequately represents the statistical model.

The two-dimensional correlation function for a single spatial channel is an important characterization of the millimeter channel. This function is measured by those experimenters who need fading statistics and it has direct application to the design of communication systems using frequency diversity. Coherence time, coherence bandwidth and fading rates can be determined directly from the two-dimensional correlation function. A two-dimensional Fourier Transform of this correlation function can be taken in order to describe the scattering function and obtain information regarding doppler and multipath spreading by the channel.

The two-dimensional spatial correlation function, for two parallel spatial channels receiving the same signal, is another important characterization of the millimeter channel. From this function the coherence aperture can be determined, which is an important measure of the maximum size antenna to be efficiently employed. In situations where space diversity schemes are being considered, the spatial correlation function specifies the antenna separation required in order to receive uncorrelated signals. A spatial spectral density function can be derived from the two-dimensional Fourier Transform of the spatial correlation function. This function describes the spatial spectrum of the wavefront and the lateral motion of wavefront with respect to the antenna baseline.

In the initial propagation experiments it is not practical to develop the complete functions just described. Modified two-dimensional correlation functions and their Fourier Transforms would be generated which are based on the amplitude envelopes rather than the complex envelopes of the received signals. Correlations of radiometric amplitude data with the received signals will accompany the modified functions during the evaluation phase.

The initial propagation experiments designed to provide the channel functions just described should be conducted with aircraft and medium to synchronous altitude manned or unmanned satellites. Low orbiting spacecraft are not ideal vehicles for basic propagation experiments since they are just too close to earth to permit reasonable time for gathering quantitative data. Low orbiting spacecraft do, however, offer payload capacities which often surpass that which is available at higher altitudes and, furthermore, the availability of man in a low orbiting spacecraft is of inestimable value in determining the operational potential of millimeter-wave communications to support future manned spacecraft missions. The experiments with low orbiting spacecraft would be communication experiments demonstrating actual modulation methods to be employed in future systems.

A series of propagation experiments with aircraft would constitute a useful phase in the overall millimeter-wave program. This phase of propagation data collection should precede the final space craft equipment design phase for the space-earth experiments with medium altitude and synchronous satellites. Slow moving aircraft which fly high above the sensible atmosphere are attractive because they provide qualitative data, at less expense, within a shorter equipment design and fabrication period. This qualitative data would be helpful in designing more intelligent space-earth experiments which are more complete and which yield quantitative results.

In the experiment designs given in the first and second quarterly reports, which use medium and synchronous altitude satellites, millimeter-wave receivers instead of millimeter-wave transmitters could be used to enhance payload reliability, reduce prime power consumption and weight and make possible the implementation of these experiments within a shorter time scale. Nevertheless, the use of satellite receivers does not appear to merit the propagation data it produces. For one thing, the spatial correlation

function and its two-dimensional spectral density transform can not be measured. Other agencies who have useful ground facilities will be discouraged from participating because of the difficulties with transmitter modifications and the lack of immediate access to raw data. Finally, coordination among the participating facilities is more difficult since the satellite has to handle each one separately.

The use of millimeter wavelengths for space-earth communication is enhanced by the large antenna gains for modest size antennas. Because of the smaller beamwidths which result, millimeter-wave antenna systems demand positioning to a greater accuracy. A ground based automatic tracking and acquisition facility utilized for millimeter-wave space-earth communications would not require that the refraction of the propagating wave be known to a high degree of accuracy. However, if this same system were to supply data required for predicting the satellite orbit, then the pointing error due to atmospheric refraction would be of prime importance. Atmospheric refraction is due to both the troposphere and the ionosphere; however, the ionosphere has negligible effect on propagating frequencies above 10 Gc. It is important to note that the pointing error in elevation due to tropospheric refraction, when observing a point on the earth from a satellite, is one to two orders of magnitude less than that which exists when viewing a satellite from the earth. This is due to the proximity of the observer with respect to the bending medium.

As discussed in previous reports, basic correlative measurements are required to classify the weather model existing in each test in order that the statistical propagation data can be translated to other geographical locations which experience similar meteorological conditions. Good correlative measurements will also help explain why certain things are happening to the test signals which are being propagated through the complex atmosphere.

In addition to the usual surface meteorological data which must be collected at each ground terminal, radiometric measurements in coincidence with the basic signal measurements are a necessity. The apparent sky temperature, which is the result of these radiometric measurements, directly relates to the atmospheric attenuation due to the water and oxygen content of the atmosphere. The test signals undergo fading due to variations in water content within the receiving beam. The radiometric measurements will therefore help distinguish between various mechanisms producing fading.

At ground terminals where considerable millimeter-wave propagation measurements are to be made, it is worthwhile to employ a weather radar (3cm to 10cm wavelength) to estimate the rainfall rate along the propagation path. In experiments involving stationary satellites where the propagation path is fixed, surface rate data from rain gauges underneath the path could be a practical supplement or alternative to the radar data. Millimeter-wave radar do not look promising for measuring rainfall rate profiles since the radar backscatter is attenuated on its return, therefore, making the radar data extremely difficult to correct.

This is the summary of work performed during the third quarter of the experiment design study. A summary of the complete program is given in Volume I.

PRINCIPAL CONTRIBUTORS

The technical officers at Goddard Space Flight Center who were responsible for this study were Mr. Abe Kampinsky and Mr. Walter Elder of the Communications Research Branch in the Systems Division. The key Ratheon participants are given in Table I.

Valuable advice regarding existing theoretical and experimental propagation data and existing experimental ground facilities was received from the following agencies:

Aerospace Corporation, El Segundo, California

Air Force Cambridge Research Laboratories, Bedford, Massachusetts

MIT, Lincoln Laboratory, Lexington, Massachusetts

Electrical Eng. Research Lab., University of Texas, Austin, Texas

TABLE 1

KEY RAYTHEON PARTICIPANTS IN MILLIMETER-WAVE COMMUNICATION PROPAGATION STUDY

Name	Raytheon Organization	Technical Area
Mr. Ira Smith	SISD[1], Sudbury, Mass.	Study Director
Dr. Eli Brookner		Atmospheric Propagation Effects, Waveform Analysis, Data Processing
Mr. Joseph Clougherty		Atmospheric Propagation Effects, Plasma Effects
Mr. Edward Gifford		Equipment Design
Mr. Ronald Porter		Correlative Measurements, Meteorology
Mr. Louis Romano		Atmospheric Propagation Effects, Signal Analysis, Equipment Design
Mr. Thomas Servey		Atmospheric Propagation Effects, Meteorology
Mr. Arthur Robichaud	(now with National Radio Astronomical Observatory)	Facilities Survey, Equipment Design
Mr. Robert Savage	SBO[2], SISD, Santa Barbara, California	Equipment Design
Mr. David Barton	SURANO[3], Equipment Division, Wayland, Mass.	Atmospheric Propagation Effects
Dr. Joseph deBettencourt	CADPO[4], Equipment Division, Norwood, Mass.	Atmospheric Propagation Effects
Dr. John Myers	Research Division, Waltham, Mass.	Atmospheric Propagation Effects
Dr. Barret Hazeltine	Consultant, Brown University, Providence, R.I.	Correlative Radiometric & Radar Measurements
Mr. Donald Snyder	Consultant, MIT, Cambridge, Mass.	Data Processing

(1) SISD - Space and Information Systems Division
(2) SBO - Santa Barbara Operation
(3) SURANO - Surface Radar and Navigation Operation
(4) CADPO - Communications and Data Processing Operation

CONTENTS

CONTENTS (Cont.)

CONTENTS (Cont.)

ILLUSTRATIONS

ILLUSTRATIONS (Cont)

ILLUSTRATIONS (Cont)

ILLUSTRATIONS (Cont)

TABLES

Section I
INTRODUCTION

This document is Volume II of the final report for the Millimeter Communication Propagation Program being performed under NASA Contract No. NAS5-9523 by Raytheon's Space and Information Systems Division for Goddard Space Flight Center. This program is a study to design experiments which will determine the effects of the propagating medium on millimeter-wave space-earth communications.

The scope of work for this study program was defined in Exhibit "A" of Contract NAS5-9523 and supplemented by the Raytheon Proposal, "A Millimeter Communication Propagation Program," BR-3011, 3 June 1964. Another report which supplements Exhibit "A" is "Program Definition Plan for Millimeter Communication Propagation Program," FR-4-498-B, 29 January 1965. The Program Definition Plan defines the objectives of the program, lists the tasks to be performed, and describes the various work activities under each task, including their time relationships with one another.

The objective of this experiment design study was to design a series of experiments which show how the objectives of a millimeter propagation program can be met. Wherever design problems could not be solved, courses of action in the form of component tests and breadboard design were recommended. This objective includes development of experiment cost estimates and time schedules, including that for data processing and evaluation. Results of the study include equipment design, source of key components, definition of basic measurements and description of how these basic measurements can be used to meet the objectives of the experiment.

The First Quarterly Report, which was a report of work accomplished during the period 1 November 1964 to 1 February 1965, discussed the effects of the propagating medium as they are known today and described a one-year space-earth experiment to be performed in 1968 with a 6000 nautical mile medium altitude satellite. The Second Quarterly Report, which was a report of work accomplished during the period 1 February 1965 to 1 May 1965, described a one-year space-earth experiment using a synchronous stationary satellite. The Second Quarterly Report also described in detail the ground and satellite equipment to be used in the experiment, most of which is compatible with either the medium altitude or synchronous altitude Applications Technology Satellites.

The Final Report consists of three volumes. Volume I is a summary of all the work performed during the program. Volume III has a descriptive bibliography of reports which were used duringthe study. Volume III also contains an outline of a propagation data handbook which is recommended as the final product of the experimental program.

This report, Volume II, is a detailed report of work accomplished during the third quarter, 1 May 1965 to 1 August 1965.

Section 2, "Propagation of Millimeter Waves," is a discussion on atmospheric refraction of millimeter waves. It describes the effects of the atmosphere on pointing large millimeter-wave ground antennas at spacecraft, and also gives the refraction errors encountered when looking down at a given point on the earth from a spacecraft. This section is a detailed continuation of the general discussion on refraction which was given in Section 3 of the first quarterly report.

Section 3, "Basic Correlative Measurements," describes the usefulness of radiometric sky temperature data and weather radar rainfall data in evaluating the causes of atmospheric effects on millimeter signal propagation.

This section completes the discussion on basic correlative measurements which was introduced in Section 4 of the first quarterly report.

Section 4, "Formulation of Experiments," discusses: the importance of aircraft flight tests during the early phases of the propagation program; the wisdom of using receivers instead of transmitters in an Applications Technology Satellite; and contains an introduction to the design of communication and propagation experiment design for low altitude and synchronous altitude manned spacecraft which includes a work statement recommending further work in this area.

Section 5 briefly discusses the design of the spacecraft receivers which were introduced in Section 4 and Section 6.

Section 6 describes the process of acquiring signals in noise using phase-locked receivers. Incidentally, Section 6 could more appropriately have been part of Section 5 in the second quarterly report under "Signal Level Analysis."

Section 7, "Data Processing and Evaluation," is the most important part of this report. It discusses the concept of processing and evaluating millimeter propagation data taken from space-earth channels. It includes the definitions of the channel parameters which apply to the millimeter communications channel and the mathematics for computing these parameters from basic phase and amplitude data.

Section 9 is a bibliography of reports referenced in the other sections. Appendices I and II supplement Section 7. Appendix III is a collection of general satellite orbital characteristics plus more detailed characteristics for synchronous and 6000 nautical mile altitude satellites. Specific orbital characteristics for low altitude (100 to 300 n mi.) satellites were given in Section 4. Appendix IV gives the general characteristics of millimeter-wave antennas.

Section 2
PROPAGATION OF MILLIMETER WAVES

This section is a supplement to Section 3 of the First Quarterly Report. The use of millimeter wavelengths for earth-satellite communications is suggested by the large operating bandwidth, increased antenna gain, and smaller antenna beamwidths. Antenna systems operating with these smaller beamwidths demand positioning to a greater accuracy, thus the effects of refraction on pointing millimeter-wave antennas must be evaluated.

2.1 Effects of Refraction on Pointing Millimeter-Wave Antennas

A ground based automatic tracking and acquisition facility utilized for millimeter-wave space-earth communication would not require that the refraction of the propagating wave be known to a high degree of accuracy. However, if this same system were to supply data required for predicting the orbit of the satellite, in addition to being a communication terminal, then the pointing error due to atmospheric refraction would be of prime importance.

Refraction or bending of electromagnetic propagation through the atmosphere is due to both the troposphere and the ionosphere. However, the ionosphere has very little effect on propagating frequencies above 10 Gc and, as seen in Figure 2-9, energy propagating at zero degrees elevation angle would exhibit an error in elevation angle of approximately 1 microradian when viewing a 270 nautical mile satellite from the Earth. Thus, the refraction due to the ionosphere is insignificant and need not be considered for millimeter-wave propagation. However, this is not the case for the troposphere as shown with the pointing error curves in Figure 2-5. Incidentally, the pointing error in elevation due to tropospheric refraction when observing a satellite from the surface of the earth is one to two orders of magnitude greater than that which exists when viewing a point on the earth from a satellite. Figure 2-8 gives

pointing errors at a satellite as a function of altitude and elevation angle.

Because of the turbulent nature of the troposphere in addition to humidity and temperature inhomogeneities, the radiowave molecular refraction is subject to fluctuations. These fluctuations in angle of arrival make predictions of refractions relatively useless for angles belowone degree. However, if the surface refractivity is know, the tropospheric refraction may be computed to within a few seconds of arc ofelevation angles greater than 10 degrees as demonstrated at Sugar Grove.[1] Yet, the surface temperature and humidity must be constantly monitored since surface refractivity could vary as much as 10 % in 4 hours.

The Aerospace Facility demonstrates an overall antenna system positioning capability of better than 0.1 milliradians with their 15 foot millimeter-wave system when surface refractivity corrections are made.[2] The pointing error due to inherent system noise in an automatic tracking state-of-the-art system is an order of magnitude better than the positioning accuracy of the Aerospace Facility. This means that many other errors have to be considered such as: tracking loop errors; mechanical errors of mount; and boresight shift due to temperature gradient.

The antenna systems of interest in space-earth communications are of the passive tracking variety. Internal errors are to be construed as errors resulting from parameters of the tracking system, while external errors are considered errors due to the propagation medium.

2.1.1 Internal Tracking System Errors

Internal errors in pointing are due to many system parameters such as:

1. The order and parameters of the tracking loop, since these dictate the lag error which will be a function of the satellite's velocity and acceleration.

2. Mechanical errors of the antenna mount including backlash.

3. Error due to inherent system noise.

4. Boresight shift due to temperature gradients.

This tracking antenna system could be either a sequential lobing system or a monopulse system. In either case, the pointing capability of the system due to the inherent system noise would be approximately the same. A single axis tracking system utilizing the sequential lobe switching technique, shown in Figure 2-1 shall be evaluated. This system is a basic Dicke type radiometer in closed loop form. The principles of operation of this type of radiometer have been described in Appendix VI of the First Quarterly Report.

The two antenna beams of this system are displaced about the boresight axis. When the antenna system is rotated, while receiving radiation emitted from a fixed point source, the output of the integrator would appear in accordance with the curve in Figure 2-2, assuming the system were operating in the open loop state. This curve goes through a maximum, when the axis of either antenna pattern is in line with the radiating source. These particular antenna beams intersect the boresight axis at their 3 db points. In addition to this signal received, there are fluctuations due to the inherent system noise. These fluctuations interfere with the pointing system and introduce pointing errors. Since the linear portion of the curve is about the boresight axis, the inverse slope of this section of the curve may be expressed as:

$$S = K \frac{\theta_A}{2P_R} \qquad (2\text{-}1)$$

where:

θ_A = Antenna Beamwidth

P_R = Power received by one antenna when the radiating source lies on the beam axis.

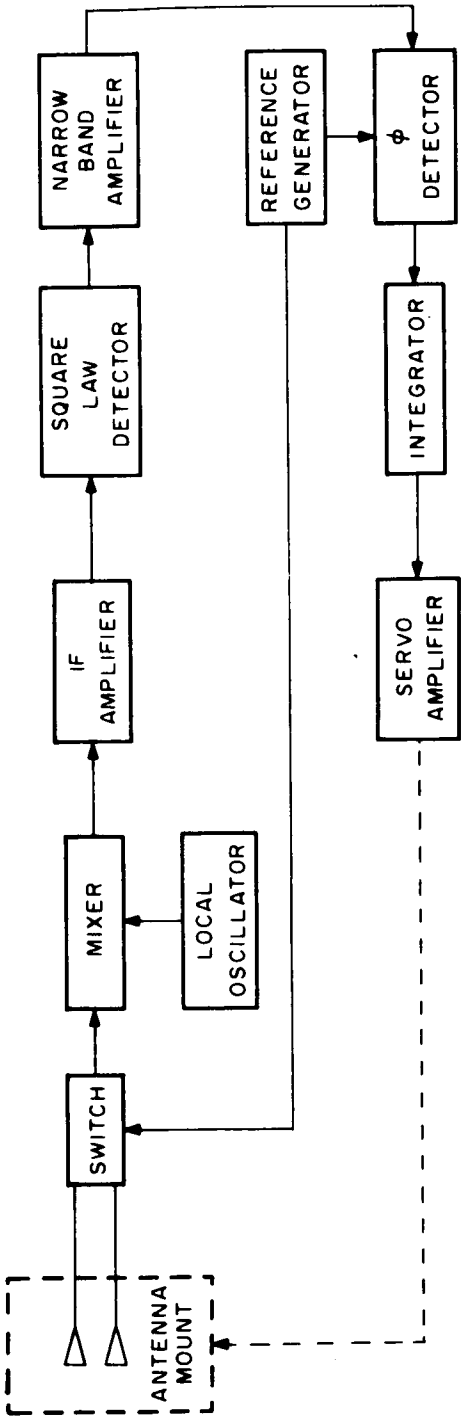

Figure 2-1. Single Axis Tracking System

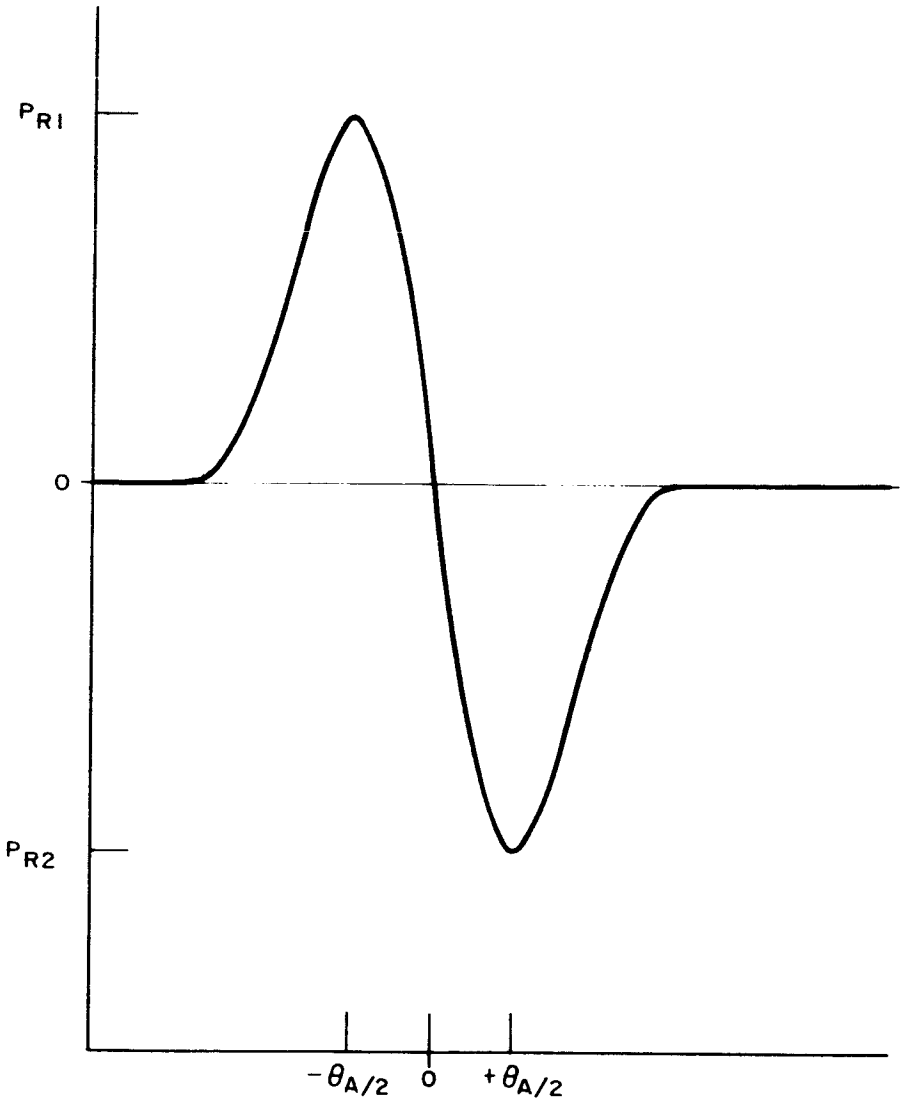

P_{R1} = Peak Power Received By Antenna No. 1

P_{R2} = Peak Power Received By Antenna No. 2

θ_A = Antenna Beamwidth

Figure 2-2. Integrator Output Vs Antenna Position

K = Constant, which is a function of beam shape, beamwidth, and beam crossover points.

The RMS fluctuations at the integrator output due to the noise in the system is defined by the classical radiometer expression:

$$T = \frac{\sqrt{\pi}\ (F-1)\ [T_o + T_A]}{\sqrt{B\ \tau}} \qquad (2\text{-}2)$$

where:

T = Fluctuations (R.M.S.)

F = System Noise figure

T_o = Ambient temperature in degrees Kelvin

T_A = Antenna temperature in degrees Kelvin

B = Predetection bandwidth in cycles per second

= Post-detection integration time is seconds

The output fluctuations due to the noise must be expressed as a function of noise power rather than noise temperature and is converted by multiplying Equation 2-2 by $K_1 B$.

$$N = \frac{\sqrt{\pi B}\ \ (F-1)\ \ [T_o + T_A]\ K_1}{\sqrt{\tau}} \qquad (2\text{-}3)$$

where:

N = Fluctuations (R.M.S.) as a function of noise power

K_1 = Boltzmann's constant

B = Predetection bandwidth in cycles per second

The receiver power is defined in equation 5-48 of the Second Quarterly Report.

$$P_R = P_T G_T G_R \sigma L \qquad (2\text{-}4)$$

where:

P_R = Power at input to receiver

P_T = Input power to transmitting antenna

G_T = Gain of transmitting antenna

G_R = Gain of receiving (tracking) antenna

$\sigma = \left[\frac{\lambda}{4\pi R}\right]^2$ = Free space attenuation

L = Atmospheric losses

The R.M.S. pointing error resulting from the total noise energy is equal to the inverse slope of the error curve multiplied by the (R. M. S.) fluctuations due to the total system noise power. This results in the following expression:

$$\delta\theta = \frac{\sqrt{\pi B}\ (F\text{-}1)\left[T_o + T_A\right] K_1\ \theta_A}{2K\ P_T G_T G_R \sigma L \sqrt{\tau}} \qquad (2\text{-}5)$$

where:

$\delta\theta$ = R.M.S. pointing error due to noise

Expression 2-5 is also valid for a CW monopulse tracking system, since it is equivalent to the expressions generated by both Manasse[3] and Barton.[4] A tracking error of approximately one arc sec has been calculated with Equation No. 2-5 for an earth-satellite communication system with the satellite in a 6000 nautical mile orbit and the following parameters:

P_T = 1 watt

G_R = 62 db

G_T = 32 db

f_o = 35 Gc

F = 13 db

B = 50 Mc

τ = 0.01 seconds

σ = 204.4 db

L = 10 db (maximum loss occuring at low evaluation angles)

T_A = 100 (maximum occuring at low evaluation angles)

K = 2

2.1.2 Tropospheric and Ionospheric Errors

If a satellite ground station is to generate data for orbit prediction, in addition to performing operational duties in a communications network, then corrections for atmospheric refractions must be made. The accuracy of these corrections depends on the accuracy with which the index of refraction profile is known along the propagation path. Refraction or bending of the propagating wave occurs in both the troposphere and ionosphere. This bending is due to the nonhomogeneous medium.

Tropospheric Refraction

The refractivity of the troposphere is represented by the following expressions:

$$N = (n-1) \times 10^6 = \frac{a}{T} \left(P + \frac{b\,\epsilon}{T}\right) \qquad (2\text{-}6)$$

where:

N = Refractivity

n = Refractive index

T = Atmospheric temperature in degrees Kelvin

ϵ = Constant $79^{o}K/mb$

b = Constant $4800^{o}K/mb$

The above expression is valid for frequencies up to 35 Gc, to an accuracy of 0.5 per cent. This expression is also valid for refractivity of infrared propagation when the second term of the expression is omitted.

The refractivity is assumed to decay exponentially at altitudes above 10 km (33k ft.) and is expressed as: (5)

$$N(h) = N_o \, e^{-\frac{h}{4.11}} \qquad (2\text{-}7)$$

where:

N_o = Refractivity at sea level

h = Altitude in nautical miles

The refractivity for a wet atmosphere (100 % relative humidity at all levels) may be computed from the following expression for altitudes less than 10 km. (6)

$$N_w = 338 - 94.4h + 15.1h^2 - 1.56h^3 + 0.084h^4 - 0.0013lh^5 \qquad (2\text{-}8)$$

Refractivity for a dry atmosphere (zero percent relative humidity at all levels) is again a polynominal expression:

$$N_d = 262 - 46.5h + 3.17h^2 - 0.102h^3 + 0.0011.8h^4 \qquad (2\text{-}9)$$

where h is in nautical miles. The reflectivity profiles which are shown in Figure 2-3 have been derived from Equations 2-7, 2-8 and 2-9.

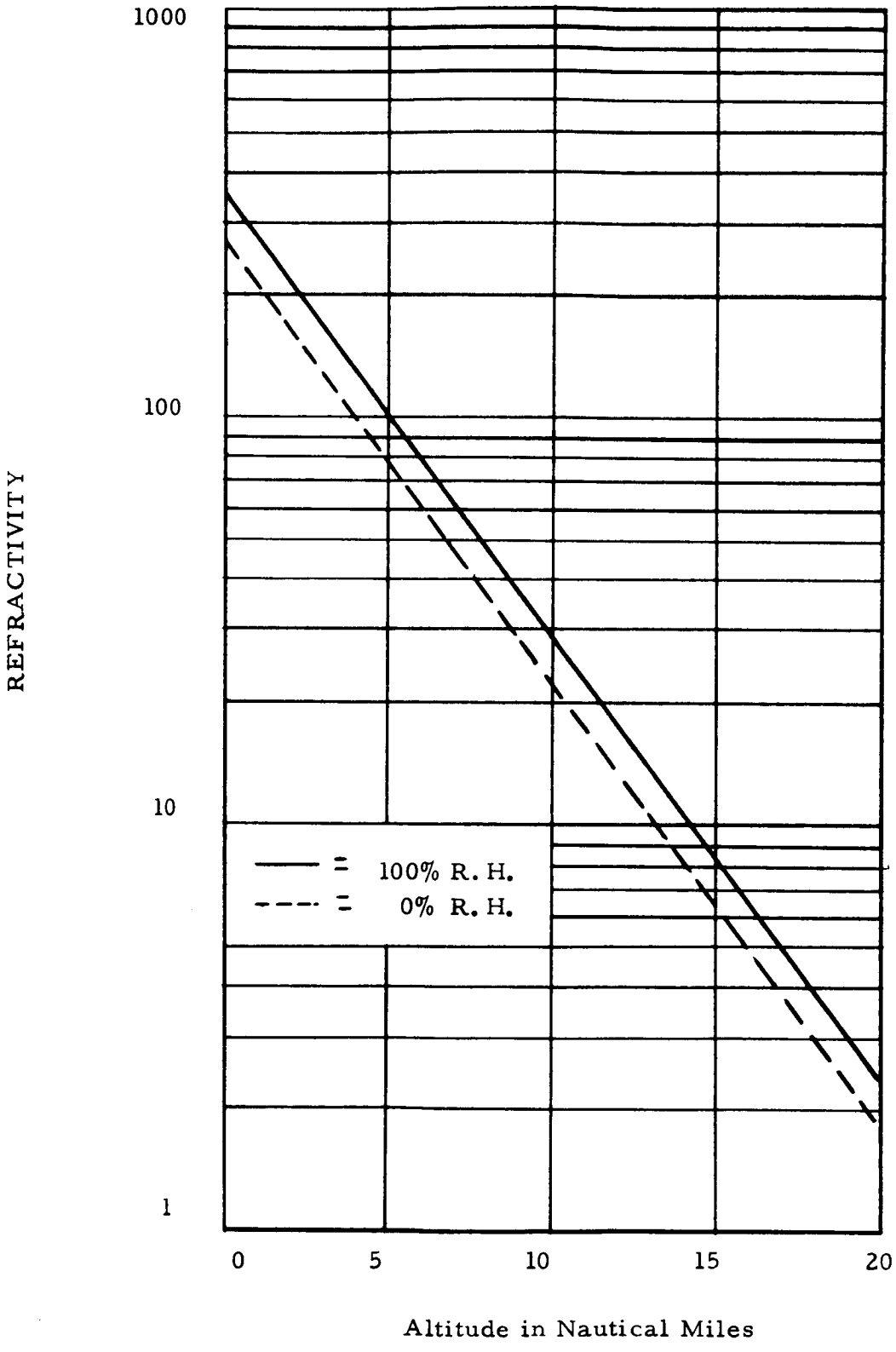

Figure 2-3 Refractivity of the Troposphere

This angular error in elevation is the difference in angle between the angle of incidence of the received energy and the true line-of-site of the radiating source. As depicted in Figure 2-4 an angular error due to tropospheric refraction is experienced at both the ground terminal and at the orbiting spacecraft. However, the error as viewed from the ground station, is greater than the error at the spacecraft by orders of magnitude. The error as observed from the ground station is a function of both elevation angle and altitude of the vehicle as readily observed in Figure 2-5 [7]. For vehicles at altitudes greater than 925Km (500 n mi) and elevation angles greater than 5 degrees, the tropospheric refraction error is approximated by: [7]

$$\delta = N_o \times 10^{-6} \cot \theta \qquad (2\text{-}10)$$

where:

δ = Error in radians

N_o = Refractivity at observing station

θ = Elevation angle of target

Curves for δ vs elevation angle for atomspheres of 100% and 0 % relative humidity are shown as Figure 2-6.

The angular error as viewed from the vehicle is much less than the errors plotted in Figure 2-6. This error has been computed for satellites orbiting at altitudes ranging from 100 to 6000 nautical miles, by dividing the atmospheric refractivity profile of Figure 2-3 into six stratified layers, as shown in Figure 2-7. The angles specified in Figure 2-7 were determined through application of Snell's law for the spherically symmetrical surface and is expressed as: [8]

$$n_{K-1}\ r_{K-1} \sin \phi_{K-1} = n_K\ r_K \sin \phi_K \qquad (2\text{-}11)$$

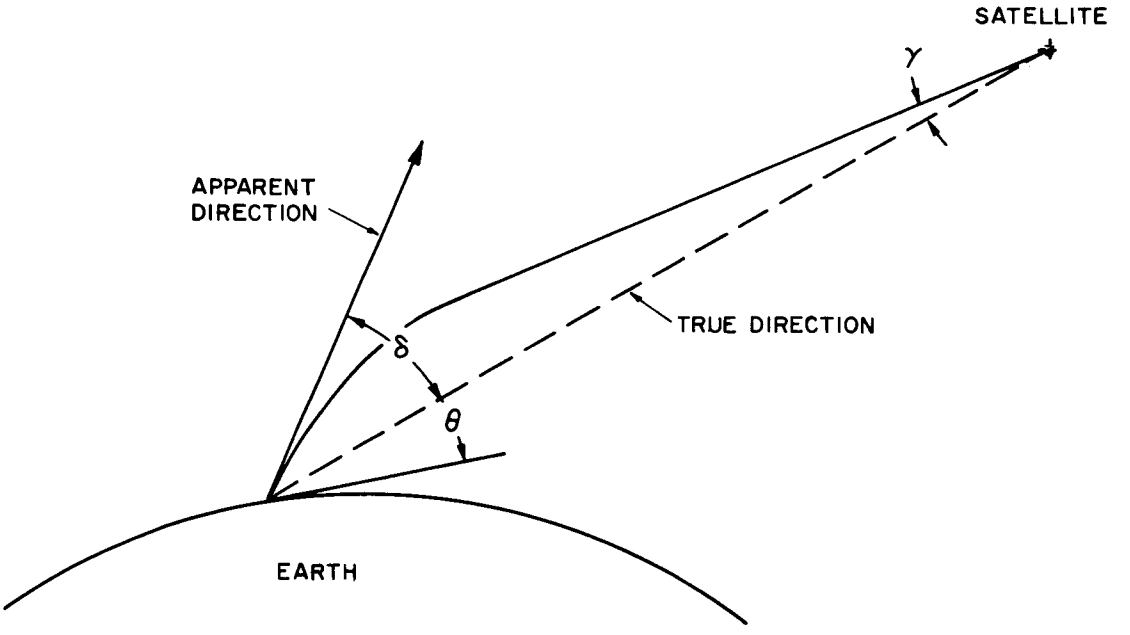

γ = Error in direction as viewed from satellite.

δ = Error in direction as viewed from earth.

Figure 2-4 Path of a Propagating Wave

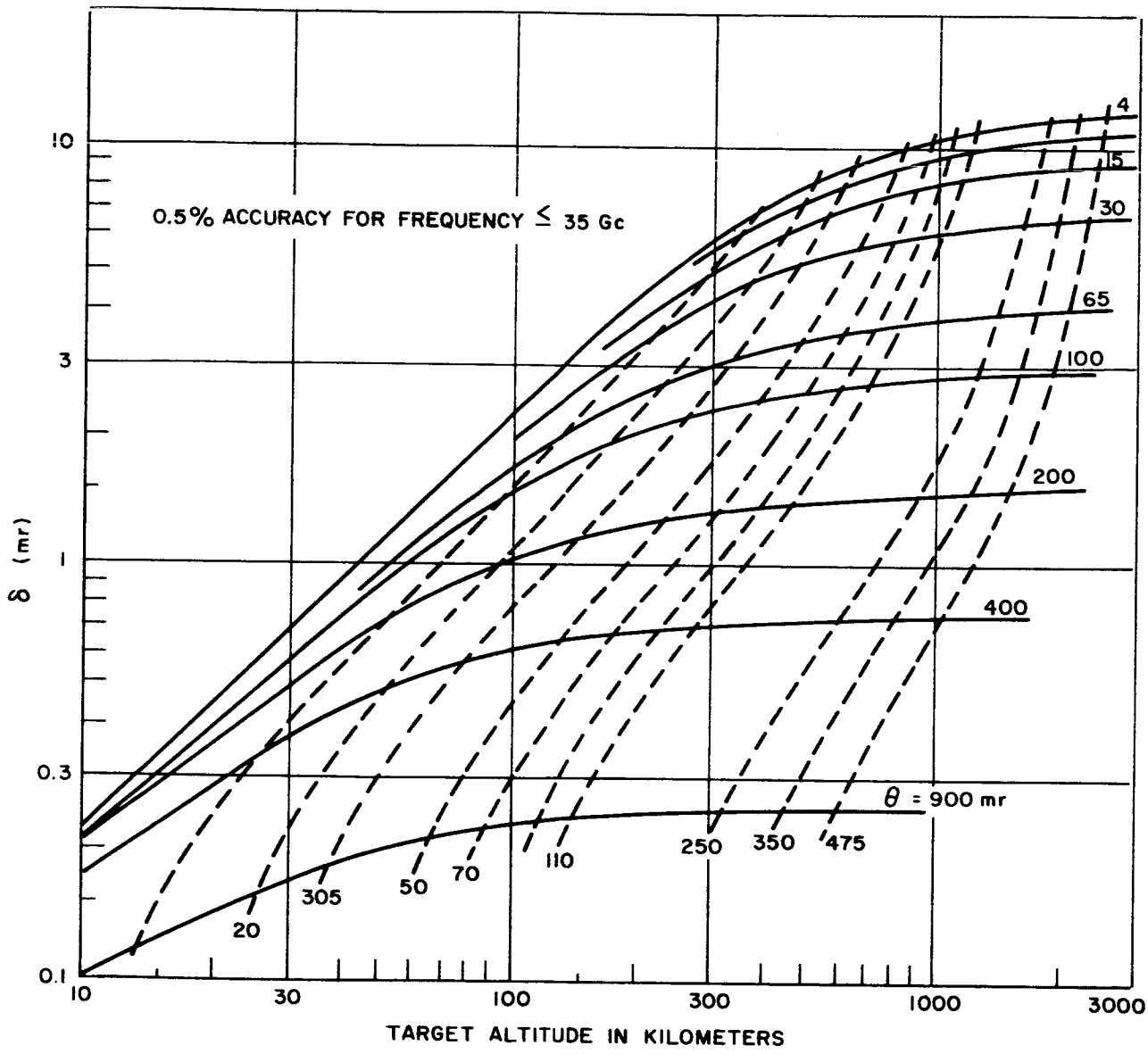

Figure 2-5 Ground Station Pointing Error Due to Tropospheric Refraction for Satellites Below 500 n. Miles

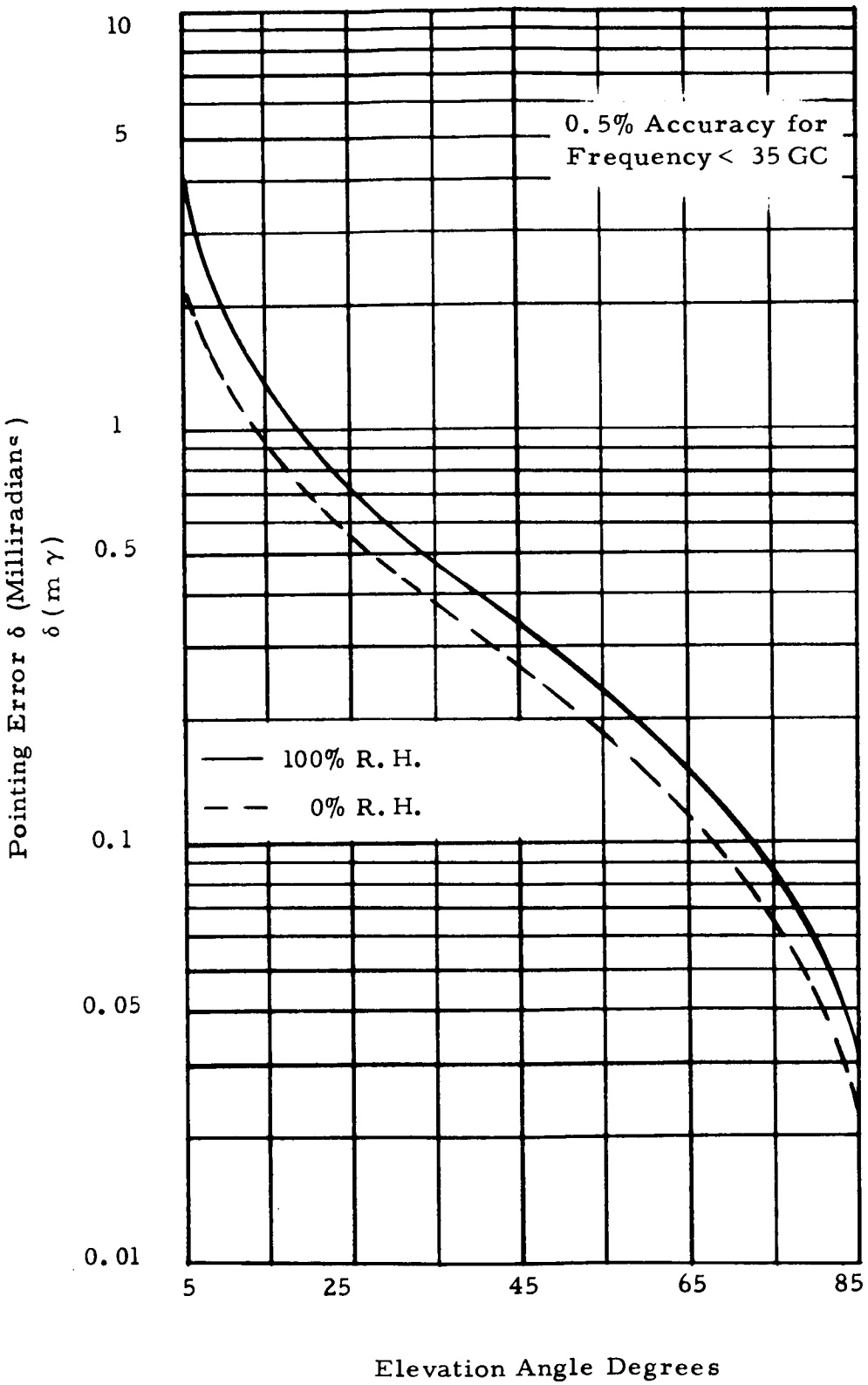

Figure 2-6 Ground Station Pointing Error Due to Tropospheric Refraction for Satellites Above 500 n. Miles

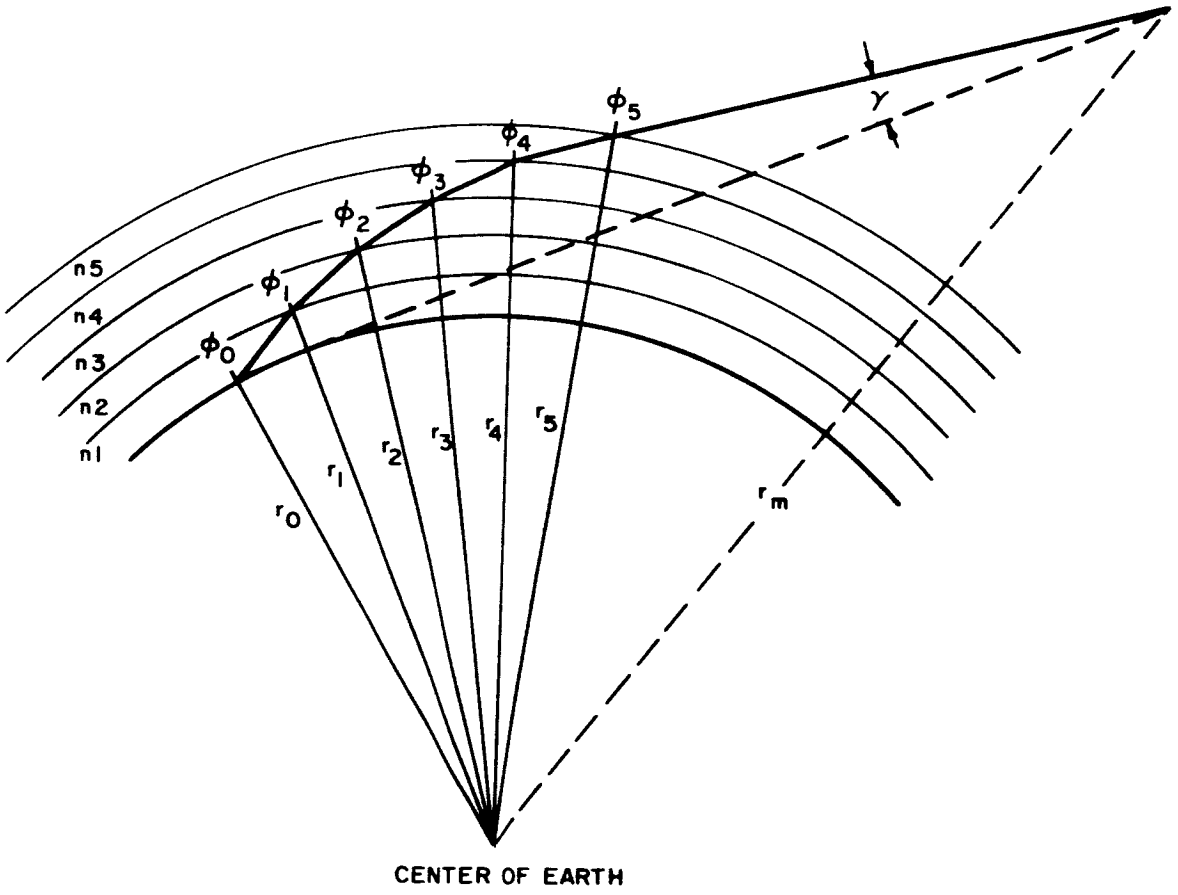

Figure 2-7 Atmospheric Layer Stratification

The final expression for the angle error is:

$$\gamma = \sin^{-1}\left(\frac{r_{m-1}}{r_m}\prod_{K=1}^{m-1}\frac{n_{K-1}\,r_{K-1}}{n_K\,r_K}\sin\phi_{K-1}\right)$$

$$-\tan^{-1}\left[\frac{r_o \sin\sum_{K=1}^{m}\left(\phi_{K-1}-\sin^{-1}\frac{r_{K-1}}{r_K}\sin\phi_{K-1}\right)}{r_m - r_o\cos\sum_{K=1}^{m}\left(\phi_{K-1}-\sin^{-1}\frac{r_{K-1}}{r_K}\sin\phi_{K-1}\right)}\right] \quad (2\text{-}12)$$

The error angle has been computed from Equation 2-12 for satellites in 100-6000 nautical mile orbits. However, since these computations are very time consuming, only the errors or low elevation angles were computed and plotted in Figure 2-8.

Ionospheric Refraction

Radio frequency propagation through the ionosphere is refracted however, the degree of refraction is not a constant for all frequencies as seen from the following expression:

$$n = \sqrt{1-\frac{4\pi N_e e^2}{m\omega^2}} \quad (2\text{-}13)$$

where:

n = Index of refraction

N_e = Electron density (electrons/cm^3)

e = Electron charge (4.8×10^{-10} e.s.u.)

m = Electron mass (9.1×10^{-28} grams)

ω = Angular frequency of incident wave (radians / sec)

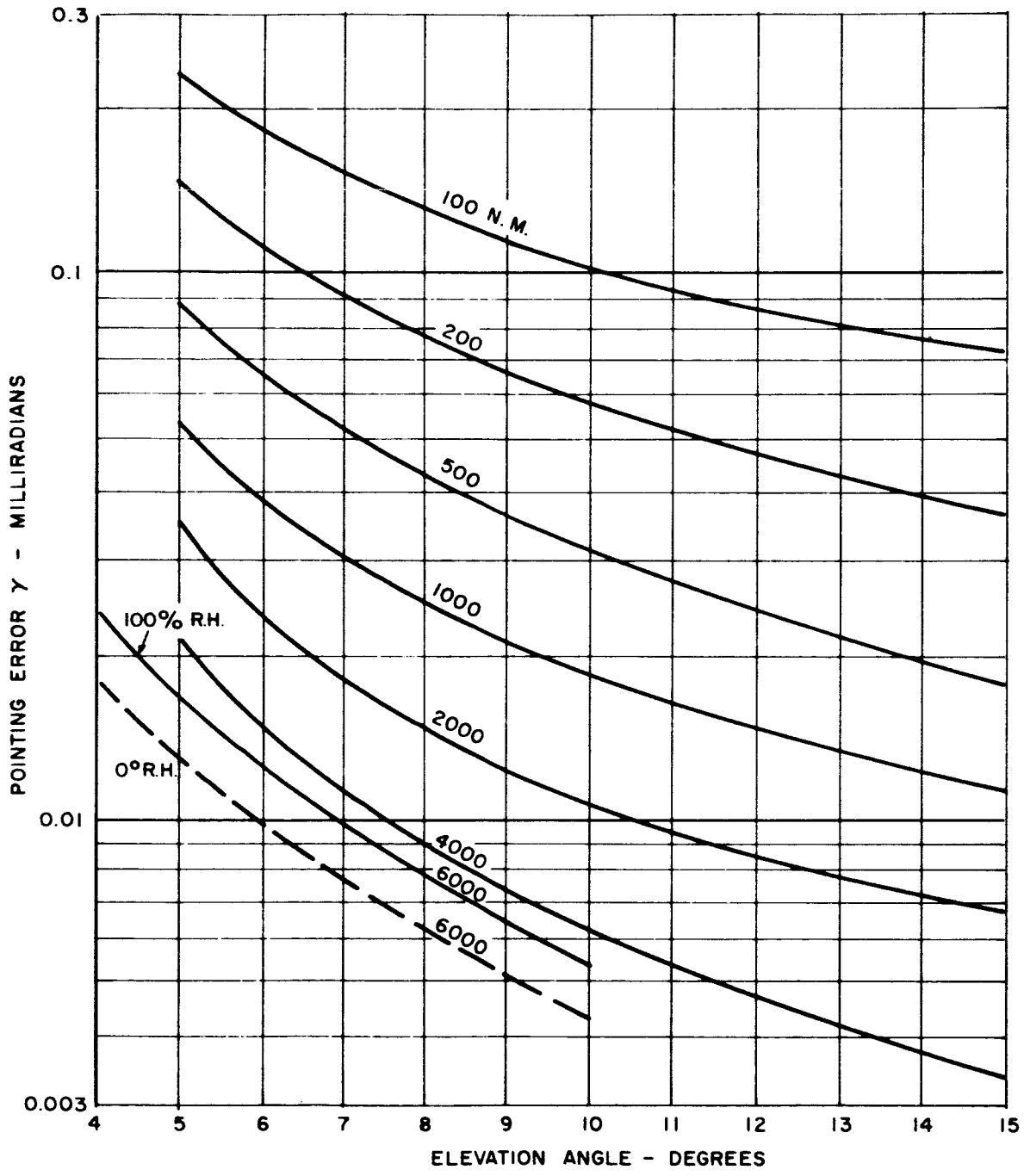

Figure 2-8 Satellite Pointing Error Due To Tropospheric Refraction

The refraction due to the ionosphere in millimeter wavelength is insignificant in comparison to the tropospheric refraction. The error angle, as observed from the ground station, due to refraction of the ionosphere only, is shown as Figure 2-9. (7)

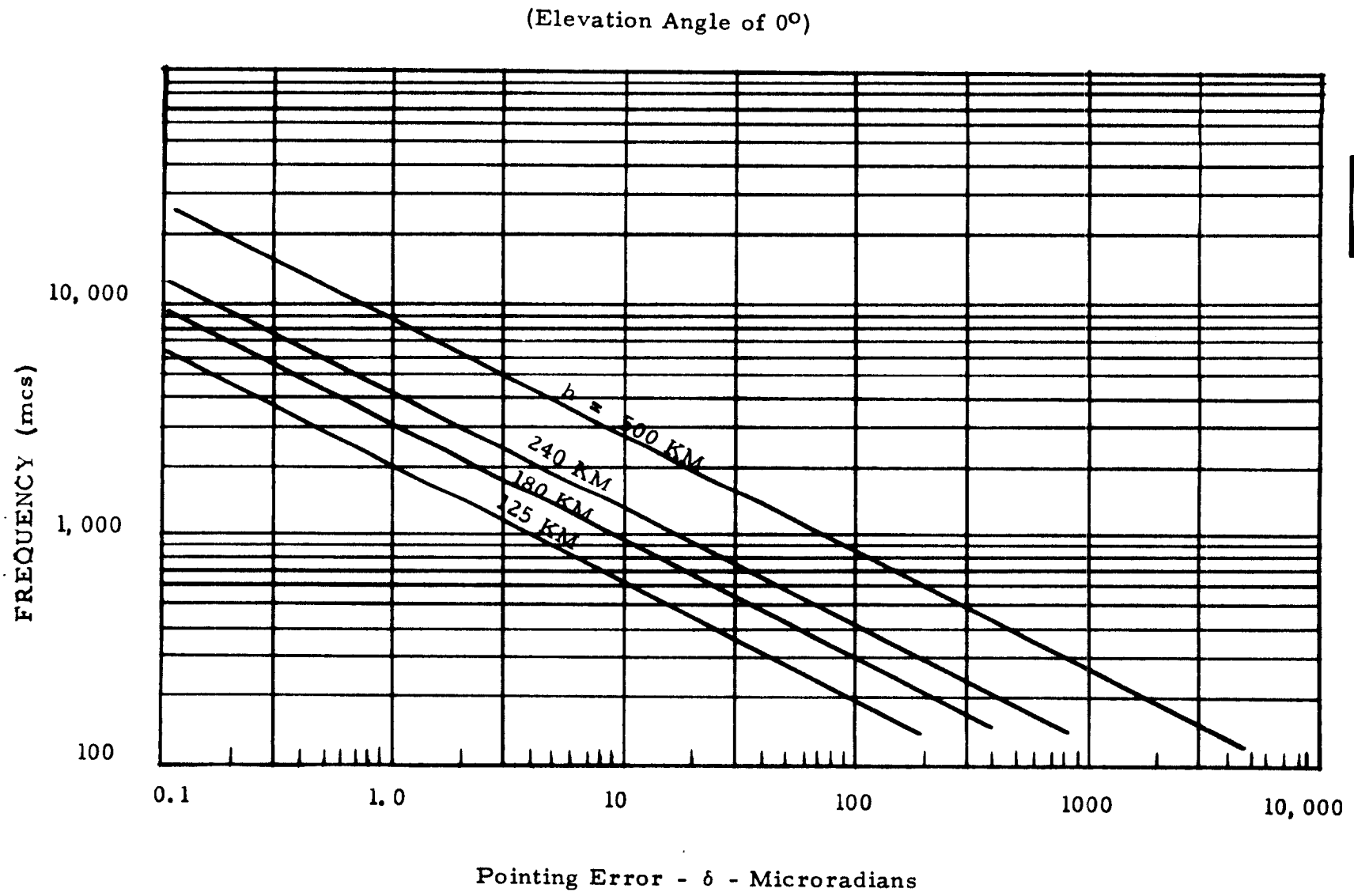

Figure 2-9 Pointing Error at Ground Station Due to Ionospheric Refraction

Section 3
BASIC CORRELATIVE MEASUREMENTS

Basic correlative experiments are required to classify the weather model existing in each test in order that the statistical propagation data can be translated to other geographical locations which experience similar meteorological conditions. Good correlative measurements will also help explain why certain things are happening to the test signals which are being propagated through the complex atmosphere. In addition to the usual surface meteorological data which must be collected at each ground terminal, radiometric measurements in coincidence with the basic signal measurements are a necessity. The apparent sky temperature, which is the result of these radiometric measurements, directly relates to the atmospheric attenuation due to the water and oxygen content of the atmosphere.

The test signals undergo fading due to multipathing as well as fading due to variations in water content within the receiving beam. The radiometric measurements should, therefore, help us to isolate these two fading effects. A weather radar, preferably located right at the ground terminal, could provide another correlative input - a rainfall rate profile along the communication path. The total effect of rain absorption and scattering can then be deduced by integration of this profile.

3.1 The Use of Radiometric Data To Distinguish Between The Various Signal Fading Mechanisms

One purpose of the experiment is to obtain information on the channel characteristics which will be useful in the design of communication systems. Conclusions about the physical mechanisms producing fading and other aspects of channel behavior will be an important part of such information. Correlative radiometric data will be taken in order to distinguish between various mechanisms producing fading.

There are evidently three major sources of fading of millimeter waves:

1. Scattering of electromagnetic energy by turbulence in the troposphere which tends to scatter energy out of (and into) the receiving antenna beam.
2. Multipath effects which produce coherent phase interference between signals received over paths which differ by an appreciable fraction of a wavelength.
3. Absorption of electromagnetic energy by gases in the troposphere, chiefly oxygen and water vapor.

It should be noted that ionospheric effects probably will not play an important role at the frequencies being considered for this experiment.[9] It should also be noted that "ducting" in the troposphere is also being neglected since it can be shown using the technique explained in "Propagation of Short Radio Waves"[10] that radio signals will not be trapped in a duct if the elevation angle is greater than 1°. This agrees with a conclusion reached by Barton.[4]

The first and third effects mentioned above influence incoherent, that is, noise-like signals as much as coherent signals, that is, signals made up of frequency components having definite phase relationships. The second effect is, of course, only present when the signal is coherent. Coherent fading can sometimes be reduced by use of such techniques as frequency diversity; thus it would, for example, be useful to the system designer to know how much of the expected fading is due to coherent interference.

3.1.1 Scattering Effects

The index of refraction varies essentially at random in a turbulent portion of the atmosphere. Because of this variation in refraction index, the turbulence tends to focus the radiation at certain places and defocus it at other places, producing areas of enhanced signals and areas of attenuated signals. These positions of enhancement and attenuation move with time; thus the signal at a fixed antenna varies with time. This phenomenon is

analagous to "scintillation" in astronomical observations.[11]

Turbulent scattering has been studied by Bergman[12] and his result requires fairly detailed knowledge of the variation of the index of refraction along the propagation path and therefore can lead to misleading results. Tatarsky[13] has also studied this problem and he shows that the mean-squared value, σ^2, of the logarithmetic variation of the amplitude of signal transmitted through a turbulent medium is:

$$\sigma^2 = 1.23\, C_n^{\,2}\, k^{7/6}\, L^{11/6} \qquad (3\text{-}1)$$

where,

$C_n^{\,2} = 10^{-9}/\text{cm}.$

$k = 2\pi/\lambda$

λ = wavelength of signal

L = pathlength in cm.

The value of C_n was calculated using optical data but Tatarsky indicates the value is useful at frequencies as low at UHF. Using representative values for λ and L, one finds there is essentially no fluctuation in the output signal due to scattering from turbulence in the atmosphere. (This agrees with some experimental results[14] which show little scintillation at elevation angles above 4 degrees.)

3.1.2 Multipath Effects

An attempt has been made to estimate the amplitude of multipath fading from published results of other experiments. One cannot predict with great confidence, however, the effect of the multipath phenomenon. (This is one reason for doing the experiment.) Some conclusions will be made here which indicate that multipath will not be an important source of fading. Data obtained from the Telstar experiment[15] shows about 1 db of fading once the satellite was above 5° in elevation. The frequency of transmission from the satellite was 4, 170 mc and the antenna beamwidth was 0.225°. It should

be noted that the total path length through the atmosphere, including refractive effects, changes from 750 km at 0° elevation to 268 km at 10° elevation. This may account for some of the diminution in fading.

Barsis, Barghausen and Kirby[16] have made measurements of fading at 9,300 mc and found as much as 20 db fading. However, they were working at low elevation angles and with fairly wide antenna beamwidths, (3°), therefore ground reflection undoubtedly was an important influence on their results. (It should be pointed out that at least 5% of the time the transmission loss obtained was less than would be observed in free space. This, presumably indicates constructive phase interference.)

The results of another experiment conducted by the Bell Telephone Laboratories is pertinent to this experiment. Fading of an 11 kmc signal was measured along an essentially horizontal path[17]. The degree of fading was found to be well correlated with the amount of rainfall along the path, even though ground reflection was certainly present and there was indication of ducting. Results obtained at the University of Texas[18] also indicate a high correlation between fading and rainfall along the propagation path. In these experiments, it seems reasonable to conclude that most, if not all, of the observed fading was due to absorption by rain rather than multipath phenomenon.

The National Bureau of Standards has published a composite power spectrum (Figure 3-12 of The First Quarterly Report) of the phase fluctuation of a signal transmitted over a 15 mile path at about a 6° elevation angle[19]. Phase fluctuations are not, of themselves, of interest in estimating the degree of fading but they are important in estimating the amount of signal degradation due to multipath and the loss of antenna gain due to phase incoherence across the antenna aperture. The first effect will be considered first. From the phase fluctuation spectrum the rms fluctuation in range and the rms fluctuation in the angular difference between the direction of arrival of the electromagnetic radiation and the actual direction between transmitter and receiver can be found[4]. Serious fading will result if there are two

paths for electromagnetic radiation from transmitter to receiver which differ by a quarter wavelength, which is about .01 feet at 34 Gc. This implies an rms change in refractivity of about 1N unit along one path. This change in refractivity will produce about .03 milliradians of bending in the delayed path. If we assume the portion of the atmosphere producing the bending is 5,000 feet high, then the horizontal distance between a path which is bent and one which is not must be about 2 inches. In other words, the refractivity must change by 2N units in 2 inches. If the path length difference were 1 foot, then the rms change in refractivity would be about 30N units, implying an rms angular change of about 0.7 milliradians. This means the horizontal distance in the troposphere along which the refractivity changes by 30N units must be about 20 inches. Measurements taken in Sweden[20] and in Japan[21] indicate that the refractivity does not, in fact, change as drastically as required. However, neither experiment was designed to measure the fine structure of the troposphere. It does seem reasonable, though, to conclude from the NBS data that there will not be appreciable fading due to the multipath phenomenon.

The second effect produced by phase fluctuation is the possible loss in antenna gain because the phase front across the antenna aperture is not planar. It will be assumed that the phase fluctuations are produced by changes in the refractive index associated with a weather pattern moving by the antenna at about 20 feet per second. If we consider the difference in phase across an antenna of 20 feet in diameter, we find the total power in the difference to be essentially zero. Therefore, from the NBS data we conclude there should be no loss in antenna gain due to phase fluctuations.

The NBS data upon which these conclusions were based represented averages over some eight years and short time variations may be obscured. For that reason, one may not have a great deal of confidence in the above conclusions. Therefore, for the millimeter-wave space-earth propagation experiment design, we will assume that multipath fading does occur, and we will estimate the corresponding change in the results of the radiometric measurement.

The presence of this multipath fading implies something about the condition of the atmosphere which, in turn, implies something about the apparent sky temperature measured by a radiometer. Estimates will be made of the change in apparent sky temperature associated with fading due to phase interference by signals transmitted along different paths.

Fading of the type being discussed arises if there are two or more paths from the transmitter to receiver and the propagation time along these paths are different. We assume there is a blob in the atmosphere through which one path travels and which is missed completely by a second path. Using elementary trigonometric arguments, one can show that a phase difference of $\pi/4$ along the two paths will produce about a 1 db fading loss. A phase difference of $\pi/4$ at 34 Gc corresponds to a range error of about .01 feet. The results of Muchmore and Wheelon[22] can be used to estimate the rms change in the refractivity which is about 2.

The refractivity can be related to the atmospheric temperature, pressure and water vapor by the (empirical) "Smith-Weintraub" equation:[6]

$$N = \frac{77.6}{T}\left(P + \frac{4810p}{T}\right) \qquad (3\text{-}2)$$

where:

N	=	refractivity
T	=	absolute temperature in degrees Kelvin
P	=	atmospheric pressure in millibars
p	=	partial pressure of the water vapor component

If we assume reference values for T, P and p as follows, $T = 300^{\circ}K$, P = 1013 millibars, and p = 20 millibars, then we can estimate directly from the above equation the required change in T, P and required to get a change in refractivity equal to 2. It should be noted that the calculations will be performed assuming that T, P and p change independently. Actually, the variations of the three quantities are probably interrelated; for example, if a blob in the atmosphere has a higher temperature than its surroundings, it will also probably have a higher water content. However,

water content (or pressure) and temperature have opposite effects on the refractivity; thus, the results will indicate bounds on the changes in temperature and water content (or pressure) required to produce the required change in refractivity.

It turns out that the required change in temperature to get an increase in refractivity of 2 units is about 3.5^{o}. It also turns out that the required change in pressure is about 7.7 millibars. Finally, it turns out that the required change in the partial pressure of water vapor is about 0.48 millibars.

Now, the effect of these changes on the radiometric measurements will be estimated. If the atmospheric blob which is 3.5^{o} hotter than the surrounding atmosphere is close to the earth's surface then the radiometric measurement will be increased by as much as 3.5^{o} although a 1.5^{o} increase is probably more realistic as the blob will undoubtedly not fill the entire receiving antenna beam. If the blob is not at the earth's surface, then radiation from it will be attenuated in passing through the atmosphere to the receiver. If we assume a 40^{o} elevation angle and a clear sky, the apparent sky temperature T_a at 35 Gc is about 17^{o}. If the blob were located in the first 2 kilometers of altitude, T_a would increase at most, 7.5%. If the blob were located in the next 2 kilometers (that is, between 2 and 4 kilometers, the increase would be about 1.27%. The apparent sky temperature would increase in these cases 1.6^{o} and 0.2^{o}, respectively. Results for these and two other altitudes are summarized in Table 3-1. These results were calculated using a method given by Barrett and Chung [23].

A 2.5% increase in the partial pressure of water vapor at the earth's surface from 20.00 to 20.48 millibars will produce about 0.1% increase in the apparent sky temperature at 17 and 35 Gc. It is unlikely that this increase will be discernible in the radiometer output. The increase in apparent sky temperature due to increased water vapor content at 94 Gc or at higher altitudes will be less than 0.1^{o}.

TABLE 3-1

BLOB TEMPERATURE AS A FUNCTION OF ELEVATION

Blob Elevation (km)	Percent Increase in T_a	Maximum Actual Temperature Increase (^{o}K)
0	21	3.5
0 - 2	7	1.3
2 - 4	1.6	.20
4 - 6	.9	.16
6 - 8	.6	.10

The absorption coefficient of water vapor is independent of the atmospheric pressure[24] while the absorption coefficient of oxygen is directly proportional to the pressure[25]. Thus at 16 and 35 Gc, where water vapor absorption is significant, there will be little effect on the apparent sky temperature caused by a blob of air at higher pressure. Even at 94 Gc the apparent sky temperature will only increase about 0.5%. These results indicate that a properly designed radiometer will be insensitive to multipath effects and therefore will help isolate signal losses due to absorption from signal losses due to multipath.

3.1.3 Atmospheric Absorption

Now the third source of fading mentioned earlier, absorption due to water vapor and oxygen in the atmosphere, will be discussed. The amount of attenuation σ due to absorption is well correlated with the apparent sky temperature T_a measured by a radiometer, especially if the apparent sky temperature is less than about $180^{o}K$. The relationship between the apparent sky temperature and the attenuation in decibels for a signal transmitted through the entire atmosphere is shown in Figure 3-1. The curve divides about $180^{o}K$ to show the area of uncertainty in our present knowledge of the relationship.

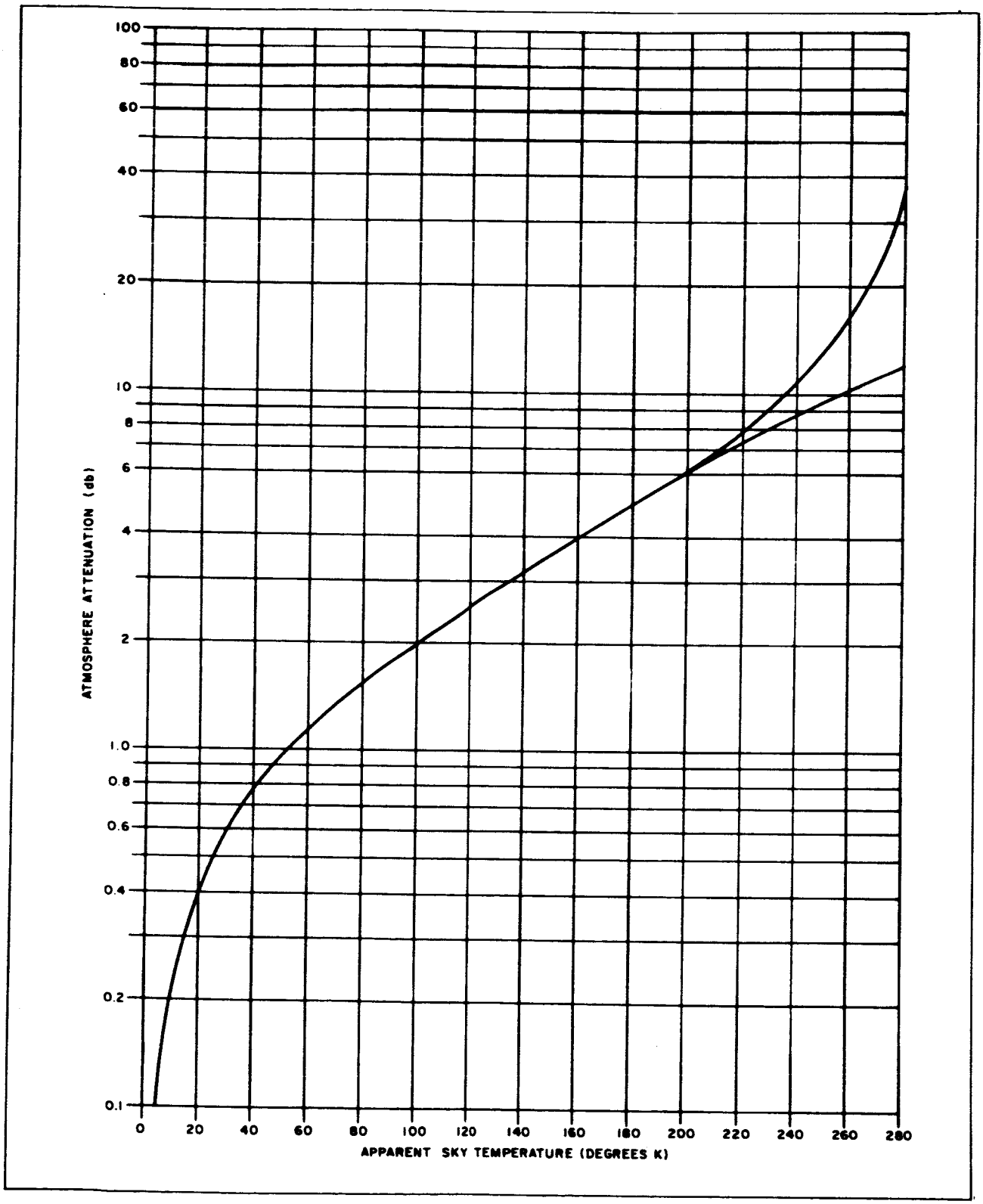

Figure 3-1 Atmospheric Attenuation as a Function of Apparent Sky Temperature

Figure 3-1 is based on results of calculations using the method given by Barrett and Chung [23]. The computer program for performing the calculations was described in Appendix II, First Quarterly Report. Points calculated for several different weather models were plotted to give the average curve shown in Figure 3-1. These twenty-one models arise as follows: each of the seven models (Cases I through IV plus revised weather model described in Section 3-1, First Quarterly Report) was considered for three conditions, "clear sky", "cloudy sky", and "moderate rain". Two other rain conditions were also considered. Finally, one weather model representing an extreme, and unrealistic, water vapor distribution, was considered in order to investigate the boundaries of the temperature-attenuation relationships. It should be noted that results for signals at three frequencies: 16, 35 and 94 Gc and for all elevation angles, were used to produce the curve in Figure 3-1.

The interesting result in this exercise was the lack of spread of the calculated points about the curve of Figure 3-1 for different weather models and different frequencies at temperatures below 180°K. This is illustrated in Figures 3-2 through 3-5. In Figures 3-2 and 3-3, the points for the revised weather model described as Case 6 in Section 3, First Quarterly Report, are plotted. In Figure 3-2, points corresponding to different frequencies are distinguished, but points corresponding to the different weather models are not; for example, points calculated for 16 Gc/clear sky and 16 Gc/cloudy sky are all indicated by circles. In Figure 3-3, points corresponding to different weather conditions are distinguished, but points corresponding to different frequencies are not. The spread of points about the curve shown in Figure 3-1 is seen to be very small.

In order to get more information on the possible distribution of points about the curve due to variations in the weather pattern, points for each weather pattern were plotted on the same axes in Figure 3-4. In order to make the graph more readable the number of points plotted was reduced by considering, for each weather model, only one frequency: 35 Gc, and one

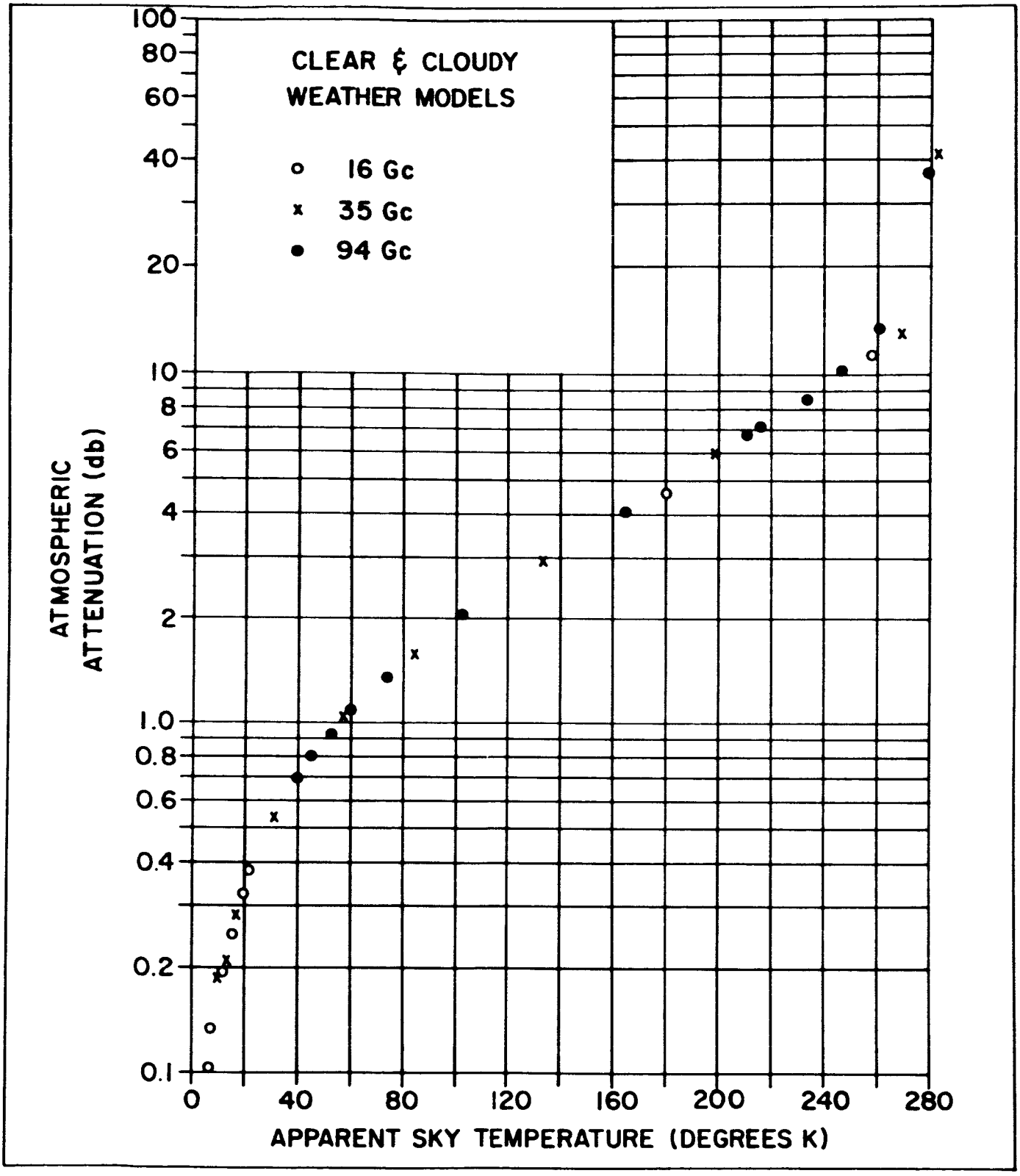

Figure 3-2 Attenuation as a Function of Apparent Sky Temperature For Various Frequencies Under Case 6

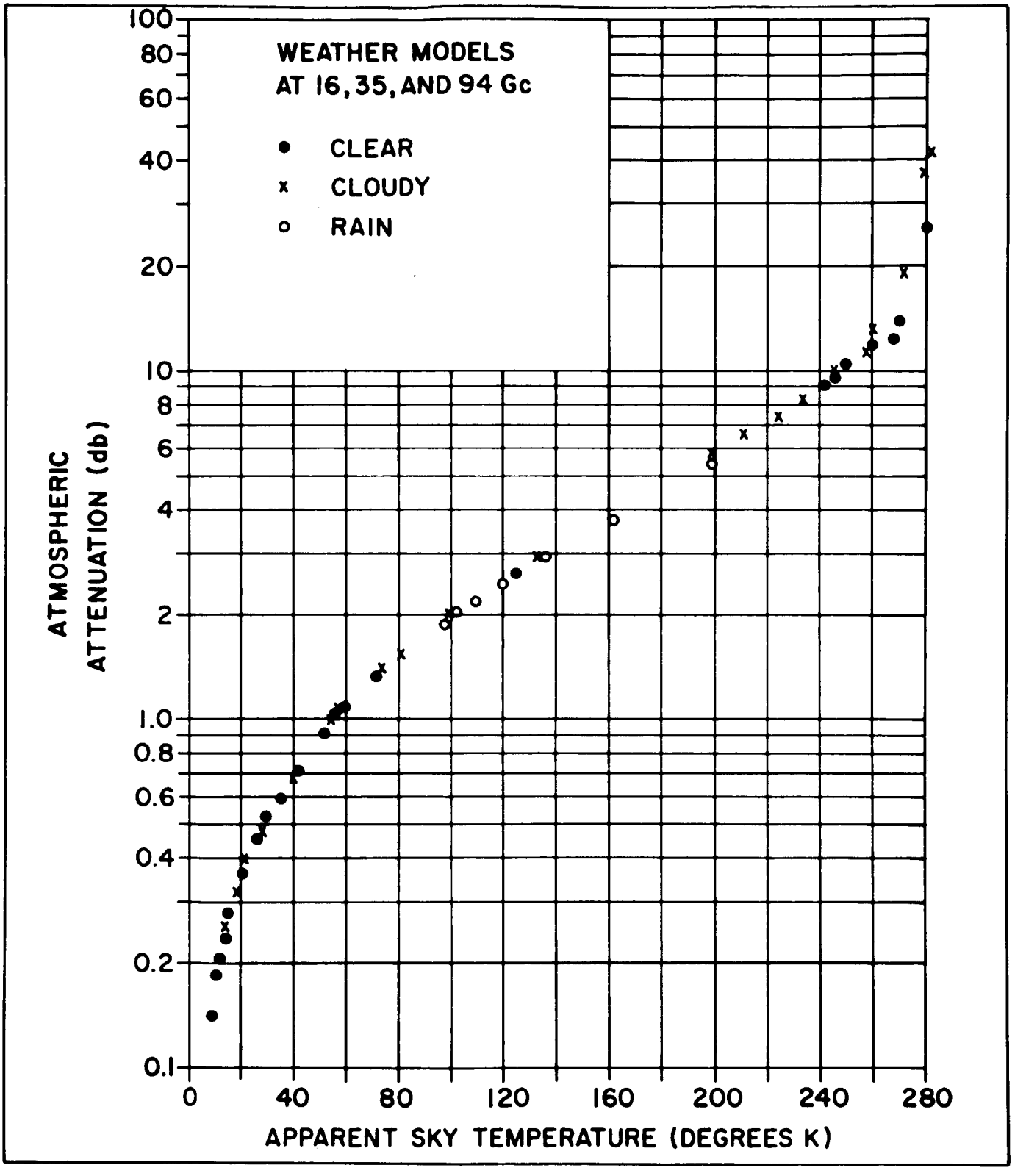

Figure 3-3 Attenuation As A Function of Apparent Sky Temperature For Case 6 Weather Models at 16, 35, and 94 Gc

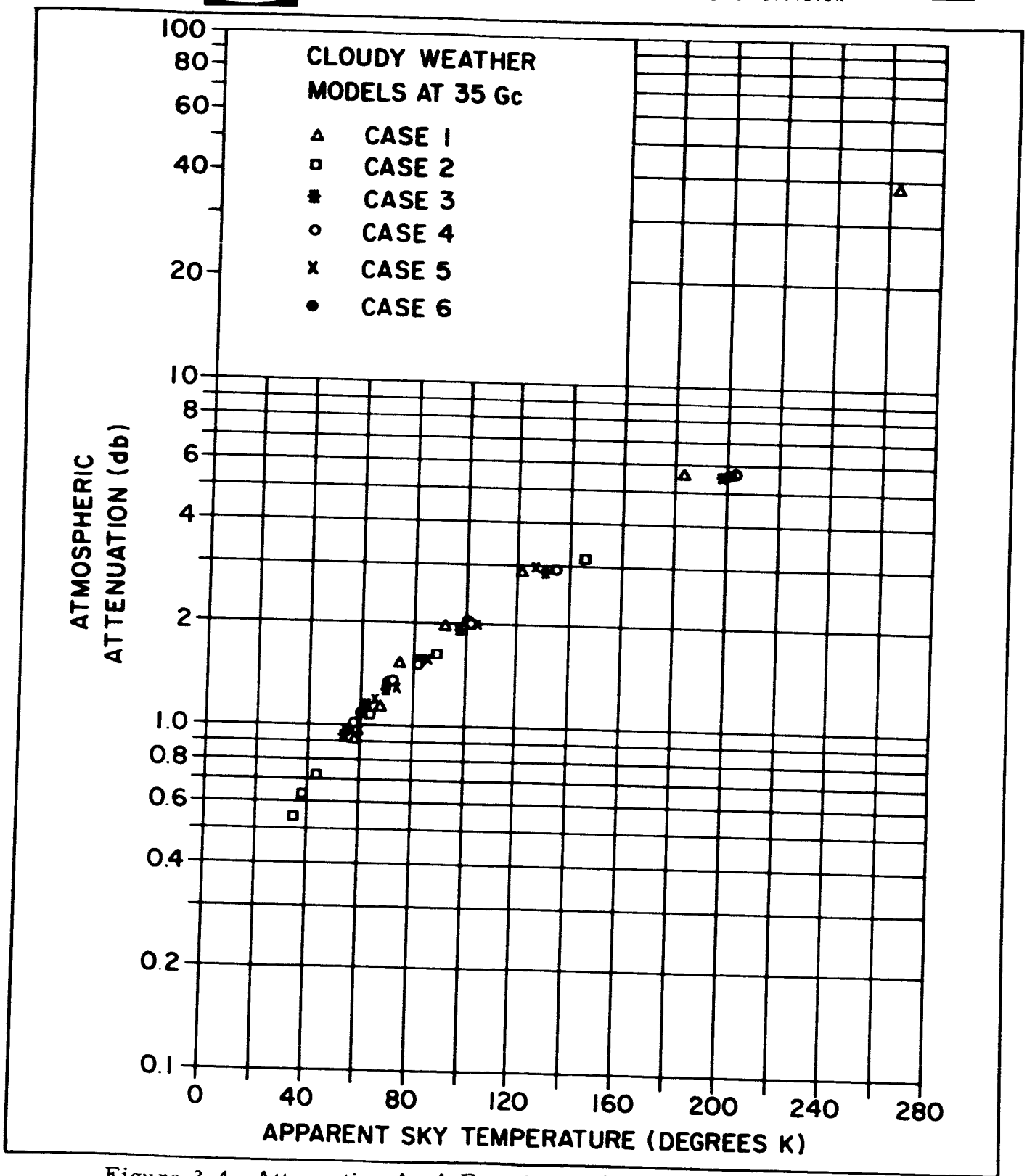

Figure 3-4 Attenuation As A Function of Apparent Sky Temperature For Various Cloudy Weather Models at 35 Gc

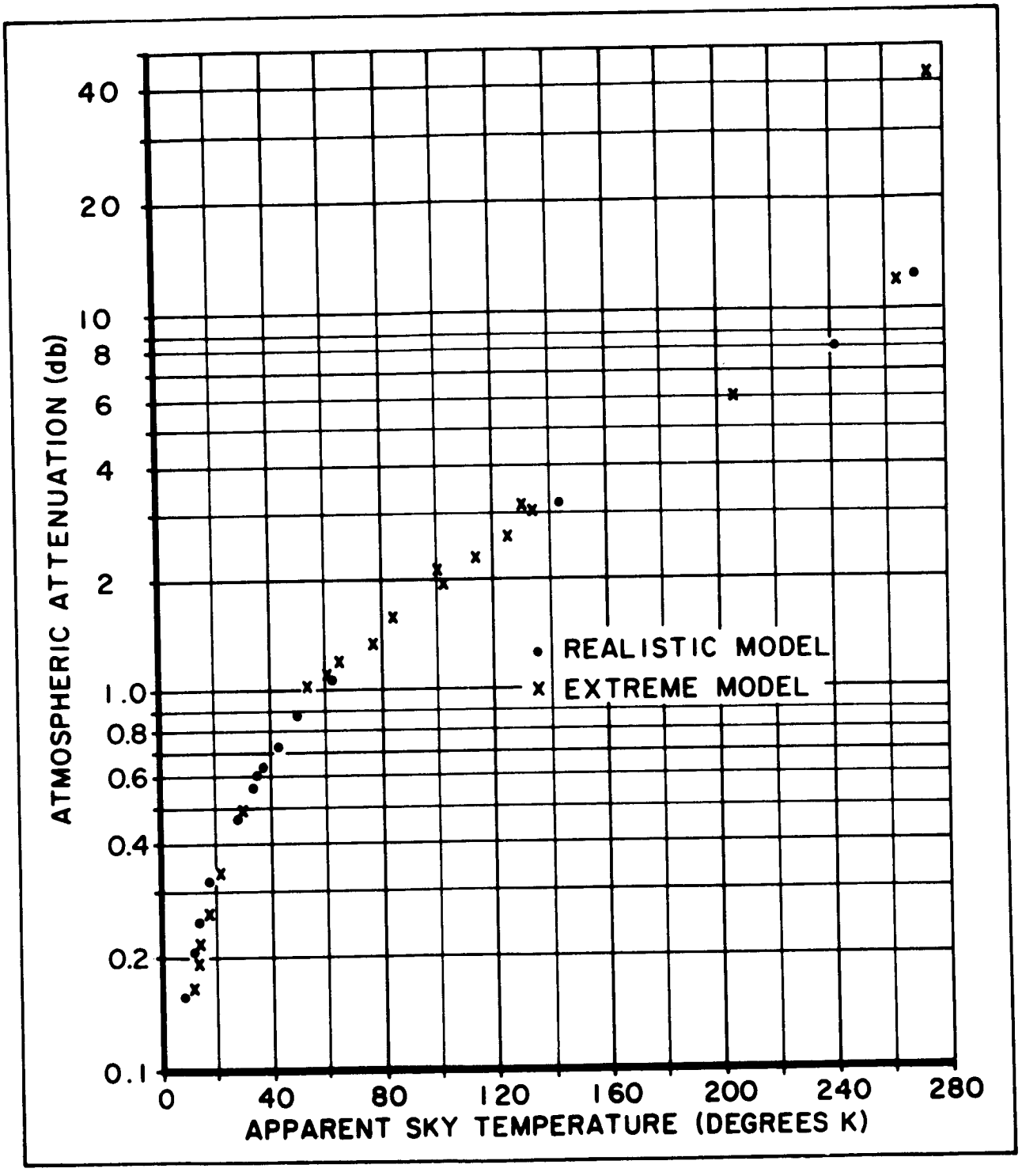

Figure 3-5 Attenuation As A Function of Apparent Sky Temperature For Realistic and Extreme Weather Models at 35 Gc

weather condition: cloudy. (It should be pointed out that the drafting difficulties tend to exaggerate the scatter of the points.) In general, the points corresponding to Case 1 and Case 2 are seen to be scattered the further from the mean of the distribution. The weather model of Case 1 has a sea level temperature of 268°K, while the weather model of Case 2 has a sea level temperature of 302°K. The sea level temperature for the various other weather models cluster about 293°K. (The temperature distributions with altitude have different shapes for the six models.) If the apparent sky temperatures for Case 1 are multiplied by $\frac{293}{268}$ and the apparent sky temperatures for Case 2 are multiplied by $\frac{293}{302}$, the resulting apparent sky temperatures are essentially indistinguishable from those obtained from other weather models for the same value of attenuation. (There are physical reasons why one would expect this to be true but the argument is fairly involved.)

As another check on the range of weather conditions for which the curve shown in Figure 3-1 is applicable, another weather model was considered. This model, while not a realistic representation of an expected actual weather, does give an extreme case with which a realistic weather model can be compared. These realistic and extreme weather models are described in Figure 3-6. The realistic weather model is the revised weather model described in the First Quarterly Report. The extreme weather model for cloudy weather consists of a cloud with a uniform water content of 0.3 grams/cubic meter extending from 0.9 kilometers to 1.8 kilometers. The rain weather models consist of the same cloud and a uniform rainfall between 0.9 kilometers and sea level. The rainfall rate is 4 millimeters per hour. The comparison between the models is shown in Figure 3-5, where clear, cloudy and rainy conditions are considered. Normalization of sky temperature with surface temperature has been accomplished.

Several important conclusions can be drawn from Figures 3-1 through 3-5.

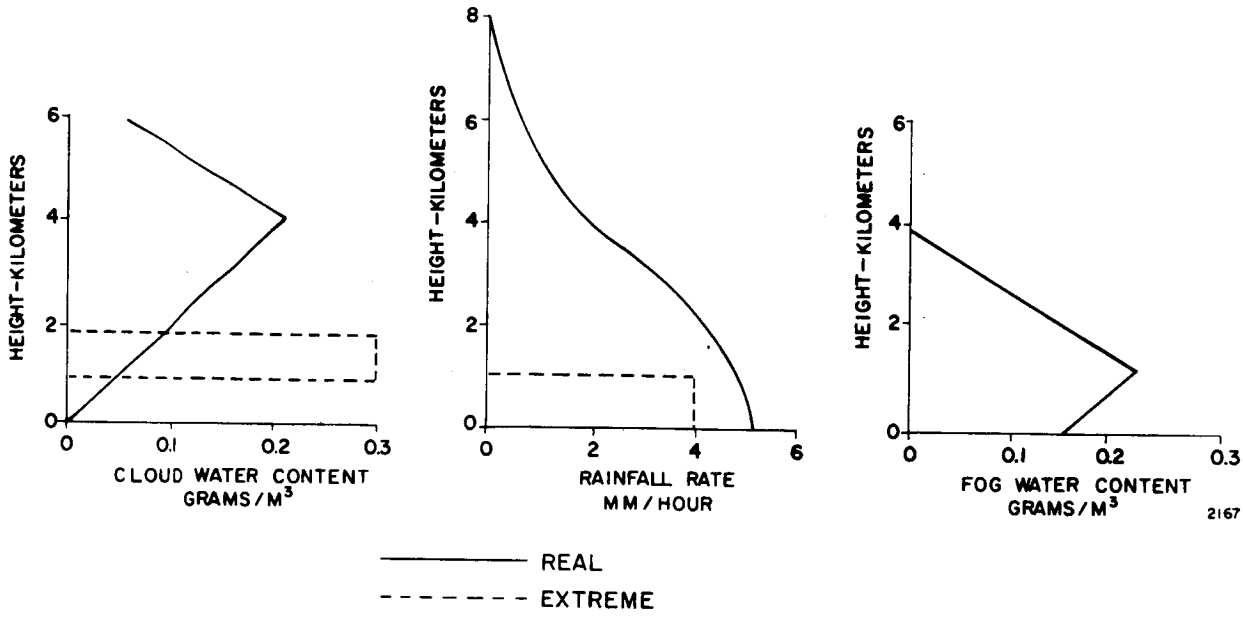

Figure 3-6 Realistic and Extreme Weather Models

(1) For $T_a \leq 200^\circ K$ ($\sigma \leq 6$ db) the uncertainty in σ is $<< 0.1$ db. With a radiometer error of 5% ($\Delta T_a = 10^\circ K$ at $T_a = 200^\circ K$), the error in σ is ≤ 0.5 db.

(2) For $T_a \leq 240^\circ K$ ($\sigma \leq 10$ db) the uncertainty in σ is ≤ 1.0 db. With a radiometer error of 5% ($\Delta T_a = 12^\circ K$ at $T_a = 240^\circ K$), the uncertainty in σ is 8.0 to 14.0 db.

(3) In the data processing operation T_a can be automatically converted to σ (within the accuracies mentioned above) using curves similar to Figure 3-1 which take into account surface temperature and pressure underneath the propagation path, receiver altitude and carrier frequency.

(4) In the data processing operation, the σ obtained from radiometric temperature can be compared with total signal losses obtained from the signal receiver data to determine if fading other than

that due to atmospheric absorption exists. As Figure 3-1 shows this can only be done effectively at $T_a \leq 240\ ^oK$ ($\sigma \leq 10$ db) because of present uncertainties in the T_a to σ conversion. If we are interested in fading when $\sigma > 10$ db (most space-earth system applications are probably not interested in that much of a penalty) then further effort is required. Table 3-2 which was derived from σ versus elevation angle data, given in Figures 5-8 through 5-10, of the Second Quarterly Report, gives the elevation angles at which $\sigma = 10$ db.

TABLE 3-2

ELEVATION ANGLES BELOW WHICH ATTENUATION DUE TO ATMOSPHERIC ABSORPTION IS 10 DB OR GREATER
(degrees)

Weather Conditions	16 Gc	35 Gc	94 Gc
Clear	0	< 5	5
Cloudy	0	5	20
Rain	< 5	10	40

The conversion from radiometric sky temperature to signal attenuation in a space-earth communications link is most accurate when the atmosphere is homogeneous in the horizontal plane. As illustrated in Section 4.1 the apparent sky temperature, as measured by a radiometer, represents an average temperature of the medium within the antenna beam while the attenuation of the actual signal depends only on the conically shaped medium between the satellite and the ground antenna. The point is that, if the medium is horizontally inhomogeneous, the received radiation may have gone through a portion of the atmosphere which absorbs significantly more or less than the average absorption indicated by the radiometer. Incidentally, the larger the antenna used by the radiometer and the signal receiver, the more accurate will be the conversion.

To get an indication of the degree of inhomogeneity in the atmosphere, a second signal receiver/radiometer located some distance from the first, could be used. The signals from the two receiver/radiometers would be cross-correlated for various relative delay times. The amount of

cross-correlation and the relative delay time at the peak of the cross-correlation function could be used to give information on the atmospheric mechanism producing the fading. For example, if the altitude of the inhomogeneities is known, the velocity of motion can be determined from the relative delay time at which the cross-correlation function is a maximum.

An estimate on the magnitude of the required spacing between antennas will now be made. The near field for a 15 ft. parabolic antenna at 35 Gc extends about 4.7 kilometers into the troposphere. Thus, a 150 ft. spacing would probably resolve inhomogeneities in the lower troposphere where there is some evidence that most of the variation in the refractive index occurs[20]. On the other hand, the center of thunderstorms occurs at about 10 kilometers altitude[26]. The beamwidth of 15 ft. parabolic antenna at 35 Gc is only 100 ft. at 10 kilometers, thus a larger antenna spacing would probably be useful if inhomogeneities associated with stormy weather are to be studied.

Another method of resolving inhomogeneities in the atmosphere is by measuring the apparent temperature of the Moon using the same receiver immediately before or after receiving from the satellite. The signal from the satellite and the sampled apparent temperature of the Moon would be cross-correlated. The size of the inhomogeneities that can be resolved depends, of course, on the angular distance between Moon and the satellite. It should be noted that the absolute temperature of the Moon need not be accurately known if only the degree of inhomogeneity in the atmosphere is of interest (as long as the Moon temperature does not change significantly between observations).

However, the absolute measurements of the apparent temperature of the Moon would give an independent value for the attenuation due to absorption. The Moon is a large source reflecting noise-like solar radiation so presumably all the fading of the signal from the Moon is due to absorption. Thus, measurements of the Moon temperature would be useful in distinguishing the various mechanisms producing fading. The accuracy of the estimate of attenuation due to absorption using the Moon depends, of course, on the

accuracy at which the apparent temperature of the Moon is known. Dr. J. Copeland of Ewen-Knight Corporation[27] has estimated the average temperature of the Moon to be 210°K. This value is accurate to at least 15°K. Measurements have been reported by Russian astronomers[28] which indicate that at 0.5 cm wavelength the apparent average temperature of the Moon is 204° K ± 4°K and that at 1.63 cm wavelength the apparent average temperature is 207°K ± 3°K.

3.2 The Use of Weather Radar to Determine Signal Attenuation Caused By Precipitation

At ground terminals where considerable millimeter-wave propagation measurements are to be made, it appears worthwhile to employ a weather radar as a correlative tool to determine precipitation rates along the propagation path. A radar such as the WSR-57 operating at 10 cm should detect precipitation at rates greater than 1 mm/hr at most altitudes of interest. In experiments involving synchronous satellites, that is, the propagation path is fixed, surface rate data from rain gauges underneath the path could be a practical supplement or alternative to the radar data.

A good general introduction to the capabilities of weather radar is given in "Radar Meteorology".[29, 30] There are two types of weather phenomena which will produce a radar return. One is moisture droplets in the atmosphere such as rain, fog or hail. The other is regions in the atmosphere where there is a marked change in the index of refraction, but no water or ice particles. (Returns from this latter type of phenomena are called "angels".) Both of these phenomena will affect the propagation of millimeter waves, the moisture particles producing absorption and scattering, and the angels producing scattering and multipath effects.

One might expect, therefore, that the number of angels detected by a weather radar would give significant information about the amount of scatter of millimeter waves or the amount of signal degradation due to multipath. Unfortunately, this does not seem to be true. For one thing, there is some disagreement as to the exact cause of angels.[31, 32] Even knowing the

mechanisms, it is difficult to predict theoretically the relation between the power scattered in different directions from turbulent variations in the refractive index.[33, 34] The signal observed by a radar is, of course, a result of radiation scattered directly back to the radar, while the signal received from a satellite is the result of radiation scattered in the forward direction. Furthermore, no applicable experimental results are available. It is expected, therefore, that while a weather radar will be quite useful in indicating if there is something invisible in the atmosphere which is producing fading, a weather radar probably cannot be used to determine whether the cause of fading is due to scattering or due to multipath.

Moisture particles in the atmosphere produce a radar return. The amplitude of the return depends upon the wavelength of the radiation. Short wavelengths (about 1 cm) can be used to detect some clouds but in one experiment only about 50% of the clouds produced a return.[35] Furthermore, because the detected clouds absorb as well as reflect, it is difficult to make quantitative estimates of the water content of the clouds from radar returns. Therefore, it does not appear to be useful to attempt to use short wavelength radars to estimate the absorption due to the water content of clouds.[36]

Radiation at 10 cm wavelengths is not appreciably scattered by the small moisture particles making up clouds, but is scattered by the larger particles making up rain, snow or hail. Therefore, a 10 cm radar would be useful in looking through a cloud cover to determine if there is precipitation along the propagation path.

3.2.1 Radar Sensitivity to Precipitation

A great deal of work both theoretical and experimental, relating to the amplitude of the power return from a rainstorm to the rainfall rate has been done.[29, 30] The major result is Equation (3-3).

$$\bar{P}_r = \frac{C}{r^2} R^{1.6} \qquad (3\text{-}3)$$

where,

$\overline{P_r}$ = the power, in watts, received from a rainstorm

r = the slant range, in meters, from the radar to the storm

R = the rainfall rate in mm/hr.

C = constant depending on the radar

The formula for C is given in Equation (3-4).

$$C = 128\pi^7 \frac{P_t A_p \gamma \beta \tau}{\lambda} K^2 N \qquad (3\text{-}4)$$

where,

P_t = transmitted power in watts

A_p = area of antenna in square meters

γ = antenna azimuth beamwidth in degrees

β = antenna elevation beamwidth in degrees

τ = pulse width in seconds

λ = wavelength in meters

$K^2 = \frac{m^2 - 1}{m^2 + 2}$ where m is the complex index of refraction. A value of .93 for K^2 is assumed which corresponds to liquid water at about $10^{\circ}C$.

N = empirical constant which relates power backscatter to rainfall rate at those frequencies where the Rayleigh approximation applies. A value of 0.4×10^{-16} is used as representative for most rains which includes a 0.2 correction factor to make the theoretical results agree with experimental data.

Based on the characteristics for the WSR-57 radar, which are given in Table 3-3, the constant C comes out to be 7×10^{-4} and, using Equation 3-3 the minimum detectable rainfall rate at any given slant range is:

$$R_{min} \simeq \left[100 \quad P_r \quad r^2\right]^{.625} \qquad (3\text{-}5)$$

Figure 3-7 is a curve of minimum detectable rainfall rate as a function of range for the radar constant of $C = 7 \times 10^{-4}$. Using this curve and the altitude versus slant range curves of Figure 3-8 (corrected for atmospheric refraction using refractive index, $n(h) = 1 + 0.000313\, e^{-0.04385h}$ with h in thousands of feet), the performance of the WSR-57 radar can be estimated. This radar should detect most rainfall rates of interest and accurately determine rates greater than 1 mm/hr at all slant ranges of interest above 2^{o} elevation.

TABLE 3-3

S-BAND CHARACTERISTICS OF THE WSR-57 WEATHER RADAR

Antenna Gain	38.5 db
Antenna Beamwidth	1.8 degrees
Antenna Diameter	12.0 feet (3.7 meters)
Peak Power	500 kilowatts
Pulse Width	0.25 & 4.0 microseconds
Pulse Repetition Freq.	658, 154 pps
Resolution	1.6 mm/hr. at 250 n mi.
Elevation Scan	-10 degrees to 45 degrees
Azimuth Scan	360 degrees

Battan[29] shows that the value of the rainfall rate calculated from radar data with Equation 3-5 can actually vary by plus or minus 50% from the rate measured by a network of rain gauges. (This conclusion is also implied by the results of Hathaway and Evans.[17] Some of this spread results from the wide variation in rainfall rates within a storm. It seems clear that the network of rain gauges was not nearly dense enough to give close estimates of rainfall rates in the experiment of Hathaway and Evans and also in other experiments.[37, 38]

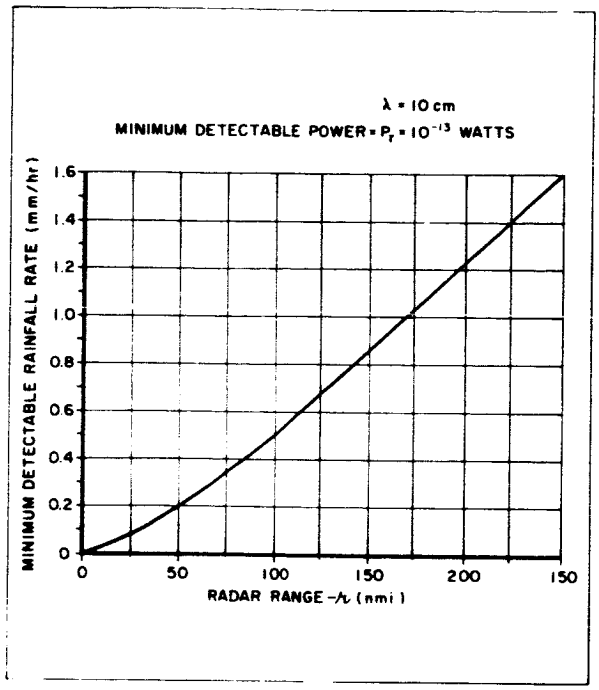

Figure 3-7 Minimum Detectable Rainfall

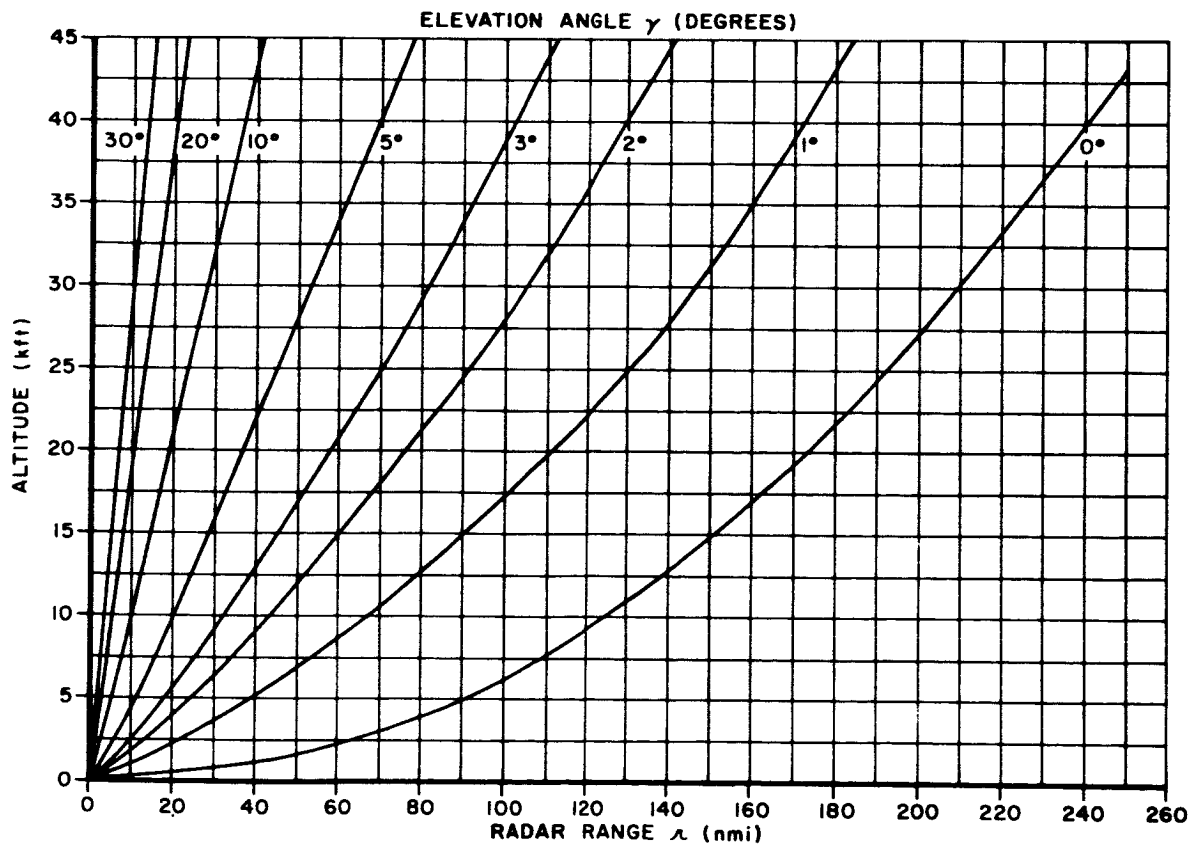

Figure 3-8 Altitude Versus Slant Range

3.2.2 The Angle Resolution Problem

It should be pointed out that the antenna beam-width for a weather radar will be much wider than that of the receiver for the millimeter waves. This will mean that the weather radar return will indicate the average amount of rainfall in a volume which may be different from the actual rainfall through which the signal from the satellite passes. There are two ways to improve the resolution of the radar:

1) Instead of letting the radar beam track the millimeter-wave beam, the radar antenna drive system is programmed to scan the beam first in the elevation plane containing the propagation path and then in the azimuth plane containing the propagation path. By knowing the shape of the beam and applying the proper coordinate conversion, the accuracy of the rate profile can be improved.

2) The WSR-57 radar also has C-band and X-band heads. With the same antenna size, each angular dimension of the resolution volume can be reduced by factors of 0.55 and 0.3 respectively. However, when operating at wavelengths below 10 cm, attenuation corrections must be made or else the conversion from power received to rainfall rate will be in error. Radiometers provide the total attenuation for the millimeter-wave signals but it does not provide an attenuation profile along the propagation path from which to make the necessary corrections. Therefore, if we increase the frequency of the radar to improve resolution we probably do not gain much in rainfall rate accuracy.

3.2.3 Conversion of Rainfall Rate to Signal Attenuation

Once the rainfall rate has been estimated, the amount of attenuation due to rain can be calculated. This attenuation is caused both by absorption and scattering. This problem has been studied theoretically and experimentally.[29, 39, 40] The theoretical result is that the attenuation is given by Equation (3-6):

$$\text{Attenuation (db)} = K_2 \int R^{\gamma} \, dr \qquad (3\text{-}6)$$

where,

R is the rainfall rate as a function of slant range r and,

K_2 = a constant dependent on the wavelength (at 1 cm, the value of K_2 is about 0.2 db/km per mm/hr)

γ = another constant also dependent on the wavelength (at 1 cm, the value of γ is about 1.0[29].

Experimental results [39] are summarized in Table 3-4 and Table 3-5. Table 3-4 indicates the spread in the value of the attenuation (per unit length, per unit rainfall) at different wavelengths and Table 3-5 indicates how well the experimental data fits the theoretical results, at least at one frequency.

It would appear then that the weather radar would be useful in giving an estimate of the rainfall rate along the propagation path and subsequently the total signal attenuation. Such an estimate could also be obtained from a line of rain gauges along the propagation path (assuming a synchronous satellite is used) and such a line might be valuable as a check on the radar estimates if one can assume accurate altitude profiles of rainfall rate. Incidentally, there is evidence of precipitation in the atmosphere which does

TABLE 3-4

SUMMARY OF ATTENUATION MEASUREMENTS

Organization	Wavelength λ(cm)	Attenuation, db/km per mm/hr.		
		Upper Bound	Lower Bound	Average
BTL	3.2	0.090	0.012	0.019
RL	1.25	0.40	0.09	0.17
NRSL	1.25	0.34	0.23	0.25
BTL	1.09	0.27	0.15	0.18
Clarendon	0.96	0.25	0.10	0.15
BTI	0.62	0.37	0.27	0.31

TABLE 3-5

COMPARISON OF EXPERIMENTAL AND THEORETICAL ATTENUATION

(λ = 0.6 cm)

Rainfall Rate R-(mm/hr)	Attenuation - (db)	
	Experimental	Theoretical
10	3.7	3.8
20	7.4	7.0
30	10.6	10.0
40	13.6	12.7
50	16.0	15.4
70	20.4	20.0
100	26.5	27.0

not reach the ground. The weather radar is especially useful in night-time measurements or measurements in the presence of fog, when the millimeter wavelength receiver operator cannot observe weather conditions along the propagation path.

Section 4
FORMULATION OF EXPERIMENTS

This section of the report discusses three topics relating to philosophy of experiment design. Two of these topics are best expressed by the following questions:

1) Isn't an aircraft flight test phase necessary to supply information for more intelligent design of propagation experiments using satellites?

2) Why not use millimeter-wave receivers in ATS type spacecraft, instead of millimeter-wave transmitters, and thus enhance payload reliability, reduce prime power consumption and weight, and make possible the implementation of these experiments within the ATS time schedule?

The third topic is related to communication and propagation experiment design for low altitude and synchronous altitude manned spacecraft. With the recent establishment of NASA and Air Force programs for manned earth-orbital missions, an attempt was made to include as much experiment design information as possible in these reports. The remaining work that needs to be accomplished, but is not within the scope of this program, is expressed in the form of a study work statement.

4.1 Use of Aircraft to Simulate Space-Earth Communication Links

A series of propagation experiments using aircraft, whose objectives are to determine the effects of the atmosphere on the characteristics of space-earth communications channels, would constitute a useful phase in

the overall millimeter-wave propagation program.

This phase of propagation data collection should precede the final spacecraft equipment design phase for the space-earth experiments. Air-ground experiments, however, should not be considered as a satisfactory substitute for the complete space-earth experiments. As compared to satellites, slow moving aircraft which can fly above most of the sensible atmosphere are attractive as vehicles for conducting propagation experiments because they provide qualitative data, without the threat of additive noise, at less expense, within a shorter equipment design and fabrication period. This qualitative data would be helpful in designing more intelligent space-earth experiments which are more complete and which yield quantitative results.

An air-ground link could quickly provide fading data as a function of elevation angle for a variety of weather models. If the experiment is properly designed, a good assessment of the effects of multipath fading near the horizon could be obtained. In addition, coherence bandwidth as a function of elevation angle for a variety of weather conditions can be determined. One problem in instrumenting air ground experiments is to equip the ground terminal with an aircraft acquisition and tracking capability. It is desirable to determine the variance of the channel characteristics as a function of beamwidth including those very narrow beams, which are expected to be used in space-earth channels. These resulting large ground apertures, far bigger than necessary to complete an air-ground link, create an aircraft acquisition and tracking problem.

The features of aircraft instrumentation which make the air-ground phase of experiments practical are the lesser payload restrictions relative to those found aboard a spacecraft. Reliability requirements are much

less because of the ability to correct malfunctions between flights. Ample prime power is available so that sufficient rf power levels can be achieved without regard to conversion efficiency and heat dissipation.

4.1.1 Effects of Aircraft Altitude and Velocity on Simulation

From a cost effectiveness standpoint, aircraft are not satisfactory substitutes for satellites when determining the complete characteristics of space-earth channels. Before giving specific reasons for this statement, it is important to briefly review the effects of the atmosphere on millimeter-wave propagation which are subject to distortion by aircraft speed and altitude.

Propagation of millimeter-waves through the atmosphere has an effect upon the maximum useful receiving aperture and the maximum useful receiver pre-detection integration time. The magnitude of these effects decrease with increasing ground terminal elevation angle and decrease with increasing distance between the receiving system and the perturbing medium. Spatial variations in index of refraction degrade lateral coherence, that is, they spoil the wavefront which is incident upon the receiving aperture. The amount of degradation in aperture gain due to these irregularities increases with aperture size. Variations in the degradation effect the signal fading spectrum along with variations in atmospheric absorption.

Temporal variations in index of refraction along the propagation path are caused by changes in the inhomogeneous atmosphere by circulation of air and the change of path position due to satellite movement with respect to the ground terminal. The degradation in aperture gain due to any temporal variations is reduced by the tracking system's ability to respond to slow variation in wave front tilt. In other words, the tracking system cancels out the low frequency spatial and temporal components of the two

dimensional spectral density function for lateral coherence which is sketched in Figure 4-1.

Temporal variations also reduce the maximum useful predetection integration time because each spectral line in the wave-form is doppler spread by changes in average speed of propagation over the total path. This pre-detection integration time, however, increases with increasing aperture size because of the averaging effects with a larger segment of wavefront.

The ideal experiment would provide a complete statistical model of this two-dimensional lateral coherence function and the accompanying cross-correlation function. However, for the early experiments, the effects of the propagation medium on spectral purity is partially masked by the short term instabilities of the millimeter-wave transmitter until

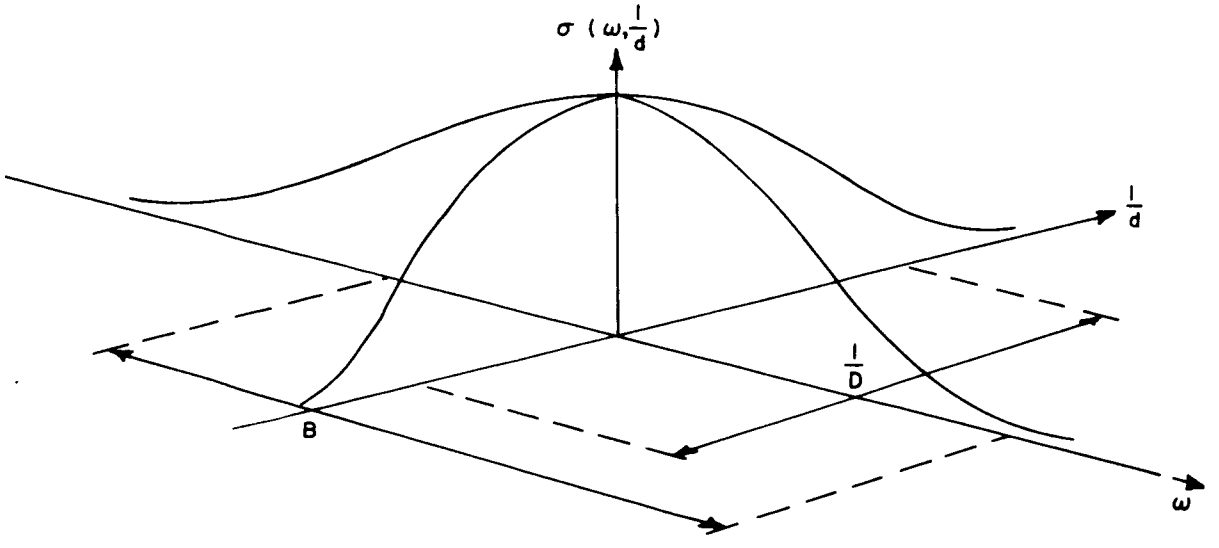

Figure 4-1 Two Dimensional Spectral Density Function For Lateral Coherence

such time that the much needed improvements in state-of-the-art have been accomplished. An indirect account of the effects on spectral purity can be obtained by observing the amplitude fading spectrum.

The inability of the geometry of air-ground links to simulate the geometry of space-earth links creates certain atmospheric effects which preclude complete substitution of aircraft for spacecraft. There are three major reasons:

1) To determine the spatial dimension for lateral coherence,it is desirable to vary the width of the spatial filter - that is, change the effective receiving aperture size; and change the baseline distance between two spatial filters. Air-ground links for this purpose are difficult to implement because the aircraft is moving. Incidentally, low-orbiting spacecraft are even more undesirable because the spacecraft is seldom within view of the ground terminal. The satellite should be stationary when lateral coherence measurements are being performed because it greatly simplifies the ground instrumentation required.

2) The drawing in Figure 4-2 illustrates another reason why aircraft data could present results which do not truly simulate space-earth channels. An aircraft flies just above the sensible atmosphere and as a result the volume of the atmosphere which effects the channel is conical in shape with the apex at the aircraft and the base being the ground antenna. When a satellite is used, even a 100 mile altitude satellite, the volume of the atmosphere approaches that of a cylinder whose diameter is equal to the diameter of the ground antenna. The effects on the channel are the same when the atmosphere is homogeneous. When the atmosphere is turbulent, especially at the higher

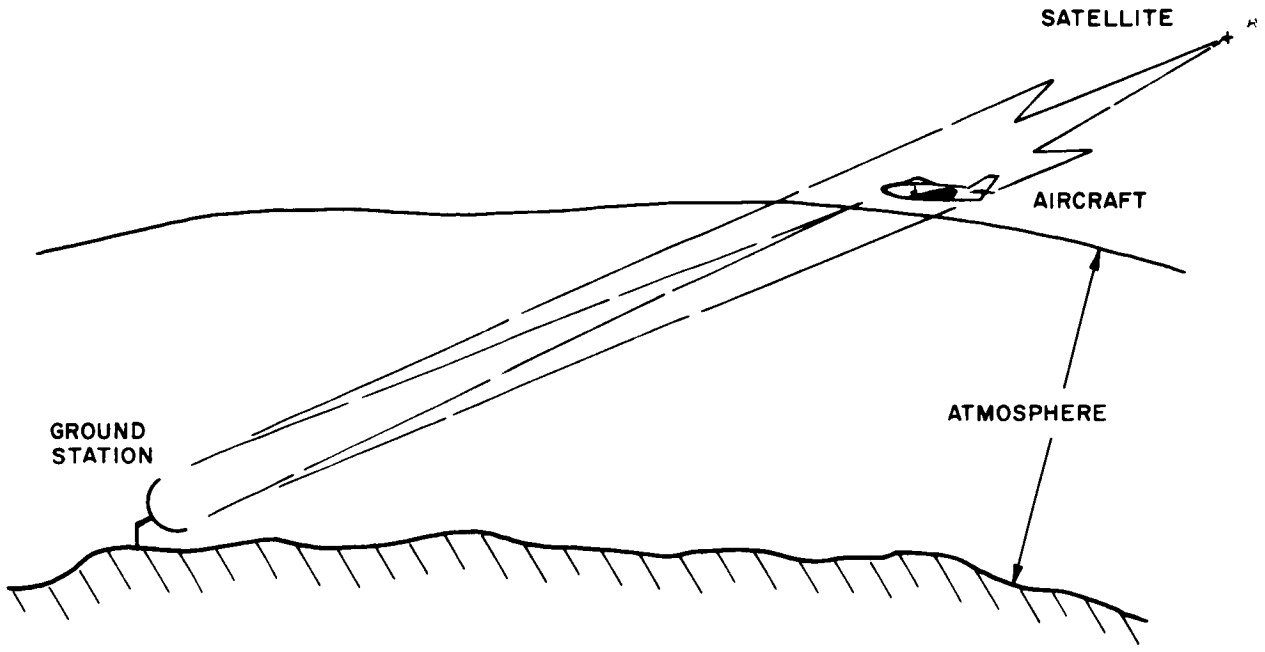

Figure 4-2 Dissimilarities of the Atmospheric Volume Involved in Space-Earth and Air-Ground Communication Channels

altitudes, the difference in channel effects might become appreciable.

Another interesting point to make concerns the use of radiometers and weather radar. An essential input to the experiment results is sky temperature which gives a measure of total atmospheric absorption. Rainfall rates along the path of propagation as measured by a weather radar are also important. The volume of the atmosphere which affects the radiometer and radar measurements are also cones.

The apex of each of these cones is at the ground receiver dish (excluding the near field which is cylindrical) and its cone angle is equal to the beamwidth of the antenna. (See Figure 4-3). When the condition of the atmosphere is homogeneous, the effects are negligible, but when the atmosphere is turbulent the effects might be significant. The final point to make,

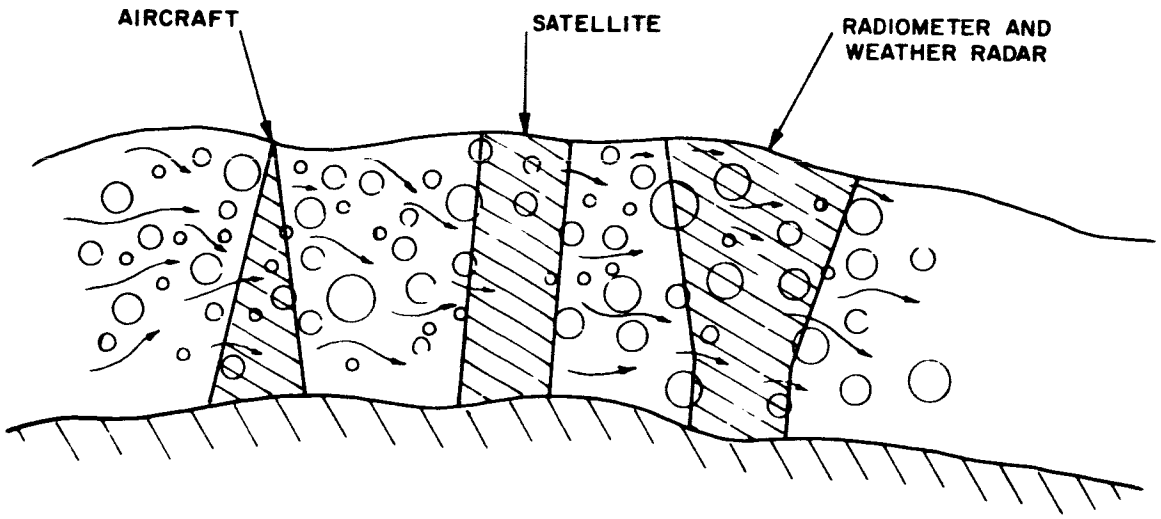

Figure 4-3 Comparison of Atmospheric Volume Involved in Radiometric and Radar Measurements with Atmospheric Volumes Which Affect Communications

is that the inverted cone will more nearly represent a cylinder in the space-earth channel than it will represent a cone in the air-ground channel.

3) The third reason why aircraft data could present results which truly simulate space-earth channels is shown in Figure 4-4. Aircraft flying just above the sensible atmosphere cause the path of propagation to change in position. The movement of the aircraft introduces an apparent wind speed which is proportional to the velocity of the aircraft and proportional to the altitude at which the turbulence exists. This apparent wind speed can be an order of magnitude greater than true wind

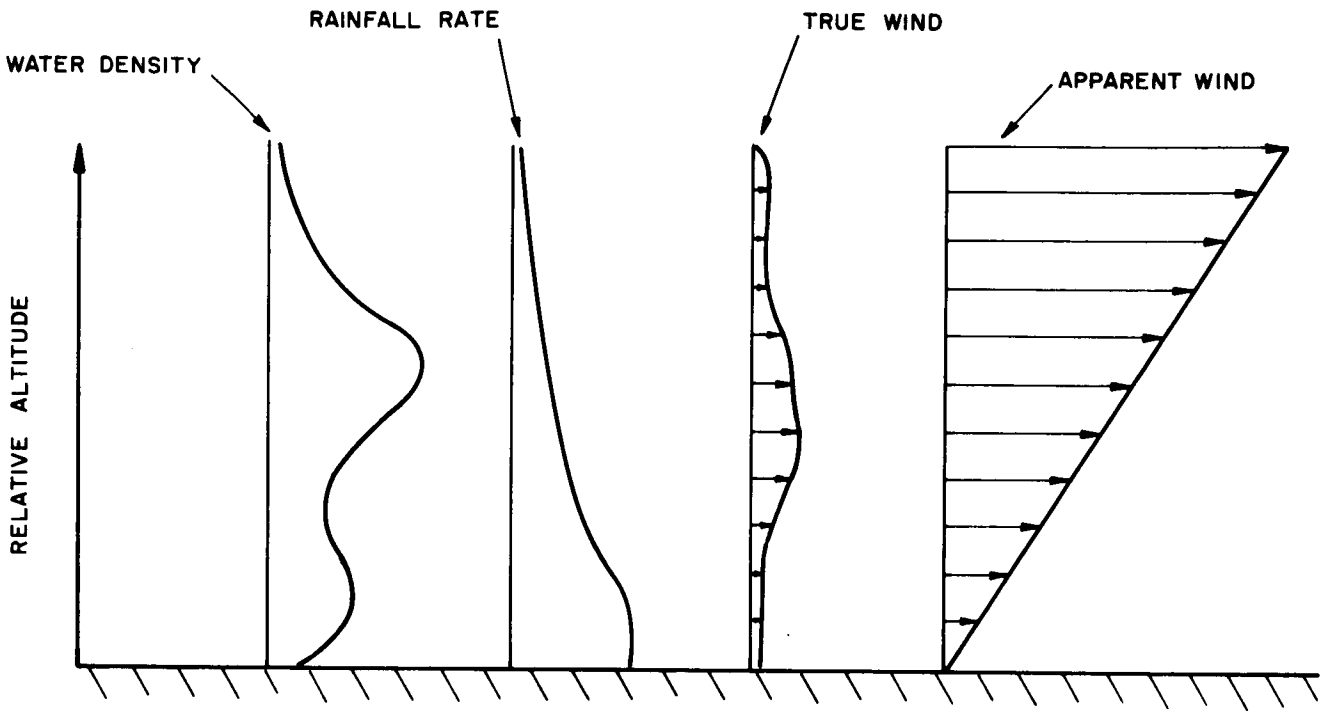

Figure 4-4 Apparent Wind Profile Caused by Aircraft Motion And Its Relation To True Wind, Rainfall Rate and Water Density Profiles

speeds which are normally encountered. This "wind" effect is not too serious when simulating space-earth channels for low orbit spacecraft, but when simulating space-earth channels for high altitude spacecraft and deep space probes, there would be some question. Aircraft movement expands the two-dimensional spectral density function in the time domain and direct compression of the time scale may not necessarily simulate the long range channels.

The differences between space-earth channels and air-ground channels as discussed above might turn out to be insignificant but one cannot be completely sure until some measurements are made. To improve the simulation one should strive to use

slow moving high altitude aircraft. The effects of atmospheric turbulence on the short term motion of the aircraft decreases with altitude. If the bulk of the perturbing medium happens to be near 8 to 15 thousand feet, then an air-ground channel with a high altitude aircraft (about 40 thousand feet) more nearly represents the space-earth channel. Also the higher the aircraft altitude and the slower the aircraft speed the smaller the apparent wind speeds. Everything that is done to improve simulation increases the costs of the aircraft flight tests. This leads the discussion to one final area - cost effectiveness of aircraft tests versus cost effectiveness of spacecraft tests. A complete cost effectiveness study is not within the scope of this report, but certain preliminary ideas can be introduced.

4.1.2 Cost Effectiveness of Aircraft Tests

One of the objectives of the overall millimeter-wave propagation program is to provide the communication system designer with the necessary statistical knowledge to accurately assess the effects of the propagation medium on: the required effective radiated power and effective receiver sensitivity to achieve given nominal data transmission capacities; the signal fidelity or error rate probability of transmitted signals after propagation through the channel; and on the reliability or percentage of time these quantities and qualities are expected to prevail.

A typical work cycle with a stationary satellite which would be satisfactory for the propagation experiments would be to operate during a five day work week, ten to twelve times, spaced seasonally during the year. A full work week every four or five weeks may be the most attractive arrangement from a manpower scheduling point of view. This several week period between tests also provides an opportunity for examining data and

making changes in test procedure and ground equipment before the next test.

Each work week could consist of four data collection sessions, four to six hours duration for each; and appropriately spaced so that each station collects data during dawn and dusk and near noon and midnight. These sessions include pre-test and post-test data collection check-out and calibration with the spacecraft simulator which is located at a remote boresight facility. No planning would be made with regard to weather since it is unpredictable and since work schedules must be established well in advance. Enough samples would be taken during the year which should result in a reasonable cross-section of the normal meteorological variables.

With three ground stations working in different parts of the country, this typical work cycle represents 864 hours of data. It is, of course, not necessary to statistically process all of the data collected in a four to six hour period, but it would be necessary to look for the occurrence of unusual propagation effects, to insure that what is processed,adequately represents the statistical model. If the expense of a high altitude aircraft is compared with the cost of a payload aboard a synchronous satellite to provide that many hours of good data, it can be shown that spacecraft can be very competitive with aircraft as platforms for conducting the propagation experiments. This is based on the assumption that the millimeter-wave experiment is one of several experiments being performed with the satellite such as in the case of the Applications Technology Satellites.

4.2 Propagation Experiments Using Only Receivers In Small Satellite Payloads

One question, which is continually being asked by those who are interested in millimeter-wave propagation experiments using satellites, is: "Why not use millimeter-wave receivers in the satellite instead of

millimeter-wave transmitters and thus enhance payload reliability, reduce prime power consumption and weight, and above all, make possible the implementation of these experiments within a shorter time scale?"

For the initial propagation experiments, the First and Second Quarterly Reports specifically recommend down-links instead of up-links and the reasons for this recommendation are repeated here. The chief purpose of this Section and Section 5.1 "Multiple Frequency Receiver Configuration for Small Payloads" is to extend the discussion on up-links versus down-links one step further by discussing the design of satellite receivers and weighing the simplification in payload against the reduction in experiment value to determine if the experiment is worthwhile. The points pro and con are made with the synchronous ATS (Applications Technology Satellites) in mind as the primary candidate for the space platform.

The key to a successful experimental program which involves the assistance of several existing ground installations, each controlled by a different agency, depends on the ease with which these facilities can participate. This ease is measured in terms of expense for any modifications required (unless absorbed by NASA), compatibility with schedules of other activities which involve these facilities, the amount of coordination required with other agencies during the operational periods, and the immediate accessibility of the resulting data to the participating agencies.

All of the existing sites under consideration (see Section 6.0, First Quarterly Report) are equipped with millimeter-wave receivers which are used in radio astronomy. Since these facilities use interchangeable rf heads to change frequency of operation, it is very reasonable to assume that new rf heads, specifically designed for propagation data collection, can be supplied to these facilities. If these existing facilities are to be

equipped with transmitters, some serious equipment difficulties can arise. The University of Texas facility, for example, does not use a Cassegrain antenna and, to eliminate long waveguide runs, the transmitter would have to be mounted near the focal point of the parabolic dish. A new transmitter and antenna feed support structure would also have to be installed.

Another very important reason for wanting to use satellite transmitters is that less coordination is required during the data collection operation. These facilities can receive test waveforms transmitted from the satellite with little or no coordination with GSFC except to obtain satellite ephemeris data and to plan the data collection schedules. Several stations can make measurements simultaneously without interfering with one another. When ground transmitters are used, coordination is much more difficult, the main reason being that a closed loop is required to confirm that the transmitted signal is being properly received. A closed loop would require that each ground facility be equipped to receive a beacon signal or a telemetry signal from the satellite which indicates that the transmit beam is properly pointed.

One objection to the down-link has been the high prime power requirements of the space transmitter. However, a good receiver local oscillator, especially one that is locked to a stable source, consumes almost as much power and, since it must be on longer than a space transmitter in order to accommodate each ground station individually, it is questionable whether the satellite receiver really provides much advantage in prime power.

One of the prime areas of interest in the propagation experiments is to define the lateral coherence function which was discussed in Section 4.1. This function is two-dimensional in that it describes the maximum useful antenna aperture and the maximum useful integration time of a space-earth channel. It is desirable in the initial experiments to determine at least some

of the points along the spatial axis (points along the frequency axis can be inferred from the amplitude fading spectral density function). These points are determined from measurements using multiple receiving apertures on the ground, and therefore, these measurements can only be made with a down-link.

An essential input to the experiment is sky temperature measurements which give a measure of total atmospheric absorption. The most meaningful measurements are made with ground radiometers which use antennas equivalent in size to those being used for the space-earth link. It is very difficult to share an antenna with a CW signal transmitter and a radiometric receiver. Use of two antennas is out of the question because of expense involved. The frequency of operation of the radiometer would have to be displaced from that of the transmitter by a substantial amount in order to preserve the sensitivity of the radiometer.

When up-links are used, the participating agencies do not have immediate access to the raw data which is being collected. There is a certain delay in obtaining this information which prevents the station operators from evaluating their performance in real time and taking corrective action. It appears certain that in addition to satisfying NASA's requirements, these agencies would want to make specific measurements or data recordings which fulfill some special requirement of their own (antenna pattern measurements is a prime example). When up-links are used, they do not have any of these liberties.

All of these negative features about up-links tend to discourage or prevent other agencies from participating in the propagation program. The absence of their participation means the loss of valuable data points. In addition to losing important weather models, their absence also means

degradation in the elevation profile if a synchronous satellite is used.

On the positive side there are some significant features of the up-link which are worth discussing. First of all, as will be apparent in Section 5.1, satellite receivers are simpler and easier to design. Inherent in the design is improved reliability and significantly lower power consumption especially in the case of the 16 Gc and 35 Gc receivers. One area of increased reliability is in signal acquisition because the ground transmitter and receiver local oscillator can now be stabilized with a crystal frequency source. A satellite transmitter could not be stabilized because of the prohibitive amounts of power required especially when considering the ATS satellites.

Even though the positive points for use of up-links are discussed briefly it does not mean that they aren't important. An early space-earth experiment has to depend completely on present technology and a satellite receiver design is considerably closer to meeting longevity and environmental requirements than the present satellite transmitter design. The main question to be answered is: Does the cost of an up-link experiment merit the propagation data it produces? This question can only be answered at such time when a specific satellite has been declared available and actual commitments have been received from the participating agencies who have usable ground terminals.

4.3 Design of Communication and Propagation Experiment for Synchronous and Low Altitude Manned Spacecraft

With the establishment of the NASA Apollo Applications Program (AAP) (formerly known as AES, Apollo Extension System) and the Air Force Manned Orbiting Laboratory (MOL) Program, it was considered appropriate to include as much experiment design information as possible in these reports. This section is therefore a preliminary discussion of millimeter-wave (EHF) communication experiment design for synchronous and low earth-orbiting manned spacecraft. Since the information contained in the First and Second Quarterly Reports covers most of the design elements for unmanned synchronous satellites, the emphasis in this section will be on low satellite altitudes between 100 and 300 nautical miles. Design philosophy for experiments using low altitude manned spacecraft is discussed. The potential of millimeter-waves in future manned spacecraft communication data links is reviewed.

Orbital analysis for low altitude spacecraft is given including some estimates of communication time per orbital pass and average communication time per day in a long duration mission (30 to 45 days).

Effects of atmosphere on millimeter-wave propagation in the 60 Gc oxygen absorption band (50 to 70Gc) is reviewed and a signal level analysis is given for 60 Gc experimental links between spacecraft and aircraft.

This section on manned spacecraft experiments is concluded with a recommended work statement for additional study which was not included in the scope of the present effort.

4.3.1 Design Philosophy for Experiments Using Low Altitude Manned Spacecraft

The design of experiments using low altitude manned spacecraft would be based on the assumption that propagation experiments using aircraft and medium to synchronous altitude unmanned or manned satellites have already been performed during preceding phases of the program. As explained in the First and Second Quarterly Reports and in Section 4.1 of this report, these preceding experiments would provide basic propagation data, under highly controlled measurement conditions. This accurate knowledge of significant atmospheric influences on power density, modulation method, and receiver performance would permit valid conclusions to be reached as to the utility of this region of the spectrum. Finally, the preceding experiments would generate statistics relating to channel reliability as a function of time and zenith angle under a representative series of meteorological conditions.

Low orbiting spacecraft are not ideal vehicles for basic propagation experiments. They are just too close to earth to permit reasonable time for gathering quantitative data by any one aircraft or ground station. Multiple aircraft and ground stations are expensive especially since the spacecraft is traveling at high angular rates relative to the other terminal. Low orbiting spacecraft do, however, offer payload capacities which often surpass that which is available at higher altitudes. Furthermore, the availability of man in a low orbiting spacecraft is of inestimable value in determining the operational potential of millimeter-wave communications, to support future manned spacecraft missions. The experiments with low orbiting spacecraft would be communication experiments demonstrating actual modulation methods expected to be employed in future systems. They would, in effect, verify the system performance inferred from the basic propagation data gathered during previous phases of the millimeter-wave communication/

propagation program.

The experiment design must include careful consideration of the orbital and payload constraints placed by the specific spacecraft and its crew. When a manned spacecraft experiment is planned, special attention must be given to the crew's capability to perform in the environment, the amount of crew time available for experiments, justification for the devotion of this time to a millimeter-wave communication experiment rather than other experiments, evaluation of functions in the experiment which requires participation of the crew, and evaluation of the degree of automation in the experiment.

The designs must be such that the success of the experiment will not depend completely upon the success of other experiments which are also being performed with the low altitude space platform. Neither should the design be dependent upon adding components, such as a complex antenna system, the operation of which would in itself constitute an experiment. Since the experiment should run for as long as possible and should include measurements made under a multitude of conditions at many different path angles, the proper use of the spacecraft must be determined from a cost-effectiveness viewpoint. One of the basic ground rules, to be observed in planning such an experimental program, is that the experiment hardware consist of proven designs and techniques with emphasis on reliable performance and simplicity of design.

4.3.2 The Potential of Millimeter-Waves in Manned Spacecraft Systems

Present aerospace communication links are using densely populated frequency bands, particularly the VHF and UHF bands, which are already crowded with non-communication-type emitters. This means that important communication channels can be highly susceptible to interference or jamming of either an intentional or unintentional nature. Bandwidths available at

SHF for communication purposes are limited by FCC, interference, and other considerations. The resulting available frequency bandwidths are inadequate to handle the steadily increasing data required of aerospace information links.

Spacecraft weight and power is at a precious premium as is room on space vehicles for antennas. The combination of radiated power and antenna gain is an important consideration in the performance of a satellite communication link. The ideal objective would be to be able to reduce the required radiated power from the vehicle and increase the antenna gain without increasing the size of the antenna. Finally, it is highly desirable to be able to construct an aerospace communication link with a high degree of privacy. This feature insures that the link information is available only to the intended receiver and should further reduce the possibility of intentional jamming.

All of these problems and requirements indicate that portions of the millimeter band, initially the 30-100 Gc frequency region, should receive consideration for use as the carrier in aerospace communication links.

Present operational equipments which are radiating power at fundamental frequencies in the millimeter band are comparatively few. Most of these EHF emitters are limited to low radiated power levels and transmission paths along the earth. As a result of these characteristics and well confined antenna sidelobes, radiated EHF power at angles other than along the earth's surface is very small. In addition, any radiated EHF power along the earth's surface is subject to comparatively high attenuation due to atmospheric losses. Consequently, there is currently little possibility of interference to EHF aerospace links from fundamental EHF emitters, either accidental or intentional. Another possible source of interfering EHF signals lies in the harmonics of high power C-band and

X-band radars. These harmonic signal levels can be of sizeable magnitudes and the antennas from which they are radiated are quite often pointed skyward. In general, however, the signal density in the EHF band is several orders of magnitude less than the signal density in the present SHF communication links.

The available rf bandwidths in the millimeter band are at least one order of magnitude greater than available SHF bandwidths. A 15 percent bandwidth at 94 Gc is about 14,000 mc wide; this is as wide as the entire combined VHF, UHV and SHF bands presently in use. A 15 percent bandwidth at X-band is about 1400 mc wide theoretically, but this 1400 mc bandwidth is further reduced by FCC regulations and other constraints. Since these constraints do not apply in the EHF band, improvements in available bandwidth greater than one order of magnitude can be theoretically obtained. This increase in available bandwidth is necessary if future aerospace communication links are to handle the steadily increasing quantities of information which must be transmitted from space vehicles, particularly if they are manned and they are performing low altitude missions. The only area of uncertainty which impedes the immediate use of EHF aerospace communication links is the subject of the propagation characteristics at EHF.

If the transmitter portion of an aerospace communication link is contained in a spacecraft, then the distribution of the product of radiated power and antenna gain is an important factor in the design of the communication link. As an example, assume that an aerospace communication link were performing satisfactorily at a frequency of 9400 mc with 10 watts of radiated rf power and a two-foot diameter paraboloid antenna. Neglecting atmospheric attenuation for a moment, the same link performance, assuming identical receiving terminal characteristics, could be obtained

at a frequency of 94 Gc with the same two-foot dish by using only 100 milliwatts of radiated rf power. Considering that tube conversion efficiencies might typically be 10 percent, the X-band system would require 100 watts of satellite power while the EHF system would require one watt of satellite power. The savings of almost 100 watts of primary power in only one instance is an important consideration when the scarcity of spacecraft power is considered.

Another advantage that is obtained by operating aerospace communication links at EHF is the aspect of transmission privacy. This advantage is due primarily to EHF atmospheric attenuation characteristics and the narrow antenna beamwidths obtainable at EHF. These two factors also help to reduce any possible interference or RFI from other EHF signals. For a given size antenna, the half power beamwidth is inversely proportional to the operating frequency. Thus, an antenna operating at 94 Gc would have 1/10th the beamwidth of the same size antenna operating in X-band. The privacy of transmission which is obtainable due to atmospheric attenuation characteristics is particularly noticeable in the 60 Gc frequency band. In this frequency band, transmissions from a satellite to an aircraft at 45,000 feet would not be received by a ground station because of the large additional attenuation due to the intervening atmosphere below the aircraft.

Thus, there are many possible operational advantages to be obtained from aerospace communication links at EHF. However, the EHF band has not received anywhere near the attention that the SHF band has received and, consequently, the EHF band got a late start and has been developing at a much slower pace than the SHF band. However, various Government agencies are now encouraging the development of the EHF state-of-the-art and considerable information and capability is being developed.

4.3.3 Experimental Ground and Airborne Facilities

Unfortunately, space-earth links for low orbiting spacecraft are limited in experimental communications time. Additionally, since millimeter-wave communications are seriously degraded by the propagation medium near the horizon, communications time is further limited. Typical low altitude space-earth communications are restricted to short intervals (2-10 minutes) at each site during each orbital pass, nevertheless, these millimeter-wave channels are attractive for certain system applications.

The advantages of aircraft as terminals in aerospace communications have been recognized. They fly above a large portion of the sensible atmosphere and therefore provide a space-air communications channel which is essentially free of both water vapor and oxygen absorption. Because of their freedom from propagation effects and the altitude of the airborne terminal, these communication links offer a considerable increase in reliable communication time per orbital pass over that for space-earth channels. In addition, the transportability of the aircraft allows one to take advantage of certain orbits, not available to ground stations, where real-time transmission from spacecraft sensors is necessary.

For potential operational systems, both ground terminals and airborne terminals have their place in millimeter-wave aerospace communications. Thus, the geometry of the space-earth and the space-air experimental links must resemble as closely as possible the geometry of those links expected to have the greatest variety of future applications.

Table 4-1 gives a typical mission outline for the manned earth-orbital phase of the APOLLO Applications Program recently defined by Dr. George Mueller, Associate Administrator for Manned Space Flight. This mission outline gives the orbits and mission times which are

TABLE 4-1

TYPICAL MISSION OUTLINE

FOR

12 THREE-MAN EARTH-ORBITAL FLIGHTS IN THE APOLLO APPLICATIONS PROGRAM

Flight No.	Mission Class	Altitude n miles	Inclination degrees	Duration days	Description
1	Remote Sensing of Earth's Surface	200	50	14	Earth mapping in visible and near-visible spectrum. Artificial gravity qualification. Medical.
2	Biomedical/Behavioral Technology	200	28 1/2	30	Biomedical/Behavorial Investigations. Lunar Orbit Survey System qualification.
3	Bioscience/Physical	200	28 1/2	45	Prolonged Weightlessness Effects. Zero-G behavior of solids, liquids and gases.
4	Space Operations/ Bioscience Laboratory	200	28 1/2	45	Rendezvous with Mission No. 3. Extravehicular cargo and personnel transfer. Rescue Operations. Spacesuit evaluation. Space Flight Effects on biological systems.
5	Remote Sensing of Earth's Atmosphere	200	83	45	Sun synchronous. Multi-spectral Sensors. Solar cell array erection and orientation.
6	Astronomy/Bioscience Laboratory No. 1	19,350	0	45	X-band, visual and IR spectral and photometric data. Deployable satellites. Extendable radio astronomy antenna
7	Artificial Gravity Laboratory	200	28 1/2	45	Evaluate Human Performance in Rotating Environment. Cable mounted CSM and LEM-Lab are rotated.
8	Remote Sensing of Earth's Surface and Atmosphere. Echo Observation	200	83	45	Sun synchronous. Multi-spectral Sensors. Solar Cell Array erection of orientation. CSM Inspection of Echo Satellite.
9	Space Physics and Subsurface Development	19,350	0	45	Space Environment near Earth. Aurora magnetic fields. Micrometeoroid fluxes. Life Support Communications. Satellite Launch
10	Astronomy/Bioscience laboratory No. 2	200	28 1/2	45	Optical Radio Astronomy. Micrometeorites. Gamma Rays. Biomedical.
11	Astronomy/ Logistics No. 1 and Bioscience Laboratory	200	28 1/2	45	Rendezvous with Mission 10. Cargo and Personnel Transfer Effects of flight duration beyond 45 days. Continue Optical and Radio Astronomy
12	Astronomy/ Logistics No. 2	200	28 1/2	45	Rendezvous with Mission 11. Extended Mission to total of 135 days. Cabin Atmosphere. Propellant Handling.

predominant and is representative of the total experimental activity in which the spacecraft crew will be involved.

Table 4-2 lists four existing millimeter-wave facilities which are possible candidates for experimental ground terminals. Detailed characteristics of these facilities were given in Section 6 of the First Quarterly Report. Their geographic distribution provides an excellent cross-section of meteorological variables. Unfortunately, the AFCRL and Lincoln Laboratory facilities are positioned too far North for effective collection of propagation data with the low altitude $28\text{-}1/2^{\circ}$ inclined orbits. New facilities at locations such as Hawaii, Ascension and Puerto Rico would be most helpful. An orbital analysis is given in Section 4.3.4. From this one can visualize the effects that orbital inclination, orbital altitude and minimum operational horizon can have upon data collection time. The orbital parameters of the spacecraft and the latitude of the ground terminal would be an important consideration in the final cost trade-offs that must be formed.

An area of chief concern in the airborne equipment is its emplacement in the aircraft. Figure 4-5 illustrates one approach which may be applicable to a U-2 aircraft. The millimeter-wave transmitter or receiver is placed forward of the cockpit. With the fixed elevation axis oriented parallel to the longitudinal axis of the aircraft, the permissible elevation coverage ranges from -10 degrees to 190 degrees. The transverse axis is perpendicular to the elevation axis. Transverse coverage of 60 degrees appears to be adequate. With a proper flight path, a spacecraft can be kept within view of the aircraft antenna from horizon to horizon. The sketches in Figure 4-6 show orientation of aircraft with respect to spacecraft orbit.

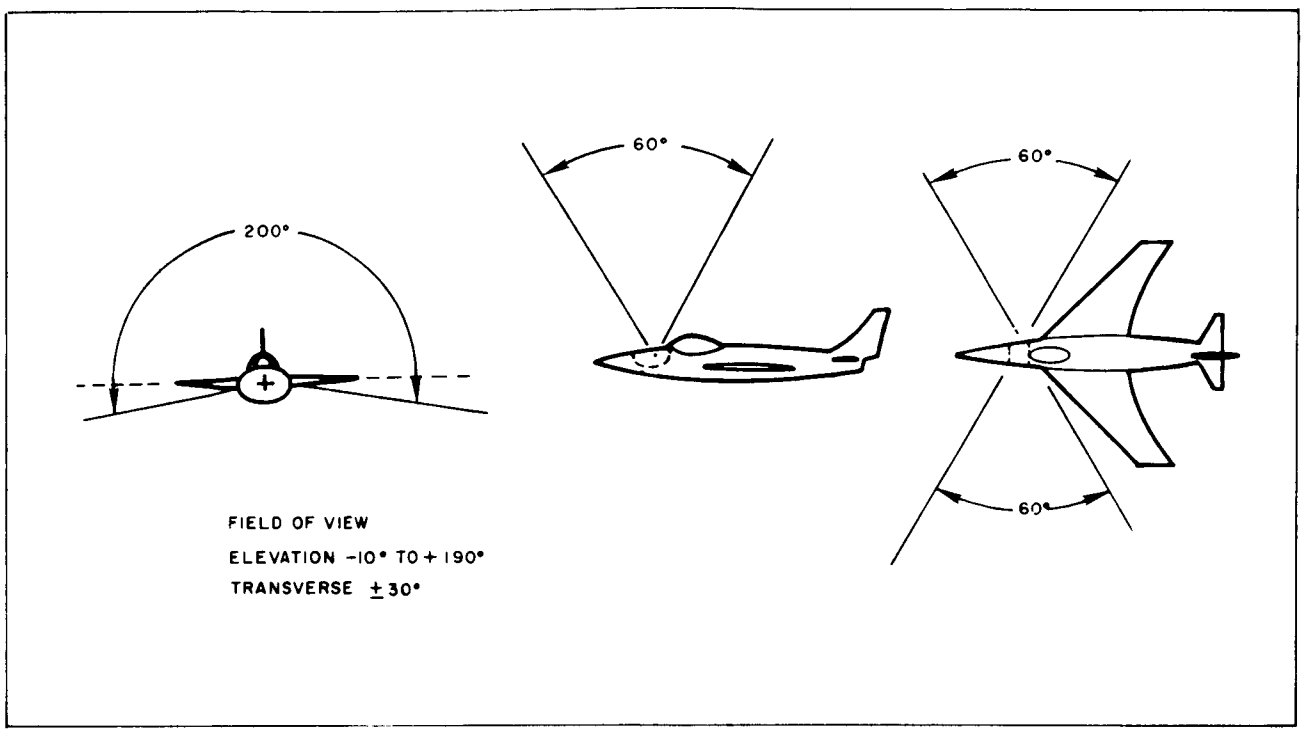

Figure 4-5 Field-of-View Aboard an Aircraft

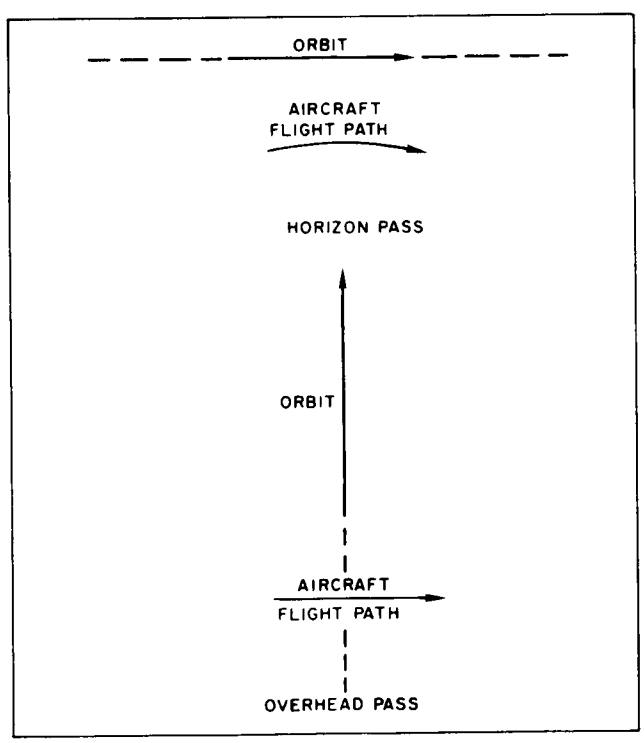

Figure 4-6 Orientation of Aircraft with Respect to Spacecraft Orbit

TABLE 4-2

APPLICABLE EXISTING MILLIMETER EXPERIMENTAL FACILITIES

Facility	Location	Features[1]
Aerospace Corporation	Southern California Latitude 34 degrees Longitude 118 degrees Altitude 0 to 300'	Clear Weather Model 10 to 20 inches annual rainfall Good Orbital Coverage[2]
University of Texas	Central Texas Latitude 30 degrees Longitude 98 degrees Altitude 1000' to 2000'	Constant Weather Model 20 to 40 inches annual rainfall Good Orbital Coverage[2]
AFCRL and Lincoln Labs	Eastern Massachusetts Latitude 42 degrees Longitude 71 degrees Altitude 100' to 500'	Variable Weather Model 40 to 60 inches annual rainfall Questionable Orbital Coverage[2]

[1] Weather Model which is likely to occur during 45-day mission

[2] With respect to $28\text{-}1/2^{o}$ inclinations or less.

4.3.4 Orbital Analysis for Low Altitude Satellites

Orbital periods and velocities for satellites at altitudes below 600 nautical miles are given in Figure 4-7. Period and velocity for a circular orbit are approximated by:

$$\text{Period} = T = \frac{(R + h)}{2390}^{3/2} \quad \text{Minutes} \qquad (4\text{-}1)$$

$$\text{Velocity} = V = \frac{250}{(R + h)}^{1/2} \quad \text{nautical miles/second} \qquad (4\text{-}2)$$

where

R = Earth's radius = 3440 nautical miles

h = satellite altitude in nautical miles

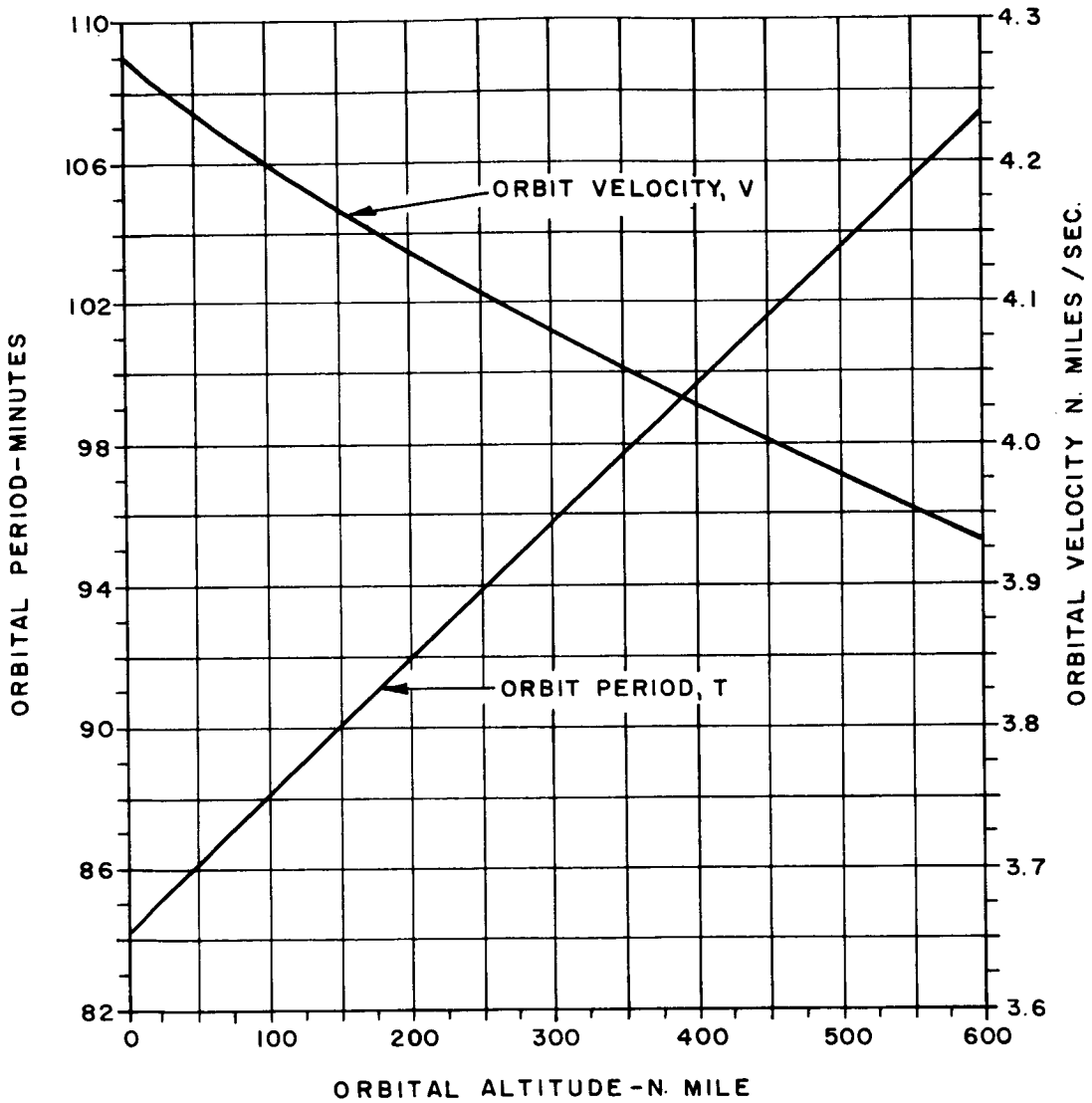

Figure 4-7 Orbital Period and Velocity Versus Altitude For Low Orbiting Spacecraft

Figures 4-8 and 4-9 give slant range and coverage radius versus altitude and elevation angle for low orbiting spacecraft. Slant range and coverage radius are defined in the geometry shown in Figure 4-10 and are calculated using:

$$\text{Slant Range} = R_s = \frac{\sin \theta/2}{\cos \gamma} (R + h) \text{ nautical miles} \quad (4\text{-}3)$$

$$\text{Coverage Radius} = R_\theta = 60 \times \theta/2 \text{ nautical miles} \quad (4\text{-}4)$$

where:

$$\theta/2 = \sin^{-1}\left[\frac{R_s}{R_s + h}\right] \cos \gamma \text{ degrees} \quad (4\text{-}5)$$

γ = elevation angle

Communications time during an orbital pass between a satellite and a given point on the Earth is the most important parameter when evaluating candidate satellites as platforms for space-earth propagation and communication experiments. Figure 4-11 gives communications time versus elevation angle during an overhead pass of polar satellites at altitudes of 100, 200 and 300 nautical miles. A correction can be made for Earth's rotation for satellites at inclinations other than 90 degrees. The correction factor is:

$$n = 1 + \frac{T}{1400} \cos \ell \quad (4\text{-}6)$$

where

T is in minutes and ℓ = inclination angle (ℓ = 0 degrees for an equatorial orbit launched from West to East). The factor n is given in Figure 4-12.

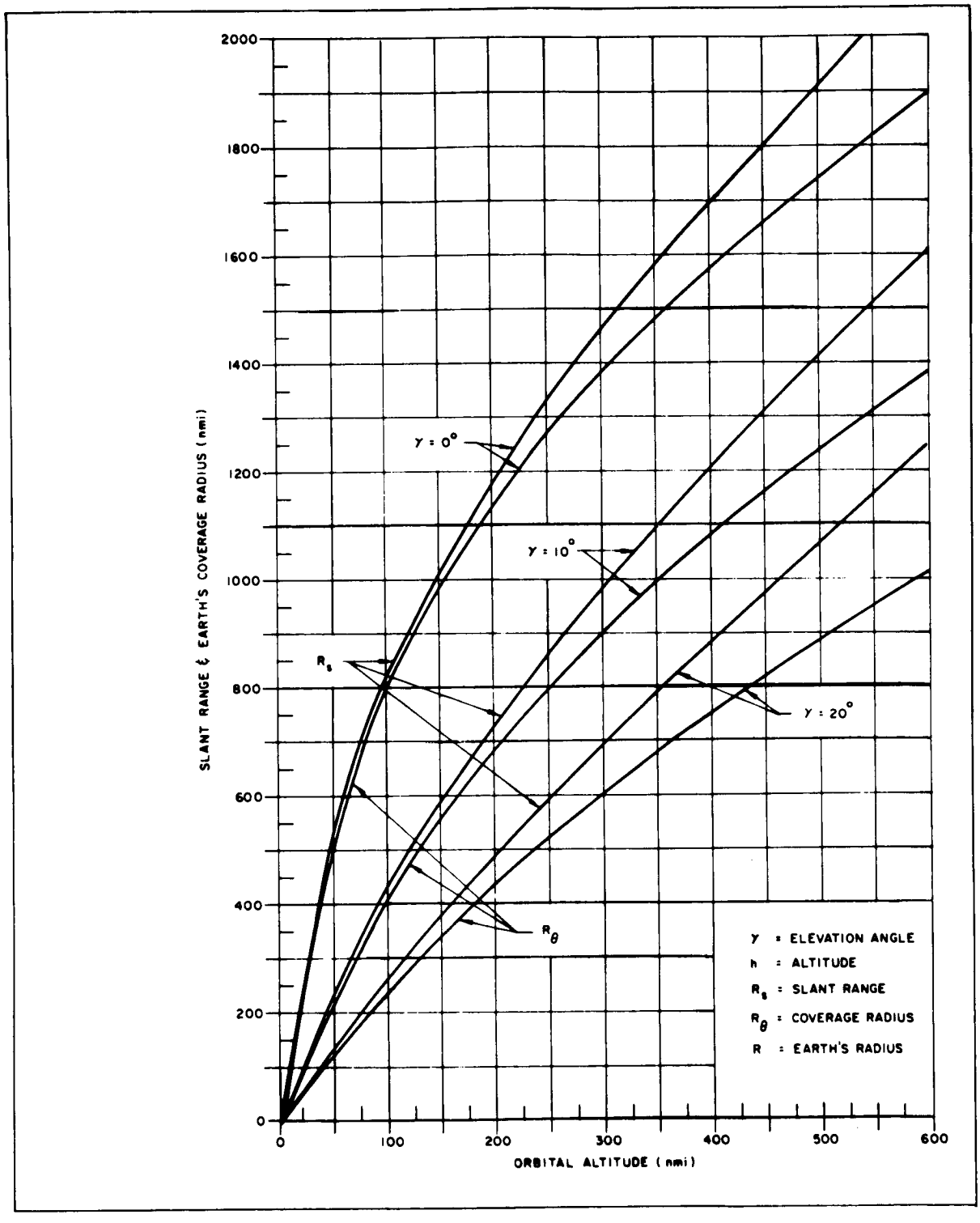

Figure 4-8 Slant Range Plus Coverage Radius Versus Altitude For Low Orbiting Spacecraft

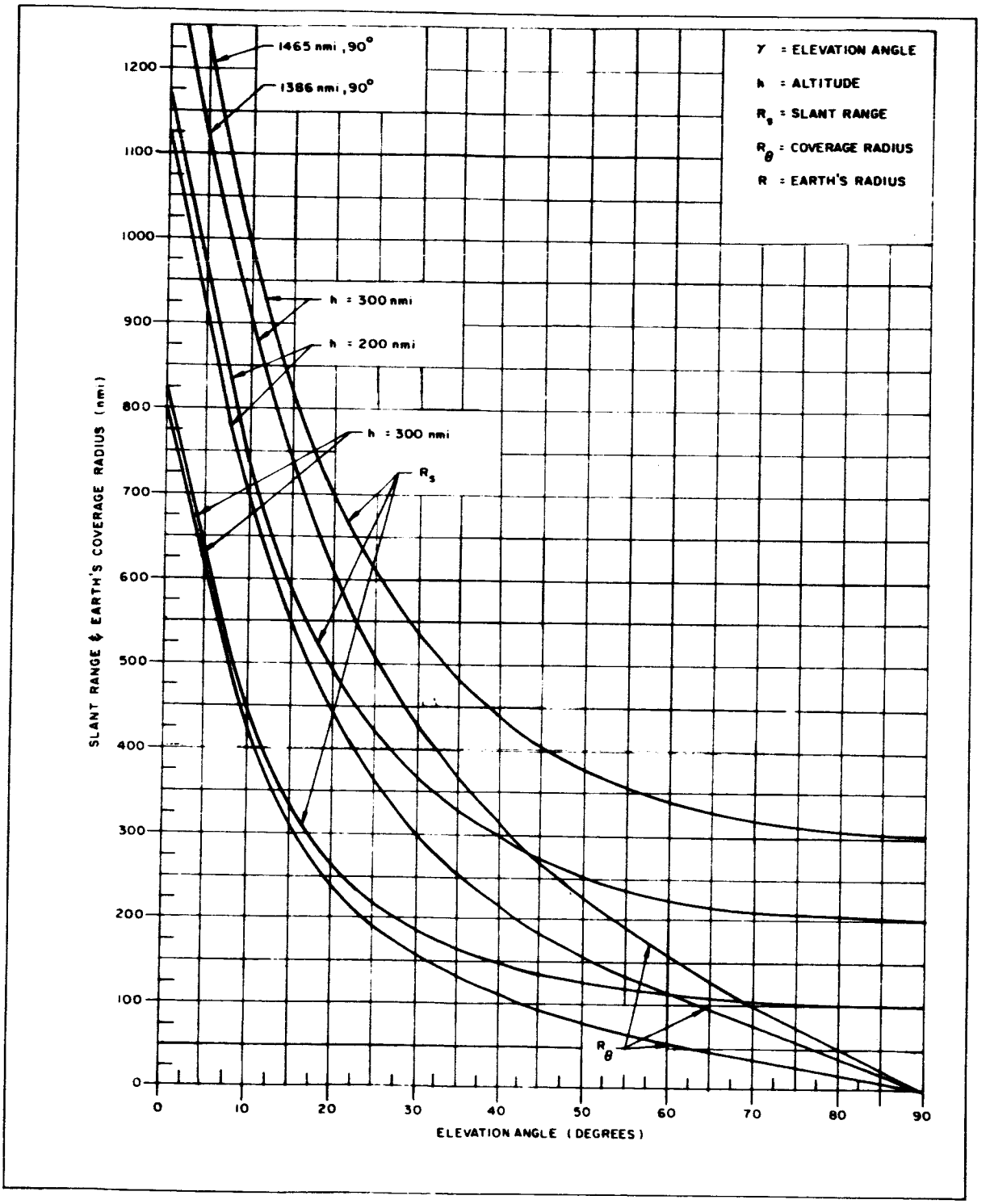

Figure 4-9 Slant Range and Earth's Coverage Radius Versus Elevation Angle for Low Orbiting Spacecraft

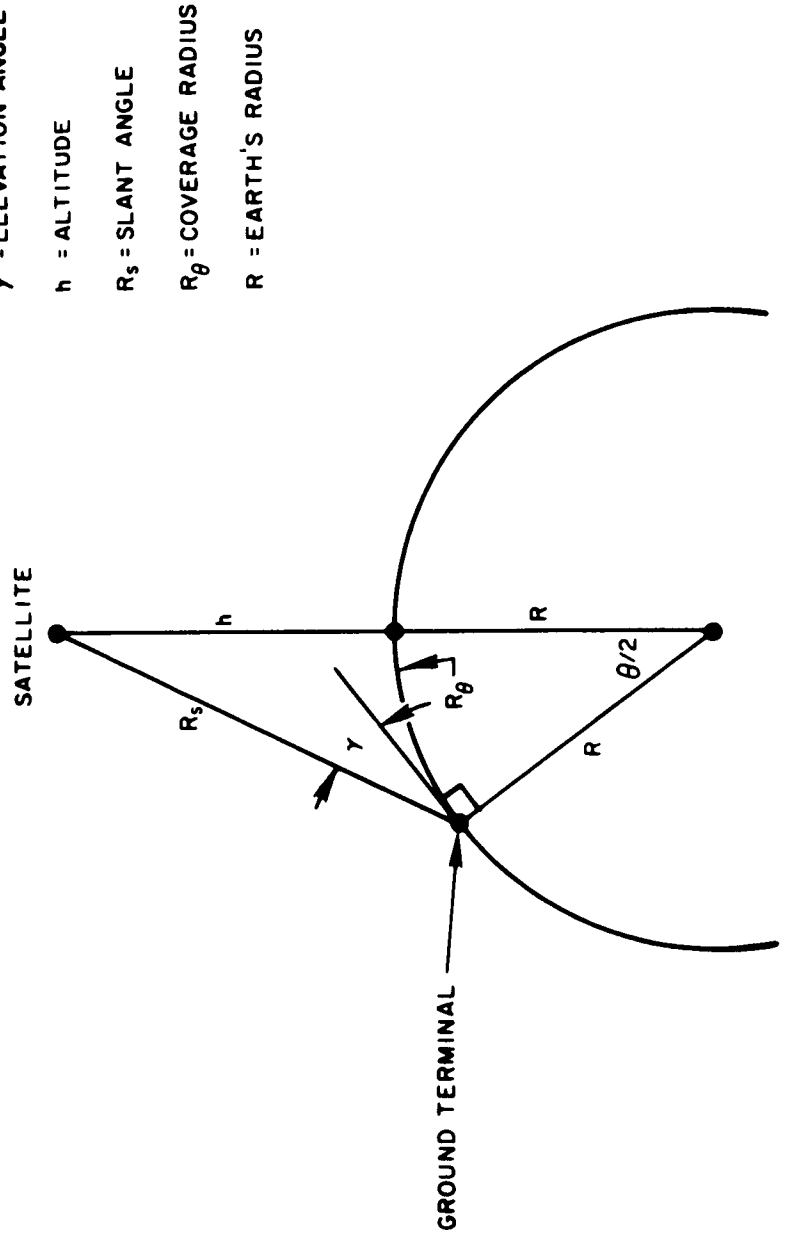

Figure 4-10. Geometry for Satellite Orbits

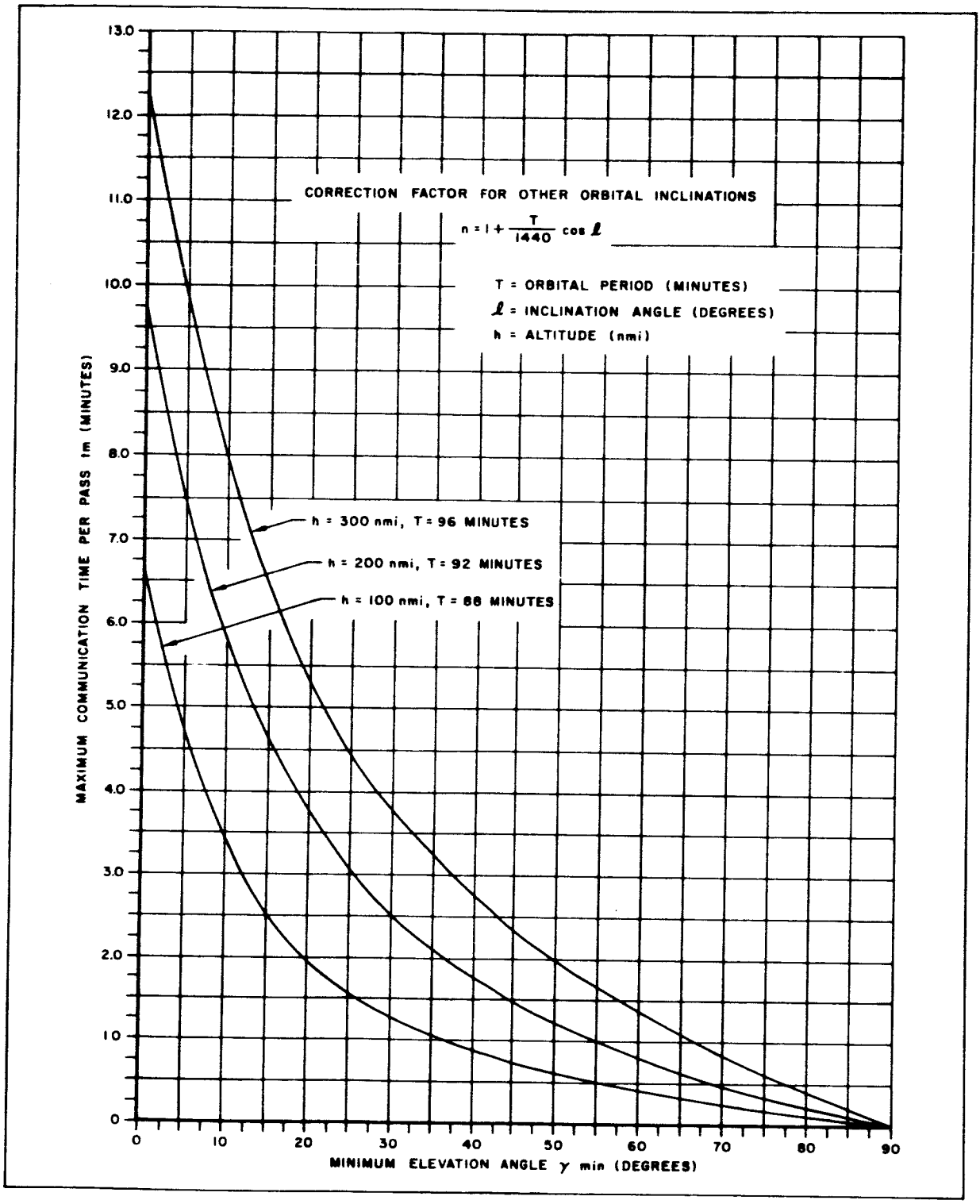

Figure 4-11 Maximum Communication Time For Low Altitude Passes (Polar Orbits)

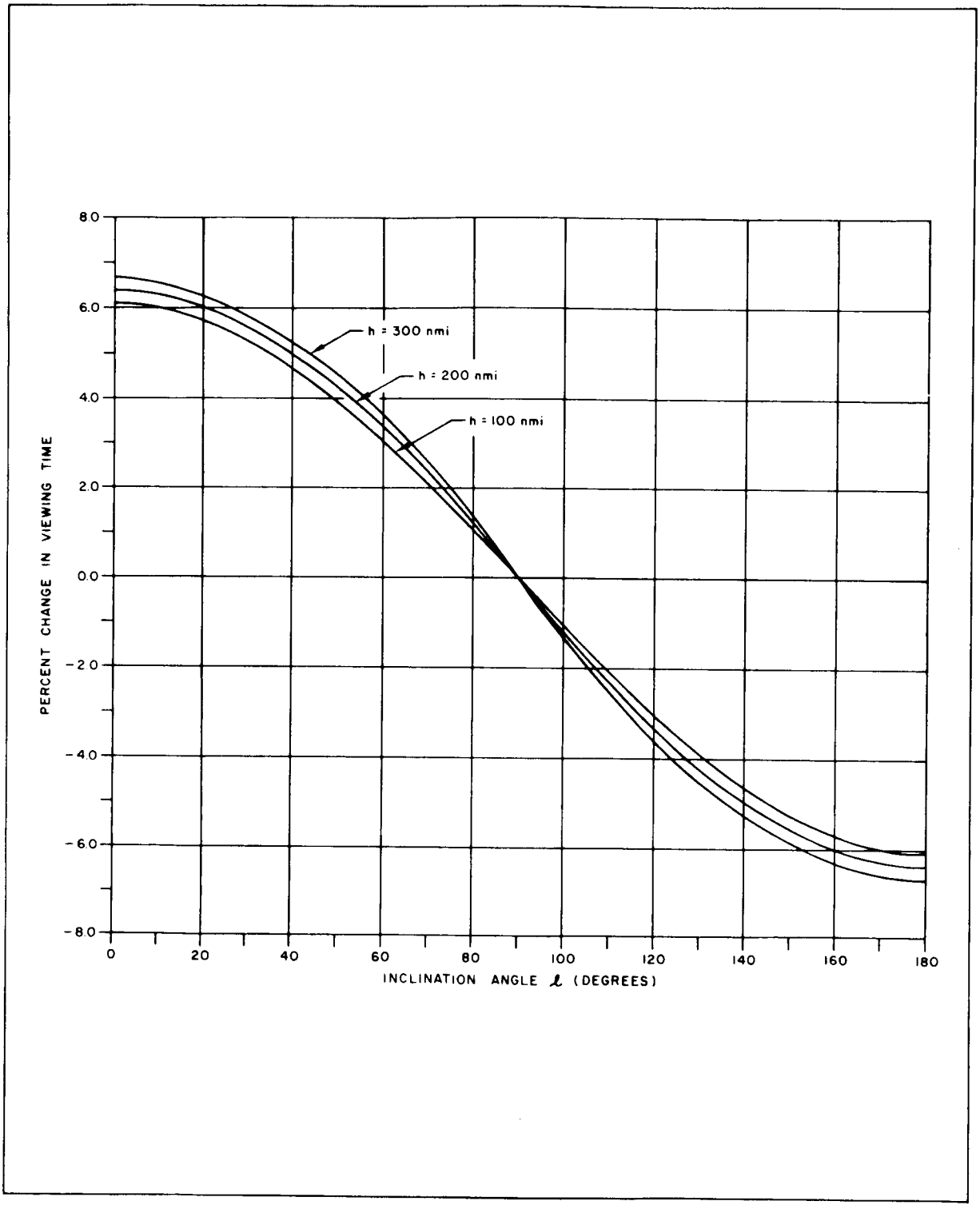

Figure 4-12 Corrections For Inclination Angle On Communication Time

The most useful curves for estimating communication time for a given orbital pass are shown in Figures 4-13 through 4-15. These curves are approximations for communications time as a function of: minimum horizon in terms of elevation angle; and minimum Earth's surface range between the ground terminal and the orbital plane which is the same parameter as Earth's coverage radius. These curves show the profound effects that the minimum operating horizon has on the usefulness of low orbiting spacecraft. Calculations for all of these curves are based on the assumption that the ground terminal latitude is somewhat less than the orbit inclination.

Finally, a three dimensional sketch is given in Figure 4-16 which shows the shape of the ground station latitude-orbital inclination function for average total communication time for a 24 hour day in a 30 to 45 day mission. Communication time is maximum at points 1 and 2 in Figure 4-16 when the ground station is on the Equator and the satellite orbit is equatorial or when the ground station is on a Pole and the satellite orbit is polar. Table 4-3 gives the average communications time in hours per day for the above two cases at satellite altitudes of 100, 200 and 300 n miles. The communications time for an equatorial station and a polar orbit is also given. Communication time is zero for values of ground station latitude.

$$L \geq \ell + (\theta/2)_{\max}$$

where:

$\theta/2$ is maximum when γ = zero degrees.

4.3.5 Effects of Atmosphere on Propagation in Oxygen Absorption Band

Using the Raytheon computer program described in Appendix II of the First Quarterly Report and the Case 6 weather model described in

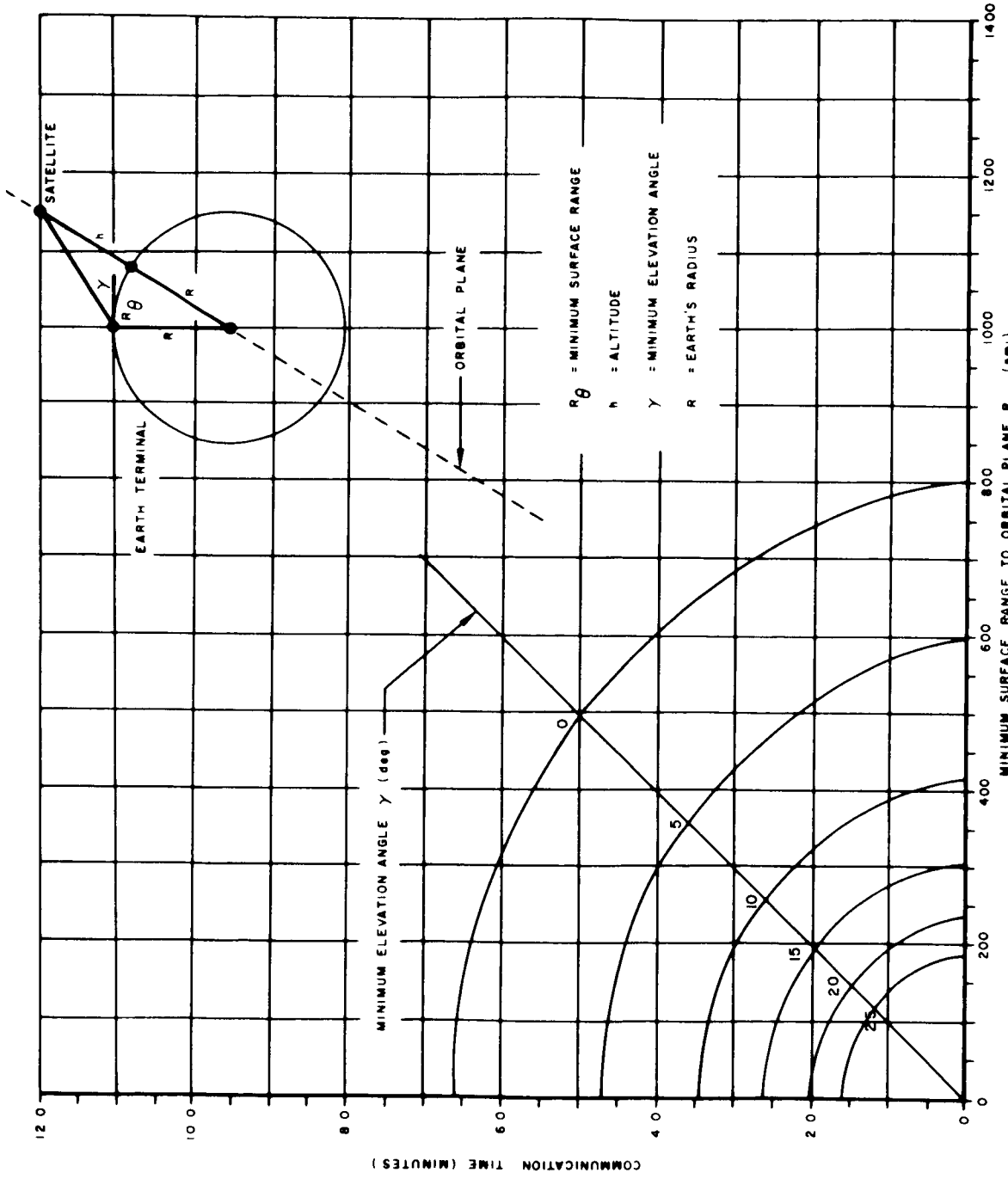

Figure 4-13. Communication Time for a 100 n. mi. Altitude Satellite Pass

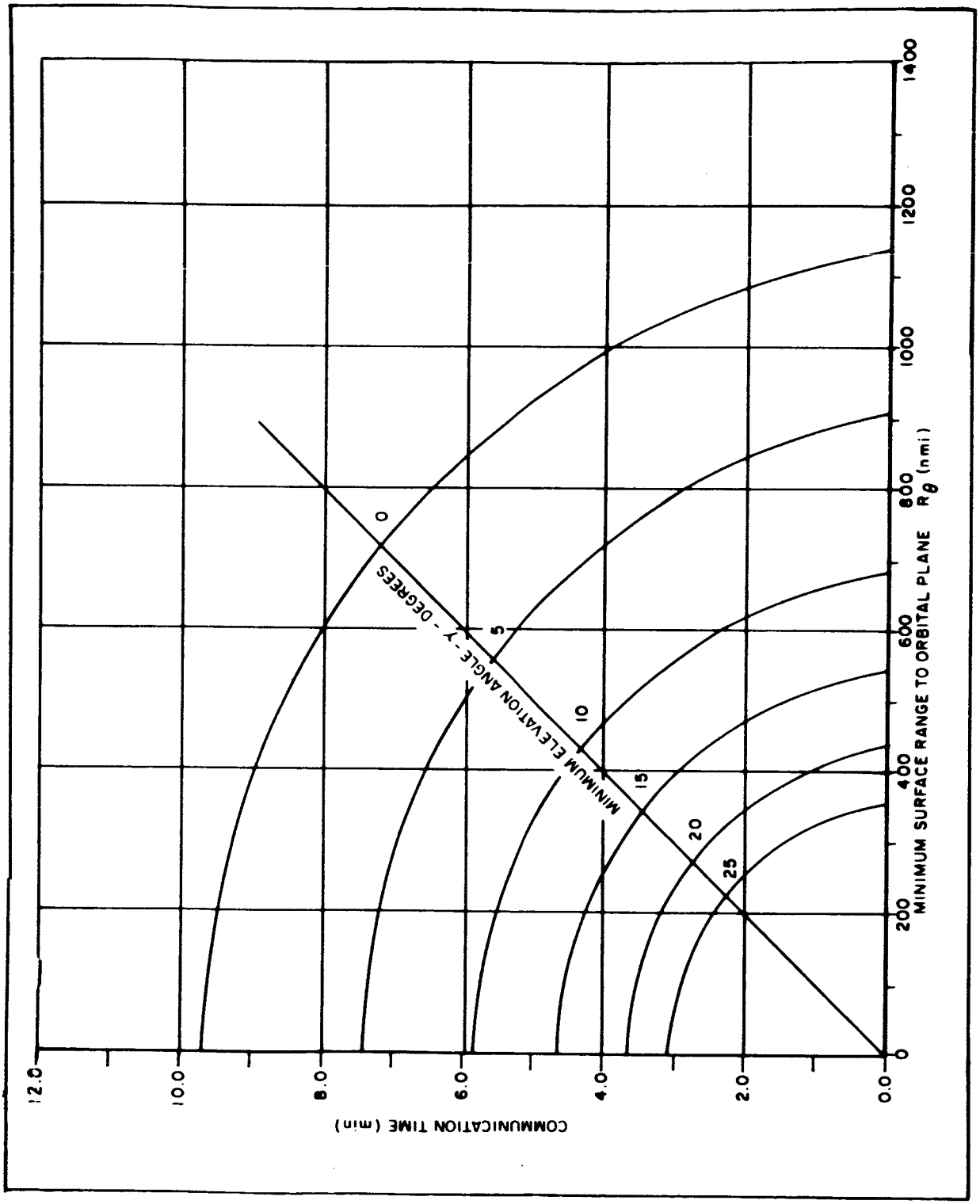

Figure 4-14. Communication Time For a 200 n mi. Altitude Satellite Pass

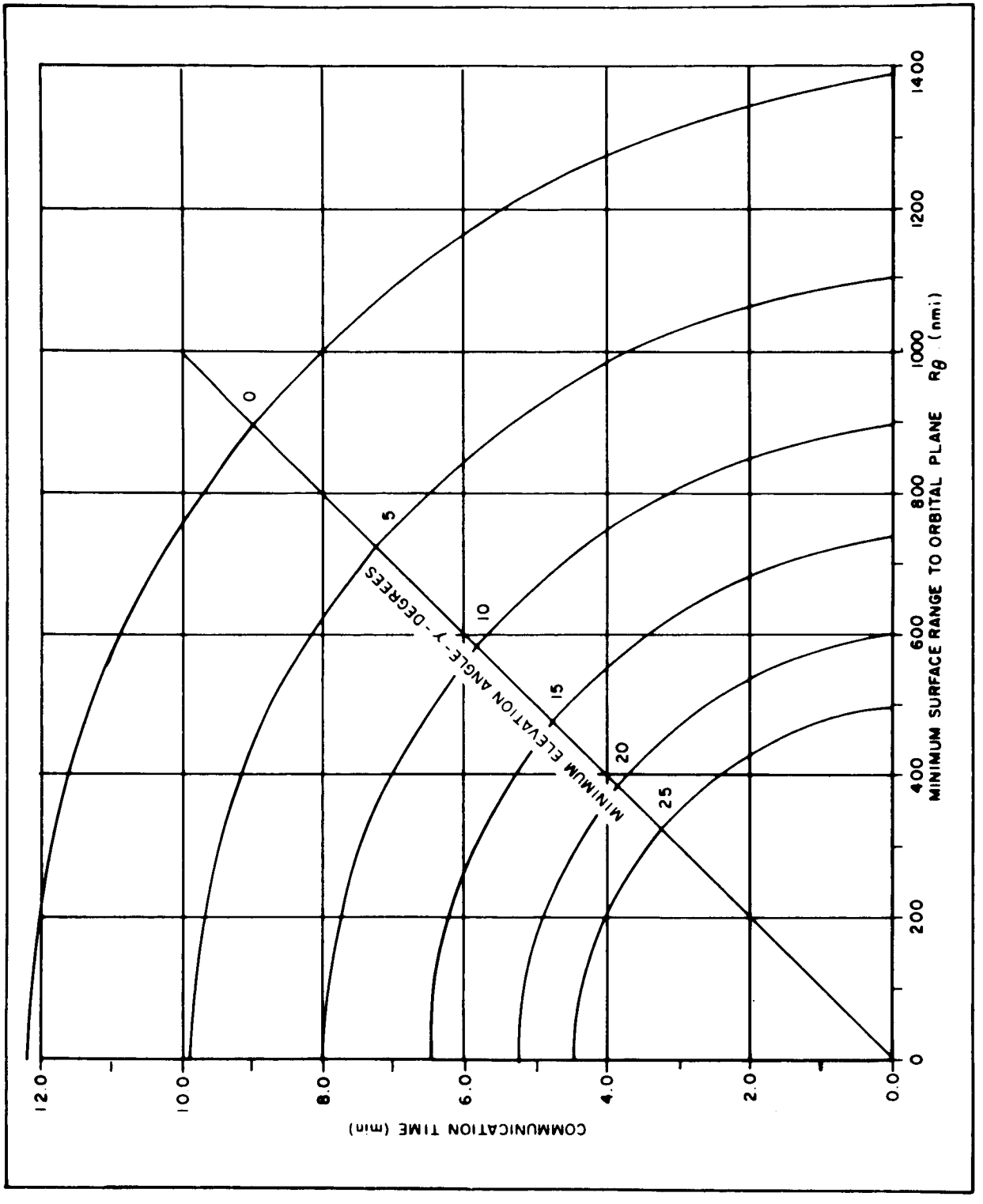

Figure 4-15. Communication Time For a 300 n mi. Altitude Satellite Pass

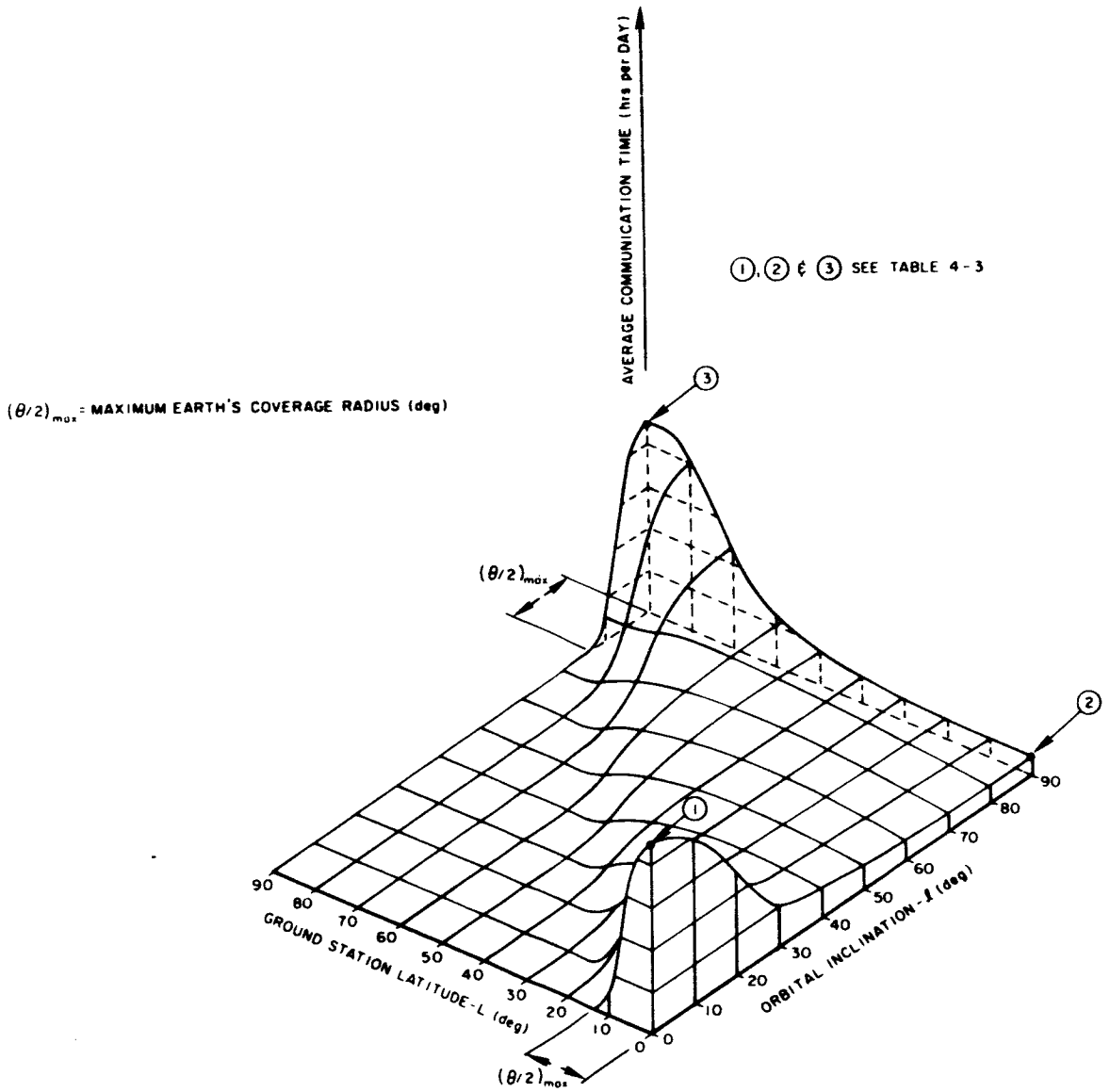

Figure 4-16. The Shape of the Ground Station Latitude/ Orbital Inclination Function.

TABLE 4-3

AVERAGE COMMUNICATION TIME FOR LOW ALTITUDE SPACECRAFT

Orbital Inclination, Station Location	Communication Time - hours		
	h = 100 n. mi. $\theta/2 = 13.5^{o}$	h = 200 n mi. $\theta/2 = 19.0^{o}$	h = 300 n mi. $\theta/2 = 23.1^{o}$
(1) 0^{o} ; equatorial	1.8	2.5	3.1
(2) 90^{o} ; equatorial	0.2	0.4	0.6
(3) 90^{o} ; polar	1.9	2.5	3.1

Section 3, also, of the First Quarterly Report, the transmission factor of the atmosphere versus zenith angle has been calculated for several frequencies assuming a ground terminal location at sea level. The resultant curves for 35, 50, 70 and 94 Gc are shown in Figures 4-17 through 4-20. Figures 4-21 through 4-24, showing apparent sky temperature versus zenith angle, were also generated from the computer program

$$\text{Atmospheric attenuation (db)} = 10 \log \frac{1}{\text{Transmission Factor}}$$

Note that the weather model used is not the "Revised Weather Model" upon which atmospheric attenuation and sky temperature curves in Section 3, First Quarterly Report, and Section 5, Second Quarterly, are based. These curves are presented here because the values for the extremities of the oxygen absorption band (50 Gc and 70Gc) were not computed for the revised model.

Satellite-to-aircraft experimental communication links are essential when considering the use of frequencies near the 60 Gc oxygen absorption band. The opacity of the atmosphere to frequencies near 60 Gc has been

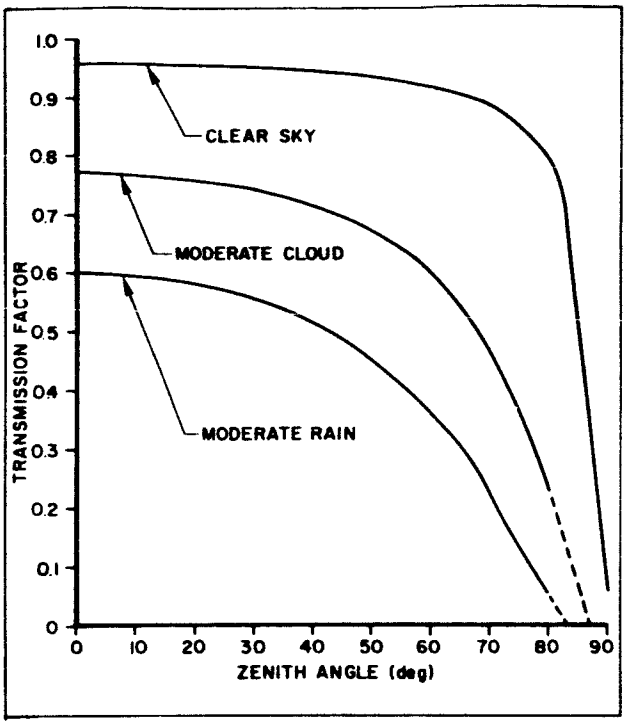

Figure 4-17 - Transmission Factor of the Atmosphere at 35 Gc

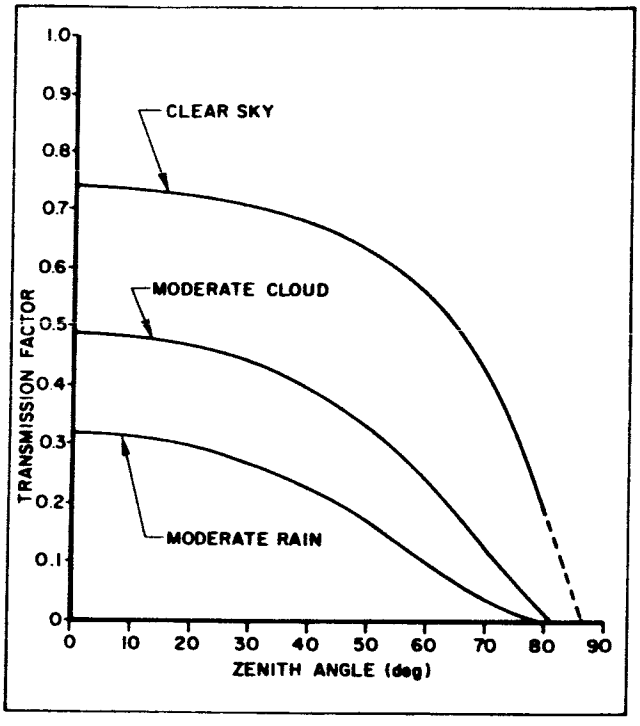

Figure 4-18 - Transmission Factor of the Atmosphere at 50 Gc

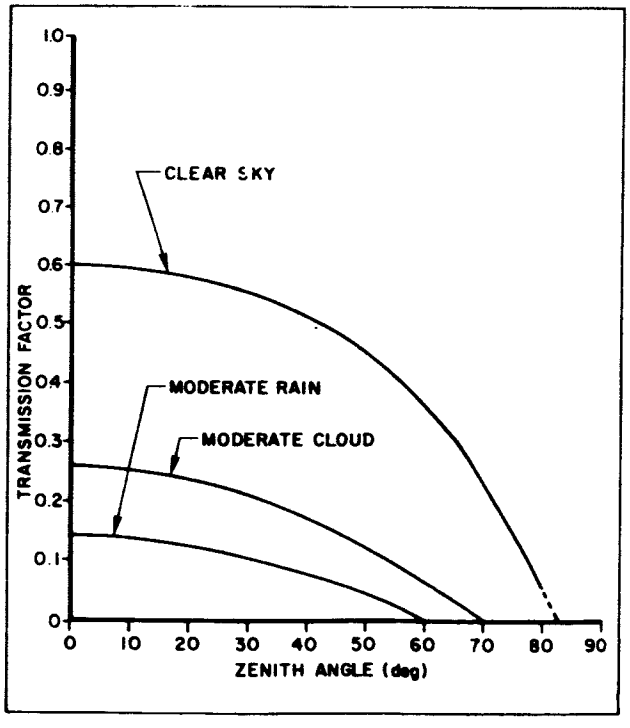

Figure 4-19 - Transmission Factor of the Atmosphere at 70 Gc

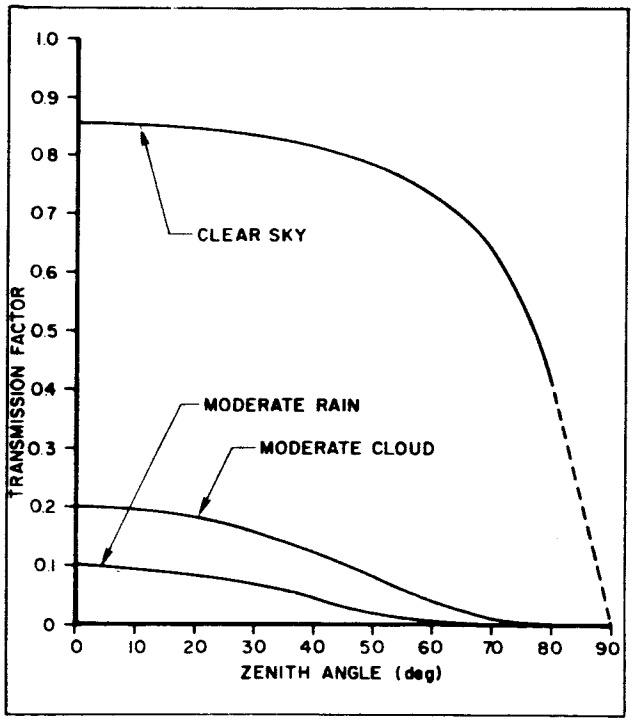

Figure 4-20-Transmission Factor of the Atmosphere at 94 Gc

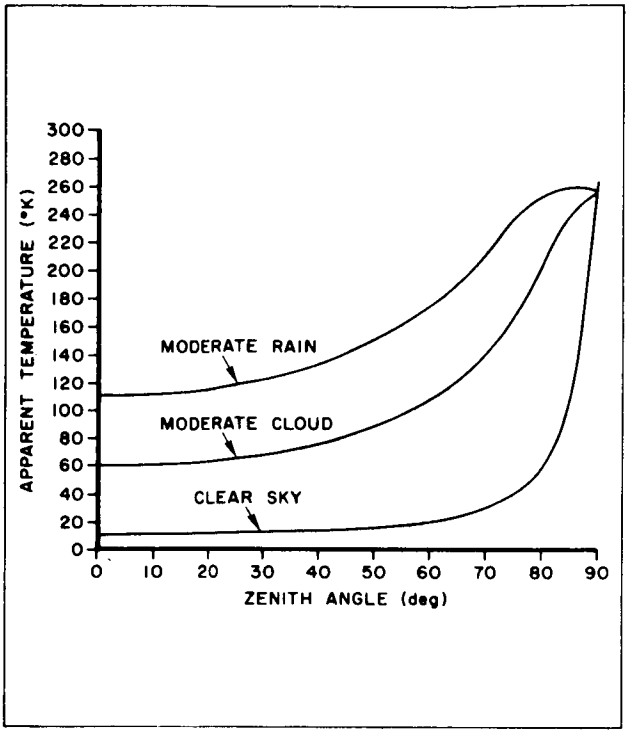

Figure 4-21 - Apparent Temperature of the Atmosphere at 35 Gc

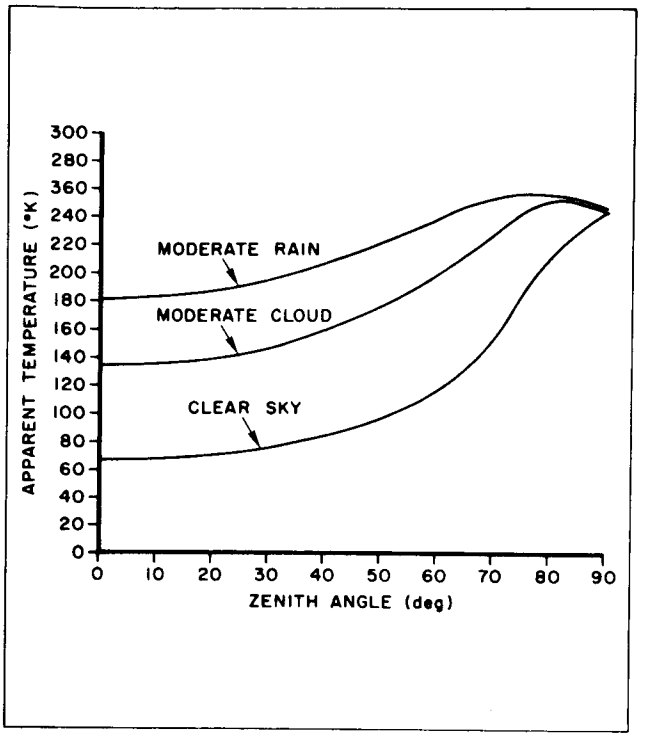

Figure 4-22 - Apparent Temperature of the Atmosphere at 50 Gc

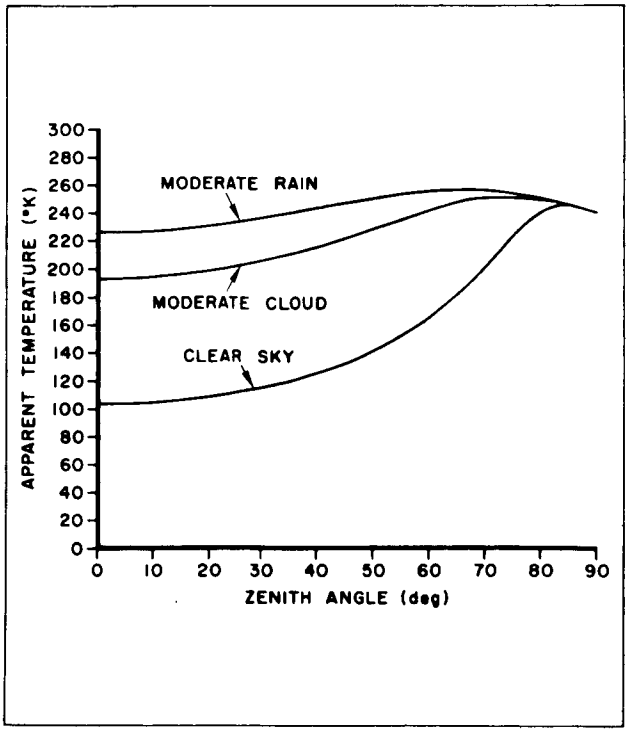

Figure 4-23 - Apparent Temperature of the Atmosphere at 70 Gc

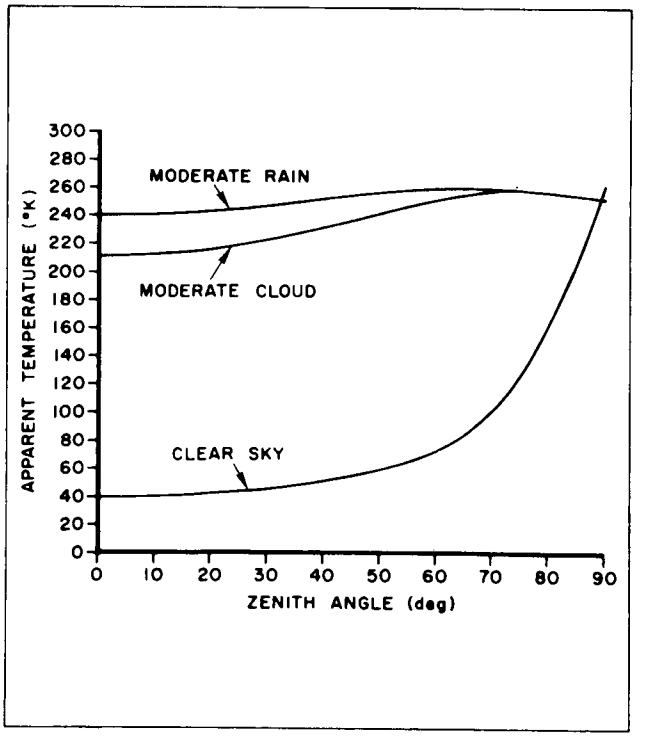

Figure 4-24 - Apparent Temperature of the Atmosphere at 94 Gc

pretty well predicted. Meeks and Lilley[25] give detailed estimates of the limitations that oxygen places on millimeter-wave propagation. Straiton and Tolbert[41] have also investigated this band using a 500-foot absorption cell at the University of Texas. What is not completely predictable is the bandwidth that the propagation medium will support and the minimum useful horizon as a function of altitude. Experimental verification with satellite-aircraft communication links using special signal waveforms are required. Opacity per unit bandwidth can vary from 2 db per megacycle near a resonant frequency such as 60.44 Gc, to 0 db per megacycle near the adjacent window at 60.8 Gc. This can have drastic effects on the phase and amplitude characteristics of the broadband communication channel.

In designing space-air experimental links operating in the 60 Gc oxygen absorption band, the required system analysis will be a bit different. From Meeks and Lilley vertical and horizontal attenuation, due to oxygen is shown in Figures 4-25 and 4-26. Zenith opacity versus altitude, and opacity versus zenith angle, have been derived for 60.8 Gc and is shown in Figures 4-27 and 4-28.

With a Computer Program, such as the one described in Appendix II of the First Quarterly, it can be used to provide parametric data describing the opacity of the absorption band as a function of frequency, altitude and zenith angle. From this, data change in opacity per unit bandwidth over the frequency band can be determined, to permit proper choice of experiment frequencies.

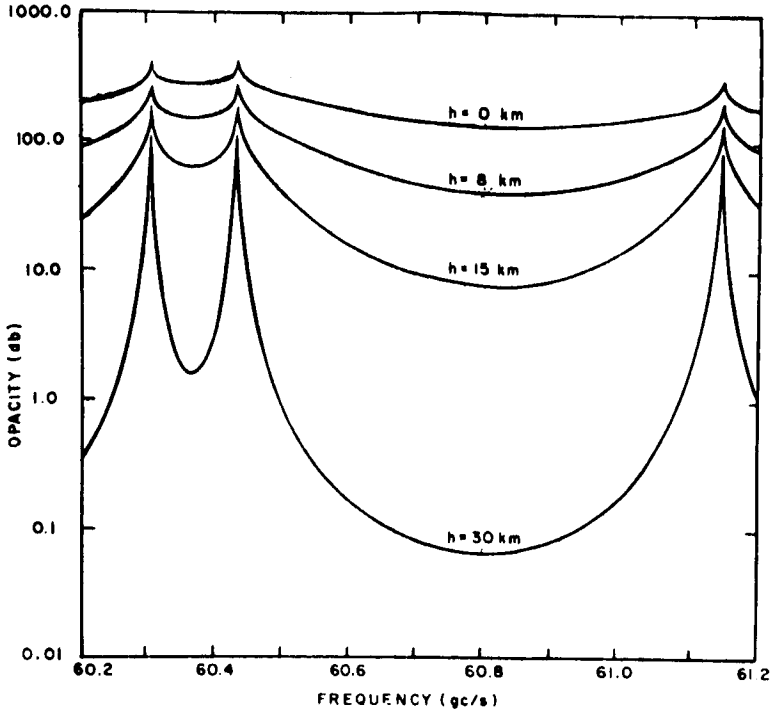

Figure 4-25. Verical Opacity Due to Oxygen

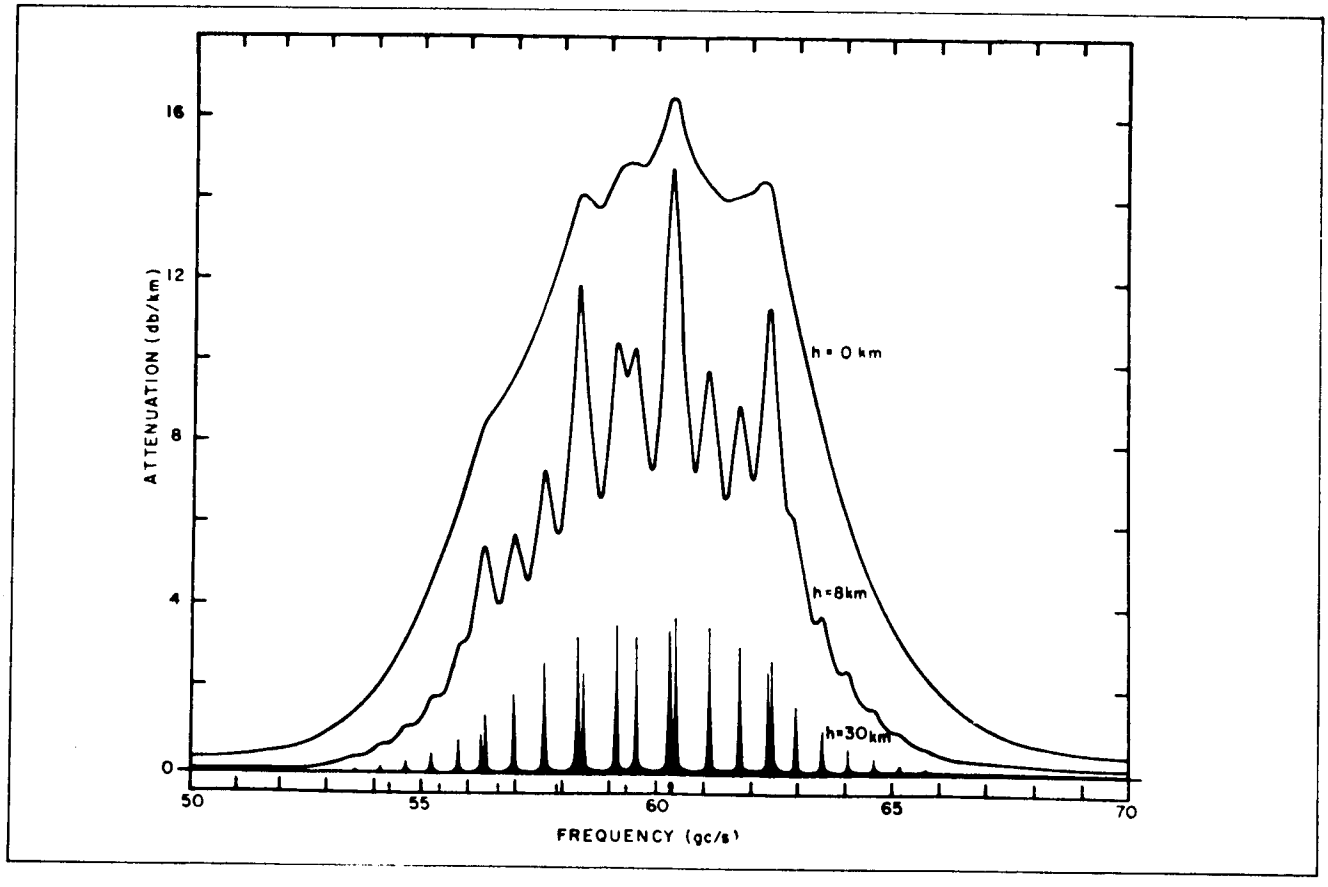

Figure 4-26. Horizontal Attenuation Due to Oxygen

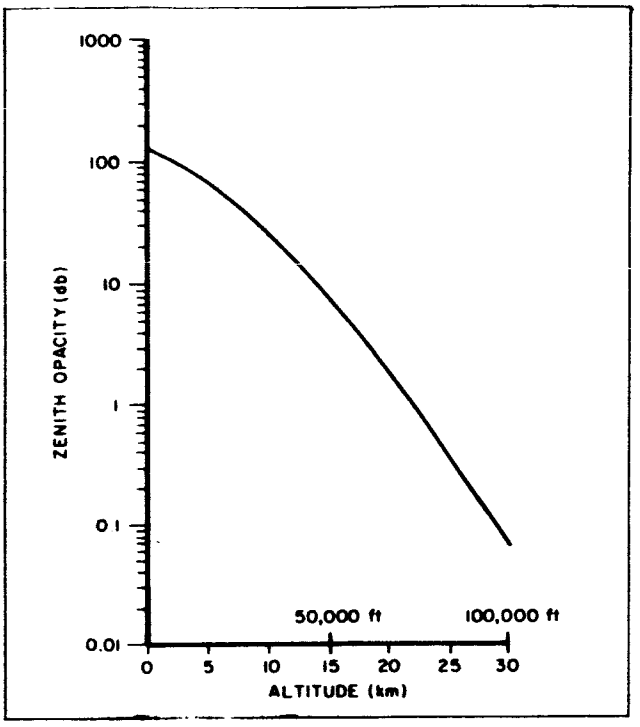

Figure 4-27.- Zenith Opacity of the Atmosphere Due to Oxygen Absorption at 60.8 Gc

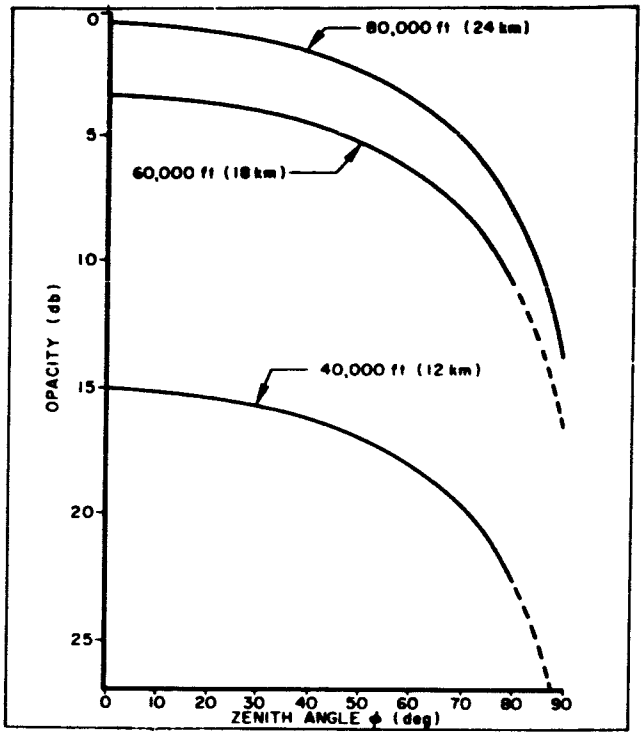

Figure 4-28.- Opacity vs Zenith Angle Due to Oxygen Absorption at 60.8 Gc

4.3.6 Signal Analysis for 60.8 Gc Experimental Links

In this section typical 60.8 Gc experimental links using synchronous stationary satellites and 200 nautical mile satellites are discussed. Because of free space attenuation, there is a penalty in signal-to-noise density when using synchronous satellites instead of those at low altitudes. However, the advantage of stationary satellites in the initial experiments is more important.

Tables 4-4 and 4-5 indicate the capacity of space-air down links which can realistically be achieved within the NASA Apollo Applications Program time schedules. Table 4-4 gives signal-to-noise densities referenced to 90 degrees elevation and zero propagation loss. Table 4-5 gives signal margin estimates for various practical configurations. The propagation losses were taken from Figure 4-28 in Section 4.3.5. Relative free space attenuation for 200 n mile satellites is given in Figure 4-29 and

TABLE 4-4

SIGNAL ANALYSIS FOR 60.8 Gc SPACE TO AIR LINKS WITH SYNCHRONOUS AND 200 n mi. ALTITUDE SATELLITES

	Synchronous	200 n. mile
Free Space Attenuation ($\lambda \simeq 5$ mm, $\gamma = 90^{\circ}$) - db	219.4	179.6
Propagation Loss (zero loss as reference) -db	0.0	0.0
Satellite Antenna Gain (24" for 0.6° beam) - db	48.7	48.7
Aircraft Antenna Gain (30" for 0.5° beam) - db	50.7	50.7
Noise Density ($T_o = 30,000^{\circ}$K, NF = 20 db, $T_A = 0^{\circ}$) - dbw/cps	-184.0	-184.0
Transmitter Power (10 w) - dbw	10.0	10.0
Polarization Loss - db	0.3	3.0
Received Signal Power (unmodulated carrier) - dbw	-110.3	- 73.2
Signal-to-Noise Density (unmodulated carrier) - db/cps	73.7	100.8
(modulated carrier) - db/cps	71.9	98.0
(each sideband) - db/cps	65.9	92.0

TABLE 4-5

SIGNAL MARGINS FOR TYPICAL SPACE TO AIR EXPERIMENTAL LINKS AT 60.8 Gc

	Aircraft Altitude = 80,000' $\gamma = 5^{\circ}$		Aircraft Altitude = 40,000' $\gamma = 10^{\circ}$	
	Synchronous	h = 200 n. mi.	Synchronous	h = 200 n. mi.
Reference Signal-to-Noise Density, $\gamma = 90^{\circ}$ - db/cps (Unmodulated Carrier)	73.7	100.8	73.7	100.8
Relative Free Space Attenuation - db	- 1.2	- 13.3	- 1.1	- 11.4
Propagation Loss (Opacity) - db	11.0	11.0	26.6	26.6
Actual Signal-to-Noise Density - db/cps	61.5	76.5	46.0	62.8
Minimum Signal-to-Noise Density - db/cps (Phase lock receiver unlock)	27.0	27.0	27.0	27.0
Signal Margin-db (Unmodulated Carrier)	34.5	49.5	19.0	35.8

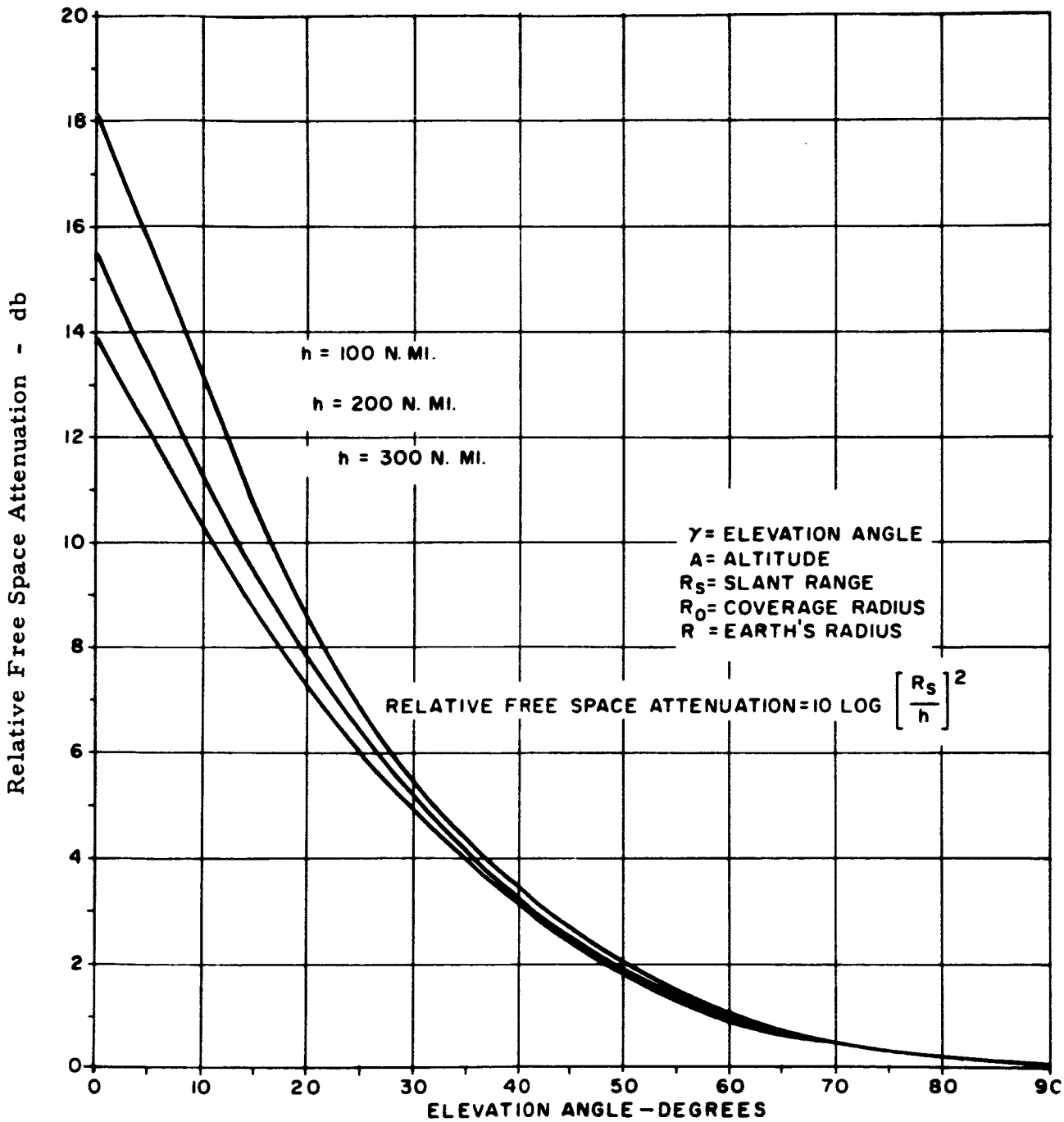

Figure 4-29 Relative Free Space Attenuation for 200 n mi. Satellite

relative free space attenuation for synchronous satellites was taken from Figure 5-7, Second Quarterly Report. The minimum allowable signal-to-noise density, that is, the signal-to-noise density level at which a phase-lock receiver unlocks, was discussed in Section 5.3.7 of the Second Quarterly.

For amplitude modulated test waveforms the modulated carrier signal margin would be 1.8 db less than those shown in Table 4-5. The signal-to-noise density levels for each of two sidebands would be 7.8 db less than those shown in Table 4-5. The AM modulated carrier could be scanned across a segment of the oxygen absorption band to determine attenuation and coherence bandwidth as a function of frequency. As the scan rate increases the minimum allowable signal-to-noise density increases (see Section 6.2). There is a serious problem with frequency scan using low altitude spacecraft. The short communications time per pass and the high rate of change of elevation, force the scan rate to be very high thus requiring high signal-to-noise densities for holding receiver phase lock. The scanning signal has to be phased-tracked by the receiver local oscillator in order that relative phase measurements among the spectral components can be made.

4.3.7 Mission Profiles

A primary result of the experiment design study using manned orbiting spacecraft should be to define one or more typical 45-day mission profiles which can be considered. The profiles should describe the specifics of each millimeter experiment, the data to be obtained, the anticipated results, the application of the data, and the manner in which each experiment relates to other experiments and to the capabilities of unmanned satellites.

The program estimates performed should reference these candidate profiles in terms of costs. Each mission profile should be a schedule of events in the manned spacecraft mission which are pertinent to the

millimeter communication experiments. Careful and thorough planning and scheduling of mission profiles would insure most efficient use of valuable experiment time. Results of these profiles would allow reasonably accurate costing of the complete communication experiment.

The mission profiles may vary with the spacecraft launching date because of the influence of the prevailing weather at the ground station at that time of the year. For each mission, predetermined alternatives should include orbital coverage from ground sites and aircraft flight paths for each pass of the 45-day mission. Daily countdown procedures for calibration and check-out of each ground site and each aircraft should be defined and scheduled. Each aircraft flight plan, which may encompass experiment data collection on three or more consecutive orbital passes, should be defined in terms type of aircraft, landing points, direction, altitude and speed, all related in time to the spacecraft orbit. All flights required for ground site and aircraft calibration and checkout, plus any flights required for aircraft-ground propagation data collection should be included.

A very important section of the mission profile would be the specification of the spacecraft crew's participation during the 45-day mission. Their duties may include calibration and maintenance checks, aid to acquisition, millimeter antenna steering and observation of signal displays. The duties of the personnel required to operate and maintain the ground and airborne experimental equipment should also be specified.

4.3.8 Work Statement for Extension of Experiment Design Study

This work statement is recommended as an extension of the current millimeter-wave communication/propagation program to include design of more extensive experiments with manned and unmanned spacecraft which have larger payload capacities than those specified in the present study.

The experiment design already accomplished shall be modified to include:

a. Communication experiments as well as propagation experiments.
b. Definition of channel characteristics in the water vapor and oxygen absorption bands.
c. Implementation of more sophisticated waveforms for direct measurement of certain channel characteristics.
d. Variable separation receiving apertures to measure angular extent of atmospheric inhomogeneities.
e. Determination of limits of refraction on the pointing of high gain spacecraft and ground antennas.
f. Spacecraft radiometers for survey of background temperature of the earth and its atmosphere.
g. Utilization of man in the spacecraft.
h. The use of spacecraft in low altitude earth-orbits.
i. Utilization of spacecraft-aircraft experiment links.
j. Data processing, evaluation and storage aboard the spacecraft.

Task 1. Define Study Objectives

Prepare a supplement to " Program Definition Plan for Millimeter Communication Propagation Program," Raytheon Report No. FR-4-498B, 29 January 1965, which describes the additional tasks to be performed, describes their relationships with the tasks already accomplished, and provides the schedule of tasks and sub-tasks.

Task 2. Define Basic Measurements

The results of the present study shall be modified to include definition of channel characteristics in the water vapor (18 to 22 Gc) and

oxygen absorption (50 to 70 Gc) bands, in addition to the windows at 16, 35 and 94 Gc which have already been considered. In addition to a simple carrier modulated by sinusoidal signals (5 Kc, 5 Mc, 50 Mc), waveforms shall be evaluated such as: multiple carrier (0.3 to 1.0 Gc spacing) for examination of channel coherent bandwidth in all bands; pulse amplitude modulation which yields indication of communication system performance for the PAM, PWM, PPM, PAM/AM, PWM/AM and PPM/AM family of modulation systems; and pulse amplitude modulation/frequency modulation which yields indication of communication system performance for the PAM/FM, PWM/FM, PCM/FM, PPM/FM and FM/FM family of modulation systems. In other words, communication experiments as well as propagation experiments shall be defined.

The present study results associated with variable separation, variable beamwidth receiving apertures shall be modified to include more sophisticated measurement of angular extent of atmospheric inhomogeneities, by measuring amplitude and phase correlation among the received signals. This experimental setup shall also be used to determine the limits of refraction on pointing high gain spacecraft and ground antennas. In those experiments which use spacecraft millimeter-wave receivers, consideration shall be given to multiple purpose utilization such as radiometer functions to survey the background temperature of the earth and its atmosphere and to observe other bodies in the solar system.

The descriptive bibliography being prepared under the present study shall be updated at the end of this study extension.

Task 3. Evaluation and Selection of Experiments

Using the approach developed in the present study, experiments shall be formulated which will make the basic measurements prescribed in

Task 2. The candidate satellite evaluation shall be expanded to include low earth-orbiting (100-300 n mile altitude, 28.5-90 degree inclination) spacecraft as well as medium altitude (6000 n miles) and synchronous altitude spacecraft. Curves shall be generated showing viewing time as a function of spacecraft altitude, inclination, horizon limitations and mission time for space-air and space-earth links. A detailed signal level analysis for each candidate satellite shall be performed showing signal attenuation and fading margin estimates as a function of elevation angle, weather model, modulation scheme, etc.

New measurement waveforms which were introduced in Task 2 of the study extension plus those measurement waveforms already evaluated in the present study, but were rejected on the basis of payload limitations, shall be considered for implementation in the new experiment design. A signal flow analysis shall be provided which traces the frequency components of the test waveform through the entire experimental links. The experiments shall be designed for various payload capacities up to 200 pounds, 3 cubic feet, 300 watts prime power and 2 foot apertures.

The use of man shall be clearly defined by comparing the manned experiment with the comparable unmanned experiment in terms of specific experimental results, operational and equipment reliability, savings in weight and prime power, etc.

Spacecraft integration and operational problems shall be defined including those associated with the conduct of multiple experiments with the same equipment, concurrent experiments which compete for operator attention, and experiments by a non-specialist member of the crew.

Typical mission profiles based on the experiments selected shall be developed to specify key test procedures and measurement techniques. The mission profiles shall include orbital coverage from ground sites and aircraft, aircraft flight plans, ground and airborne operational procedures, astronauts' duties, and available data collection time.

Task 4. Ground and Airborne Facilities Evaluation

The evaluation of the ground facilities considered in the present study (Aerospace, University of Texas, AFCRL, Lincoln and GSFC) shall be updated and expanded during the course of the study extension. Additional facilities such as those located at University of Ohio; NAA, Columbus, Ohio; DRTE, Ottawa, Canada; NOL, Corona, California, shall be included. Important geographic locations such as Hawaii and Ascension at which millimeter facilities presently do not exist shall be considered in the overall ground facilities evaluation. Various types of aircraft shall be evaluated in terms of performance as an airborne terminal for the space-air experiments.

Task 5. Equipment Design

The equipment design already accomplished in the present study shall be used as a base from which to show the hardware implementation of the new experiments selected in Task 3. The equipment design for the new experiments shall be carried out to the level specified in "Program Definition Plan for Millimeter Communication Propagation Program" for Task 5 of the present study. Since the selected experiments will, of necessity, require component development time and costs.

Task 6. Data Processing and Evaluation

The data processing and evaluation requirements already specified in the present study will be applied to the new experiments. Additional methods of data processing required by the new measurement waveforms shall be added.

Section 5
EQUIPMENT DESIGN

This section completes the equipment design phase of the study. Most of the results of this task were given in the first and second quarterly reports.

5.1 Multiple Frequency Receiver Configuration for Small Payloads

As previously mentioned in Section 4.1, the First and Second Quarterly Reports recommend propagation experiments in which the down-link would be utilized at 35 Gc and 16 Gc. A down-link could not be recommended for a 94 Gc experiment because of the risk in attempting to develop a space-worthy transmitter within a two year time period. This particular experiment configuration has been studied to the extent that anticipated carrier signal-to-noise density ratios have been calculated for the available sites assuming certain synchronous satellite positions. These carrier signal-to-noise density ratios, which were listed in Table 5-1 of the Second Quarterly Report and are again listed here in Table 5-1, range from 27 db to 49 db when amplitude modulation is used.

5.1.1 Improvement in Signal-to-Noise Margins

The modulated carrier signal-to-noise density ration is a prime concern since it is this energy that is translated and phase-locked to the stable reference frequency in the phase-locked receiver. The ability of the phase-locked receiver to hold lock is defined in Section 5.3, Second Quarterly Report as the modulated carrier signal-to-noise density ratio at which the receiver unlocks. This signal-to-noise density ratio at unlock is a function of both the post-detection noise bandwidth and the combined frequency drift of the received signal and the first local oscillator frequency. If the assumption is made that the maximum frequency drift due to the combined frequency stabilities of the receiver carrier and local oscillator is 1 part per 10^9 per

TABLE 5-1
RECEIVER SIGNAL-TO-NOISE DENSITY IN db FOR MODULATED AND UNMODULATED CARRIES IN SYNCHRONOUS SATELLITE EXPERIMENT LINKS

Frequency (Gc)	Station	Satellite Position (2)			
		PA-45	SA-30	PP-145	SP-165
35	Aerospace (10)	5/33/27(3)		41/39/33	31/38/32
35	WSMR (10)	15/38/32			22/39/33
35	U. of Texas (16)	24/43/37	10/41/35	29/44/38	10/41/35
35	Rosman (10)			15/38/32	
35	GSFC (15)	33/42/36	23/41/35	7/38/32	
35	AFCRL (29)	35/47/41	26/46/40		
35	Lincoln (28)	35/48/42	26/47/41		
35	Haystack (120)	35/51/45	26/50/44		
16	Aerospace (10)	5/39/33		41/43/37	31/42/36
16	WSMR (10)	15/43/37			22/43/37
16	U. of Texas (16)	24/47/41	10/46/40	29/48/42	10/45/39
16	Rosman (10)			15/43/37	
16	GSFC (15)	33/46/40	23/45/39	7/44/38	
16	AFCRL (29)	35/51/45	26/50/44		
16	Lincoln (28)	35/52/46	26/51/45		
16	Haystack (120)	35/55/49	26/54/48		
94	Aerospace (15)	5/21/19		41/42/40	31/40/38
94	GSFC (15)	33/44/42	23/41/39	7/35/33	

Code:
(1) Number in parenthesis represents antenna diameter.
(2) PA-45 Primary Atlantic Position = 45° W Lg.
SA-30 Secondary Atlantic Position = 30° W Lg.
PP-145 Primary Pacific Position = 145° W Lg.
SP-165 Secondary Pacific Position = 165° W Lg.
(3) Ground Terminal Elevation Angle/Unmodulated Carrier S/N_c(db)/ Modulated Carrier S/N_c (db)

0.1 second, then curve No. 2 of Figure 5-1 defines a modulated carrier signal-to-noise density of 27 db as the point of receiver phase unlock. As seen in Table 5-1, the margin or difference between the anticipated modulated carrier signal-to-noise density ratio and the 27 db ratio at receiver phase-unlock ranges from 0 db to 22 db.

The ability to determine amplitude variations due to the transmission medium is also a function of a signal to noise density ratio. The output of the amplitude processor is a function of the sideband signal to noise density ratio, and with present circuit parameters, a sideband signal to noise density ratio of 45 db results in an output signal to peak noise ratio of the amplitude processor of 20 db.

It is evident from the above, that every attempt must be made to increase signal to noise density ratios in the signal receivers. An increase in signal to noise density ratio may be attained through alteration of system parameters in the present configurations or through changes in experiment configurations.

One possible alternate experiment would consist of only an up-link with all three receivers located in the satellite. This approach would increase all signal to noise density ratios at 35 Gc in Table 5-1 by 24 db due to the fact that a Litton 50 watt klystron may be utilized in a ground station. The 16 Gc propagation experiment with this approach would experience a 27 db increase in signal to noise density ratio because a good 100 watt tube is available. The signal-to-noise densities in Table 5-1, are based on steerable satellite antennas which cover the United States from synchronous altitude. To simplify the payload a fixed horn which looks at the whole Earth could replace the steerable horn at an expense of 9 db in signal-to-noise density margin.

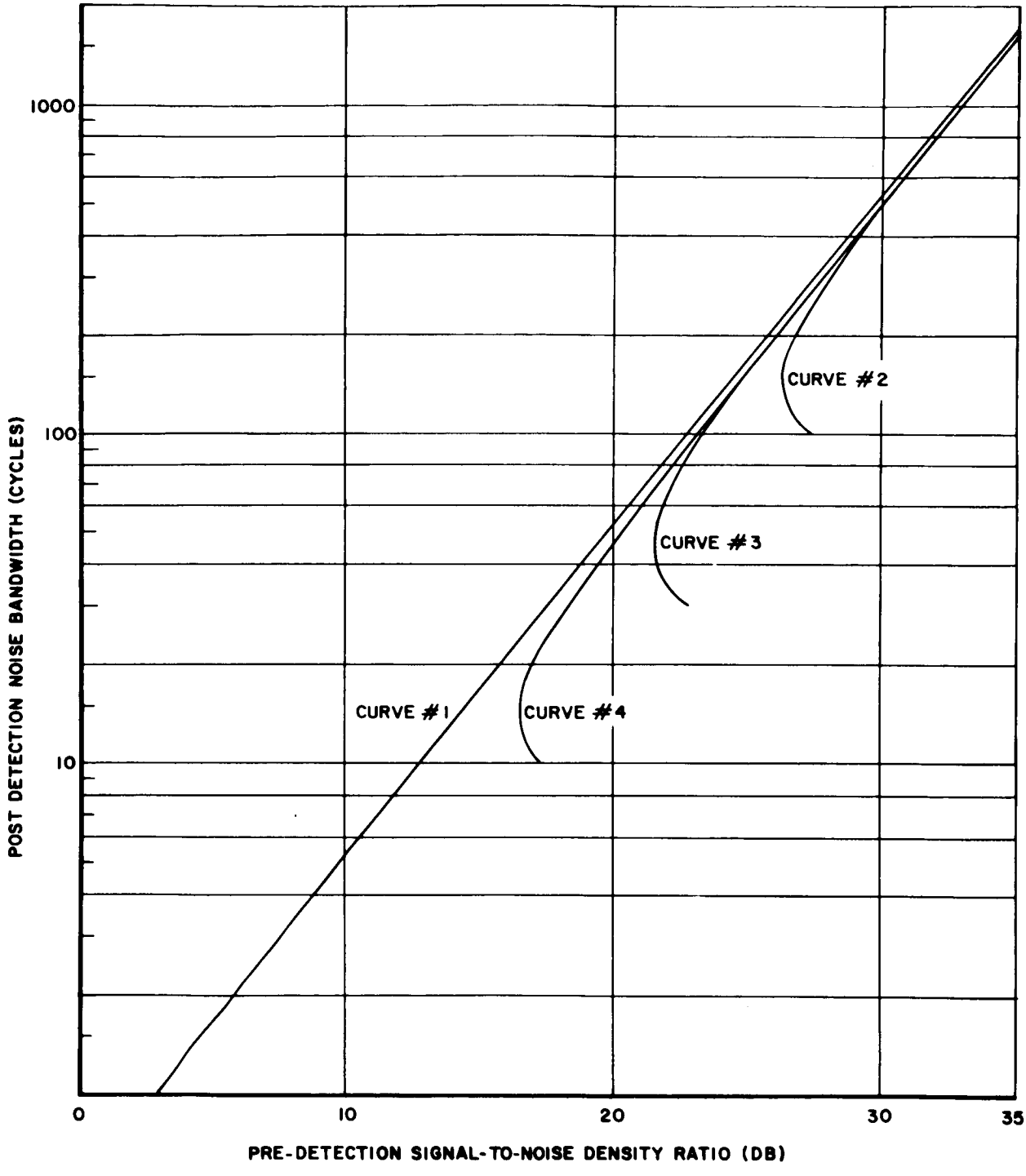

Figure 5-1. Post Detection Noise Bandwidth vs Signal-to-Noise Density when Carrier Phase-Lock Loop Unlocks

5.1.2 Satellite Receiver Design

A block diagram of the system in the satellite, capable of receiving any one of the three propagation frequencies is shown as Figure 5-2. This system consists of three separate mixers connected to a common receiver I-F amplifier. This satellite package will require 33 watts of prime power if the 66 mcs reference is available at a 40 milliwatt drive level. If this reference is not available, a crystal controlled oscillator must be added to the satellite receiver, thus increasing the total prime power required to 48 watts. Table 5-2 lists the prime power required for one, two and three channel receivers with and without an oven controlled crystal frequency standard.

TABLE 5-2

PRIME POWER REQUIREMENTS FOR SPACECRAFT RECEIVERS

Channel Frequency (Gc)	Prime Power (watts)	
	With Xtal. Std.	Without Xtal. Std.
16	22	8
16 and 35	44	29
16, 35 and 94	48	33

Another approach considered was a crystal video receiver shown as Figure 5-3 which has a very high reliability factor, but an unacceptable degradation in post detection signal to noise ratio, thus no further evaluation is being considered at this time.

It must be kept in mind that many questions remain unanswered and some will only be solved through breadboard evaluation. Some of the questions to be answered are listed as follows:

1. Is a drift of 1 part per 10^9 per 0.1 second with a crystal oscillator physically realizable?
2. Does the pound type of discriminator exhibit better short term frequency stability than a multiplied frequency standard?
3. What is the present state of the art noise figure for a 94 Gc harmonic mixer?

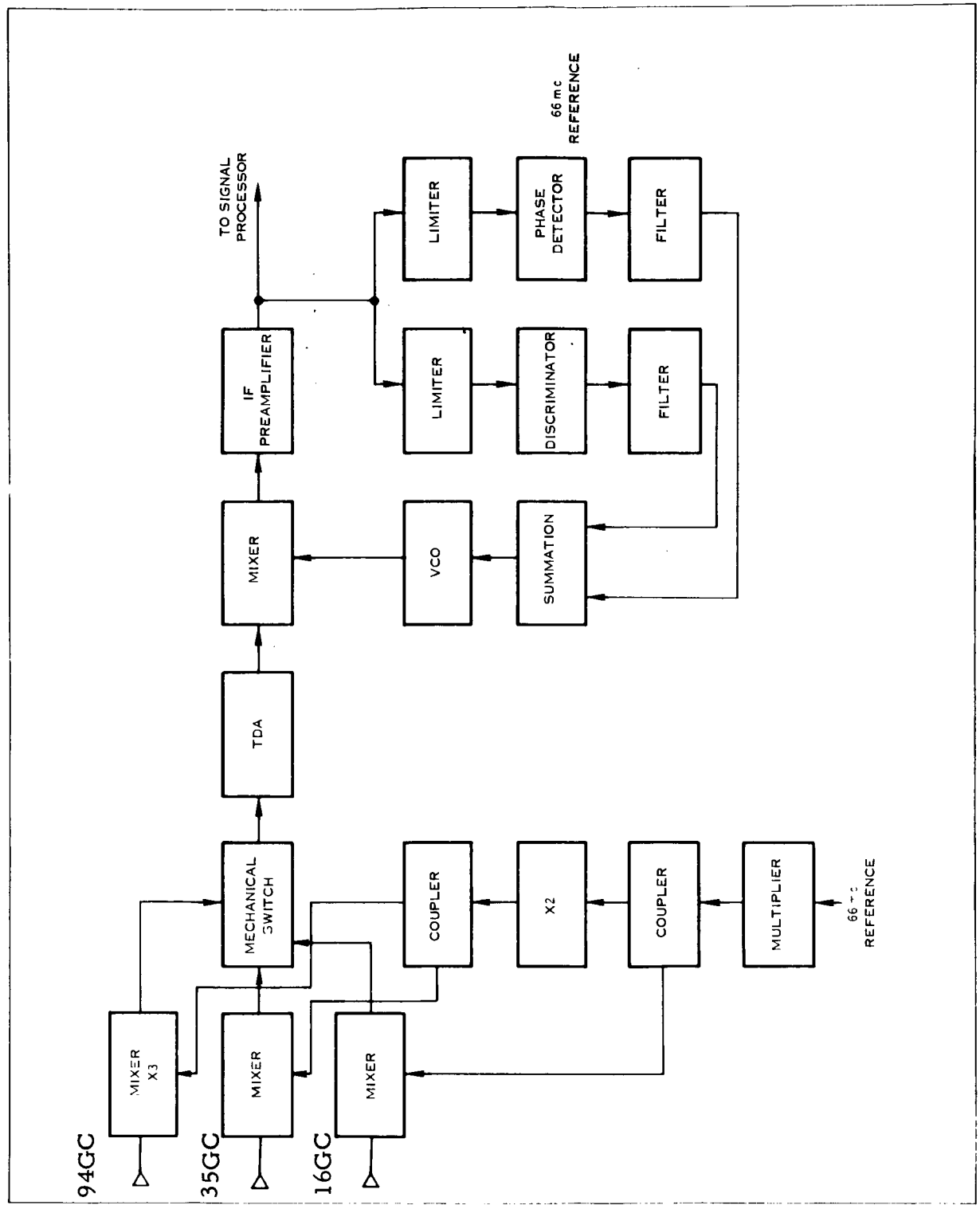

Figure 5-2. Multi-Frequency Satellite Receiver using Tunnel Diode Intermediate Amplifier

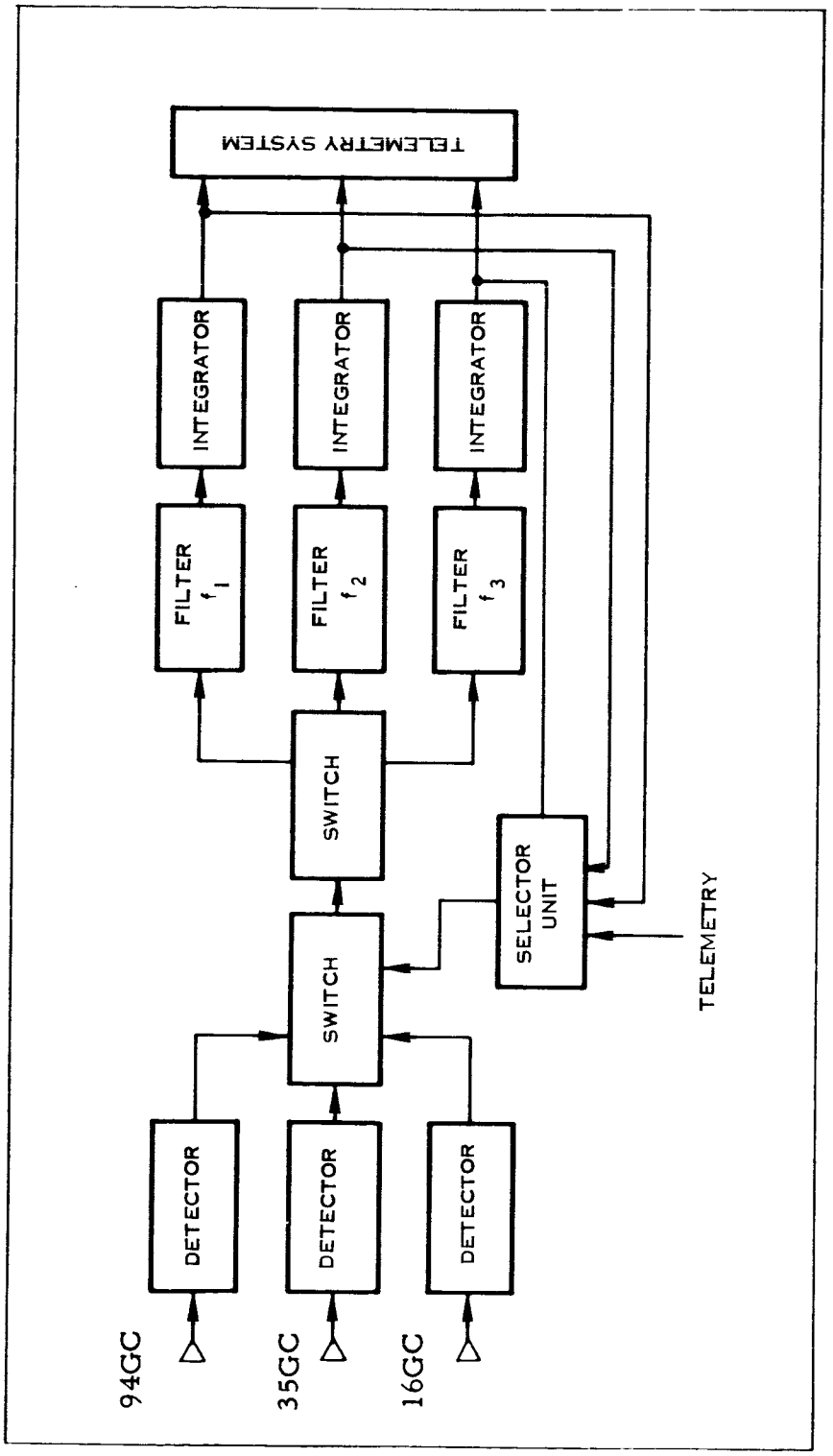

Figure 5-3. Multi-Frequency Satellite Receiver Using Crystal Video Detection

Section 6
SIGNAL ANALYSIS

This section on phase-lock receivers supersedes Section 5.3.7 of the Second Quarterly Report.

6.1 Signal Acquisition and Tracking With Phase-Lock Receivers

A spacecraft or ground based receiving system must have a frequency acquisition and tracking capability due to the fact that very small predetection bandwidths are required. The receiver circuit parameters for such a capability are derived from the anticipated signal-to-noise density ratio and the frequency offset, or the difference in frequency of the actual received signal and the frequency for which zero error signal is required for the receiver voltage controlled oscillator.

The discussion which follows shows the superiority of the bandpass limiter over automatic gain control when optimizing the dynamic range of a phase tracking loop. It is also shown that, for the frequency offsets anticipated, signal acquisition cannot be accomplished without sweeping the output frequency of the voltage controlled oscillator. Finally maximum frequency sweep rate versus loop noise bandwidth is given for various valves of signal-to-noise density.

6.1.1 Signal-to-Noise Density

The spacecraft and ground receiver configurations are dictated by many parameters. A convenient expression in which some of these parameters are included is the signal-to-noise density ratio. This ratio is the received signal power to the noise power per cycle bandwidth at the receiver input and is derived from Equations 5-48 and 5-50 of the Second Quarterly Report.

$$\frac{P_R}{N_c} = \frac{P_T G_T G_R \sigma L_p}{KT_o(FL_s - 1) + KT_A} \qquad (6\text{-}1)$$

P_T = transmitter power

G_T = gain of transmitting antenna

G_R = gain of receiving antenna

σ = free space attenuation

L_p = polarization and atmospheric losses

K = Boltzmann's constant (1.38×10^{-23} watt-seconds/^{o}Kelvin)

T_o = ambient temperature of the system

F = receiver noise figure

L_s = system losses prior to mixer

Ta = effective antenna temperature

The anticipated signal-to-noise density ratios for the propagation experiments, are in the order of 40 to 60 db, which is equivalent to a 0 to 20 db signal-to-noise ratio in a 10 Kc bandwidth.

6.1.2 Maximum Frequency Offset

The acquisition or pull-in-range of the phase-lock receiver is a second parameter to be considered. The receiver, as seen in Figure 6-1, anticipates a frequency at the receiver input, which results in zero error at the phase detector output. This frequency is the resting frequency of the system. Any frequency other than the resting frequency, will require movement of the voltage controlled crystal oscillator and will be known as a frequency displacement. The maximum frequency offset is expressed by the following:

$$f_D = K_T f_T + K_{LO} f_{LO} + f_d + K_V M f_{VCO} + K_S f_{FS} \qquad (6\text{-}2)$$

where:

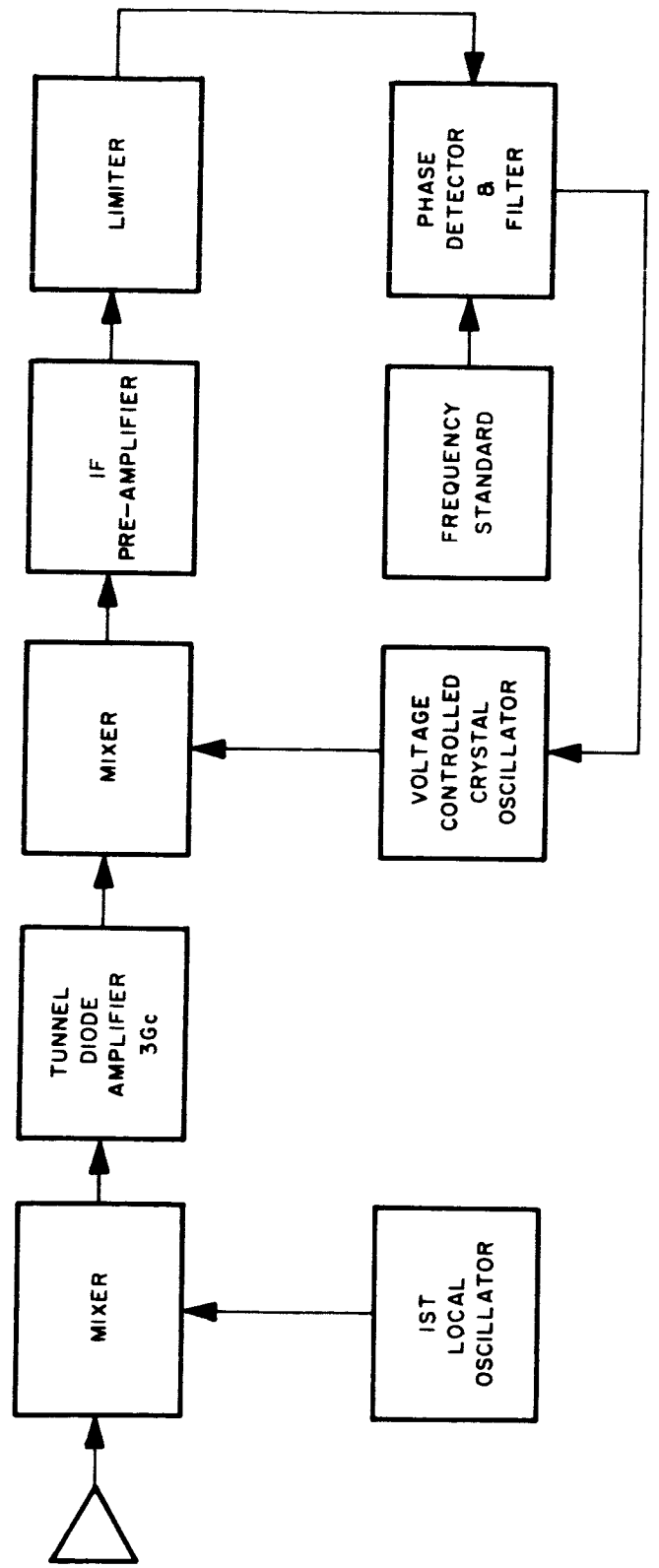

Figure 6-1 Phase Lock Receiver

K_T = uncertainty of transmitted frequency (1 part in 10^5 to 1 part in 10^6)

f_T = transmitter frequency

K_{LO} = uncertainty of receiver first local oscillator (1 part in 10^5 to 1 part in 10^6)

f_{LO} = first local oscillator frequency

f_d = doppler frequency due to relative motion of receiver and transmitter

K_V = uncertainty of voltage controlled crystal oscillator (1 part in 10^5)

M = multiplication factor required to generate second local oscillator frequency starting with voltage controlled crystal oscillator frequency

f_{VCO} = frequency of voltage controlled crystal oscillator

K_S = uncertainty of frequency standard (1 part in 10^6)

f_{FS} = frequency for the frequency standard

The doppler frequency term may be eliminated from the above expression, since it is insignificant when a vehicle is in synchronous stationary orbit. The frequency standard term may also be eliminated, since it's contribution is less than 0.1%. Frequency displacement of 950 Kc for the worst case to 95 Kc in the best case, may be anticipated for a system operating at 35 Gc. Since one does not have prior knowledge of whether the displacement frequency is above or below the system resting frequency, the system must have a pull-in-range equal to twice the displacement frequency.

6.1.3 Dynamic Range

Many papers and articles have been written describing phase-locked loops and their parameters. One parameter of interest, the dynamic range of a phase tracking loop may be optimized through the application of a bandpass limiter prior to the phase detector.[42] Comparison of a phase-locked-loop incorporating automatic gain control with a loop utilizing a bandpass limiter is shown in Figure 6-2. The loop had the following parameters:

Filter = optimum, proportional plus integral

Noise-to-signal ratio at match point = 1

Predetection bandwidth = 1 mc

Loop noise bandwidth = 5 cps

Phase displacement = 1 radian

As clearly evident from Figure 6-2, the limiter configuration approaches the optimum system, thus justifying a limiter prior to phase detection.

6.1.4 Frequency Pull-in Range

The pull-in-range of a phase-lock-loop is theoretically infinite for the case of a perfect integrating filter. For the case of the second order system incorporating an imperfect filter, the pull-in-range is finite and may be expressed as;[43]

$$\omega_p < \frac{8\sqrt{2B_N}}{3}\frac{\sqrt{4B_N}}{3\phi} + 1 \quad \frac{\text{radians}}{\text{second}} \qquad (6\text{-}3)$$

where:

B_N = loop noise bandwidth

ϕ = inverse time constant of the optimum filter.

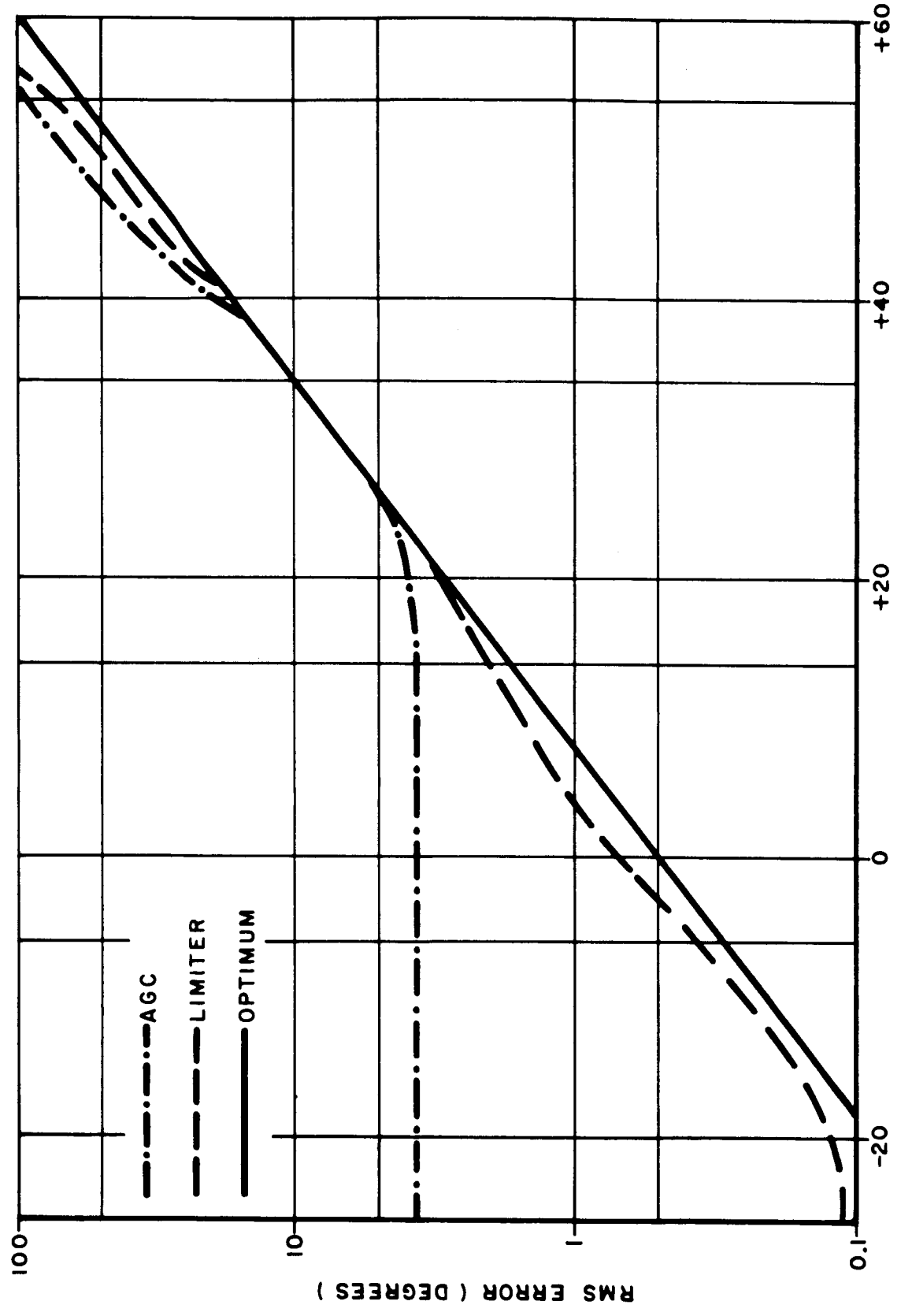

Figure 6-2 Performance of Phase-Locked Loops

Assuming a loop noise bandwidth of 100 cycles; a predetection bandwidth of 10 Kc; and velocity loop gains of 10^5 and 10^6, curves of pull-in-range versus signal-to-noise density ratio are plotted in Figure 6-3. The signal power in this case is to be considered as only the power in the carrier. It is evident from Figure 6-3, that a maximum pull-in-range of 10 Kc may be achieved for a signal-to-noise density ratio of 40 db and a loop gain of 10^7. This pull-in-range does not meet the acquisition requirement which is twice the frequency displacement of 1.8 Mc for the worst case. Figure 6-4 is another curve of maximum pull-in-range vs. signal-to-noise density with a system designed at 30 db signal-to-noise density ratio at the match point. One must conclude, that the acquisition requirement cannot be met with the system in Figure 6-1.

6.1.5 Frequency Sweeping

Thus, we must consider the frequency swept phase lock receiver configuration as shown in block diagram form in Figure 6-5. This approach has been widely used and is essentially sweeping the voltage controlled oscillator at a fixed rate until the signal is acquired at which time the sweep voltage is deactivated.

Frazier and Page[44] have derived a formula, from experimental results, to determine the rate at which a VCO may be swept for a 0.9 probability of acquisition and is expressed as:

$$S(\text{cps/sec}) = \frac{\left(\frac{\pi}{2} - 2.2\sigma_o\right)\left(0.9\frac{\alpha}{\alpha_o}\right)\omega_{no}^2}{2\pi\ (1+\delta)} \qquad (6\text{-}4)$$

where:

σ_o = rms phase jitter

α = suppression factor of limiter

δ = overshoot

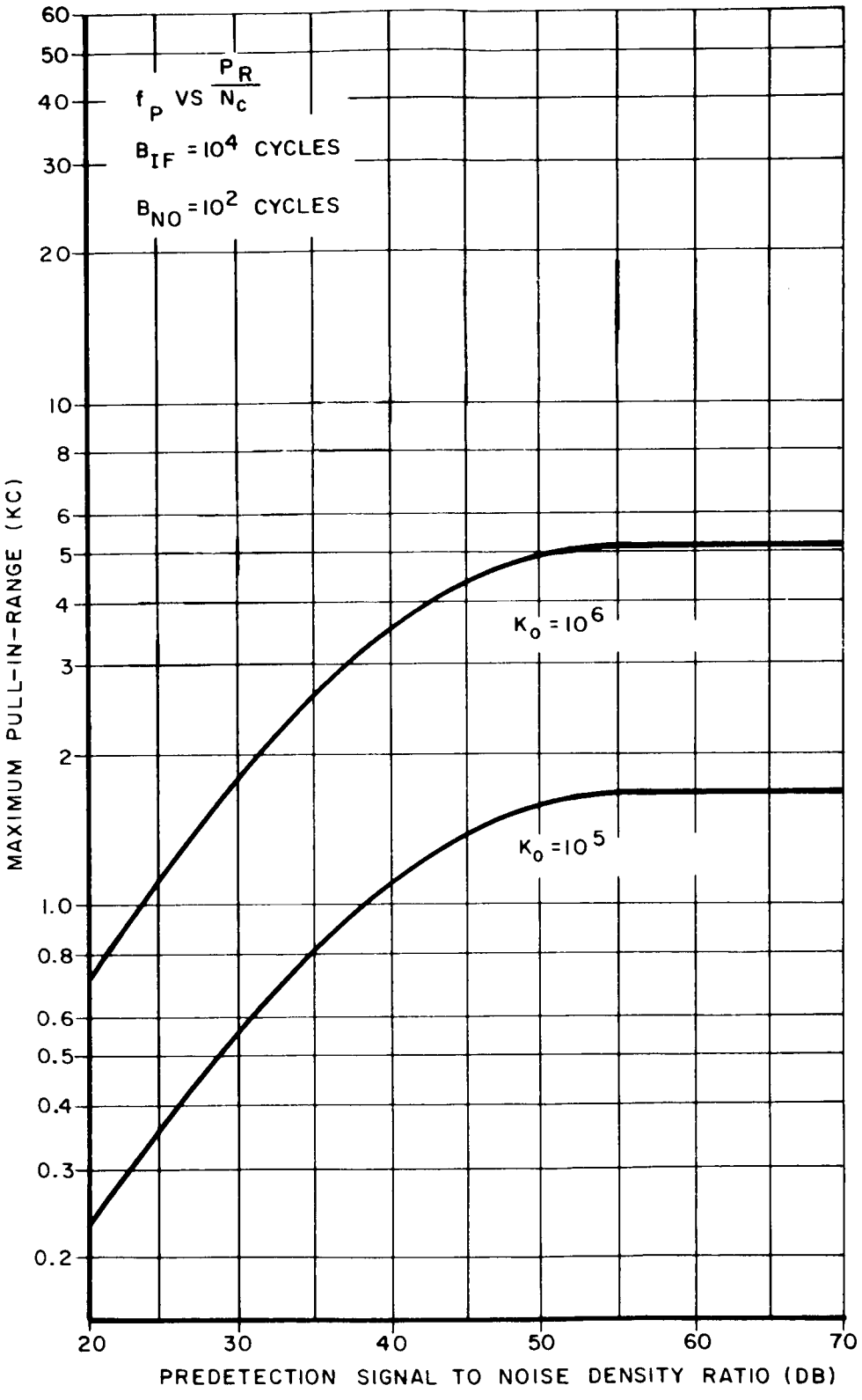

Figure 6-3 Pull-in Range of Phase Lock Receivers ($B_{IF} = 10^4$ Cycles) ($B_{NO} = 10^2$ Cycles)

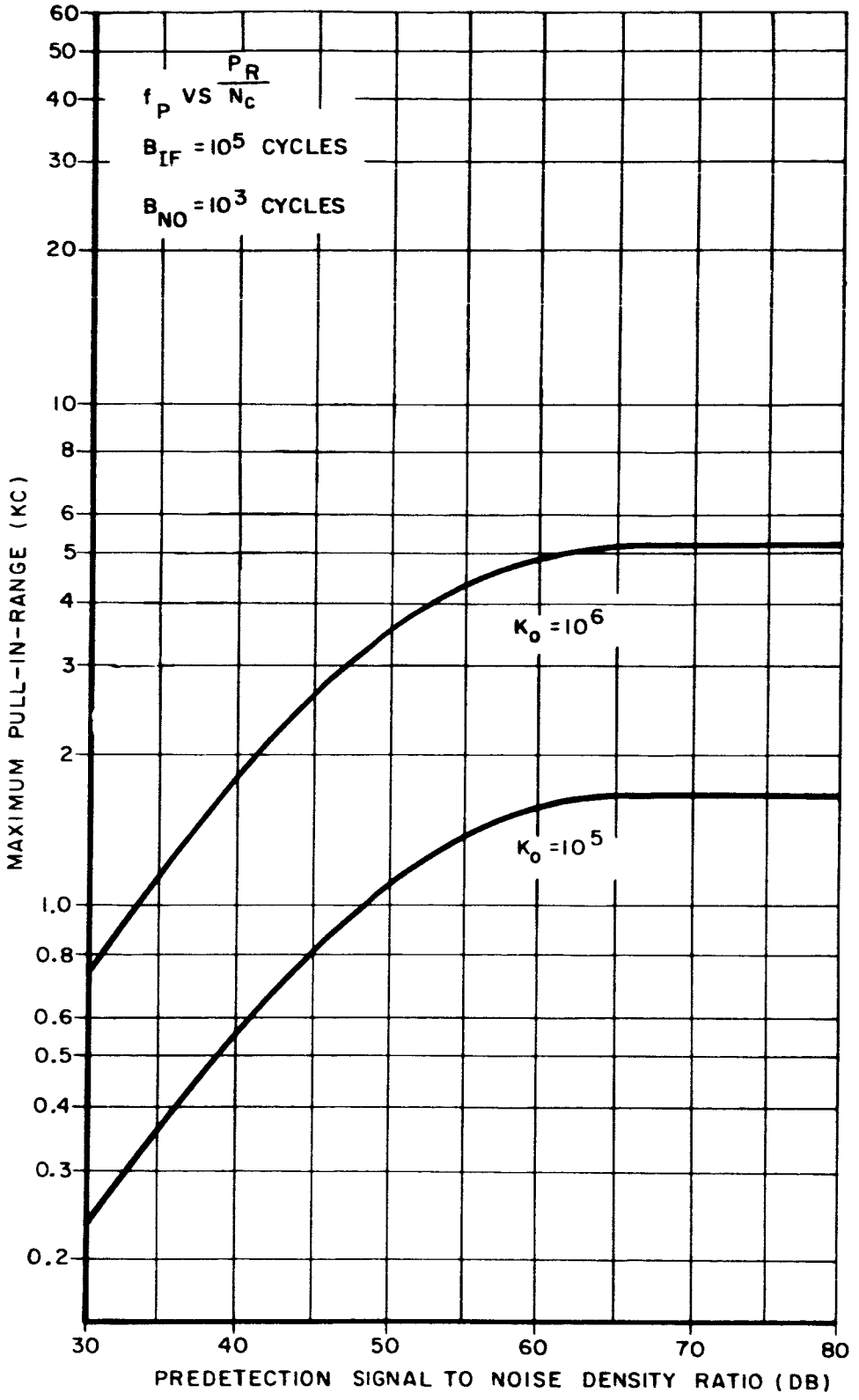

Figure 6-4 Pull-in Range of Phase Lock Receivers ($B_{IF} = 10^5$ Cycles) ($B_{NO} = 10^3$ Cycles)

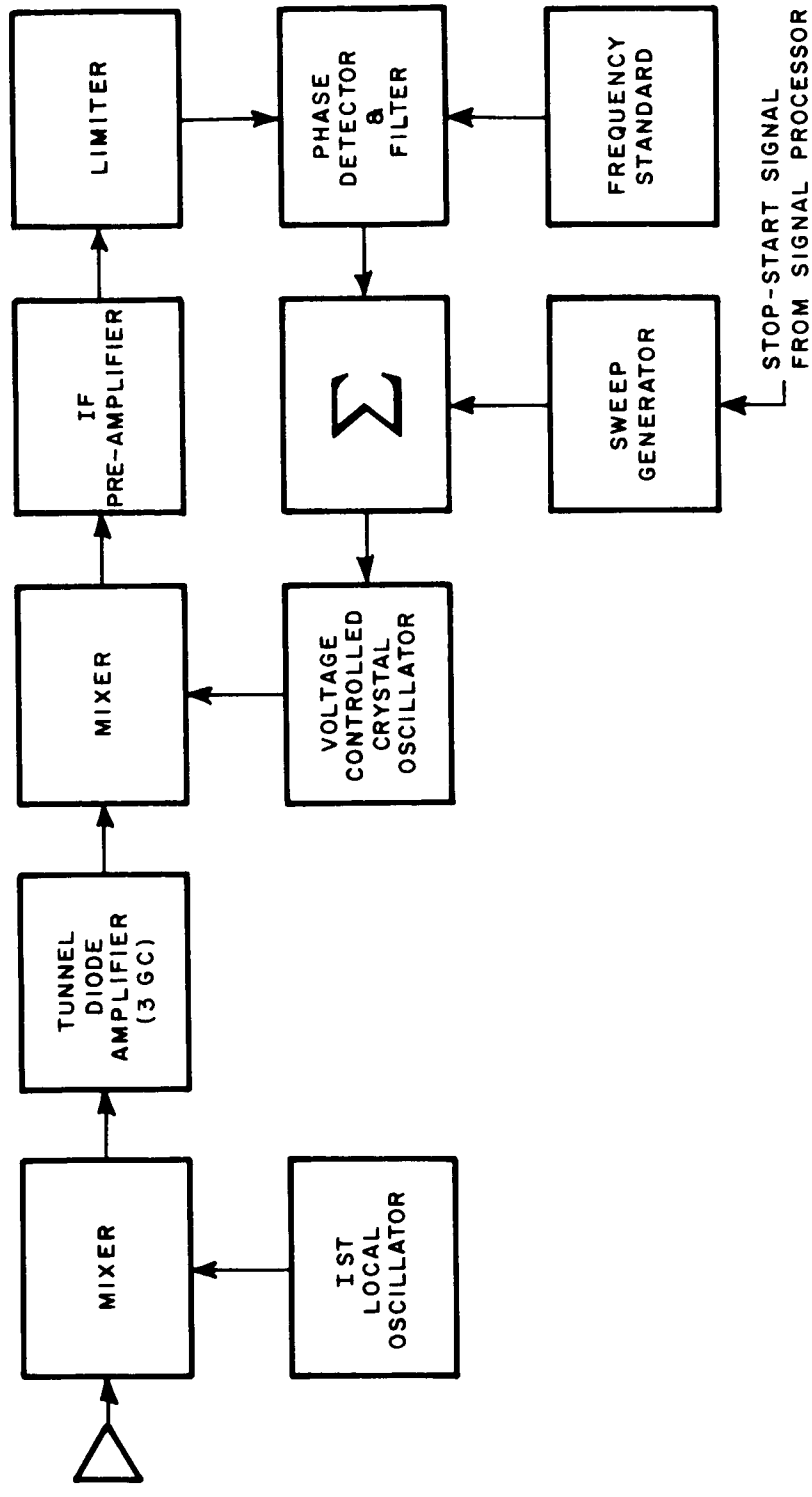

Figure 6-5 Frequency Swept Phase Lock Receiver

α_o = suppression factor of limiter at which the loop is matched.

ω_{no} = natural frequency of the loop at match point.

With Equation 6-4, the maximum sweep rate versus loop noise bandwidth for various signal to noise densities were plotted in Figure 6-6. These curves were plotted assuming the plotted points to also be the system match or design point; that is, the system is designed for the minimum anticipated signal-to-noise density ratio of 36 db. This ratio satisfies the requirements for unmodulated carrier acquisition in the majority of experiment links listed in Table 5-1. Then, from Figure 6-6, the maximum sweep rate is 0.14Mc per second and our loop noise bandwidth is to be 2 Kc. When sweeping at this rate there is a 0.9 probability of acquiring the signal in the first sweep. However, the final system design will include a margin, thus sweeping at lower rates, thus increasing the probability of acquisition. If, however, a swept rate of 0.10Mc/sec is used, the maximum time required to acquire, under the worst condition, would be 18 seconds assuming that 1.8 Mc had to be swept. On the other hand, if the minimum anticipated signal-to-noise density ratio were 40 db, the VCO could be swept at 1 Mc/sec, thus acquiring the signal in 2 seconds. The maximum frequency displacement can be as large as 1.8 Mc which will produce a steady state phase error. This error is expressed as:

$$\phi = \frac{\omega_d}{K} \qquad (6-5)$$

where:

K = Velocity loop gain constant

ω_d = displacement frequency in radians per second

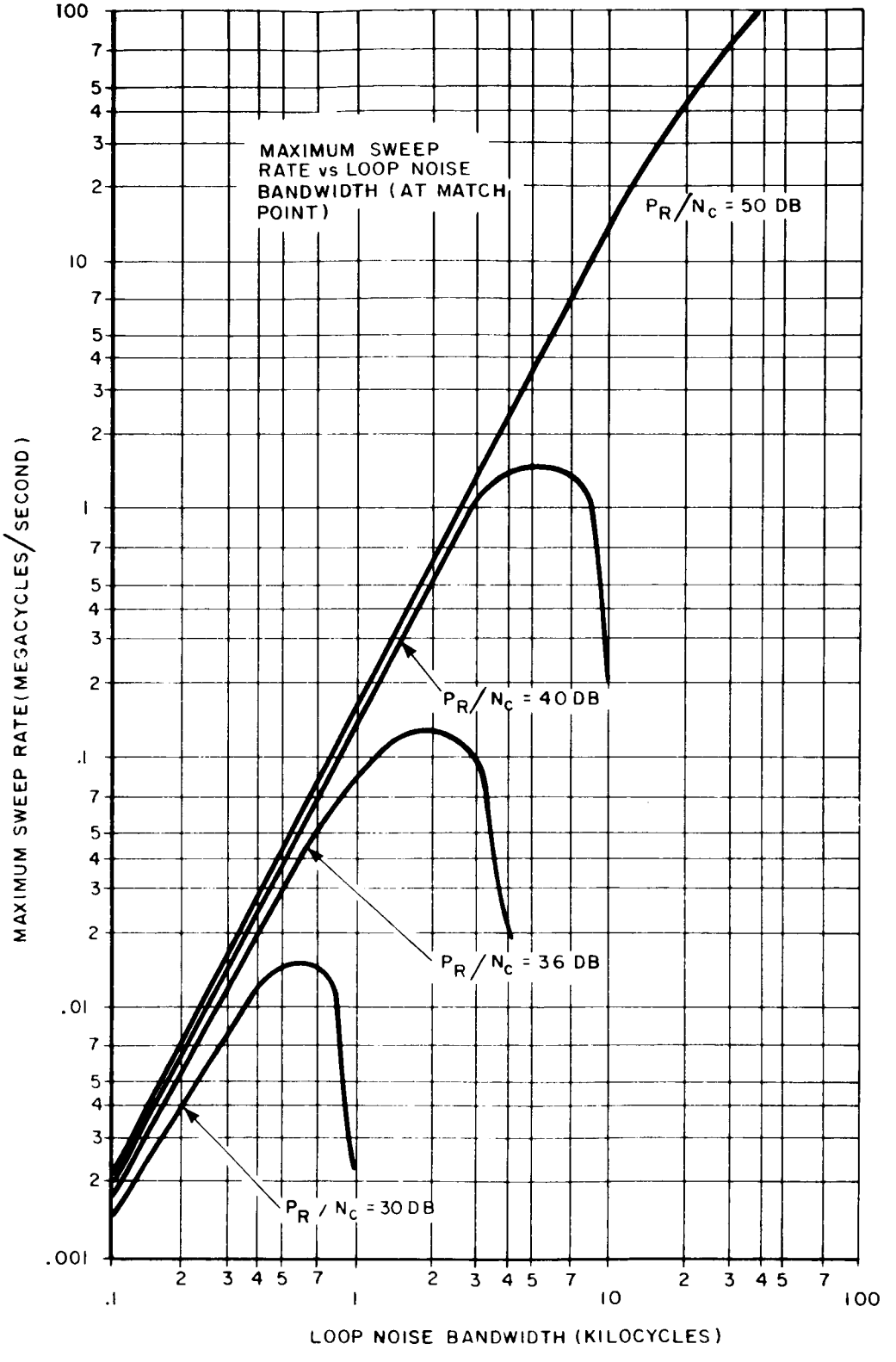

Figure 6-6 Maximum Sweep Rate vs Loop Noise Bandwidth (at Match Point)

The loop will stay in its locked state as long as the phase error due to all sources is less than $\frac{\pi}{2}$ radians. It is concluded from Equation 6-5 that a loop gain of 10^7 to 10^8 is required for this system.

Section 7
DATA PROCESSING AND EVALUATION

The design of a millimeter propagation experiment is not complete without describing the data processing and evaluation required to define the parameters of the channel through the propagating medium.

Existing computer facilities are equipped to handle the data processing required for the propagation data collection program. Special-computer programs, which are based on the mathematics presented in this section, can be generated to provide estimates of the channel parameters. Little computation is required to infer, from these basic parameters, the effects of propagation on commonly used waveforms and modulation systems because this has already been done for similar effects at lower frequencies. Information on the estimation of system performance with these basic parameters is given in Section 4.2 of the First Quarterly Report and in the open literature such as Reference 45 through 49.

The first part of this section discusses the general concept of processing and evaluating millimeter propagation data taken from space-earth channels. This is followed by definitions of the channel parameters which apply to any communication channel and then the mathematics for computing these parameters from basic phase and amplitude data is given. Finally the application of these mathematical methods to millimeter channels is the conclusion of this section.

7.1 General Concept

The actual processing of the collected data can be performed by off-the-shelf equipment. The important consideration is that when the experiment hardware is purchased, the data processing equipment must be specified

in detail so that its procurement or lease becomes an integral part of the experiment design package. Labor required for data processing and analysis must be specified in the program plan.

Data to be used in the final description of the propagating medium will come from three principal sources. They are:

a) Spacecraft position data from a satellite tracking facility.

b) Amplitude and phase data either telemetered from spacecraft receivers or extracted from ground and airborne receivers.

c) Meteorological and radiometric data from correlative sensors.

Proper emphasis must be placed upon correlative sensors and correlative data processing. It does little good to determine atmospheric absorption, atmospheric noise, selective frequency fading and channel capacity unless we accurately classify the meteorological conditions existing during each measurement period and determine the probability of recurrence of each class of conditions during the annual cycle. Good correlative data will allow prediction of propagation effects for many future ground terminal locations from data taken with a few ground terminals.

Three phases of data processing will be considered for the experiments. They are:

a) Real-time on-site space, ground, and airborne data recording and processing which will be useful for operational monitoring and last minute changes in test schedule during the spacecraft pass or measurement interval.

b) Non-real time on-site data processing which is necessary for short range test schedule planning for the subsequent spacecraft passes or measurement intervals.

c) Non-real time off-site data processing performed by existing contractor and/or government computer facilities required to develop the final data in tabular and graphical form.

The taped analog data from the satellite and from all the ground facilities would be converted to digital form and processed at a central data processing facility. The relationship of this facility with the other facilities involved in the propagation data collection program is illustrated in Figure 7-1.

Each ground facility receiver should be equipped with identical signal processors and analog tape recorders to minimize data processing expense. Each ground receiver would share its rf head with a radiometer in order to make sensitive sky temperature measurements using the same antenna beam. Short term and long term variations of antenna azimuth and elevation angle are recorded on tape along with the signal amplitude, relative sideband phase and radiometric temperature. It should also be noted that the boresight installation for each of the participating ground facilities should be equipped for calibration and checkout purposes, with a spacecraft simulator which consists of the appropriate transmitters and/or receivers which function like those aboard the satellite.

Real-time analog strip line recoder presentations of the same data which is being recorded on magnetic tape will be made at each site for calibration, checkout and operational monitoring; and to provide the cooperating agencies with immediate access to the raw data. A coarse evaluation on the analog presentations can be made at the site for the purposes of planning follow-on experiments.

An extensive quantity of data will result from the experimental program, and, of course, it is not necessary to statistically process all of the data collected. However, it is necessary to look for the occurrence of unusual propagation effects to insure that the data which is processed adequately represents the statistical model. When the magnetic tape arrives at the central processing facility, an analog presentation, similar to that made at the side, is made from the tape playback in order to select those samples

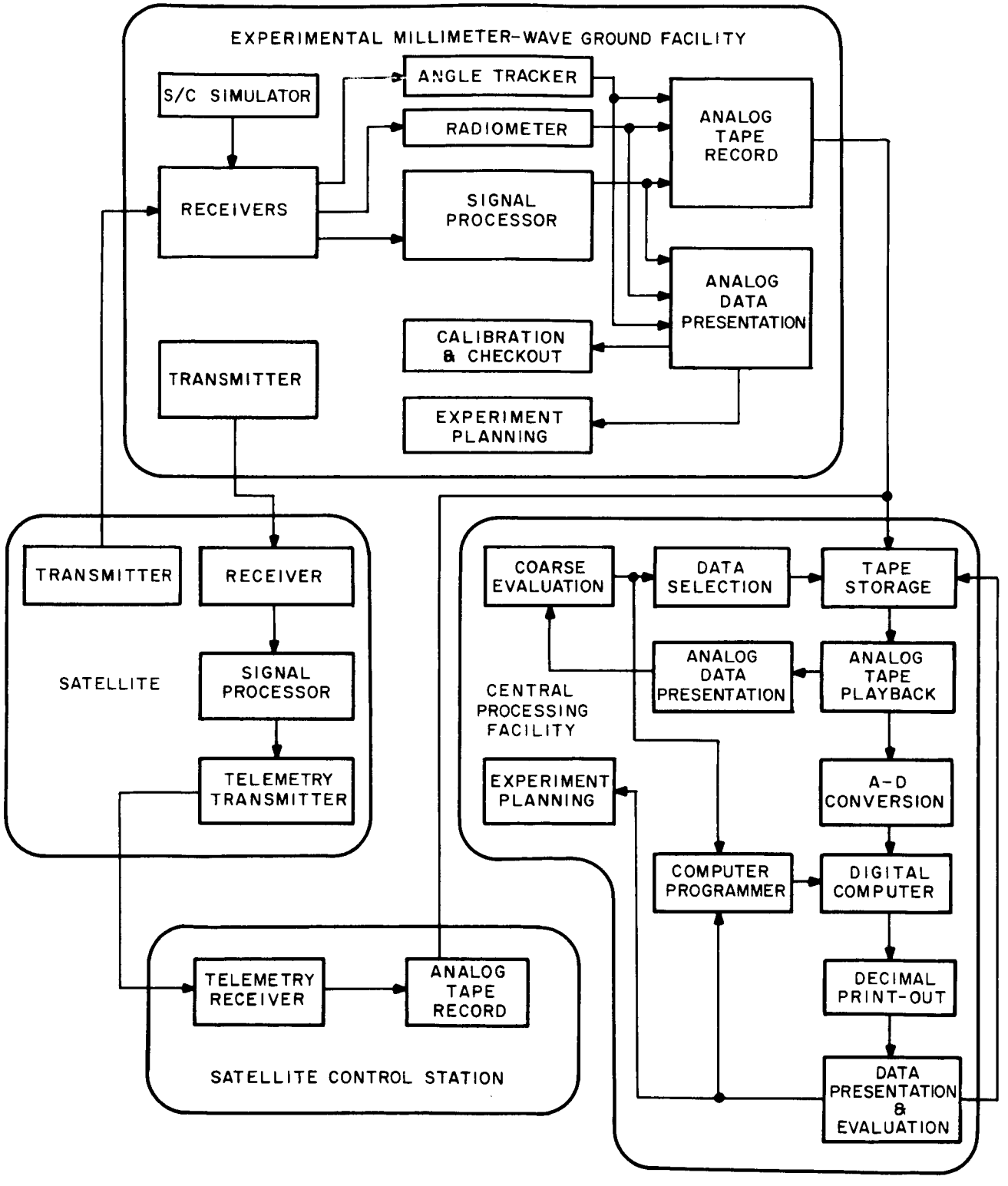

Figure 7-1 General Concept of Data Processing and Evaluation

of data which are to be processed. As more and more samples are processed it is expected that evaluation of these results will indicate improvements to be made in the computer program, and choose new samples for computer processing and old samples for rerun.

The spacecraft position data taken by the tracking facility in the satellite control station is programmed into the computer in order to cancel out free space attenuation from the total path losses of the space-earth link. Calibration runs, just prior to the actual propagation tests, are performed with the spacecraft simulator so that the proper receiver and transmitter constants can be used at the central processing facility. During the test itself, operational performance is monitored by recording certain data on one or more channels of the magnetic tape. Pre-test calibration and operational monitoring is also performed on the spacecraft equipment and telemetered to the satellite control station with the raw propagation data.

7.2 Definition of Channel Parameters

A pictorial display, provided by Green[50], which shows the functions of a single channel, to be defined, as well as their interrelationships, is given in Figure 7-2. A second pictorial display showing the functional relationships between two spatial channels is given in Figure 7-3. An explanation of each of the single and dual channel functions now follows.

7.2.1 The Two-Dimensional Correlation Function

The Two-Dimensional Correlation Function for a single spatial channel is an important quantity characterizing the millimeter channel. This function is measured by those experimentors who measure fading and fading statistics and it has direct application to the design of communication systems using frequency diversity. The importance of this function is discussed by Green[50], Gallagher[51], and Price and Green[52].

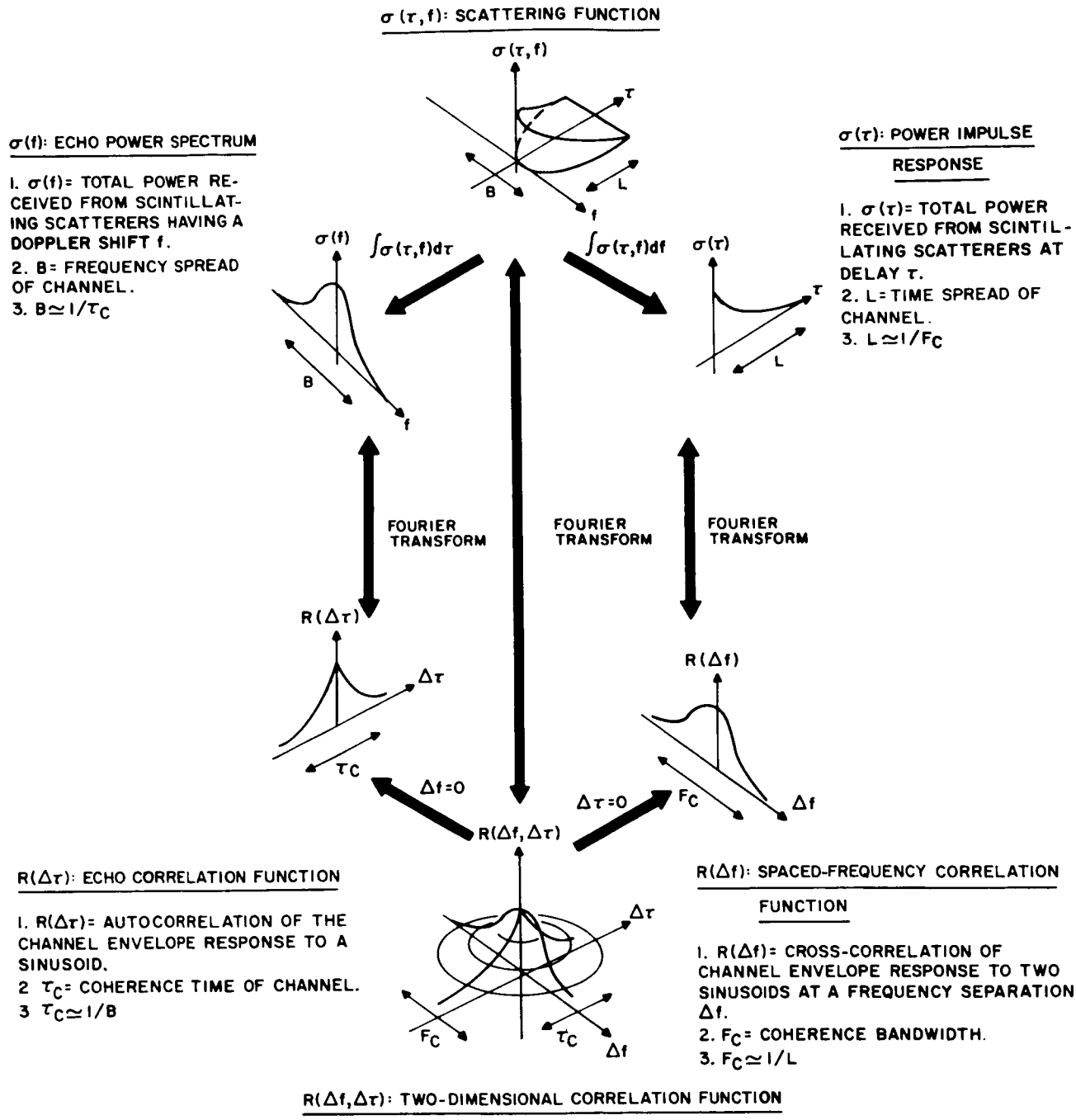

Figure 7-2 Functional Interrelationship of a Single Spatial Channel

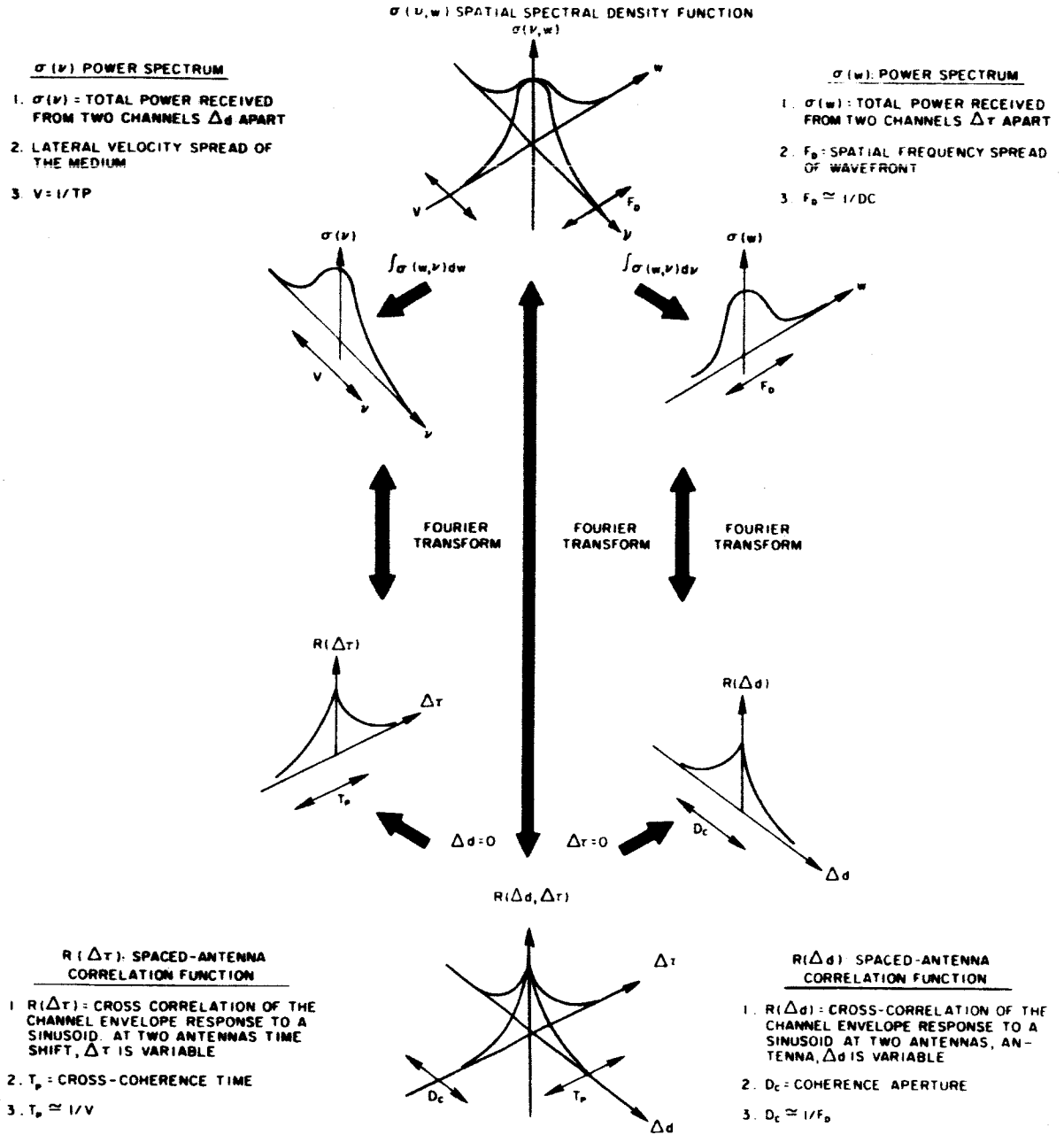

R(Δd), Δr): Two-Dimensional Spatial Correlation Function

Figure 7-3. Functional Relationships Between Two Spatial Channels

The following quantities may be determined directly from the two-dimensional correlation function, $R(\Delta f, \Delta t)$: the coherence time and the coherence bandwidth of the channel; the duration of fades; the Echo-Correlation Function, $R(\Delta t)$; and the Spaced-Frequency Correlation Function, $R(\Delta f)$. Moreover, the Scattering Function, $\sigma(\tau, f)$, which is the two-dimensional Fourier Transform of $R(\Delta f, \Delta \tau)$, provides direct information regarding doppler and multipath spreading by the channel.

That $R(\Delta f, \Delta \tau)$ and $\sigma(\tau, f)$ are important is demonstrated by the fact that $\sigma(\tau, f)$ can be used to determine the probability of error in deciding which of m waveforms has been transmitted through the channel (53, 54, 55). The function, $\sigma(\tau, f)$ also arises in the consideration of optimum analog communication systems and bounds on their performance[56].

For the purposes of investigating the physical significance of the various quantities associated with $R(\Delta f, \Delta \tau)$ and $\sigma(\tau, f)$, the observations of Green[50] and Gallager[51] are summarized.

The time-frequency-spread channels under consideration have the property that a transmitted sinusoid is received as a narrow-band random process. That is, a transmitted signal of the form:

$$s_t(\tau) = \mathrm{Re}\left\{ e^{j2\pi f \tau} \right\} \tag{7-1}$$

is received as

$$s_r(\tau) = \mathrm{Re}\left\{ \tilde{s}_r(f,\tau)\, e^{j2\pi f \tau} \right\}, \tag{7-2}$$

where $\tilde{s}_r(f,\tau)$ is the complex envelope of the received signal; since $s_r(\tau)$ is narrow-band, the envelope of the received signal is $\left|\tilde{s}_r(f,\tau)\right|$ where $\tilde{s}_r(f, \tau)$ may be interpreted as a randomly-varying transfer function.

The Two-Dimensional Correlation Function is defined in terms of complex envelopes by:

$$R(\Delta f, \Delta\tau) = 2E\left\{ \tilde{s}_r^{*}\left(f - \frac{\Delta f}{2}, \tau\right) \tilde{s}_r\left(f + \frac{\Delta f}{2}, \tau + \Delta\tau\right) \right\}, \qquad (7\text{-}3)$$

where "E" signifies taking the expected value of the bracketed quantity and "*" indicates complex conjugate.

In order to interpret $R(\Delta f, \Delta\tau)$, we closely follow Callager[49] and consider $R(o, \Delta\tau)$ and $R(\Delta f, o)$ separately.

Referring to Equation 7-3, $R(o, \Delta\tau)$ is seen to be the autocorrelation function of the complex envelope of the channel response to an input sinusoid of frequency f cps. This autocorrelation function, $R(\Delta\tau) = R(o, \Delta\tau)$, is called the "Echo-Correlation Function;" it provides coherence time and fading duration information.

The coherence time of the channel, τ_c, is loosely defined as the range in $\Delta\tau$ over which $R(\Delta\tau)$ is non-zero. Very often τ_c is taken to be the solution to:

$$R(T_c) = 1/2\ R(o). \qquad (7\text{-}4)$$

The fact that $R(\Delta t)$ approaches zero largely results from fading in the channel. τ_c is related, therefore, to the duration of fades.

Again referring to Equation 7-3, $R(\Delta f, o)$ is seen to be the cross-correlation function of the complex envelope of the channel response to a sinusoid at $f - \frac{\Delta f}{2}$, cps. with the complex envelope of the response to a sinusoid at $f + \frac{\Delta f}{2}$. The cross correlation function, $R(\Delta f) = R(\Delta f, o)$, is called the "Spaced-Frequency Correlation Function;" it provides coherence bandwidth information.

The coherence bandwidth, F_c, of the channel is loosely defined to to be the range in Δf over which $R(\Delta f)$ is non-zero. If frequency diversity modulation schemes are used to transmit information, the F_c is a measure of how far apart the separate channels must be in order to receive uncorrelated signals on each.

If a signal of bandwidth W, centered around f, is transmitted and W is such that $R(W, o) \simeq R(o, o)$, then the received signal will be the same as the transmitted signal except for an overall amplitude and phase that change over a period of time which is on the order of τ_c. Conversely, if $R(W, o) \simeq o$, the amplitude and phase of different frequency components of the input signal will be changed relative to each other, and the received waveform will no longer bear a simple resemblance to the transmitted waveform.

If $R(\Delta f, \Delta \tau)$ is unimodal, the τ_c is approximately the reciprocal of the doppler spreading and F_c is approximately the reciprocal of the time spreading of the channel.

7.2.2 The Scattering Function

The channel scattering function, which is the two-dimensional Fourier transform of the correlation function, is directly applicable to communication system design. The scattering function, $\sigma(\tau, f)$ has a convenient physical interpretation; it represents the power received from a scintillating scatterer at delay τ and doppler shift f.

Consider the two functions, $\sigma(f) = \int \sigma(\tau, f)\, dt$ and $\sigma(\tau) = \int \sigma(\tau, f)\, df$, separately. $\sigma(f)$ is called the "Echo Power Spectrum" and $\sigma(t)$ is called the "Power Impulse Response."

The scattering function represents the total power received from all scatters producing a doppler shift of f cps. The doppler spread of the channel, B, is loosely defined to be the range in f over which $\sigma(f)$ is non-zero.

As previously mentioned, if $\sigma(\tau, f)$ and $R(\Delta f, \Delta\tau)$ are well behaved, then $B \simeq 1/\tau_c$.

The functions, $\sigma(\tau)$ represents the total power received from all scatterers at a delay τ. The time spread of the channel, L, is loosely defined to be the range in τ over which $\sigma(\tau)$ is non-zero. If $\sigma(\tau, f)$ and $R(\Delta f, \Delta\tau)$ are well behaved, than $L \simeq 1/F_c$.

The Echo-Correlation Function, $R(\Delta\tau)$, is the Fourier Transform of the Echo Power Spectrum, $\sigma(f)$, and the Spaced-Frequency Correlation Function $R(\Delta f)$, is the Fourier Transform of the Power Impulse Response, $\sigma(t)$.

7.2.3 The Modified Two-Dimensional Correlation Function

A frequently measured quantity, which has no simple relation to $R(\Delta f, \Delta\tau)$, is a modified two dimensional correlation function. The modified function, which is denoted by $\hat{R}(\Delta f, \Delta\tau)$, is defined in terms of the channel envelope response by:

$$\hat{R}(\Delta f, \Delta\tau) = 2E\left\{\left|\tilde{s}_r\left(f - \frac{\Delta f}{2}, \tau\right)\right|\left|s_r\left(f + \frac{\Delta f}{2}, \tau + \Delta\tau\right)\right|\right\}. \tag{7-5}$$

Since $\hat{R}(\Delta f, \Delta\tau)$ depends on the envelope of the channel response, rather than the complex envelope, it is insensitive to phase fluctuations, and therefore provides less information than $R(\Delta f, \Delta\tau)$. $\hat{R}(\Delta f, \Delta\tau)$ is used in practice because of the relative ease in measuring it compared to measuring $R(\Delta f, \Delta\tau)$, (by 14). Associated with $\hat{R}(\Delta f, \Delta\tau)$ is a complete set of quantities; $\hat{R}(\Delta f)$, $\hat{R}(\Delta\tau)$, $\hat{\tau}_c$, $\hat{F}_c$, $\hat{\sigma}(\tau, f)$, etc., each of which is defined, in a parallel fashion, to its counterpart associated with $R(\Delta f, \Delta\tau)$.

7.2.4 The Two-Dimensional Spatial Correlation Function

The two-dimensional correlation function for two parallel spatial channels receiving the same signal will provide the communication system

designer with information on spatial diversity, limitations of atmosphere on antenna size, and the physical structure of the propagating medium. The correlation function is obtained by receiving a single sinusoid at two receivers separated by a distance (Δd) and correlating them with time shift ($\Delta \tau$).

The two-dimensional spatial correlation function, $R(\Delta d, \Delta \tau)$ which is shown in Figure 7-3 is defined by:

$$R(\Delta d, \Delta \tau = 2E \left\{ \tilde{s}_r^* \left(d - \frac{\Delta d}{2}, \tau\right) \tilde{s}_r \left(d + \frac{\Delta d}{2}, \tau + \Delta \tau\right) \right\} \quad (7\text{-}6)$$

which is analogous to the two-dimensional correlation function given in Equation (7-3).

The coherence aperture, D_c, of a channel is loosely defined as the range in Δd over which $R(\Delta d)$ is non-zero. If very large antennas are to be used in a communication system D_c is an important measure of the maximum diameter aperture which can be efficiently employed. In situations where space diversity schemes are being considered as a means of enhancing channel reliability, D_c is a measure of antenna separation required in order to receive uncorrelated signals. When Δd is zero and $\Delta \tau$ is variable, the two-dimensional spatial correlation function becomes the echo correlation function for a single channel. In Figure 7-3, D_c is thought of in seconds, that is, the coherence distance (in units of length) divided by the speed of propagation.

The cross coherence time, T_p, is loosely defined as the range in $\Delta \tau$ over which $R(\Delta \tau)$ is non-zero. $R(T_p)$ is often referred to as $1/2\ R(o)$. If $R(\Delta \tau)$ is maximum at some point other than $\Delta \tau = 0$, it indicates that the relative structure of the atmosphere has remained essentially unchanged as it moves a certain distance (Δd).

7.2.5 The Spatial Spectral Density Function

The dual channel spectral density function, $\sigma(v, w)$, which is the

two-dimensional Fourier Transform of the spatial correlation function, is useful in understanding the physical structure of the atmosphere.

The spatial frequency spread, F_D, is loosely defined to be the range in wavefront frequency W over which σ (w) is non-zero. If σ (w, v) and R (Δd, $\Delta \tau$) are well behaved, then $F_D \simeq {}^1/D_c$. In other words, the larger the coherence aperture, the narrower the spatial spectrum of the wavefront. When D_C is expressed in seconds, F_D becomes cycles per second.

The lateral velocity, V_s is loosely defined as the velocity of the propagating medium across a distance (Δd); and it is the range of the lateral velocity v over which σ (v) is non-zero. If σ (w, v) and R (Δd, $\Delta \tau$) are well behaved, then $V \simeq {}^1/T_p$ (in cycles per second). When multiplied by Δd in units of length, V is expressed in linear velocity dimensions.

7.2.6 The Modified Two-Dimensional Spatial Correlation Function

In simpler experiments, a modified spatial correlation function, R (Δd, $\Delta \tau$), is usually measured. It is defined in terms of the envelopes of the received signals by:

$$\hat{R}(\Delta d, \Delta \tau) = 2E\left\{\left|\tilde{s}_r\left(d - \frac{\Delta d}{2}, \tau\right)\right|\left|\tilde{s}_r\left(d + \frac{\Delta d}{2}, \tau + \Delta \tau\right)\right|\right\} \quad (7\text{-}7)$$

The function $\hat{R}$ (Δd, $\Delta \tau$) provides no information about decorrelation effects due to phase fluctuations because of the use of only amplitude envelopes rather than complex envelopes.

7.3 Measurement of Channel Parameters

A variety of correlation functions and spectral densities are useful in the characterization of the millimeter communication channel. The quantities listed in Tables 7-1 and 7-2, can be used to determine the fundamental limitations imposed by the channel upon commonly used modulation schemes. The purpose of this section is to review the mathematics for estimating

TABLE 7-1

CORRELATION FUNCTIONS

Name	Definition	Associated Quantities
Two-Dimensional Correlation Function	$R(\Delta f, \Delta\tau) = \mathcal{E}E\left[\tilde{s}_r^*(f - \frac{\Delta f}{2}, \tau - \frac{\Delta\tau}{2}) s_r(f + \frac{\Delta f}{2}, \tau + \frac{\Delta\tau}{2})\right]$	
Modified Two-Dimensional Correlation Function	$R(\Delta f, \Delta\tau) = \mathcal{E}E\left[\left\lvert\tilde{s}_r(f - \frac{\Delta f}{2}, \tau - \frac{\Delta\tau}{2})\ s_r(f + \frac{\Delta f}{2}, \tau + \frac{\Delta\tau}{2})\right\rvert\right]$	
Spaced Frequency Correlation Function	$R(\Delta f) = R(\Delta f, o) = \mathcal{E}E\left[\tilde{s}_r^*(f - \frac{\Delta f}{2}, \tau)\tilde{s}_r(f + \frac{\Delta f}{2}, \tau)\right]$	Coherence Bandwidth F_c
Modified Spaced-Frequency Correlation Function	$R(\Delta f) = R(\Delta f, o) = \mathcal{E}E\left[\left\lvert\tilde{s}_r(f - \frac{\Delta f}{2}, \tau)\ \tilde{s}_r(f + \frac{\Delta f}{2}, \tau)\right\rvert\right]$	Modified Coherence F_c Bandwidth
Echo Correlation Function	$R(\Delta\tau) = R(o, \Delta\tau) = \mathcal{E}E\left[\tilde{s}_r^*(f, \tau - \frac{\Delta\tau}{2})\tilde{s}_r(f, \tau + \frac{\Delta\tau}{2})\right]$	Coherence Time τ_c
Modified Echo Correlation Function	$\hat{R}(\Delta\tau) = R(o, \Delta\tau) = \mathcal{E}E\left[\left\lvert\tilde{s}_r(f, \tau - \frac{\Delta\tau}{2})\ \ s_r(f, \tau + \frac{\Delta\tau}{2})\right\rvert\right]$	Modified Coherence τ_c Time
Spatial Correlation Function	$R(\Delta d, \Delta\tau) = \mathcal{E}E\left[\tilde{s}_r^*(d - \frac{\Delta d}{2}, \tau - \frac{\Delta\tau}{2})\tilde{s}_r(d + \frac{\Delta d}{2}, \tau + \frac{\Delta\tau}{2})\right]$	
Modified Spatial Correlation Function	$R(\Delta d, \Delta\tau) = \mathcal{E}E\left[\left\lvert\tilde{s}_r(d - \frac{\Delta d}{2}, \tau - \frac{\Delta\tau}{2})\ \tilde{s}_r(d + \frac{\Delta d}{2}, \tau + \frac{\Delta\tau}{2})\right\rvert\right]$	
Spaced-Antenna Correlation Function (Variable Separation)	$R(\Delta d) = \mathcal{E}E\left[\tilde{s}_r^*(d - \frac{\Delta d}{2}, \tau)\tilde{s}_r(d + \frac{\Delta d}{2}, \tau)\right]$	Coherence Aperture D_c
Modified Spaced-Antenna Correlation Function (Variable Separation)	$R(\Delta d) = \mathcal{E}E\left[\left\lvert\tilde{s}_r^*(d - \frac{\Delta d}{2}, \tau)\ \tilde{s}_r + \frac{\Delta d}{2}, \tau)\right\rvert\right]$	Modified Coherence Aperture D_c
Spaced-Antenna Correlation Function (Constant Separation)	$R(\Delta\tau) = \mathcal{E}E\left[\tilde{s}_r^*(d, \tau - \frac{\Delta\tau}{2})\tilde{s}_r(d, \tau + \frac{\Delta\tau}{2})\right]$	Cross-Coherence Time T_p
Modified Spaced-Antenna Correlation Function (Constant Separation)	$\hat{R}(\Delta\tau) = \mathcal{E}E\left[\left\lvert\tilde{s}_r^*(d, \tau - \frac{\Delta\tau}{2})\ \tilde{s}_r(d, \tau + \frac{\Delta\tau}{2})\right\rvert\right]$	Modified Cross-Coherence Time T_p

TABLE 7-2

SPECTRAL DENSITIES

Name	Definition	Associated Quantity
Scattering Function	$\sigma(\tau, f) = \iint R(\Delta f, \Delta\tau) e^{j2\pi\tau\,\Delta f + j2\pi f\Delta\tau} d\Delta f\, d\Delta\tau$	
Modified Scattering Function	$\sigma(\tau, f) = \iint R(\Delta f, \Delta\tau) e^{J2\pi\tau\,\Delta f + j2\pi f\Delta\tau} d\Delta f\, d\Delta\tau$	
Power Impulse Response	$\sigma(\tau) = \int \sigma(\tau, f)\, df = \int R(\Delta f)\, e^{j2\pi\tau\Delta f} d\Delta f$	Frequency Spread B
Modified Power Impulse Response	$\sigma(\tau) = \int \sigma(\tau, f)\, df = \int \hat{R}(\Delta f) e^{j2\pi\tau\Delta f} d\Delta f$	Modified Frequency Spread $\hat{B}$
Echo Power Spectrum	$\sigma(f) = \int \sigma(\tau, f)\, d\tau = \int R(\Delta\tau)\, e^{j2\pi f\Delta\tau} d\Delta\tau$	Time Spread L
Modified Echo Power Spectrum	$\sigma(f) = \int \sigma(\tau, f)\, d\tau = \int \hat{R}(\Delta\tau)\, e^{j2\pi f\Delta\tau} d\Delta\tau$	Modified Time L Spread
Spatial Spectral Density Function	$\sigma(v, w) = \iint R(\Delta d, \Delta\tau) e^{j2\pi\tau\Delta d + j2\pi d\Delta\tau} d\Delta d\Delta\tau$	
Modified Spectral Density Function	$\sigma(v, w) = \iint \hat{R}(\Delta d, \Delta\tau) e^{j2\pi\tau\Delta d + j2\pi d\Delta\tau} d\Delta d\Delta\tau$	
Power Spectrum (Vraiable Antenna Separation)	$\sigma(w) = \int \sigma(\tau, d)\, dd = \int R(\Delta d) e^{j2\pi\tau\,\Delta d} d\Delta d$	Wavefront Frequency Spread F_D
Modified Power Spectrum (Variable Antenna Separation)	$\sigma(w) = \int \sigma(\tau, d)\, dd = \int \hat{R}(\Delta d)\, e^{j2\pi\,\tau\Delta d} d\Delta d$	Modified Wavefront Frequency Spread $\hat{F}_D$
Power Spectrum (Constant Antenna Separation)	$\sigma(v) = \int \sigma(\tau, d)\, d\tau = \int R(\Delta\tau) e^{j2\pi d\,\Delta\tau} d\Delta\tau$	Lateral Velocity Spread V
Modified Power Spectrum (Constant Antenna Separation)	$\sigma(v) = \int \sigma(\tau, d)\, d\tau = \int \hat{R}(\Delta\tau)\, e^{j2\pi d\Delta\tau} d\Delta\tau$	Modified Lateral Velocity Spread $\hat{V}$

correlation functions and spectral densities.

The correlation functions and spectral densities associated with the millimeter communication channel are defined by ensemble averages. However, an ensemble of received waveforms will never be available in practice and, therefore, these functions cannot be measured experimentally by ensemble averaging. Instead, time averages on individually received waveforms must be used. The interchange of ensemble and time averages is justified provided the ensemble is ergodic, in which case infinite time averages are entirely equivalent to ensemble averages.

A further compromise must be made in practice. Because of long-term equipment instabilities, the satellite passing over the horizon, etc., coherent waveform observations for indefinitely long periods cannot be made so that only finite, rather than infinite, time averages are feasible. The result of using finite duration observations is that an estimate of the correlation function or spectral density is obtained rather than the actual function. The estimate is subject to statistical variations and it is upon these variations that we focus our attention.

The estimation of correlation functions and spectral densities on the basis of finite duration observations has been treated in detail by Blackman and Tukey[57], Bello[58], Hannan[59], Watts[60] and Bendat[61]. Use of these studies has been made in writing this section.

When considering the estimation of the correlation function, $R(\tau)$, and the spectral density, $S(f)$, of a random process, the estimate should be made on the basis of an observed sample function of the process of duration T seconds. Let $R_T(\tau)$ and $S_T(f)$ be the estimates of $R(\tau)$ and $S(f)$, respectively. Let $x(t)$, $-\frac{T}{2} \leq t \leq +\frac{T}{2}$, be the observed sample function and considers (τ) to be real. The extension to complex $x(t)$ and the extension to the estimation of cross-correlation functions and cross-spectral densities are straightforward.

As an application of the model described in (Figure 7-4) to the estimation of a particular correlation function associated with the millimeter channel, consider the measurement of the Modified Echo-Correlation Function, $\hat{R}(\Delta\tau)$. In this case, x (t) corresponds to the envelope function $\left|\tilde{s}_r(f, t)\right|$. An estimate, $\hat{R}_T(\Delta\tau)$, is made of $\hat{R}(\Delta\tau)$ on the basis of an observation of $\left|\tilde{s}_r(f, t)\right|$ for T seconds. Estimates of the coherence time of the channel, $\hat{\tau}_c$, are obtained from $\hat{R}(\Delta\tau)$.

It should be noted that at this point we are assuming a noise free observation of the received process. This is done so that the measurement error arising solely because of the use of a finite duration sample can be determined. The effects of observation noise can be introduced subsequently.

7.3.1 Estimation of Correlation Functions

The correlation function to be estimated is given by the infinite time average:

$$R(\tau) = \lim_{T\to\infty} \frac{1}{T} \int_{-T/2}^{+T/2} x\left(t - \frac{\tau}{2}\right) x\left(t + \frac{\tau}{2}\right) dt \qquad (7\text{-}8)$$

On the basis of this definition, we shall develop a reasonable definition for the estimate, $R_T(\tau)$.

A typical observed sample, and its shifted versions, are shown in Figures 1a, 1b and 1c; the length of the observation interval for each is T seconds. The product to be averaged, $x\left(t - \frac{\tau}{2}\right) x\left(t + \frac{\tau}{2}\right)$, is shown in Figure 7-4d. Because of the shifts, the observation interval for the product has decreased to $T - |\tau|$ seconds, and this is the total length of averaging time which can be employed in the estimation of $R(\tau)$. It is clear, for this reason, that as τ increases a longer observation interval, T, is required to obtain a good estimate of $R(\tau)$. Moreover, for fixed T, it is not possible to estimate $R(\tau)$ accurately for τ greater than some

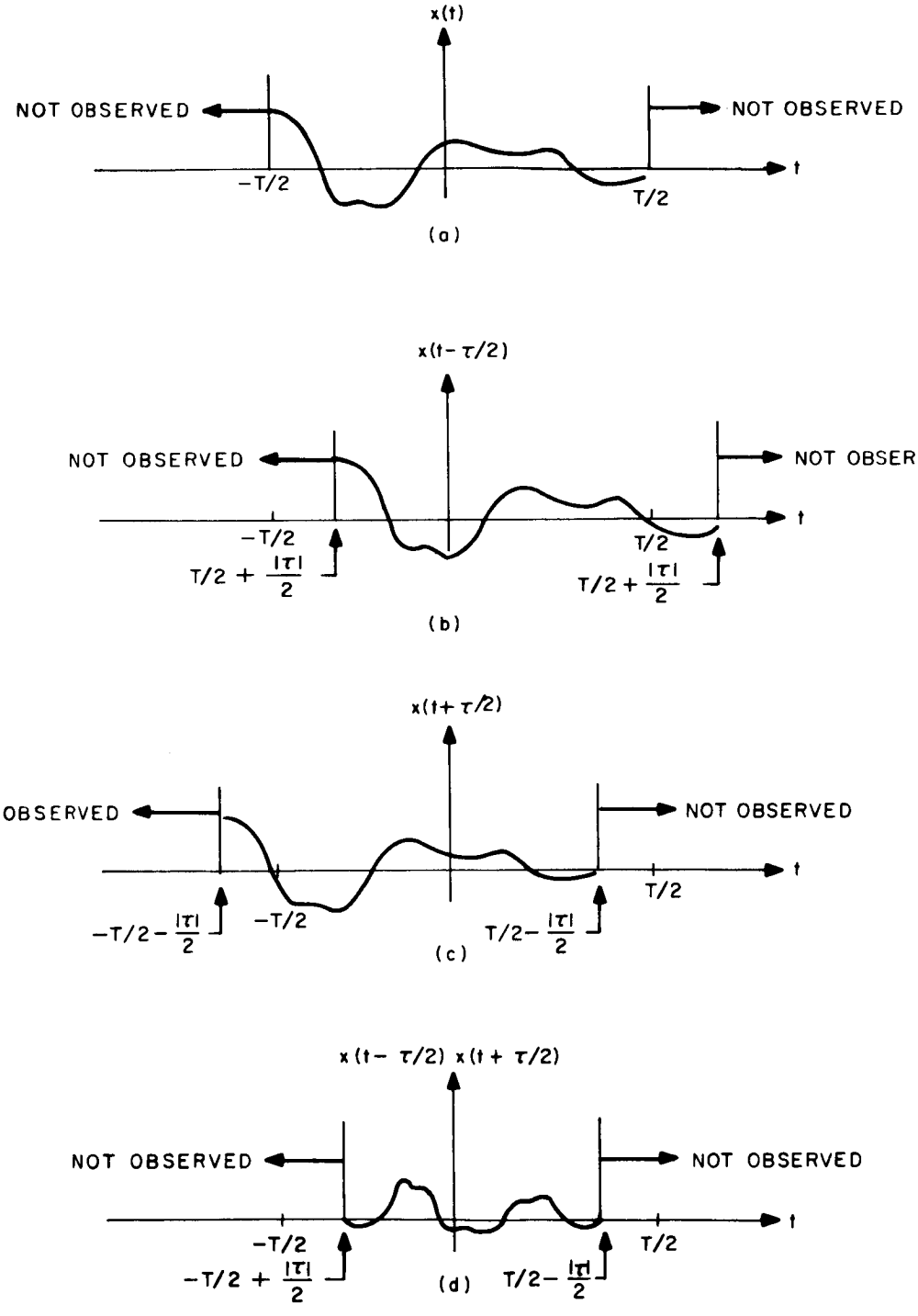

Figure 7-4 Observed Waveforms

fraction of T. The definition of the estimate, $R_T(\tau)$, which we shall employ is:

$$R_T(\tau) = \frac{1}{T - |\tau|} \int_{-\frac{1}{2}(T-|\tau|)}^{\frac{1}{2}(T-|\tau|)} x\left(t - \frac{\tau}{2}\right) x\left(t + \frac{\tau}{2}\right) dt \qquad (7\text{-}9)$$

This definition is reasonable because it makes full use of the available data and it reduces to the definition of $R(\tau)$ when the observation interval becomes arbitrarily large; that is, $\lim_{T \to \infty} R_T(\tau) = R(\tau)$.

To investigate the error, $e_T(\tau) = R_T(\tau) - R(\tau)$, consider an ensemble of observed processes, say, $x^{(1)}(t)$, $x^{(2)}(t)$, ... each of duration T. Corresponding to each observed process is an estimate and an error, $e_T^{(1)}(\tau)$, $e_T^{(2)}(\tau)$, ... These quantities are indicated in Figure 7-5. It is easily demonstrated that the expectation (ensemble average) of $R_T(\tau)$, has a zero average value. A measure of the spread of the error is provided by the error variance, defined by:

$$\sigma_T^2(\tau) = E\left[e_T^2(\tau)\right]$$

$$= E\left[R_T(\tau) - R(\tau)\right]^2$$

$$= E\left[R^2{}_T(\tau)\right] - R^2(\tau) \qquad (7\text{-}10)$$

Under the assumption that x (t) is a sample function from a Gaussian process, it is possible to derive an expression for $\sigma_T^2(\tau)$ in terms of $R(\tau)$. This is done in Appendix I, and the result is:

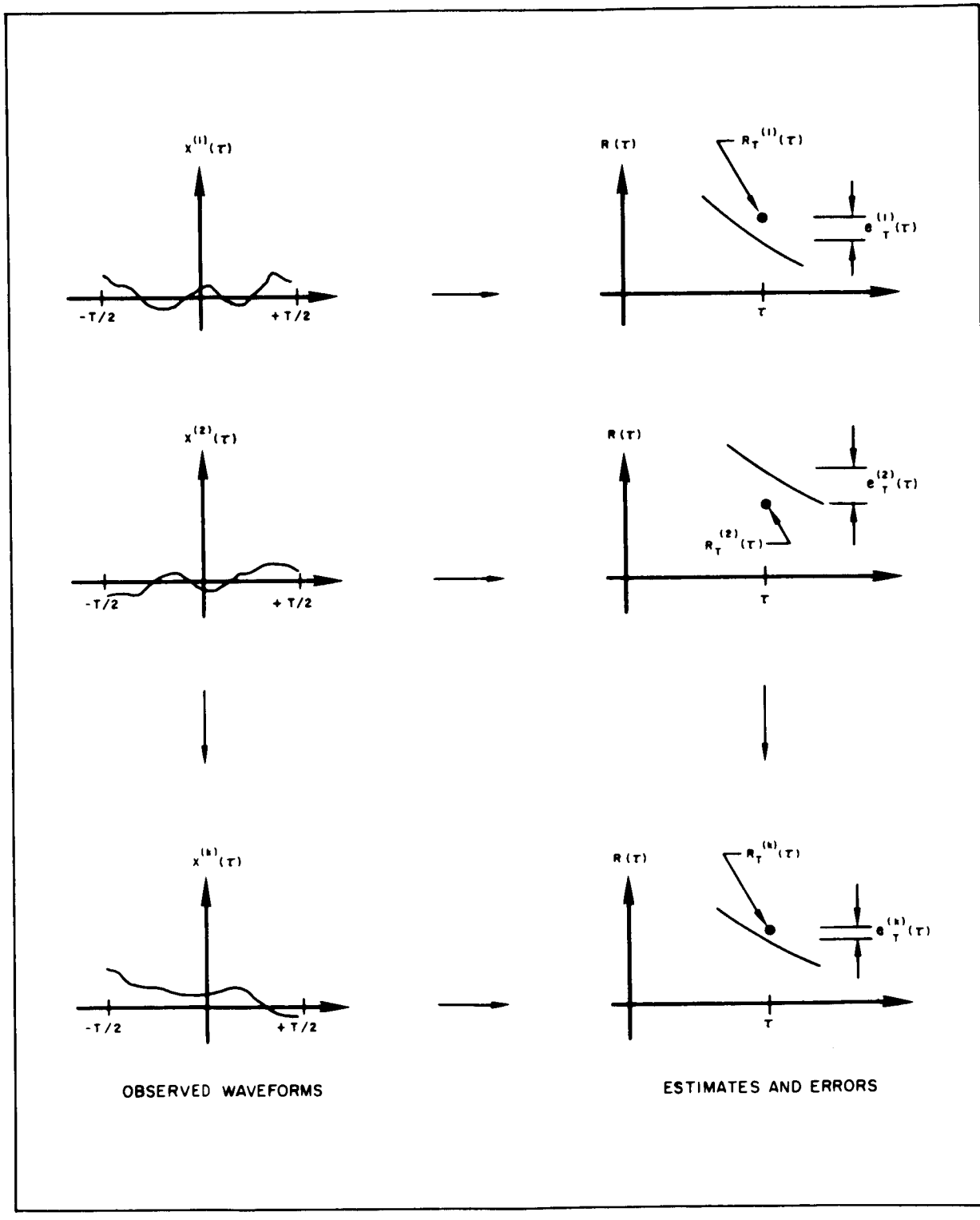

Figure 7-5 Ensemble of Observed Waveforms And Their Corresponding Estimates and Errors

$$\sigma_T^2(\tau) = \frac{1}{\left[T - |\tau|\right]^2} \int_{-(T-|\tau|)}^{+(T-|\tau|)} (T - |\tau| - |u|)\left[R^2(u) + R(u-\tau)\, R(u+\tau) - 2m_x^4\right] du \qquad (7\text{-}11)$$

where $m_x = E(x)$ is the expected value of x.

The assumption that x (t) is a sample function from a Gaussian process, essential for the derivation of Equation 7-11 needs to be discussed because in some instances the observed processes associated with the millimeter channel will be definitely non-Gaussian. As pointed out by Blackman and Tukey[57], the equation for the error variance obtained with the Gaussian assumption usually gives a good approximation to the error variance even for processes which are not closely Gaussian. Bendat[61], in discussing the measurement of correlation functions associated with Rayleigh processes, also indicates that the equation obtained with the Gaussian assumption is a good approximation. Thus, Equation 7-11 has practical value although it may not be strictly correct for some of the signals to be processed in the millimeter propagation experiment. The quantitative results to be derived below must be taken as approximations to what may actually occur in practice; the approximations will generally be good.

The error variance constitutes one measure of the quality of the estimate of $R(\tau)$. A second measure, which may be interpreted as a

signal-to-noise power ratio out of the correlator is defined by:

$$SNR_T(\tau) = \frac{R^2(\tau)}{\sigma_T^2(\tau)} = \frac{R^2(\tau)\left[T - |\tau|\right]^2}{\int_{-(T-|\tau|)}^{(T-|\tau|)} (T - |\tau| - |u|)\left[R^2(u) + R(u-\tau) - 2m_x^4\right]du} \quad (7\text{-}12)$$

$SNR_T(\tau)$ is a useful measure in practice because it can be easily related to a level of confidence for estimates based on an arbitrary sample function. In order to do this we assume that the Estimates $R_T^{(1)}(\tau)$, $R_T^{(2)}(\tau)$, ... form a Gaussian distribution with mean, $R(\tau)$, and variance, $\sigma_T^2(\tau)$. Then 68% of the estimates fall within one standard deviation, $\sigma_T(\tau)$, of the mean, $R(\tau)$; or 95% fall within two standard deviations, $2\sigma_T(\tau)$, of the mean, $R(\tau)$; etc. It follows that if we want 68% of the estimates to fall within ρ% of the mean, then we require:

$$\sigma_T(\tau) = 0.01\,\rho\,R(\tau); \quad (7\text{-}13)$$

of, if we want 95% to fall within ρ of the mean, then we require

$$2\,\sigma_T(\tau) = 0.01\,\rho\,R(\tau). \quad (7\text{-}14)$$

Equations 7-13 and 7-14 define a level of confidence of 68% and 95%, respectively, associated with ρ. Other confidence levels could be similarly defined. From these equations, it can be seen that a confidence level of 68% corresponds to a required signal-to-noise ratio of

$$SNR_T(\tau) = \left(\frac{100}{\rho}\right)^2 \quad (7\text{-}15)$$

or a confidence level of 95% to:

$$SNR_T(\tau) = 4\left(\frac{100}{\rho}\right)^2 \quad (7\text{-}16)$$

From Equations 7-15 and 7-16, it is seen that as we decrease ρ, requiring a more accurate estimate, or increase the desired level of confidence, we required a larger $SNR_T(\tau)$.

In examining $SNR_T(\tau)$ for a typical correlation function which might occur in practice, assume that $R(\tau)$ has the form:

$$R(\tau) = R(o)\, e^{\frac{-|\tau|}{\tau_c}} \tag{7-17}$$

where τ_c is the correlation time of the process. Since $\lim_{\tau \to \infty} R(\tau) = 0$, the process has a zero-mean; non-zero mean processes could be treated in a parallel fashion. For this correlation function, $\sigma_T^2(\tau)$ becomes:

$$\sigma_T^2(\tau) = \frac{R^2(o)}{2\left(\frac{T'}{\tau_c}\right)^2}\left[2\left(\frac{T'}{\tau_c}\right) - 1 + 2e^{-2\left(\frac{T'}{\tau_c}\right)} + \left\{\left[2\left(\frac{T'}{\tau_c}\right) - 1'\right]\left[2\left(\frac{\tau}{\tau_c}\right) + 1\right] - 2\left(\frac{\tau}{\tau_c}\right)^2\right\} e^{-2\left(\frac{\tau}{\tau_c}\right)}\right] \tag{7-18}$$

for $\tau > o$, and $T' = T - \tau > o$.

and the signal-to-noise ratio, $SNR_T(\tau)$, becomes:

$$SNR_T(\tau) = \frac{2e^{-2\left(\frac{\tau}{\tau_c}\right)\left(\frac{T'}{\tau_c}\right)^2}}{2\left(\frac{T'}{\tau_c}\right) - 1 + 2e^{-2\left(\frac{T'}{\tau_c}\right)} + \left\{\left[2\left(\frac{T'}{\tau_c}\right) - 1\right]\left[2\left(\frac{\tau}{\tau_c}\right) + 1\right] - 2\left(\frac{\tau}{\tau_c}\right)^2\right\} e^{-2\left(\frac{\tau}{\tau_c}\right)}} \tag{7-19}$$

for $\tau > o$, and $T' = T - \tau > o$

The dimensionless parameters:

$$\bar{T} = \frac{T}{\tau_c} \tag{7-20}$$

and

$\bar{\tau} = \frac{\tau}{\tau_c}$ are now introduced and the signal-to-the-noise ratio now becomes:

$$SNR_{\bar{T}}(\bar{\tau}) = \frac{2e^{-2\bar{\tau}}(\bar{T}-\tau)^2}{2\bar{T}-1+2e^{-2\bar{T}}+\left\{\left[2\bar{T}-2\bar{\tau}-1\right]-2\tau^{-2}\right\}e^{-2\bar{\tau}}} \tag{7-21}$$

A limiting case of interest exists when $\bar{T} >> \bar{\tau}$; that is, when the sample duration (measured in correlation times) is much greater than the time shift (also measured in correlation times).

In this limiting case $SNR_{\bar{T}}(\bar{\tau})$ becomes approximately:

$$SNR_T(\bar{\tau}) \simeq \frac{\bar{T}\,e^{-2\bar{\tau}}}{1+(2\bar{\tau}+1)e^{-2\bar{\tau}}} = \frac{\bar{T}\,e^{-2\bar{\tau}}}{z} \tag{7-22}$$

where k is a constant, $1 \leq z \leq 2$.

Equation 7-21 can be employed to obtain a useful set of curves. To illustrate this, we shall consider an example for which the approximate expression, Equation 7-22, is valid. Figure 7-6 shows plots of $SNR_{\bar{T}}(\bar{\tau})$ for $\bar{T} = 10^2$, $\bar{T} = 10^3$, and $\bar{T} = 2.7 \times 10^3$ and k = 2.

Example 1.

The curve is used in the following way. Suppose we wish to measure $R(\tau)$, over a range of values of τ equal to two correlation times, with a 68% level of confidence that all measured values are within 20% of their true value. From Equation 7-15 this is equivalent to specifying the following constraint on $SNR_{\bar{T}}(\bar{\tau})$:

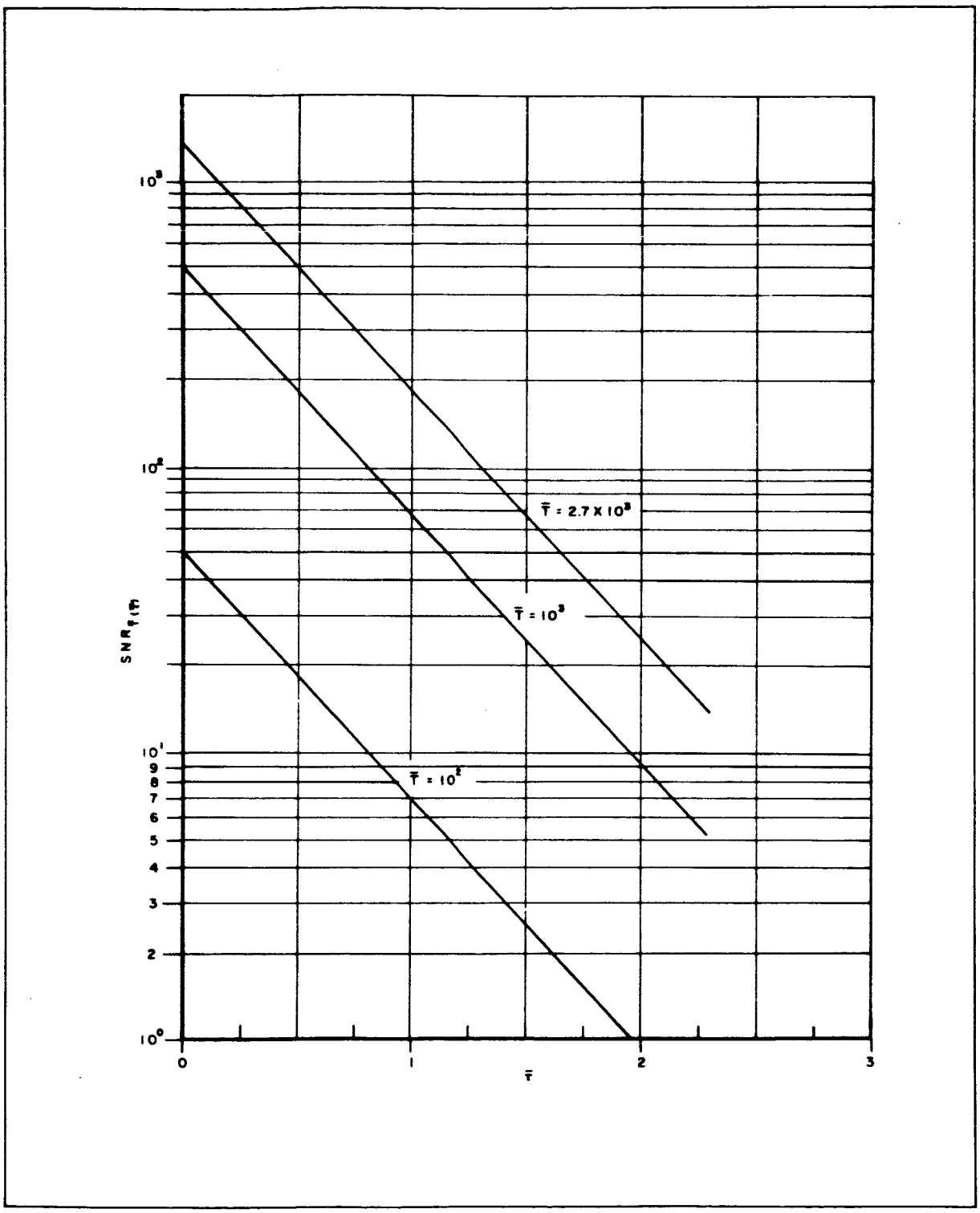

Figure 7-6 Plot of $SNR_{\bar{T}}(\bar{\tau})$

$$SNR_T(\tau) \geq 25 \quad \text{for } 0 \leq \bar{\tau} \leq 2$$

From Figure 7-6, we find that the observation time must be equal to, or greater than, 2.7×10^3 correlation times.

Example 2.

Another way in which the curves may be used is illustrated by the following. Suppose that a sample function having a duration of 10^3 correlation times is available and that we desire to estimate $R(\tau)$ with a 95% level of confidence that the measured values are within 20% of the true values. From Equation 7-16 we require $SNR_T(\bar{\tau}) \geq 100$. The range of $\bar{\tau}$ for which this constraint is satisfied can be determined from Figure 7-6 to be $0 \leq \bar{\tau} \leq 0.8$.

The processing of a single sample is now extended to include the processing of multiple records and the processing of sampled records.

Estimation of Correlation Functions with Multiple Records

The expressions for $\sigma^2_{\bar{T}}(\bar{\tau})$ and $SNR_{\bar{T}}(\bar{\tau})$, which are given by Equations 7-11 and 7-12, apply to the estimation of $R(\tau)$ on the basis of a single observation of length T. In practice, however, more than one observation will be made. We assume that these observations, denoted by $R_{k_r\bar{T}}(\bar{\tau})$, is given by the average

$$R_{k_r\bar{T}}(\bar{\tau}) = \frac{1}{k_r} \sum_{i=1}^{k_r} R_{\bar{T}}^{(i)}(\bar{\tau}) \qquad (7\text{-}23)$$

where $R_{\bar{T}}^{(i)}(\bar{\tau})$ is the estimate obtained from the i-th observation.

The error variance associated with $R_{k\bar{T}}(\bar{\tau})$ is given by:

$$\sigma^2_{k_r\bar{T}}(\bar{\tau}) = \frac{1}{k_r} \sigma^2_{\bar{T}}(\bar{\tau}) \qquad (7\text{-}24)$$

where $\sigma^2_{\bar{T}}(\bar{\tau})$ is given by Equation 7-11. The signal-to-noise ratio associated

with $R_{k_r T}(\tau)$ is

$$SNR_{k_r \bar{T}}(\bar{\tau}) = k_r SNR_{\bar{T}}(\bar{\tau}), \qquad (7\text{-}25)$$

where $SNR_T(\tau)$ is given by Equation 7-12.

Example 3.

In order to indicate how k_r enters into data-processing calculations, we reexamine the estimation problem of Example 2. Suppose k_r sample functions each of 10^3 correlation times duration are available and that we desire to estimate $R(\tau)$ with a 95% level of confidence that the measured values are within 20% of the true value. Now suppose that we want to measure $R(\tau)$ over a range of two correlation times. From Equation 7-16 we require $SNR_{k_r \bar{T}}(\bar{\tau}) \geq 100$. From Figure 7-6, it is found that $SNR_{k_r \bar{T}}(\bar{\tau}) = k_r SNR_{\bar{T}}(\bar{\tau})$, we need $\frac{100}{9} \simeq$ 12 records to achieve the desired confidence

Processing Sampled Records for the Estimation of Correlation Functions

It is desirable to obtain expressions for the estimation of correlation functions on the basis of sampled data, rather than continuous data because of the expected use of digital computer processing. For this purpose, we consider that the data available for the estimation of $R(\tau)$ is $x(k\Delta)$ for $k = o, 1, \ldots, N$. Δ is the distance between samples and there are $N+1$ samples of $x(t)$ in the observation interval $o \leq t \leq T$. (This interval is more convenient than $-\frac{T}{2} \leq t \leq \frac{T}{2}$ used in the continuous case.) Estimation of $R(\tau)$ is made at discrete points according to a slightly modified and sampled-data version of Equation 7-9:

$$R_N(\nu\,\Delta) = \frac{1}{N - |\nu|} \sum_{k=o}^{N-\nu} x\left[k\Delta \quad x \quad (k-|\nu|)\Delta\right] \qquad (7\text{-}26)$$

$\nu\Delta$, where ν is an integer, is the point on the correlation function where the estimate is desired.

The error variance, $\sigma_n^2(\nu\Delta)$, and the signal-to-noise ration, $SNR_N(\nu\Delta)$ are given by sampled-data versions of Equations 7-12 and 7-13, respectively:

$$\sigma_N^2(\nu\Delta) = \frac{1}{(N-|\nu|)^2} \sum_{k=-(N-|\nu|)}^{(N-1\nu 1)} (N-|\nu|-|k|)\Big\{ R^2(k\Delta) + R\Big[(k-\nu)\Delta\Big] R\Big[(k+\nu)\Delta\Big] - 2 m_x^4 \Big\} \quad (7\text{-}27)$$

and

$$SNR_N(\nu\Delta) = \frac{R^2(\nu\Delta)\big[N-|\nu|\big]^2}{\sum_{k=-(N-|\nu|)}^{(N-|\nu|)} (N-|\nu|-|k|)\Big\{ R^2(k\Delta) + R\Big[(k-\nu)\Delta\Big] R\Big[(k+\nu)\Delta\Big] - 2M_x^4 \Big\}} \quad (7\text{-}28)$$

As in the case of continuous processing, $SNR_N(\nu\Delta)$ can be very useful in determining the amount of data required in order to obtain a given level of confidence about the estimate. The sampling interval, Δ, or sampling rate, $1/\Delta$, now enters as an additional parameter.

For the typical correlation functions previously considered (Equation 7-17) $SNR_N(\nu\Delta)$ becomes:

$$SNR_N(\nu\Delta) = \frac{e^{-2\nu\Delta}(N-\nu)^2}{2}\left\{\frac{(N-\nu+1) + (N-2\nu+1)e^{-2\nu\Delta}}{1-e^{-2\overline{\Delta}}} - \frac{1-2e^{-2\Delta(N-\nu+1)}+e^{-2\nu\Delta}}{\left(1-e^{-2\Delta}\right)^2} + \nu e^{-2\nu\Delta}\left[N-\frac{3}{2}-\frac{1}{2}\right] - \frac{N-\nu}{2}\left[1+e^{-2\nu\Delta}\right]\right\}^{-1} \quad (7\text{-}29)$$

where $\overline{\Delta} = \frac{\Delta}{\tau_c}$, so that $\frac{1}{\overline{\Delta}}$ equals the number of samples in one correlation time.

When $N >> \nu$, Equation 7-29 approximately satisfied:

$$SNR_N(\nu\overline{\Delta}) \simeq \frac{Ne^{-2\nu\overline{\Delta}}\left[1-e^{-2\overline{\Delta}}\right]}{2\left[1+e^{-2\nu\overline{\Delta}} + \nu\left(1-e^{-2\overline{\Delta}}\right)e^{-2\nu\overline{\Delta}} - \frac{1}{2}\left(1+e^{-2\nu\overline{\Delta}}\right)\left(1-e^{-2\overline{\Delta}}\right)\right]} \quad (7\text{-}30)$$

If $\overline{\Delta}$ is also small:

$$SNR_N(\nu\overline{\Delta}) \simeq \frac{(N\Delta)e^{-2\nu\overline{\Delta}}}{1+(2\nu\overline{\Delta}+1)e^{-2\nu\overline{\Delta}}} \quad (7\text{-}31)$$

Comparison of Equation 7-31 with Equation 7-22 shows that as the sampling rate increases, such that $N\overline{\Delta} = \overline{T}$ and $\nu\overline{\Delta} = \overline{\tau}$, the performance of the continuous and sampled-data processing are nearly equal.

It is of interest to compare $SNR_N(\nu\Delta)$ and $SNR_T(\overline{\tau})$ as a function of the sampling rate, $\frac{1}{\Delta}$. We assume that the total observation time and the point on the correlation function to be estimated are the same for the two methods of processing; i.e., $N\overline{\Delta} = \overline{T}$ and $\nu\overline{\Delta} = \overline{\tau}$. A degradation factor due to finite sampling rates can be defined by:

$$D_{\bar{\tau}}\left(1/\bar{\Delta}\right) \equiv 10 \log_{10}\left[\frac{SNR_T(\bar{\tau})}{SNR_N(\nu\bar{\Delta})}\right] \qquad (7\text{-}32)$$

How much degradation occurs depends upon $\bar{\tau}$

It has been observed that as $\bar{\Delta} \rightarrow o$, the sampled-data processing and the continuous data processing are equally satisfactory. Thus, $\lim_{\Delta \rightarrow o} D_{\bar{\tau}}\left(1/\bar{\Delta}\right) = o$.

Assuming that $\bar{T} >> \bar{\tau}$, an expression for $D_{\bar{\tau}}\left(1/\bar{\Delta}\right)$ can be obtained by using Equations 7-22, 7-30 and 7-32, along with the restrictions that $N_{\bar{\Delta}} = \bar{T}$ and $\nu\bar{\Delta} = \bar{\tau}$.

$$D_{\bar{\tau}}\left(1/\bar{\Delta}\right) = 10 \log_{10}\left[\frac{\bar{\Delta}\left(1+e^{-2\bar{\Delta}}\right)\left(1+e^{-2\bar{\tau}}\right) + 2\bar{\tau}\, e^{-2\bar{\tau}}\left(1-e^{-2\bar{\Delta}}\right)}{\left(1-e^{-2\bar{\Delta}}\right)\left[1+(2\bar{\tau}+1)\, e^{-2\bar{\tau}}\right]}\right] \qquad (7\text{-}33)$$

Example 4.

The usefulness of Equation 7-33 will be deomonstrated by considering a particular value of $\bar{\tau}$; namely, $\bar{\tau} = o$. In this case Equation 7-33 reduces to:

$$D_o\left(1/\bar{\Delta}\right) = 10 \log_{10}\left[\bar{\Delta}\,\frac{1+e^{-2\bar{\Delta}}}{1-e^{-2\bar{\Delta}}}\right] \qquad (7\text{-}34)$$

$$= 10 \log_{10}\left[\bar{\Delta}\ \operatorname{ctnh}\bar{\Delta}\right]$$

where $\operatorname{ctnh}\bar{\Delta}$ is the hyperbolic cotangent of $\bar{\Delta}$. A plot of Equation 7-34 is shown in Figure 7-7. It is seen that a sampling rate above two or three samples per correlation time results in very little decrease in the degradation. On the other hand, lower sampling rates result in a significant increase in degradation.

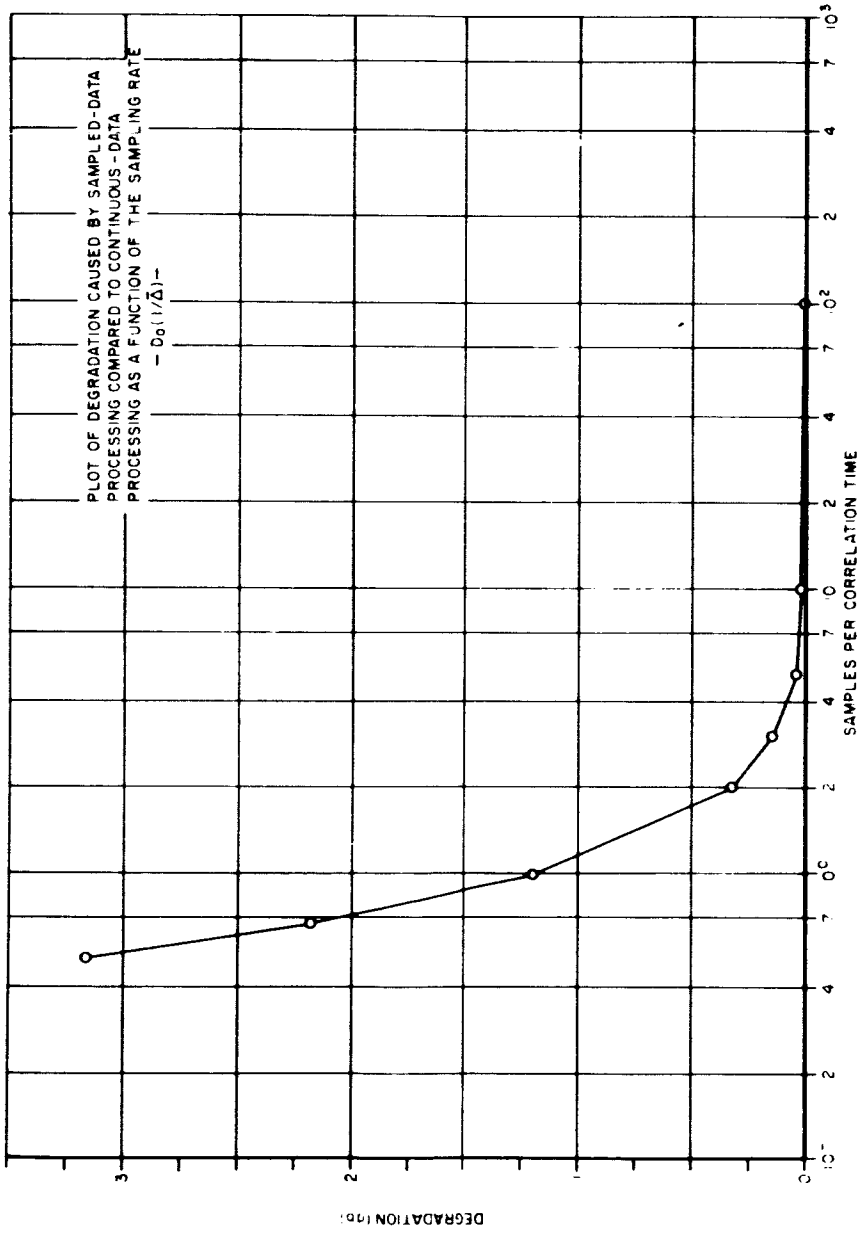

Figure 7-7 A Plot of Equation 7-34

Summary for the Measurement of Correlation Functions

An estimate of a point on a correlation function is obtained by implementing 7-9 and 7-23 in the case of continuous processing and Equations 7-26 and 7-23 in the case of sampled-data processing. The emplementations are shown schematically in Figures 7-8.
for the more general case of cross-correlation measurements based on a single sample length T.

The procedure for determining the amount of data which is required for a particular measurement is:

1) An approximate value for $\hat{\tau}_c$, the coherence time of the channel must be chosen. If no prior information is available, then a guess of $\hat{\tau}_c$ must be made. Subsequent to initial measurements, the guess can be appropriately modified.

2) Specify the level of confidence desired for the experiment. This, in turn, specifies the minimum allowable value for $SNR_{kT}(\tau)$. (Assuming at least 3 samples per correlation time are used, the signal-to-noise ratios for continuous and sampled processing are nearly equal.)

3) Specify a value of τ, or a range of values of τ, for which the estimate is desired. Use Figure 7-6 to determine k T, the required amount of data.

7.3.2 The Measurement of Power Density Spectra

This discussion on the measurement of power density spectra associated with the millimeter communication channel will be on the general problem of spectral density measurement with the results being applicable to the measurement of a particular spectral density listed in Table 7-1.

The spectral density, S (f), of a random process is to be estimated on the basis of an observed sample of the process of duration, T. Let $x(t)$, $-\frac{T}{2} \leq t \leq \frac{T}{2}$, be the observed sample function and $S_T(f)$ the estimate of S(f). As in the case of the estimation of correlation functions, we shall consider x(t) to be real.

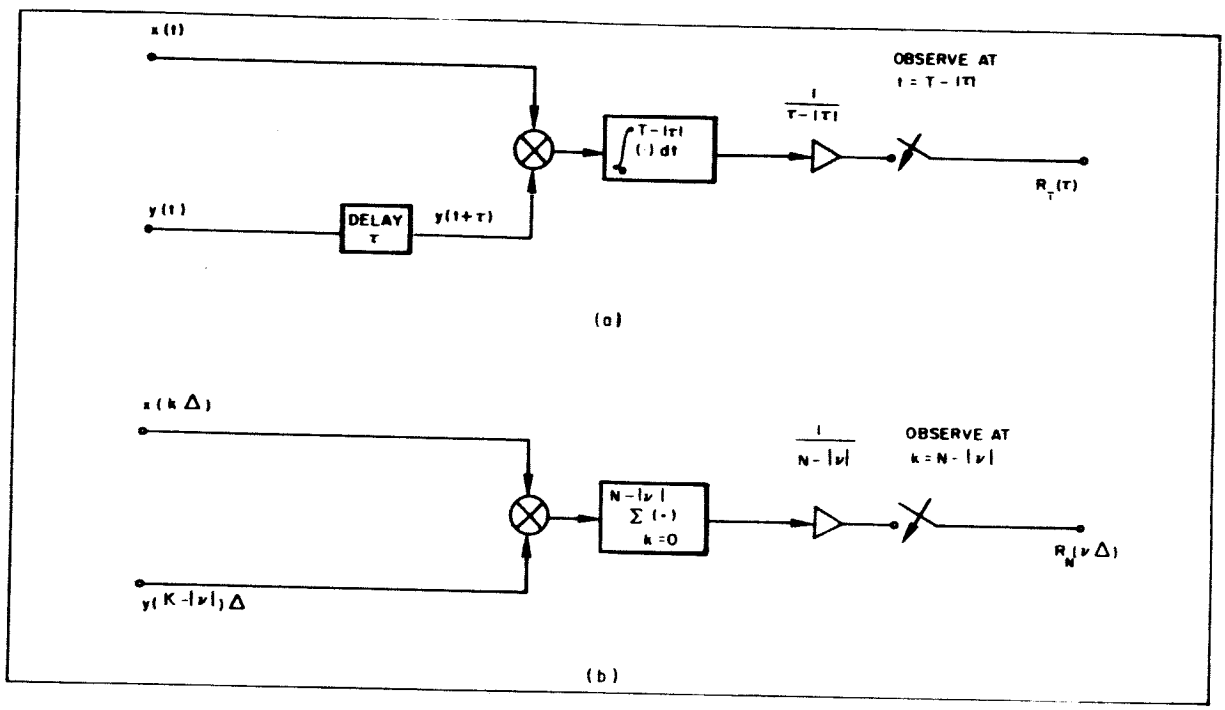

Figure 7-8 Implementation for Cross-correlation estimates based on (a) continuous records (b) on sampled-data records

Let X(f) be the Fourier transform of x(t) when it is assumed that x(t) is zero outside the observation interval; that is

$$X(f) = \int_{-T/2}^{T/2} x(t)\, e^{j2\pi ft}\, dt \qquad (7\text{-}35)$$

The total power in the observed waveform is given by:

$$P_{total} = \frac{1}{T} \int_{-T/2}^{T/2} x^2(t)\, dt$$

$$= \frac{1}{T} \int_{-\infty}^{\infty} \left| X(f) \right|^2 df \qquad (7-36)$$

The second expression follows from Parseval's theorem. Let $\left[P_T(f)\right]$ be defined by:

$$P_T(f) = \frac{1}{T} \left| X(f) \right|^2 \qquad (7-37)$$

$P_T(f)$ is the power density associated with the observed waveform and is frequently called the "periodogram." It can be easily demonstrated that $P_T(f)$ is an asymptotically unbiased estimate of S(f); i.e., $\lim_{T \to \infty} \left[E\, P_T(f)\right] = S(f)$.

The use of $P_T(f)$ as an estimate of S(f) is intuitively plausible and somewhat justified by the above observations. However, in spite of its apparent usefulness, $P_T(f)$ is not a consistent estimate of S(f) because the error variance, $E\left[P_T(f) - S(f)\right]^2$, does not approach zero as T becomes large. In fact, $P_T(f)$ is a very poor estimate of S(f) since, for any T, the standard deviation of the error is at least as large as the height of the spectrum at the point of interest[62], that is $E^{1/2}\left\{\left[P_T(f) - S(f)\right]^2\right\} \geq S(f)$.

It is possible to obtain a consistent estimate of a smoothed version of S(f). The modified estimate is defined by:

$$S_T(f) = \int P_T(f') \; W_i(f-f') \, df' \tag{7-38}$$

where $W_i(f)$ is called a window function and will be defined below. It is easily seen that

$$E\left[S_T(f)\right] = \int_{-\infty}^{\infty} S(f') \; W_i(f-f') \, df' \; . \tag{7-39}$$

and it can be shown[60] that the error variance is satisfied

$$E\left[S_T(f) - S(f)\right]^2 \simeq S^2(f) \; \frac{\tau_m}{T} \tag{7-40}$$

where τ_m is defined below.

A variety of window functions which have been used in practice are listed in Table 7-3; the function sinc x is defined by $\text{sinc } x = \frac{\sin \pi x}{\pi x}$. The width of $W_i(f)$ is approximately equal to $\frac{1}{\tau_m}$ and this quantity is defined to be the resolution in cps[58]. Windows $W_2(f)$ and $W_3(f)$ are most commonly used and are called hanning and hamming-windows, respectively.

From the definition of $S_T(f)$ and from Equation 7-40, it is observed that the "width" of $W_i(f)$ has a significant influence on the quality of $S_T(f)$ as an estimate of S(f). If $W_i(f)$ is an impulse, therefore having zero width, then $S_T(f) = P_T(f)$ and $E\left[S_T(f)\right] = S(f)$. At the opposite extreme, if $W_i(f)$ = constant, then $E\left[S_T(f)\right] \propto R(o)$, which is obviously a very poor estimate of S(f). From the point of view of estimating S(f) with good resolution, it is therefore desirable for $W_i(f)$ to have a "narrow" pulse-like shape. According to Equation 7-40, on the other hand, the rate at which the error variance approaches zero as a function of T is inversely dependent on the width of $W_i(f)$. The choice of the width of $W_i(f)$ is, therefore, based upon a trade-off between resolution and accuracy.

Blackman and Tukey[57] give four equations describing the trade-off between resolution and accuracy as a function of the duration of the observation. Associated with each equation is a level of confidence in the estimate; an 80% level of confidence means, for example, that each estimate has an 80% chance of having a specified accuracy. The equations are:

80% Confidence Level

$$T = \left[\frac{1}{2} + \frac{125}{(\text{spread})^2} + \frac{n}{3}\right] \Big/ (\text{resolution}) \qquad (7\text{-}41)$$

90% Confidence Level

$$T = \left[\frac{1}{2} + \frac{200}{(\text{spread})^2} + \frac{n}{3}\right] \Big/ (\text{resolution}) \qquad (7\text{-}42)$$

96% Confidence Level

$$T = \left[\frac{1}{2} + \frac{313}{(\text{spread})^2} + \frac{n}{3}\right] \Big/ (\text{resolution}) \qquad (7\text{-}43)$$

98% Confidence Level

$$T = \left[\frac{1}{2} + \frac{420}{(\text{spread})^2} + \frac{n}{3}\right] \Big/ (\text{resolution}) \qquad (7\text{-}44)$$

where n is the number of records, each of length T'; T, the total duration of the observation, satisfied $T = n\,T'$. "Spread" relates to the accuracy and is defined by:

$$\text{spread} = 10 \log \frac{100 + P_+}{100 - P_-} \text{ (db)} \qquad (7\text{-}45)$$

where P_+ and P_- define an error band around the true mean; the errors are contained within $+P_+$% and $-P_-$% of the true mean.* Equations 34a, b, c, and d are plotted in Figures 7-9, a, b, c & d, respectively for the special case of one record of length T. The use of the curves is illustrated by Example 5.

*The units of T are seconds, of resolution are cycles-per-second, and of spread are decibels.

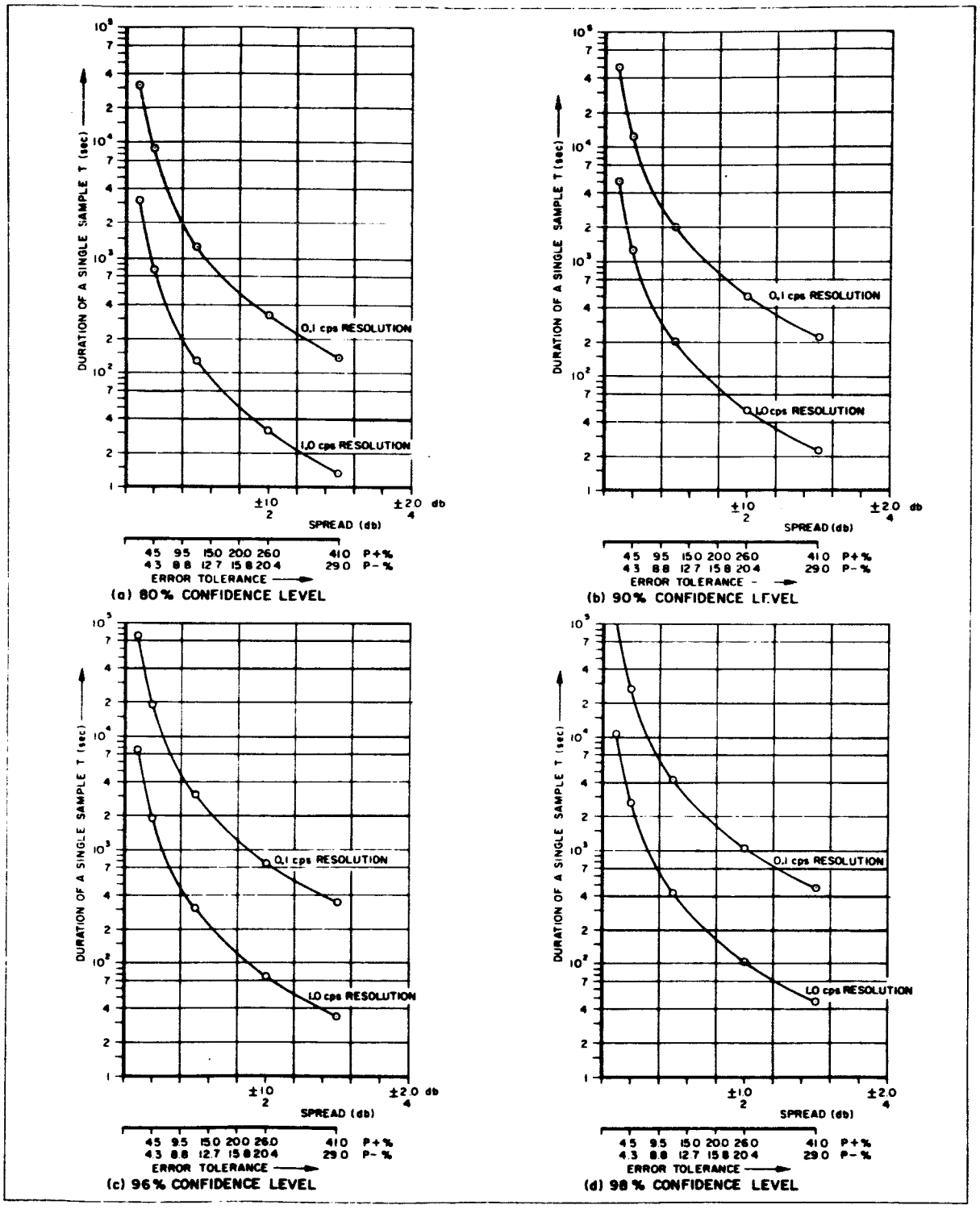

Figure 7-9. Sample Time Versus Error Tolerance

Example 5.

It is desired to have a 90% certainty that an estimate of the spectrum at a given frequency lies within ±0.5 db. (spread = 1 db.) of the true value. The desired resolution is 0.1 cps. What is the minimum required duration of a single observation? From Figure 7-9b, the required duration is at least 2000 seconds. (A single record of this duration is not easily obtained in practice, so that more than one record would be used.)

TABLE 7-3

WINDOW - LAG WINDOW PAIRS

$W_o(f) = 2\tau_m \operatorname{sinc} 2\tau_m f$	$W_o(\tau) = \begin{cases} 1 & \lvert\tau\rvert < \tau_m \\ 0 & \lvert\tau\rvert > \tau_m \end{cases}$
$W_1(f) = \tau_m \operatorname{sinc}^2 \tau_m f$	$W_1(\tau) = \begin{cases} 1 - \frac{\lvert\tau\rvert}{\tau_m} & \lvert\tau\rvert < \tau_m \\ 0 & \lvert\tau\rvert > \tau_m \end{cases}$
$W_2(f) = \tau_m \operatorname{sinc} 2\tau_m f + \frac{1}{2}\tau_m \left[\operatorname{sinc}(2\tau_m f+1) + \operatorname{sinc}(2\tau_m f-1)\right]$	$W_2(\tau) = \begin{cases} \frac{1}{2}(1+\cos\frac{\pi\tau}{\tau_m}) & \lvert\tau\rvert < \tau_m \\ 0 & \lvert\tau\rvert > \tau_m \end{cases}$
$W_3(f) = 1.08\,\tau_m \operatorname{sinc} 2\tau_m f + 0.46\,\tau_m \left[\operatorname{sinc}(2\tau_m f+1) + \operatorname{sinc}(2\tau_m f-1)\right]$	$W_3(\tau) = \begin{cases} 0.54+0.46\cos\frac{\pi\tau}{\tau_m} & \lvert\tau\rvert < \tau_m \\ 0 & \lvert\tau\rvert > \tau_m \end{cases}$

Relations Between $S_T(f)$ and $R_T(\tau)$

Before discussing the processing of sampled-data records, it is convenient to develop an alternate expression for $S_T(f)$. This can be done by investigating the relationship between $S_T(f)$ and $R_T(\tau)$. The processing for sampled-data records follows easily from the alternate expression.

The periodogram, $P_T(f)$, and the estimate of the correlation-function, $R_T(\tau)$, are shown in Appendix II to be related by:

$$P_T(f) = \int_{-T}^{T} \frac{T - |\tau|}{T} R_T(\tau)\, e^{j2\pi f\tau}\, d\tau$$

$$= \int_{-T}^{T} \frac{T - |\tau|}{T} R_T(\tau) \cos 2\pi f\tau \, d\tau \qquad (7\text{-}46)$$

It follows that $\frac{T - |\tau|}{T} R_T(\tau)$ and $P_T(f)$ are a Fourier transform pair. Based on this relation between $P_T(f)$ and $R_T(\tau)$, a relation between $S_T(f)$ and $R_T(\tau)$ can be easily obtained. Let $S_T(\tau)$ be the inverse Fourier transform of $S_T(f)$. Then it is clear from Equation 7-38 that

$$S_T(\tau) = \frac{T - |\tau|}{T} R_T(\tau)\, W_i(\tau) \qquad (7\text{-}47)$$

where $W_i(\tau)$ is the inverse transform of $W_i(f)$, as given in Table 7-3 and is called a lag window. Hence:

$$S_T(f) = \int_{\infty}^{\infty} S_T(\tau)\, e^{j2\pi f\tau} d\tau$$

$$= \int_{-\infty}^{\infty} \frac{T - |\tau|}{T} R_T(\tau)\, W_i(\tau)\, e^{j2\pi f\tau} d\tau \qquad (7\text{-}48)$$

$$= \int_{-\tau_m}^{\tau_m} \frac{T - |\tau|}{T} R_T(\tau)\, W_i(\tau) \cos 2\pi f\tau \, d\tau, \qquad (7\text{-}49)$$

where τ_m is defined in Table 7-3.

This relation provides an alternate method for implementing the estimation of $S_T(f)$. Namely, we first estimate $R(\tau)$, then use Equation 7-48 to obtain the estimate of S(f). Clearly, $R_T(\tau)$ is required only over the range of τ for which $W_i(\tau)$ is non-zero; that is, for $|\tau| < t_m$.

An inverse relationship can also be given which determines $R_T(\tau)$ in terms of $S_T(f)$. Of course, it is valid only for $|\tau| < \tau_m$. Using inverse transforms, we have, from Equation 7-48:

$$R_T(\tau) = W_i^{-1}(\tau) \frac{T}{T - |\tau|} \int_{-\infty}^{\infty} S_T(f)\, e^{j2\pi f\tau}\, df \quad \text{for } |\tau| < \tau_m \qquad (7\text{-}50)$$

Processing of Sampled Records for the Estimation of Spectral Densities

We now consider that the data available for the estimation of S(f) is $x(k\Delta)$ for $k = 0, 1, \ldots, N$. Δ is the distance between samples and there are N + 1 samples of x(t) in the observation interval $o \leq t \leq T$.

For the purpose of processing sampled data, it is convenient to use a sampled-data version of Equation 7-48 for the estimation of S(f). It is:

$$S_T(f) = \sum_{\nu = -\nu_m}^{\nu_m} \frac{N - |\nu|}{N} R_N(\nu\Delta)\, W_i(\nu\Delta)\, e^{j2\pi f\nu\Delta}, \qquad (7\text{-}51)$$

where $R_N(\nu\Delta)$ is defined by Equation 7-52:

$$R_N(\nu\Delta) = \frac{1}{N - |\nu|} \sum_{k=0}^{N} x(k\Delta)\, x\left[(k - |\nu|)\Delta\right] \qquad (7\text{-}52)$$

$R_N(\nu\Delta)$ is required for the range $|\nu| < \nu_m$ (where $t_m = \nu_m \Delta$.)

Summary for the Measurement of Spectral Densities

An estimate for a point on a spectral density is obtained by first estimating $R(\tau)$ then using either Equation 7-49 for continuous processing

or Equation 7-51 for sampled-data processing. The implementations are shown in Figures 7-10.

The initial steps in determining the amount of data required for the estimation of $S_T(f)$ are:

1. Specify the desired frequency resolution (in cycles per second).
2. Specify the confidence level and accuracy desired.
3. Use Equations 7-45a, b, c, and d, or Figures 7-9a, b, c, and d, to determine the amount of data required.

The next steps relate to the construction of an estimate of S(f) over a range of frequencies. The procedure is:

1. Specify the range of frequencies of interest.
2. Divide the range into intervals of width approximately equal to the resolution.
3. Estimate S(f) at a point within each of these intervals.

Several issues have been avoided in the brief review of the estimation of spectral densities given above. First, the relative merits of the

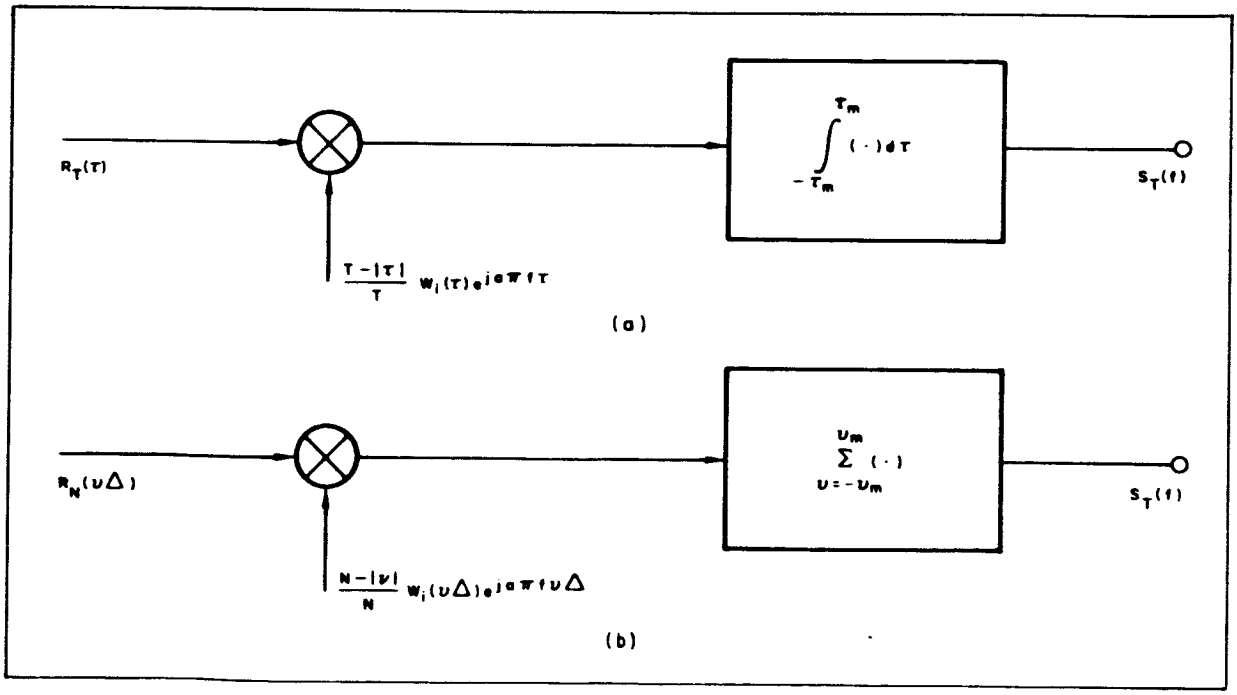

Figure 7-10 - Implementation for Spectral Density Estimates Based on (a) continuous records (b) sampled-data records

various window functions have not been examined. Secondly, the effect of aliasing errors has not been discussed. These and other issues are discussed in references 57 through 61.

7.4 Application of Measurements to the Initial Propagation Experiments

This section gives the procedure for applying the results of the preceding section to the measurement of correlation functions and spectral densities associated with the initial millimeter-wave propagation experiments. Because of difficulties in implementing the hardware required to perform the propagation experiments, it is wiser to restrict the initial tests, in many instances, to the determination of the modified functions. The results of the initial tests can be used for the intelligent design of more complex tests which define the complete function.

A number of test signals have been considered for probing the channel (Sections 4.1 and 5.3, First Quarterly Report). The AM waveform was selected for the initial experiments since it represents a reasonable compromise between the resulting data and the complexity of measurement equipment. While this section deals mainly with the application of the results from the AM waveform, the procedure for treating other waveforms is quite similar.

7.4.1 Channel Functions Derived from Initial Experiments

The channel functions most likely to be measured directly during the initial phase of the space-earth propagation experiments are:

a) Modified echo correlation function

b) Spaced-frequency correlation function

c) Modified echo power spectrum

d) Modified spatial correlation function

e) Modified spatial spectral density function

In addition to these channel functions, other functions derived

from radiometric data should be useful in investigating some of the causes of these channel functions. They are:

a) Sky temperature autocorrelation function

b) Sky temperature - Signal amplitude cross-correlation function

c) Sky temperature spatial correlation function

7.4.2 Application of the AM Test Waveform

Consider the processing of data received as a result of probing the channel with the AM test waveform discussed in the First Quarterly Report. This waveform consists simply of a sinusoidal carrier amplitude modulated by a single sinusoidal signal so as to produce two sidebands symmetrically positioned around the carrier at a distance equal to the modulation frequency. For the purpose of this discussion, we consider that the signals available for processing are the envelopes of the signals received at the carrier and each of the sideband frequencies. These signals are available for a finite observation interval of which we seek to determine minimum requirements. Of course, signals other than the envelopes are available for processing. These would be used to estimate channel quantities other than those considered here.

Let the signal be received at the carrier frequency be given by:

$$s_r(f_c:\tau) = \mathrm{Re}\left[\tilde{s}_r(f_c:\tau)\, e^{j2\pi f_c \tau}\right] \tag{7-53}$$

and at the two sideband frequencies by:

$$s_r(f_c \pm f_m:\tau) = \mathrm{Re}\left[\tilde{s}_r(f_c \pm f_m:\tau)\, e^{j2\pi (f_c \pm f_m)\tau}\right] \tag{7-54}$$

where Re [·] denotes the real part of the bracketed expression and $\tilde{s}_r(\cdot\ :\tau)$ are complex envelope functions. The frequencies f_c and f_m are the carrier and modulation frequencies, respectively. The three signals available for processing are then:

$\left| \tilde{s}_r(f_c + f_m : \tau) \right|$ = envelope of the signal received at the upper sideband frequency, $f_c + f_m$.

$\left| \tilde{s}_r(f_c : \tau) \right|$ = envelope of the signal received at the carrier frequency, f_c.

$\left| \tilde{s}_r(f_c - f_m : \tau) \right|$ = envelope of the signal received at the lower sideband frequency, $f_c - f_m$.

Measurement of the Modified Echo-Correlation Function

The complete echo-correlation function would not be measured because of the short term instability of the millimeter-wave frequency sources. Fade rates are expected to be one cycle per second or less for stationary or slow-moving satellites, so that coherent measurements are not terribly important in the initial experiments.

The modified echo-correlation function, $\hat{R}(\Delta\tau)$, has been defined by:

$$\hat{R}(\Delta\tau) = 2E\left[\left|\tilde{s}_r(f:\tau - \frac{\Delta\tau}{2})\right| \left|\tilde{s}_r(f:\tau + \frac{\Delta\tau}{2})\right|\right]$$

where $E[\cdot]$ denotes ensemble of infinite-time averaging, which are assumed to be equivalent. $\hat{R}(\Delta\tau)$ is the correlation function associated with the fluctuating envelope of the response of the channel to a single sinusoid. We seek to obtain an estimate of $\hat{R}(\Delta\tau)$, denoted by $\hat{R}_T(\Delta\tau)$, based on an observation of $\left[\tilde{s}_r(f_c:\tau)\right]$ for a duration of T seconds (the envelopes at the sideband frequencies could also be used).

In order to determine the amount of data required for the estimation of $\hat{R}(\Delta\tau)$ (that is, T), the following information is required:

1) an approximate value for $\hat{\tau}_c$, the coherence time of the channel. If no a priori information is available, then a guess of $\hat{\tau}_c$ must be made. Subsequent to initial measurements, the guess can be appropriately modified.

2) a value, or a range of values, of $\Delta\bar{\tau} = \Delta\tau/\overset{\Delta}{\tau}_c$ for which the estimate is desired.

3) a specification of the desired accuracy and level of confidence in the measurement. These can be conveniently expressed by the single quantity, $SNR_{\bar{T}}(\Delta\bar{\tau})$.

In the case of the millimeter channel, Lee and Waterman[61] have reported that $\hat{\tau}_c$ is slightly less than 1 second. Their measurements were made at 35 Gc over a 17 mile line-of-sight path. Therefore, an appropriate first guess would be: $\tau_c = 1$ sec.

Suppose we wish to estimate $\hat{R}(O)$, then $\Delta\bar{\tau} = O$. This quantity would be required for an estimate of the variance of the amplitude fading. Various accuracies and confidence levels, along with the corresponding values of $SNR_T(\Delta\tau)$, as determined from Equations 7-15 and 7-16 in Section 7.3.1, are tabulated in Table 7-4. The corresponding minimum observation times are also tabulated; these are determined from Figure 7-6 or from Equation 7-22 in Section 7.3.1. If, for example, a 95% confidence level and a ± 10% accuracy in the measurement of $\hat{R}(O)$ had been specified, then an observation interval of about 14 minutes duration would be required.

TABLE 7-4
FACTORS DETERMINED FROM EQUATIONS 7-15 AND 7-16

Confidence Level	Accuracy	$SNR_{\bar{T}}(\Delta\bar{\tau})$	Observation Time	
(%)	(±%)	(db)	(sec)	(min)
95	10	400	800	14.0
95	20	100	200	3.4
95	33	36	72	1.2
68	10	100	200	3.4
68	20	25	50	0.8

This lengthy requirement can be reduced in three ways:

a) take multiple observations and average (The total duration should still be about 14 min.);

b) reduce the specified level of confidence; and

c) reduce the specified accuracy.

As an example, a reduction of the confidence level to 68% for the same accuracy (± 10%) results in a reduction in the data required by a factor of four which is 3.4 minutes.

Measurement of the Spaced-Frequency Correlation Function

The measured space-frequency correlation function will not be complete, however, it is not modified in the same sense that the other functions are modified. The relative phase between the two sidebands can be measured. Therefore, the function will be sensitive to phase fluctuation. However, since only one pair of sidebands is used at any given time and since the choice of modulating frequency is limited, the correlation function will be based on a small number of points in the frequency domain.

The spaced-frequency correlation function, $R(\Delta f)$, has been defined by:

$$R(\Delta f) = 2E\left[\tilde{s}_r^*(f - \frac{\Delta f}{2}; \tau)\ \ \tilde{s}_r(f + \frac{\Delta f}{2}; \tau)\right]$$

$R(\Delta f)$ is the cross-correlation function associated with the fluctuating envelope of the response of the channel to two sinusoids separated by Δf cps. An estimate of $R(\Delta f)$ is obtained, based on the observation of $\tilde{s}_r(f_c + f_m; \tau)$ and $\tilde{s}_r(f_c - f_m; \tau)$ for a duration of T seconds. The information required for determining the value of T for the estimation of $R(\Delta f)$ is:

a) an approximate value for F_c, the coherence bandwidth of the channel;

b) a value, or a range of values, of $\Delta\bar{f} = {}^{\Delta f}/_{F_c}$ for which the estimate is desired; and

c) a specified accuracy and level of confidence.

In the case of the millimeter channel, approximate values of F_c apparently are not available. Consequently, a reasonable guess of F_c must be made for initial calculations. Subsequent to measurements, the guess can be modified. When a value of F_c is given, the procedure for determining T parallels that for determining T in the modified echo-correlation function.

Measurement of the Modified Spatial Correlation Function

The spatial correlation function will probably be modified because of the difficulties in providing a common receiver local oscillator signal to two separate antenna systems. Measurement of the complete function is certainly out of the question with moving satellites.

The modified spatial correlation function $\hat{R}(d)$, has been defined by:

$$\hat{R}(\Delta d, \Delta\tau) = 2E\left[\left|\tilde{s}_r(d-\frac{\Delta d}{2}, \tau)\right|\left|\tilde{s}_r(d+\frac{\Delta d}{2}, \tau+\Delta\tau)\right|\right]$$

where

$\left|\tilde{s}_r(d-\frac{\Delta d}{2}, \tau)\right|$ and $\left|\tilde{s}_r(d+\frac{\Delta d}{2}, \tau+\Delta\tau)\right|$ are the envelopes of the channel response to a single sinusoid at two receivers which are spatially separated a distance, Δd_s. $\hat{R}(\Delta d, \Delta\tau)$ is the cross-correlation function associated with the two fluctuating envelopes. For the spaced-antenna measurement, the estimate of $\hat{R}(\Delta d)$ is based on the observation of the two envelopes for a duration of T seconds.

As before, the required information for determining the minimum value of T is:

a) an approximate value for $\hat{D}_c$, the coherence distance and $\hat{T}_p$, the cross-coherence time;

b) a value, or a range of values, of $\Delta\bar{d} = \Delta d/D_c$ and $\Delta\tau = \Delta\tau/\hat{T}_p$ for which the estimate is desired; and

c) a specified accuracy and level of confidence.

In the case of the millimeter channel, Lee and Waterman (63) have reported that $\hat{D}_c$ is about 20 feet, (measured at 35 Gc over a 17 mile horizontal path) and Mondlock [64] has reported the $\hat{D}_c$ to be in the same range (measured at 50 Gc over a 10.4 mile horizontal over-water path with vertical baseline).

Suppose we want to estimate $\hat{R}(\Delta d, 0)$ over a range of Δd of 15 to 30 feet, (one correlation distance). Various accuracies and confidence levels, along with the corresponding values of $SNR_{\bar{T}}(\bar{d})$, are tabulated in Table 7-5 .

TABLE 7-5

ACCURACIES, CONFIDENCE LEVELS AND CORRESPONDING VALUES OF $SNR_1(d)$

Confidence Level (%)	Accuracy ($\pm$%)	$SNR_T(d)$ (db)	Observation Time (sec)	(min)
95	10	400	5700	95.0
95	20	100	750	12.5
95	33	36	270	4.5
68	10	100	650	12.5
68	20	25	180	3.0
68	33	9	67	1.1

The corresponding minimum observation times are also tabulated. These are determined from Figure 7-6 or from Equation 15 of Section 7.3.1. Time requirements can be reduced by:

(a) using multiple observations and averaging(total observation time remains the same),

(b) reducing the specified accuracy;

(c) reducing the level of confidence or

(d) reduce the range of d for which the estimate is required.

Measurement of the Modifed Echo-Power Spectrum

The modified echo-power spectrum, $\hat{\sigma}(f)$ is the spectral density associated with the fluctuating envelope of the response of the channel to a single sinusoid. We seek to estimate $\hat{\sigma}(f)$ based on an observation of $|s_r(f_c: \tau)|$ for a duration of T seconds.

In order to determine the amount of data required for the estamation of $\hat{\sigma}(f)$, the following information is required:

(a) the desired resolution;

(b) the desired level of confidence, and

(c) the desired accuracy.

When these quantities are specified, T can be determined from Equations 34a, b, c, and d, or from Figures 7-9a through 7-9d in Section 7.3.2.

As an example, suppose the desired resolution is 0.1 cps, the desired accuracy is $\pm$ 0.4db (or about $\pm$ 10%), and the desired level of confidence is 90%. Then, from Figure 7-9b, the minimum duration of a single observation is about 50 minutes. This requirement can be reduced by:

(a) taking multiple observations and averaging;

(b) requiring less resolution;

(c) reducing the level of confidence; or

(d) reducing the accuracy.

For example, if the accuracy requirement is reduced to ± 1 db (or about ± 23%) and all other requirements remain unchanged, the required duration is reduced to approximately 8 minutes.

7.4.3 Processing Radiometric Data

The three functions involving rediometric sky temperature data are processed in much the same manner as those for some of the channel functions.

Table 7-6 lists the three sky temperature functions and the corresponding channel functions which require the same mathematical approval for processing.

TABLE 7-6
SKY TEMPERATURE FUNCTIONS AND THEIR SIMILAR CHANNEL FUNCTIONS

Function Radiometric	Channel Function
SkyTemperature Autocorrelation	Modified Echo Correlation
Sky Temperature- Signal Amplitude Cross-Correlation Function	Modified Spaced Frequency Correlation
Sky Temperature Spatial Correlation	Modified Space Antenna Correlation

Section 8
BIBLIOGRAPHY

1. Nicholson, P. F., "Atmospheric Refraction Considerations for the 150-Foot Paraboloidal Antenna at Sugar Grove", NRL Memorandum Report 1599, April 1965.

2. Hoffman, L. A., Wintroub, H. J., Garber, W. A., "Propagation Observations in the 3.3 Millimeter-wave Window", Aerospace Corporation, Presentation to Millimeter-wave and Far Infrared Conference, Estes Park, Colorado, August 1965.

3. Manasse, R., "Maximum Angular Accuracy of Tracking a Radio Star by Lobe Comparison", IRE Transaction on Antennas and Propagation, January 1960.

4. Barton, D. A. "Radar System Analysis" Prentice-Hall EE Series, 1964.

5. Millman, G. H., "Atmospheric Effects on VHF and UHF Propagations" Proceedings IRE August 1958,

6. Smith, E. K., and Weintraub, S. "The Constants in the Equation for Atmospheric Refractive Index at Radio Frequencies" Proceedings IRE August 1953.

7. Barton, D. A. etal, "Report of the Ad Hoc Panel on Electromagnetic Radiation" Final Report, Air Force Systems Command Contract AF18 (600) - 1895, February 1963.

8. Westinghouse Electric Corporation, "Navigation Satellite System" Volume 1, January 1964.

9. Krassner, G.N. and Michaels, J.V., "Introduction to Space Communication Systems", McGraw-Hill Book Co., New York, 1965.

10. Kerr, R.B., "Propagation of Short Radio Waves", Mc-Graw Hill Book Co., New York, 1947.

11. Stock, J. and Keller, G., "Astronomical Seeing", in Telescopes, edited by Kuiper, G.P., and Middlehurst, B.M., The University of Chicago Press, Chicago, 1960.

12. Bergman, P.G., "Propagation of Radiation in a Medium With Random Inhomogeneities", Physical Review, Vol. 70, No.7, October 1950, pp. 486-493.

13. Tatarsky, V.I., "Wave Propagation in a Turbulent Medium", McGraw-Hill Book Co., Inc., New York, 1961. Also see, Krasilnikov, V.A., and Tatarsky, V.I., "Atmosphere Turbulence and Radio Wave Propagation", in Monograph on Radio Wave Propagation in the Troposphere, Elsevier Publishing Co., New York, 1962.

14. Maio, A.D., Castelli, J.P., and Harney, P.J., "Wavefront Distortion Due to Atmospheric Inhomogeneities", Proceedings 1964 World Conference on Radio Meteorology, Boulder, Colorado.

15. Hatch, R.W., Bennett, S.B., Kinzer, J.P., "Results of the Telstar System Communication Tests", Bell System Technical Journal, Vol. 42, No.4, Part 2, pp. 1561-1631, July 1963.

16. Barsis, A.P., Barghausen, A.F., and Kirby, R.S., "Studies of Within-the Horizon Propagation at 9,300 mc", IEEE Trans. on Antennas and Propagation, Vol. AP-11, No. 1, pp. 24-38, Jan. 1963.

17. Hathaway, S.D. and Evans, H.W., "Radio Attenuation at 11 kmc and Some Implications Affecting Relay System Engineering", Bell Systems Tech. Journal, Vol.38, pp. 73-97, Jan. 1959.

18. University of Texas, "Final Report on Research Activities in Millimeter Radiowaves and Geomagnetics", June 1, 1951 to 30 April 1961, Contract No. 375(01)NR-371-032.

19. Janes, H.B., and Thompson, M.C., Jr., "Errors Induced by the Atmosphere in Microwave Range Experiments", Radio Science Journal of Research NBS, Vol. 68D., No.11, November 1964.

20. Wickerts, S., "An Investigation of the Semi-Fine Structure of the Refractive Index Field in a Coastal Area", Proceedings 1964 World Conference on Radio Meteorology, Boulder, Colorado.

21. Fukushima, M. & Irige, H. "Preliminary Study of Spatial Distributions of Atmospheric Refractive Index from Aircraft Observations", Proceeding 1964 World Conference on Radio Meteorology, Boulder, Colorado.

22. Muchmore, R.B., & Wheelon, A.D., "Line-of-Sight Propagation Phenomena" Proc. IRE, Vol. 43, No. 10, pp. 1437-66, Oct. 1955.

23. Barrett, A.H., & Chung, V.K., "Method for the Determination of High Altitude Water-Vapor Abundance From Ground-Based Microwave Observations" Journal of Geophysical Research, Vol. 67, No. 11, October 1962.

24. Van Vleck, J.H., "The Absorption of Microwaves by Oxygen" and "The Absorption of Microwaves by Uncondensed Water Vapor", Physical Review, Vol. 71, No.7, pp. 413-33, April 1, 1947.

25. Lilley, A.E., & Meeks, M.L., "The Microwave Spectrum of Oxygen in the Earth's Atmosphere", Journal of Geophysical Research, Vol. 68, No. 6, March 15, 1963.

26. Browning, K.A., "Interaction of Two Severe Local Storms" in Proceedings 1964 World Conference on Radio Meteorology, Boulder, Colorado.

27. Copeland, J., Personal Communication.

28. Krotikiv, V.D., Troits kii, V.S., "Radio Emission and Nature of the Moon", Soviet Physics, Uspekhi, Published by American Institute of Physics, Vol. 6, No. 6, pp. 841-863, May-June 1964.

29. Battan, L.J., Radar Meteorology, The University of Chicago Press, Chicago, 1959.

30. Kessler, E., "Use of Radar Measurements for the Assessment of Areal Rainfall", U. S. Weather Bureau Presentation at 17th Session of WMO Executive Committee, Geneva, Switzerland, May 1965.

31. Atlas, D., "Angels in Focus," 1964 World Conference on Radio Meteorology, Boulder, Colorado.

32. Geotis, S. G., "On Sea Breeze Angels," 1964 World Conference on Radio Meteorology, Boulder, Colorado.

33. Doviak, R.J., Goldhirsch, J., and Lombardini, P.P., "Electromagnetic Scattering from Electron Irregularities in an Inhomogeneous Electron Density Distribution," Raytheon Company Report FR-65-275, 18 August 1965.

34. Ottersen, H., "Occurrence and Characteristics of Radar Angels Observed with a Vertically-Pointing Pulse Radar," 1964 World Conference on Radio Meteorology, Boulder, Colorado.

35. Plank, V.G., Atlas, D., and Paulsen, W.H., "The Nature and Detectability of Clouds and Precipitation as Determined by 1.25 cm Radar," Journal of Meteorology, Vol. 12, No. 4, August 1955.

36. Hitschfield, W. and Bordan, J., "Errors Inherent in the Radar Measurement of Rainfall at Attenuating Wavelengths," Journal of Meteorology, Vol. 11, No. 1, February 1954.

37. Brown, E. N. and Braham, R. R., Jr., "Precipitation Particle Measurements in Cumulus Congestion," Journal of Atmospheric Sciences, Vol. 20, No. 1, January 1963.

38. Braham, R. R., Jr., "Cumulus Cloud Precipitation as Revealed by Radar - Arizona 1955", Journal of Meteorology, Vol. 15, No. 1, February 1958.

39. Kerr, R. B., Propagation of Short Radio Waves, McGraw-Hill Book Co., New York, 1947.

40. Deir Mendjian, D., "Complete Scattering Parameters of Polydispersed Hydrometeors in the $\lambda 0.1$ to $\lambda 10$ cm Range," 1964 World Conference on Radio Meteorology, Boulder, Colorado.

41. Stroiton, A. W., Tolbert, C. W., "Factors Affecting Earth - Satellite Millimeter Wavelength Communications," IEEE Tranactions on Microwave Theory and Techniques, September 1963.

42. Jaffee, R. and Rechtin, E., "Design and Performance of Phase-Lock Circuits Capable of Near-Optimum Performance Over a Wide Range of Input Signal and Noise Levels," IRE Transactions on Information Theory, March 1955.

43. Viterbi, A. J., "Acquisition and Tracking Behavior of Phase-Locked Loops," J. P. L. External Publication #677.

44. Frazier, J. P., and Page, J., "Phase-Lock Loop Frequency Acquisition Study," IRE Transactions On Space Electronics and Telemetry, September 1962.

45. Turin, G. L., "Error Probabilities for Binary Symmetric Ideal Reception through Nonselective Slow Fading and Noise", IRE, September 1958.

46. Lindsey, W. C., "Error Probabilities for Rician Fading Multichannel Reception of Binary and N-ary Signals," IEEE Trans. on Information Theory, October 1964.

47. Lindsey, W. C., "Error Probabilities for Random Multichannel Reception of N-ary Signals," (original version of Reference 46).

48. Sunde, E. D., "Digital Troposcatter Transmission and Modulation Theory," The Bell System Technical Journal, Part 1, January 1964.

49. Sunde, E. D., "Intermodulation Distortion in Analog FM Troposcatter Systems," The Bell System Technical Journal, Part 2, January 1964.

50. Green, P. E., Jr., "Radar Astronomy Measurement Techniques," Technical Report 282, Lincoln Laboratory, M. I. T., Lexington, Mass. December 1962.

51. Gallager, R. G., "Characterization and Measurement of Time and Frequency Spread Channels", Technical Report 352, Lincoln Laboratories, M. I. T., Lexington, Mass.; April 1964.

52. Price, R. and Green P. E., Jr., "Signal Processing in Radar Astronomy-Communication via Fluctuating Multipath Media", Technical Report 234, Lincoln Laboratory, M. I. T., Lexington, Mass.; October 1960.

53. Kennedy, R., "Design Considerations for Ionospheric Channels" Raytheon Internal Memo. BL-1039; July 1964.

54. Lebow, I. L., et al., "The West Ford Belt as a Communications Medium" Proc. IEEE, 52, 5, pp. 543-563; May 1964.

55. Bello, P. A. and Nelin, B. D., "The Effect of Frequency Selective Fading on the Binary Error Probabilities of Incoherent and Differentially Coherent Matched Filter Receivers", IEEE Trans. on Communication Systems, pp. 170-186; June 1963.

56. Van Trees, H. L., Class Notes for Course 6.576, Massachusetts Institute of Technology; Spring 1965.

57. Blackman, and Tukey, J.W., "The Measurement of Power Spectra from the Point of View of Comminication Engineering", Dover Publications, Inc., New York, 1958.

58. Bello, P.A., "Measurement of the Complex Time-Frequency Channel Correlation Function", Radio Science Journal of Research NBS/USNCu-URSI, Vol. 68D, No. 10; October 1964.

59. Hannan, E.J., "Time Series Analysis", Methuen and Co., Ltd., London, and John Wiley and Sons, Inc. New York; 1960.

60. Watts, D.G., "Optimal Windows for Power Spectra Estimation", Mathematics Research Center, United States Army, University of Wisconsin, MRG Report No. 506; Sept. 1964. Also, available as ASTIA AD-607-822.

61. Bendat, J.S., "Principles and Applications of Random Noise Theory" John Wiley and Sons, Inc., 1958.

62. Davenport W. and Root, W., "Random Signals and Noise", McGraw-Hill Book Co., Inc. New York, 1958.

63. Lee, R. and Waterman, A., "Some Millimeter Wave Propagation Measurements" Stanford University, Contract AF04(695)-353, Project 2274.

64. Mondlock, A., "Observations of Short-Term Fading at Millimeter Wave-Length", Presentation to Boulder Millimeter Wave and Fan Infra-Red Conference, Estes Park, Colorado, August 1965.

Appendix I
DERIVATION OF AN EQUATION FOR ERROR VARIANCE

This appendix shows the derivation of Equation 7-10 in Section 7.3.1 for error variance. By definition, error variance is

$$\sigma^2_T(\tau) = E\left[R^2_T(\tau)\right] - R^2(\tau). \qquad \text{(I-1)}$$

The principle term we need to determine is $E\left[R^2_T(\tau)\right]$.

$$E\left[R^2_T(\tau)\right] = E\frac{1}{\left[T-\tau\right]^2} \int_{-1/2\left[T-|\tau|\right]}^{1/2\left[T-|\tau|\right]} \int x\left(t_1 - \frac{\tau}{2}\right) x\left(t_1 + \frac{\tau}{2}\right) x\left(t_2 - \frac{\tau}{2}\right) x\left(t_2 + \frac{\tau}{2}\right) dt_1\, dt_2 \qquad \text{(I-2)}$$

Interchange the order of expectation and integration. Using the assumption that x(t) is a sample function from a Gaussian process, as discussed in the main text, the expectation occurring within the integral is:

$$R^2(\tau) + R^2\left(t_1 - t_2\right) + R\left(t_1 - t_2 - \tau\right) R\left(t_1 - t_2 + \tau\right) - 2m_x^4$$

where $m_x = E(x)$ is the expected value of x. Making the change variable, $u = t_1 - t_2$, Equation I-2 becomes:

$$u = 1/2\left[T-|\tau|\right] - t_2$$

$$t_2 = 1/2\left[T-|\tau|\right]$$

$$E\left[R_T\,\tau\right] = R^2(\tau) - 2m_x^4 + \frac{1}{\left[T\,\tau\right]^2} \iint \left[R^2(\mu) + R(\mu-\tau)\, R(\mu+\tau)\right] d\mu\, dt_2$$

$$u_2 = -1/2\left[T - |\tau|\right] \quad t_2 \qquad \text{(I-3)}$$

$$t_2 = -1/2\left[T - |\tau|\right]$$

where the integration is over the area shown in Figure DS-8.

By interchanging the order of integration in Equation I-3, it is possible to obtain:

$$E\left[R_T^2(\tau)\right] = R^2(\tau) - 2m_x^4 + \frac{1}{\left[T-|\tau|\right]^2} \int_{-\left[T-|\tau|\right]}^{+\left[T-|\tau|\right]} \left[T-|\tau|-|\mu|\right]\left[R^2(u) + R(u-\tau)R(u+\tau)\right]du \qquad \text{(I-4)}$$

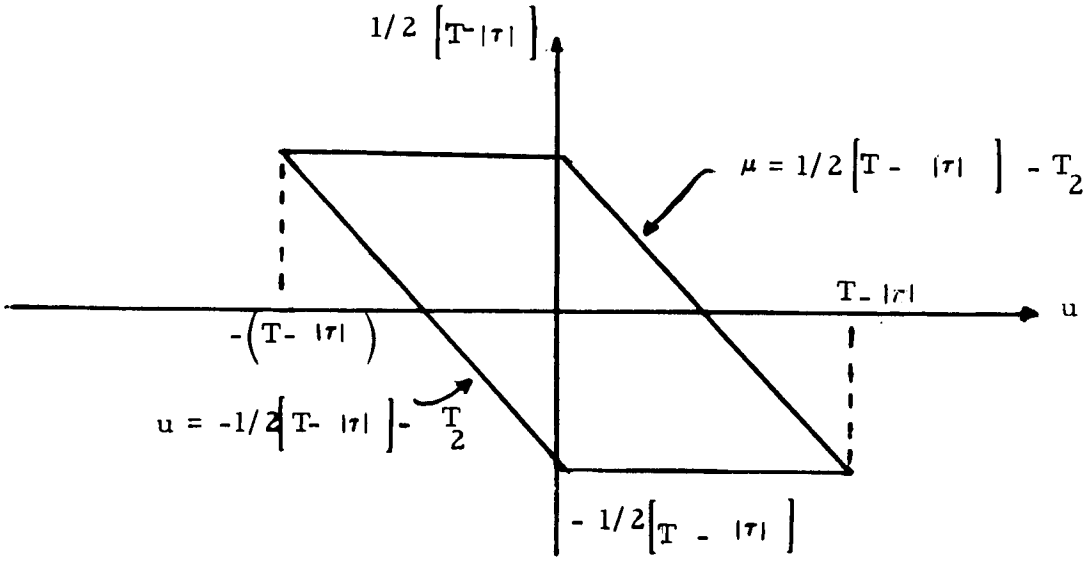

Figure DS-8 Area of Integration

Usine Equation I-1:

$$\sigma_T^2(\tau) = \frac{1}{\left[T-|\tau|\right]^2} \int_{-\left[T-|\tau|\right]}^{\left[T-|\tau|\right]} (T-|\tau|-|\mu|)\left[R^2(u) + R(u-\tau)\,R(u+\tau)\right]du - 2m_x^4 \qquad \text{(I-5)}$$

An alternate equation for $\sigma_T^2(\tau)$, which is obtained by using

$$\frac{1}{\left[T-|\tau|\right]^2}\int_{-\left[T-|\tau|\right]}^{\left[T-|\tau|\right]}(T-|\tau|-|\mu|)\,du=1,\ \text{is:}$$

$$\sigma_T^2(\tau)=\frac{1}{\left[T-|\tau|\right]^2}\int_{-\left[T-|\tau|\right]}^{\left[T-|\tau|\right]}(T-|\tau|-|\mu|)\left[R^2(u)+R(u-\tau)\,R(u+\tau)-2m_x^4\right]du \qquad (I\text{-}6)$$

Appendix II
DEFINITION OF THE PERIODOGRAM

This Appendix demonstrates that the periodogram (Equation 35, Section 7.3.2) is:

$$P_T(f) = \int_{-T}^{T} \frac{T - |\tau|}{T} R_T(\tau)\, e^{j2\pi f \tau} d\tau, \qquad \text{(II-1)}$$

where $P_T(f)$ is defined by Equation 30 in Section 7.3.2;

$$P_T(f) = \frac{1}{T} |X(f)|^2 \qquad \text{(II-2)}$$

and $R_T(\tau)$ is defined by Equation 2 in Section 7.3.1.

$$R_T(\tau) = \frac{1}{T - |\tau|} \int_{-\frac{1}{2}(T - |\tau|)}^{\frac{1}{2}(T - |\tau|)} x(t - \frac{\tau}{2})\, x(t + \frac{\tau}{2})\, dt \qquad \text{(II-3)}$$

The definition of (x(b) is given by Equation 28 from Section 7.3.2.

$$X(f) = \int_{-T/2}^{T/2} x(t)\, e^{j2\pi f t} dt \qquad \text{(II-4)}$$

With x(f) substituted into $P_T(f)$:

$$P_T(f) = \frac{1}{T} \int_{-T/2}^{T/2} \int_{-T/2}^{T/2} x(t_1,) x(t_2)\, e^{j2\pi f(t_1 - t_2)}\, dt_1\, dt_2 \qquad \text{(II-5)}$$

Let

$t_1 - t_2 = \tau$, then

$$P_T(f) = \frac{1}{T} \int_{t_2 = T/2}^{T/2} \int_{\tau = T/2 - t_2}^{T/2 - t_2} x(t_2 + \tau)\, x(t_2)\, e^{j2\pi f \tau}\, d\tau\, dt_2 \qquad \text{(II-6)}$$

By interchanging the order of integration (as in Appendix I), it is easy to obtain:

$$P_T(f) = \frac{1}{T} \int_{\tau=-T}^{o} \int_{t_2 = -T/2 - \tau}^{T/2} x(t_2 + \tau)\, x(t_2)\, e^{j2\pi f \tau}\, d\tau\, dt_2$$

$$+ \frac{1}{T} \int_{\tau=o}^{T} \int_{t_2 = -T/2}^{T/2 - \tau} x(t_2 + \tau)\, x(t_2)\, e^{j2\pi f \tau}\, d\tau\, dt_2 \qquad \text{(II-7)}$$

Let $t_2' = t_2 + \tau/2$

$$P_T(f) = \frac{1}{T}\int_{\tau=T}^{o}\int_{t_2'=-\frac{1}{2}(T+\tau)}^{\frac{1}{2}(T+\tau)} x(t_2+\tau/2)\, x\,(t_2-\tau/2)\, e^{j2\pi f\tau}\, d\tau\, dt_2$$

$$+\frac{1}{T}\int_{\tau=o}^{T}\int_{t_2'=-\frac{1}{2}(T-\tau)}^{\frac{1}{2}(T-\tau)} x(t_2+\tau/2)\, x\,(t_2-\tau/2)\, e^{j2\pi f\tau}\, d\tau\, dt_2' \qquad \text{(II-8)}$$

$$P_T(f) = \frac{1}{T}\int_{\tau=T}^{T}\int_{t_2'=-\frac{1}{2}(T-|\tau|)}^{\frac{1}{2}(T-|\tau|)} x(t_2+\tau/2)\, x\,(t_2-\tau/2)\, e^{j2\pi f\tau}\, d\tau\, dt_2' \qquad \text{(II-9)}$$

Then, using the definition for $R_T(\tau)$ given by Equation II-3,

$$P_T(f) = \int_{-T}^{T} \frac{T-|\tau|}{T} R_T(\tau)\, e^{j2\pi f\tau}\, d\tau \qquad \text{(II-10)}$$

Appendix III
SATELLITE ORBITAL CHARACTERISTICS

Symbols (See Figure III-1)

r = Earth's radius = 3440 nautical inches

h = satellite altitude - nautical miles

T = orbital period - minutes

γ = elevation angle - degrees

θ = coverage on earth's surface - degrees

α = vision angle - degrees

R_S = slant range - nautical miles

V = satellite velocity - miles/second

V_d = doppler velocity - miles/second.

Formulas

$$T = \frac{(r + h)^{3/2}}{2390} \quad \text{minutes}$$

$$V = \frac{250}{(r + h)\frac{1}{2}} \quad \text{nautical miles per second}$$

$$\text{Maximum } R_S = h^{1/2}(2r + h)^{1/2} \text{ nautical miles}$$

$$\theta = \cos^{-1}\left[\frac{r}{r + h} \cos \gamma\right] - \gamma \text{ degrees}$$

$$\alpha = 2 \sin^{-1}\left[\frac{r}{r + h}\right] \text{ degrees}$$

$$\text{Maximum } V_d = V \sin \frac{\alpha}{2} \frac{250\ r}{(r + h)\ 3/2} \text{ nautical miles per second}$$

Graphs

Figure III-1	Orbital Characteristics of a Satellite
Figure III-2	Periods of Circular Orbits
Figure III-3	Velocity of Circular Orbits
Figure III-4	Maximum Slant Range vs Satellite Altitude
Figure III-5	Coverage of Earth's Surface by a Satellite
Figure III-6	Vision Angle of a Satellite
Figure III-7	Slant Range vs Elevation Angle for a 6000 nmi Satellite
Figure III-8	Slant Range vs Elevation Angle for a Synchronous Satellite
Figure III-9	Coverage vs Elevation Angle for 6000 nmi Synchronous Altitude Satellites
Figure III-10	Vision Angle vs Elevation Angle for 6000 nmi and Synchronous Altitude Satellites
Figure III-11	Ground Range Versus Ground Station Latitude for a Synchronous Satellite
Figure III-12	Elevation Angle Versus Longitude Difference between Synchronous Satellite and Ground Station for various Ground Station Latitudes.

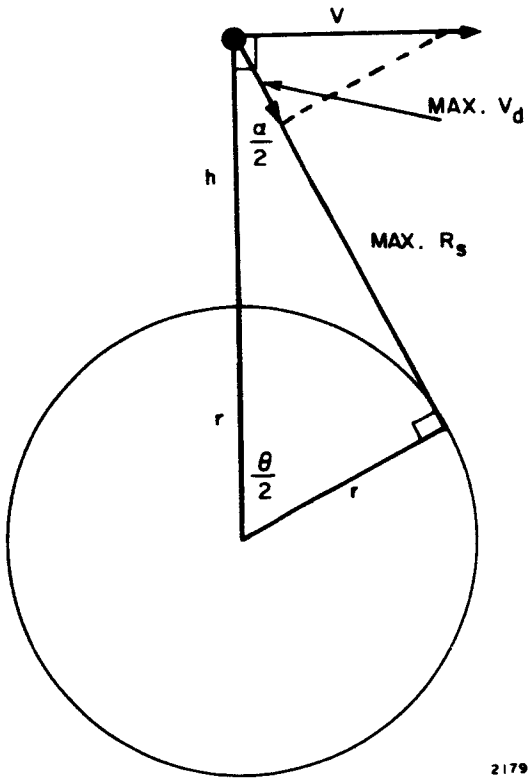

Figure III-1 Orbital Characteristics of a Satellite

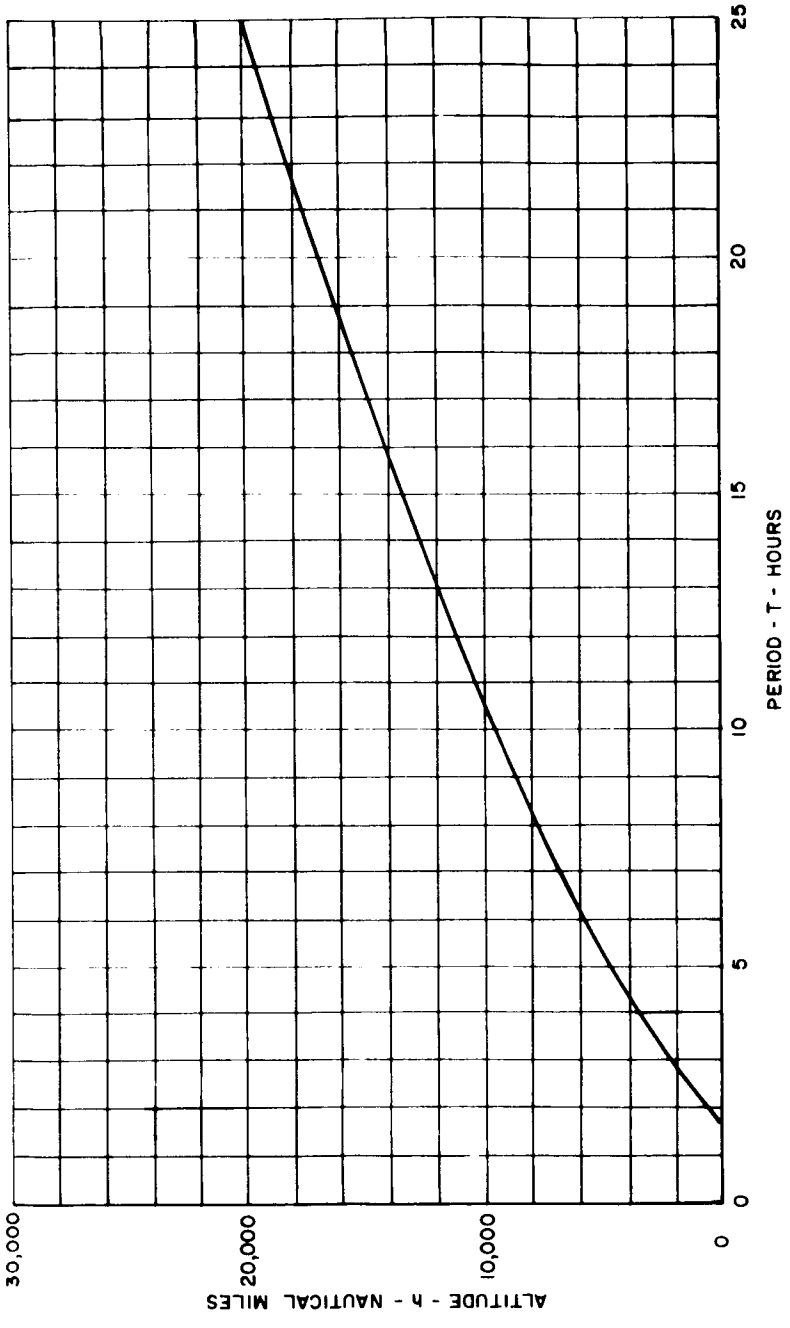

Figure III-2 Periods of Circular Orbits

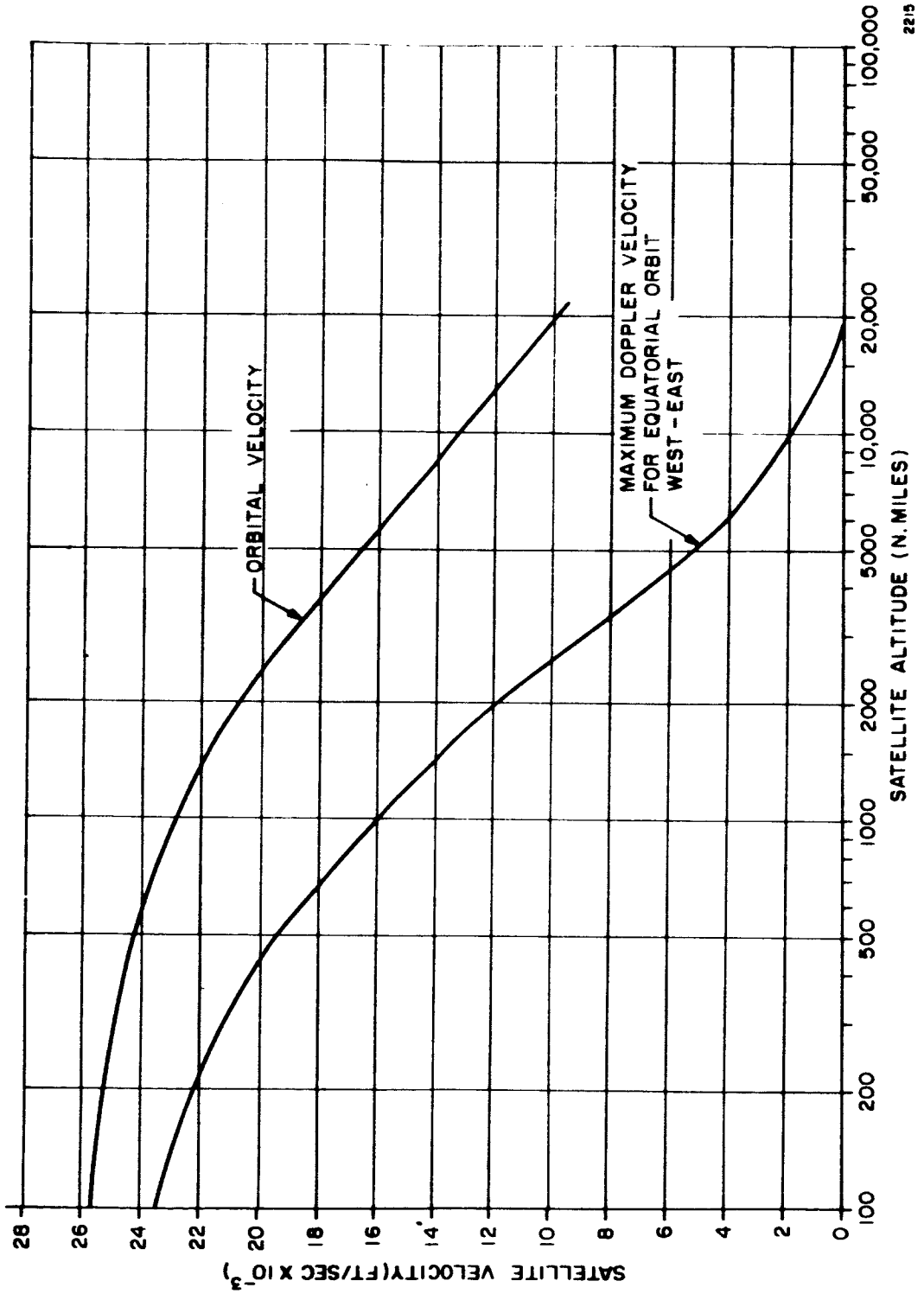

Figure III-3 Velocity of Circular Orbits

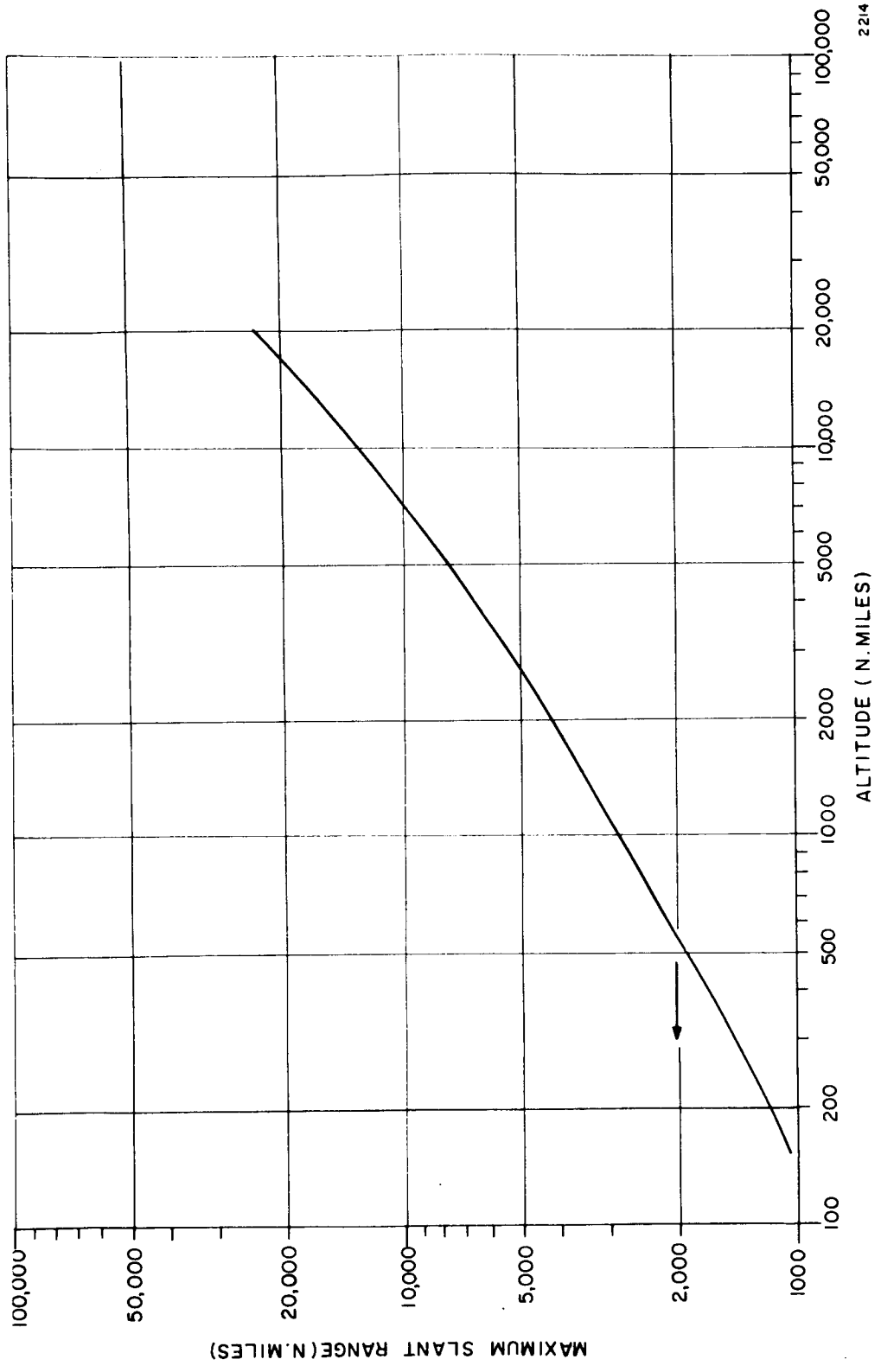

Figure III-4 Maximum Slant Range vs Satellite Altitude

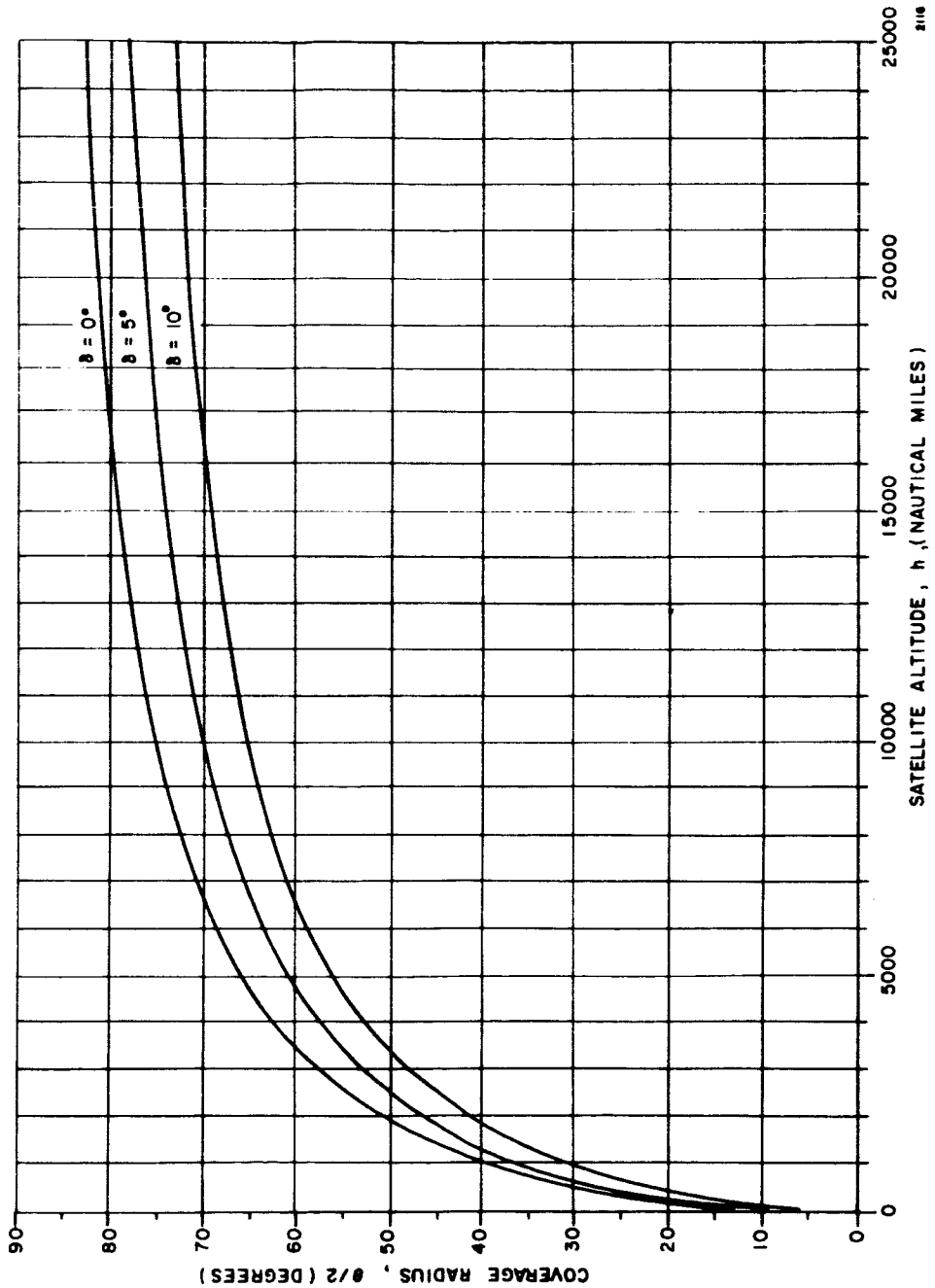

Figure III-5 Coverage of Earth's Surface by a Satellite

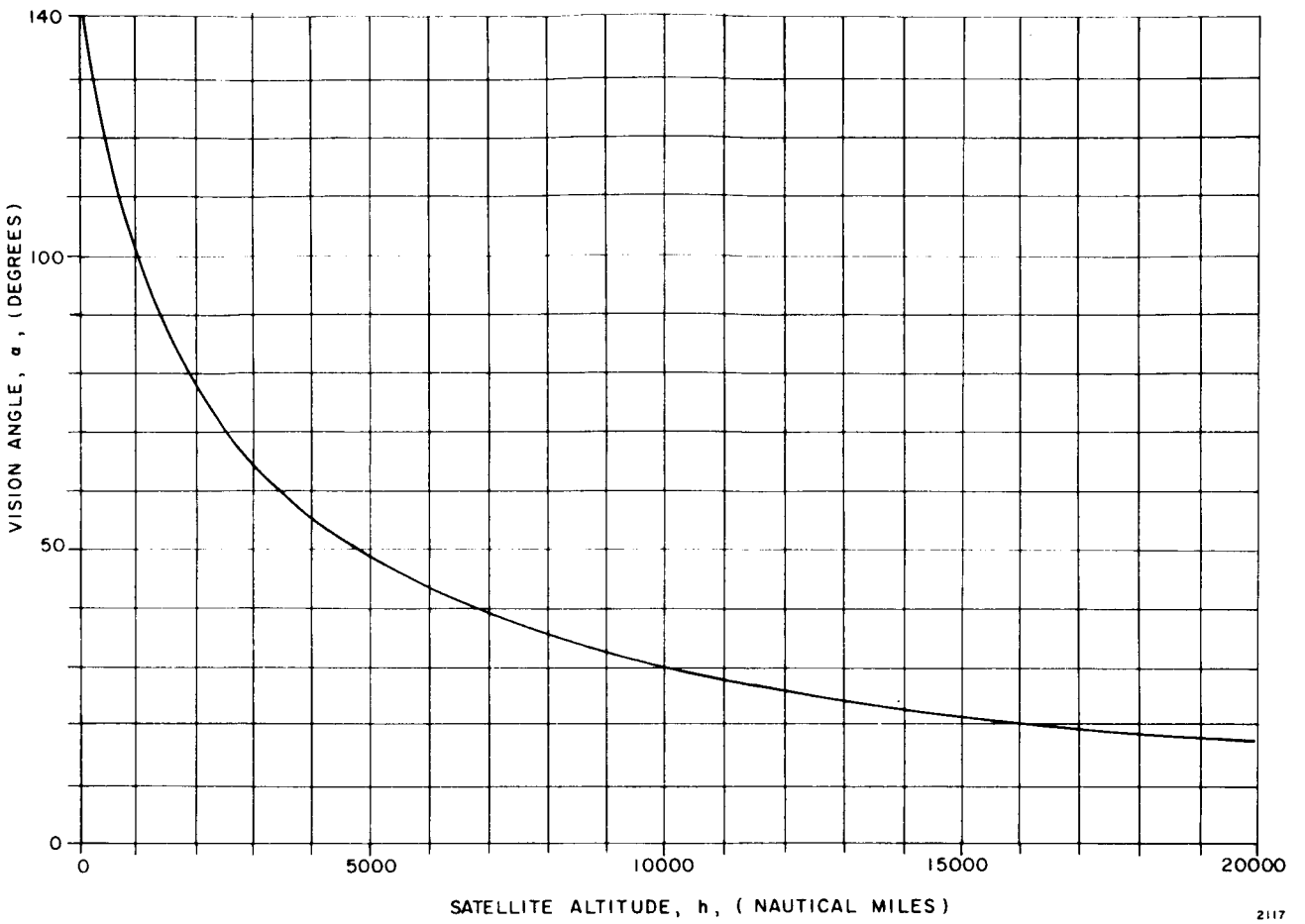

Figure III-6 Vision Angle of a Satellite

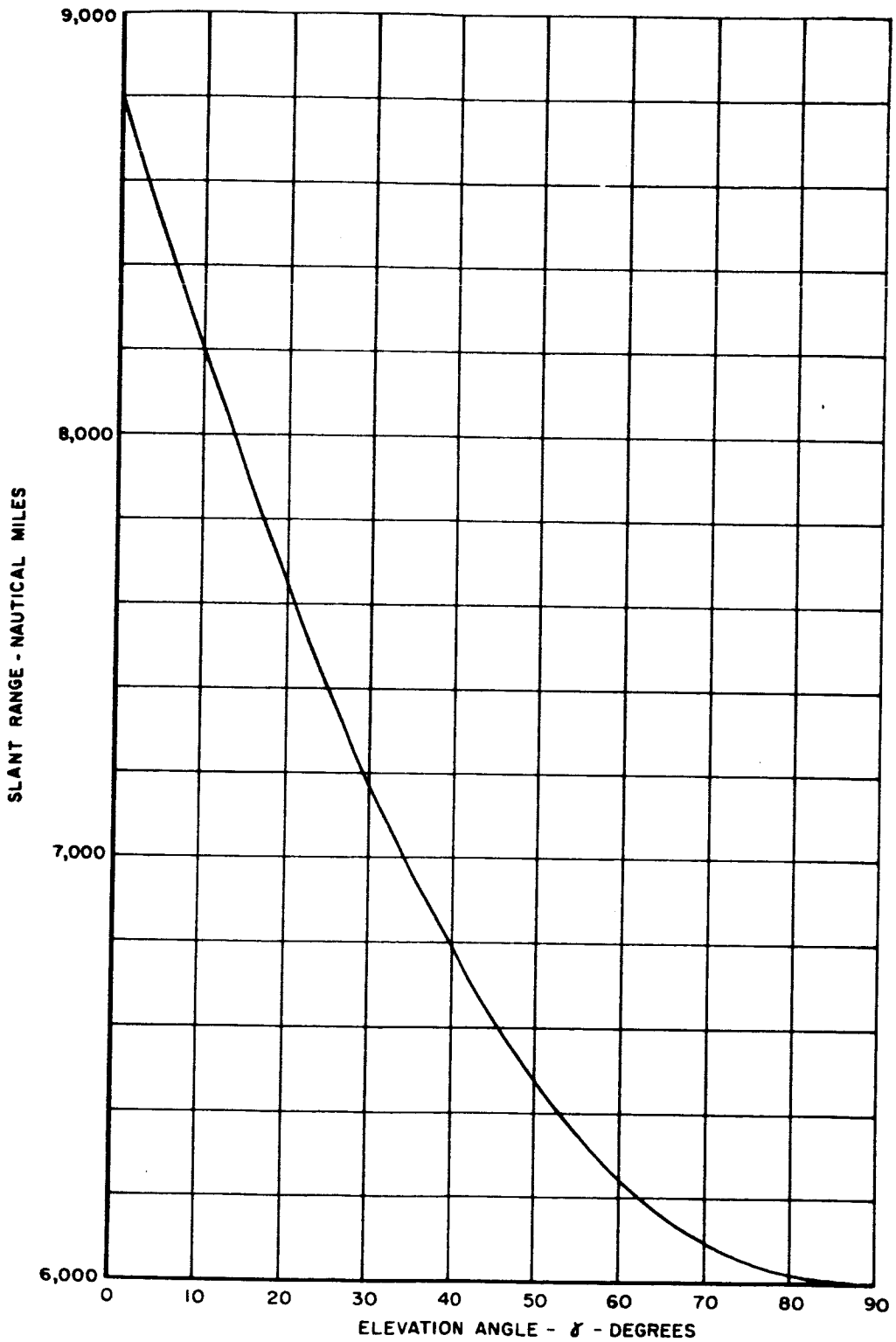

Figure III-7. Slant Range vs Elevation Angle for a 6000 nmi Satellite

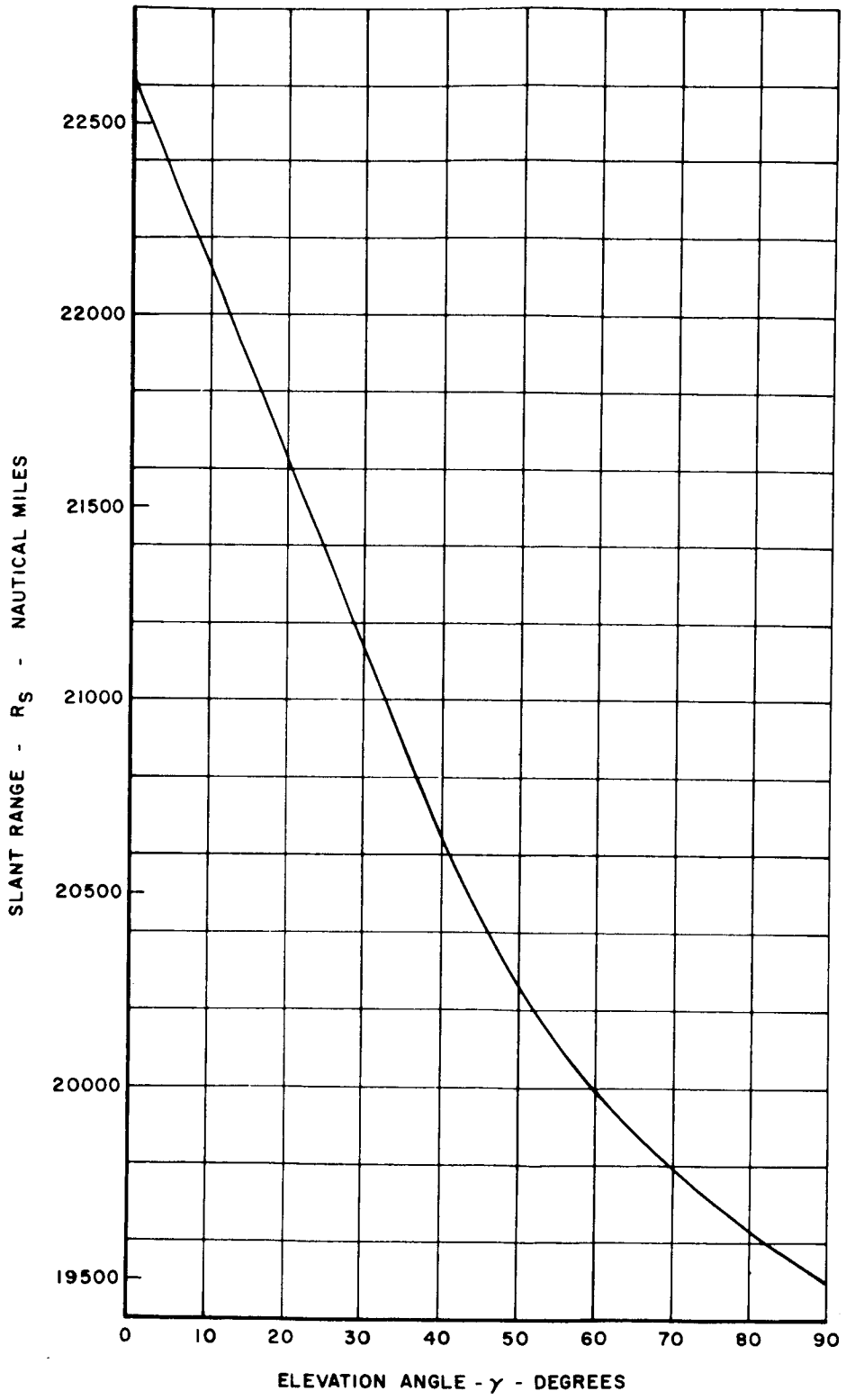

Figure III-8. Slant Range vs Elevation Angle for a Synchronous Satellite

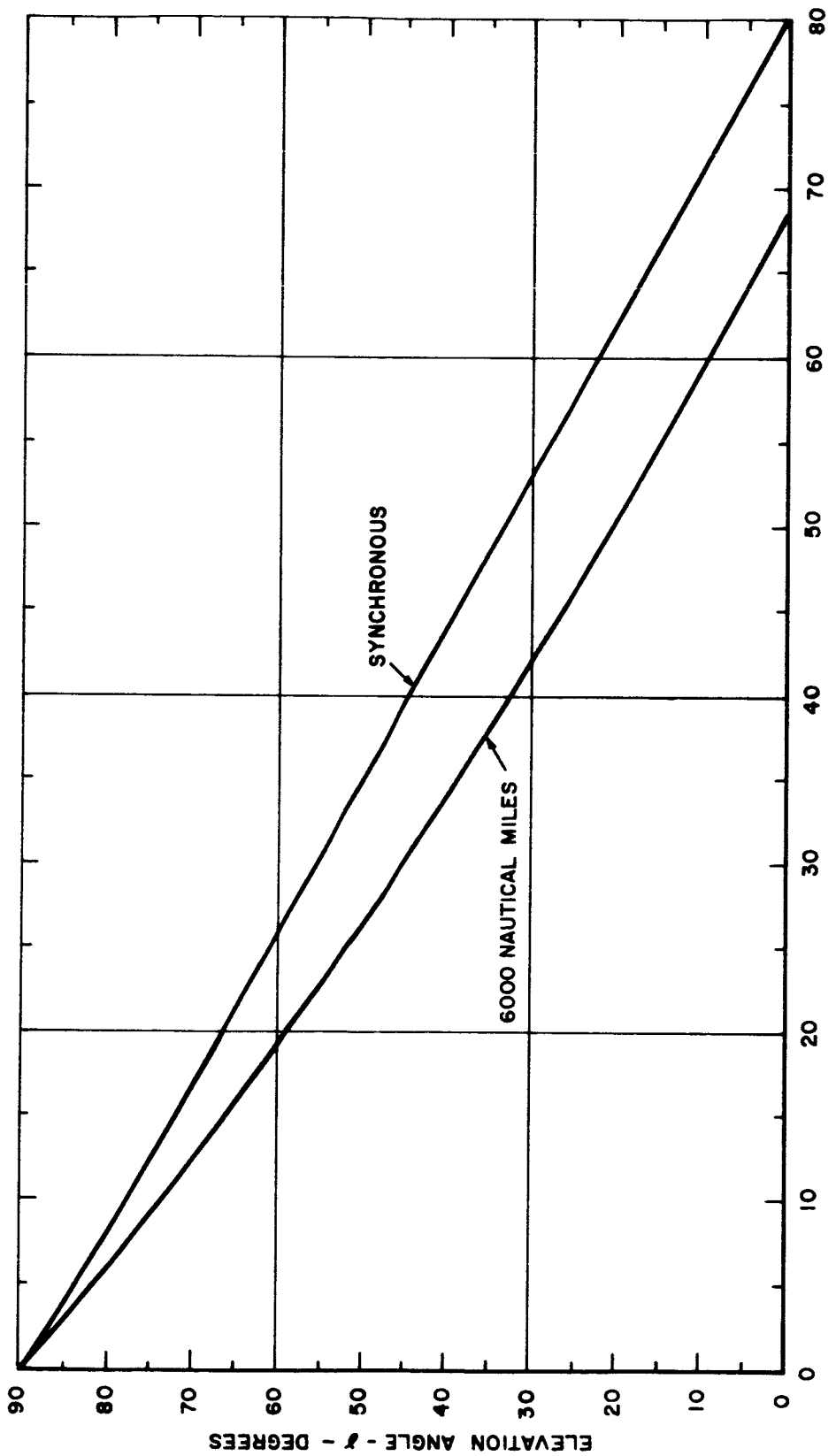

Figure III-9 Coverage vs Elecation Angle for 6000 nmi Synchronous Altitude Satellites

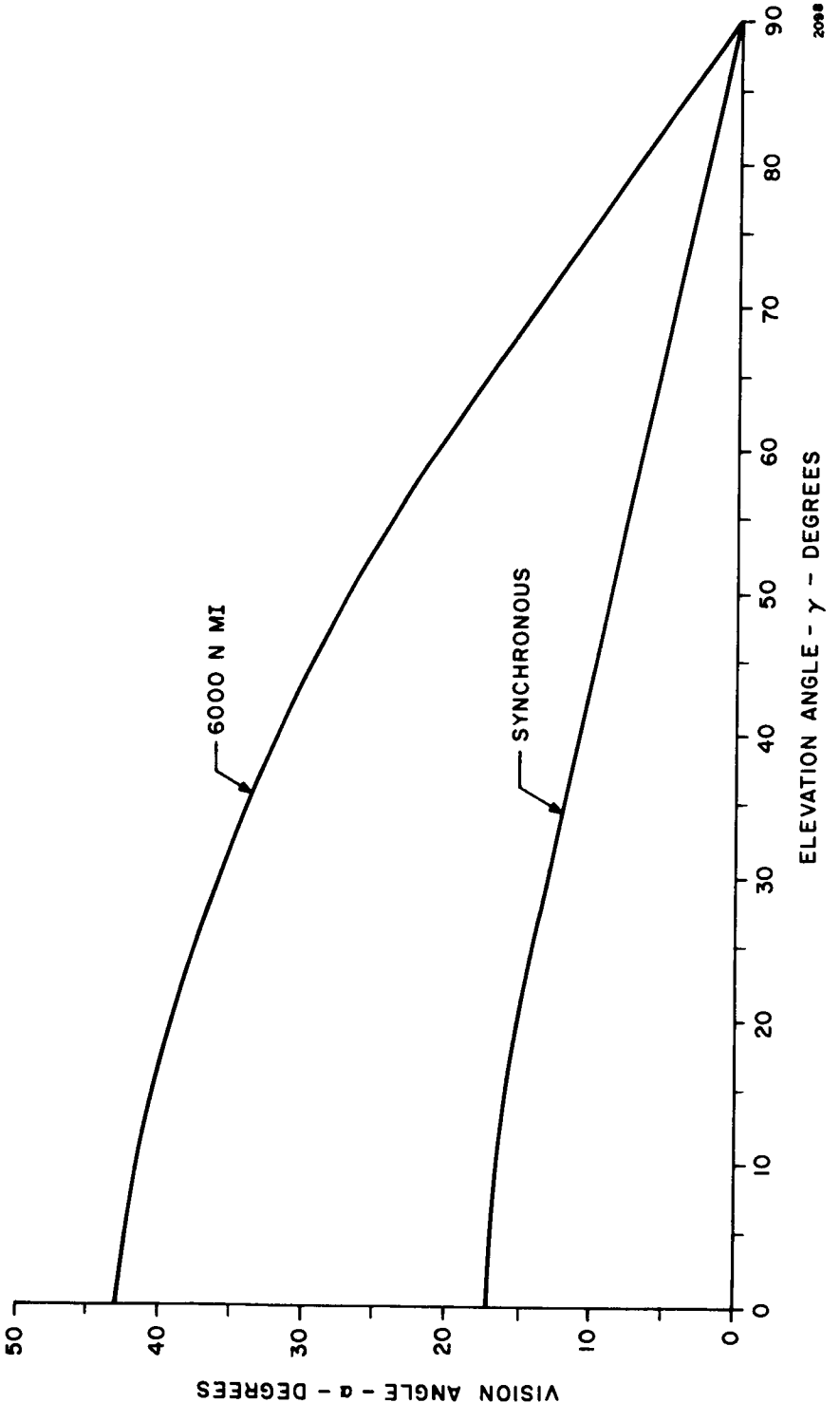

Figure III-10 Vision Angle vs Elevation Angle for 6000 nmi Synchronous Altitude Satellites

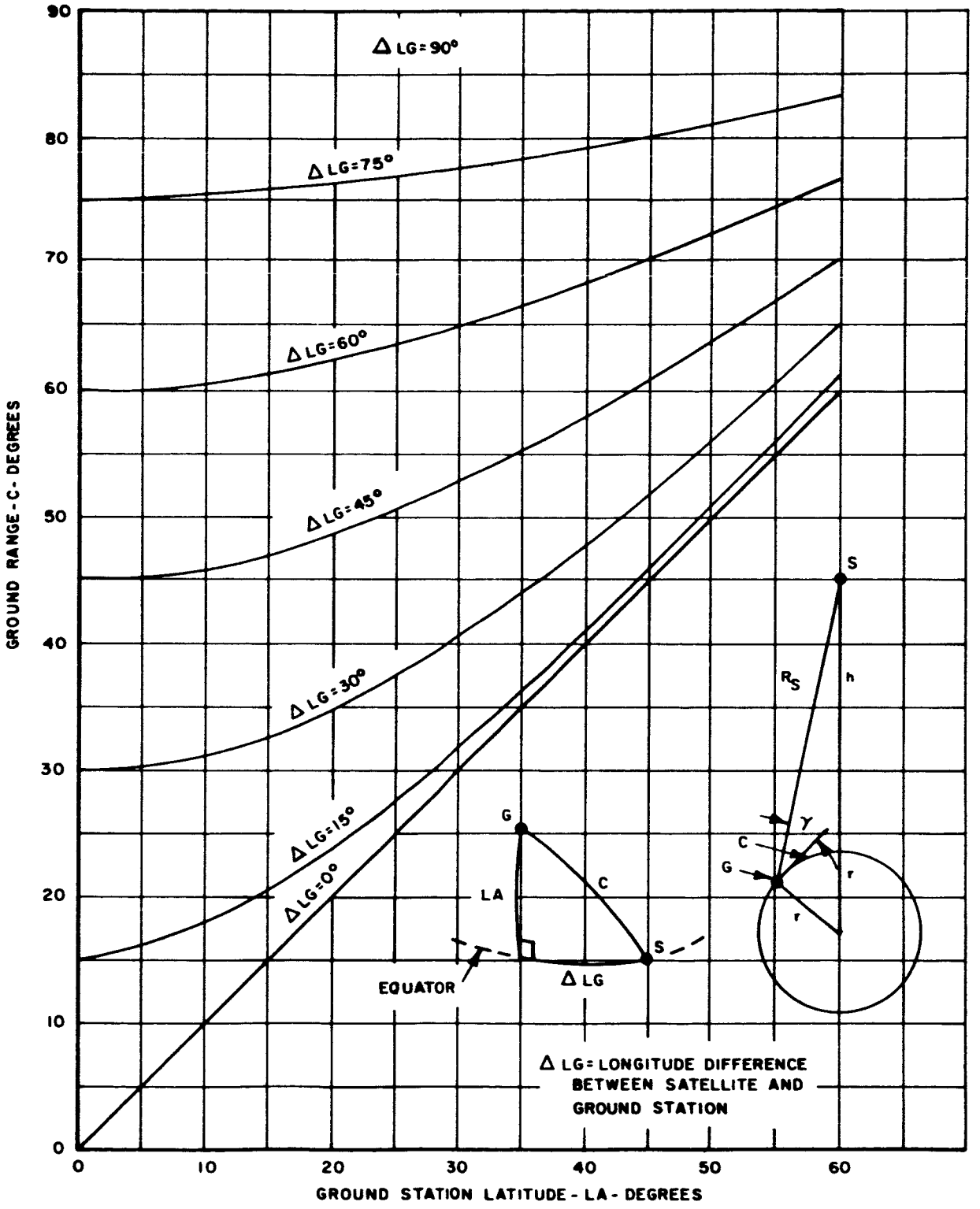

Figure III-11 Ground Range vs Ground Station Latitude for a Synchronous Satellite

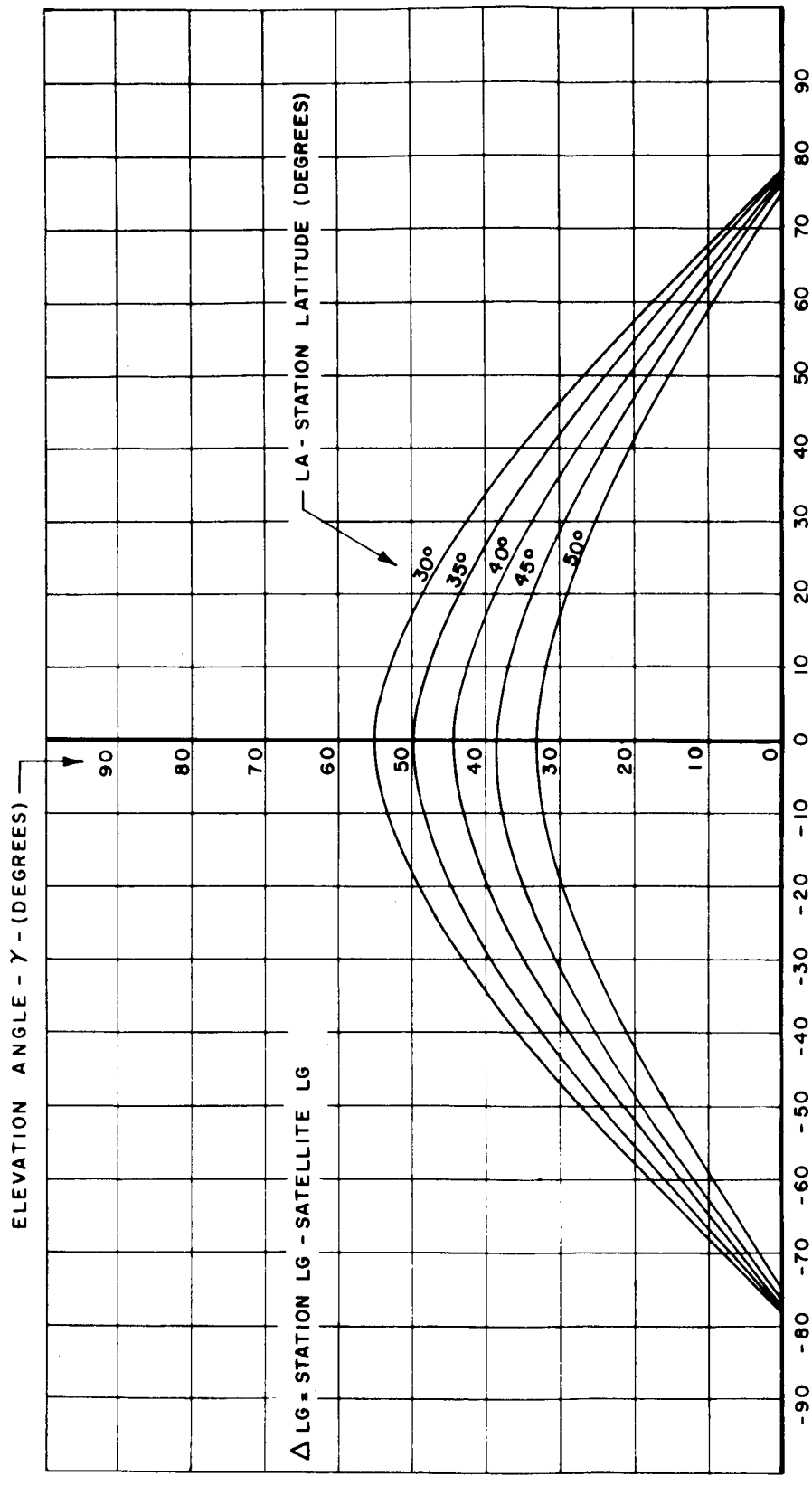

Figure III-12 Elevation Angle Versus Longitude Defference Between Synchronous Satellite and Ground Station for Various Ground Station Latitudes

Appendix IV
GAIN AND BEAMWIDTH OF MILLIMETER-WAVE ANTENNAS

Figure No.

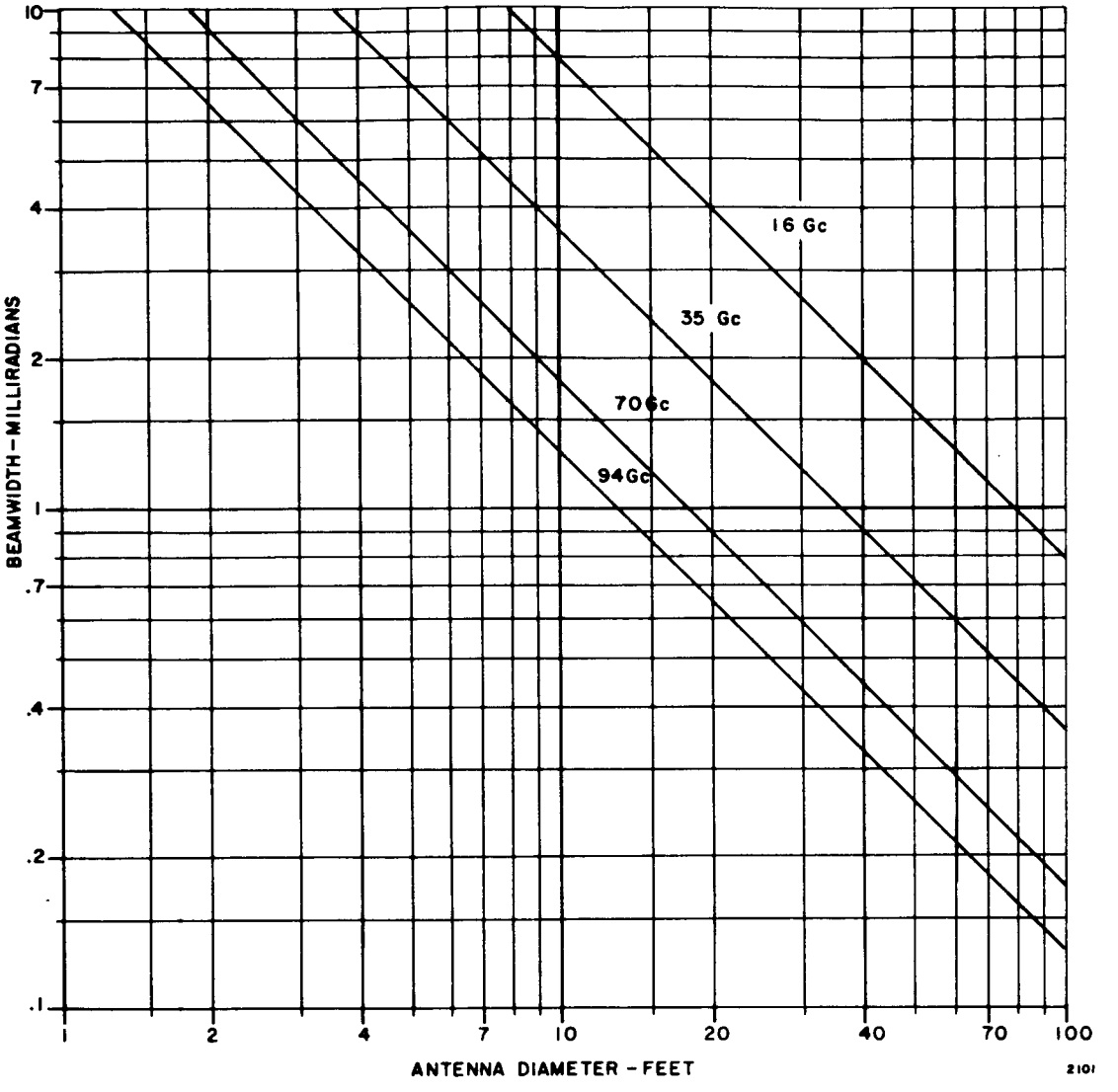

Figure IV-1 Beamwidth vs Diameter for Large MM Antennas

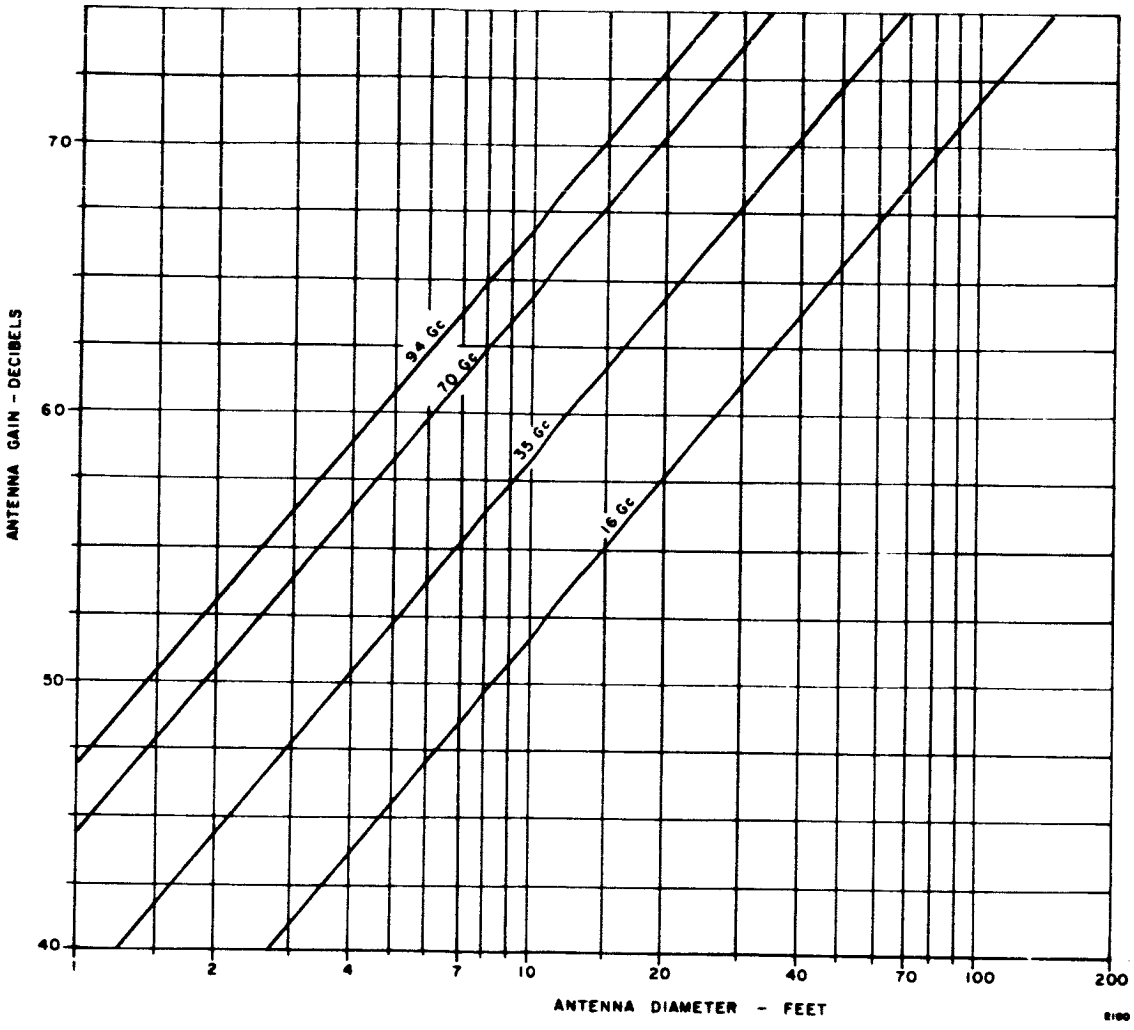

Figure IV-2 Gain vs Diameter for Large MM Antennas

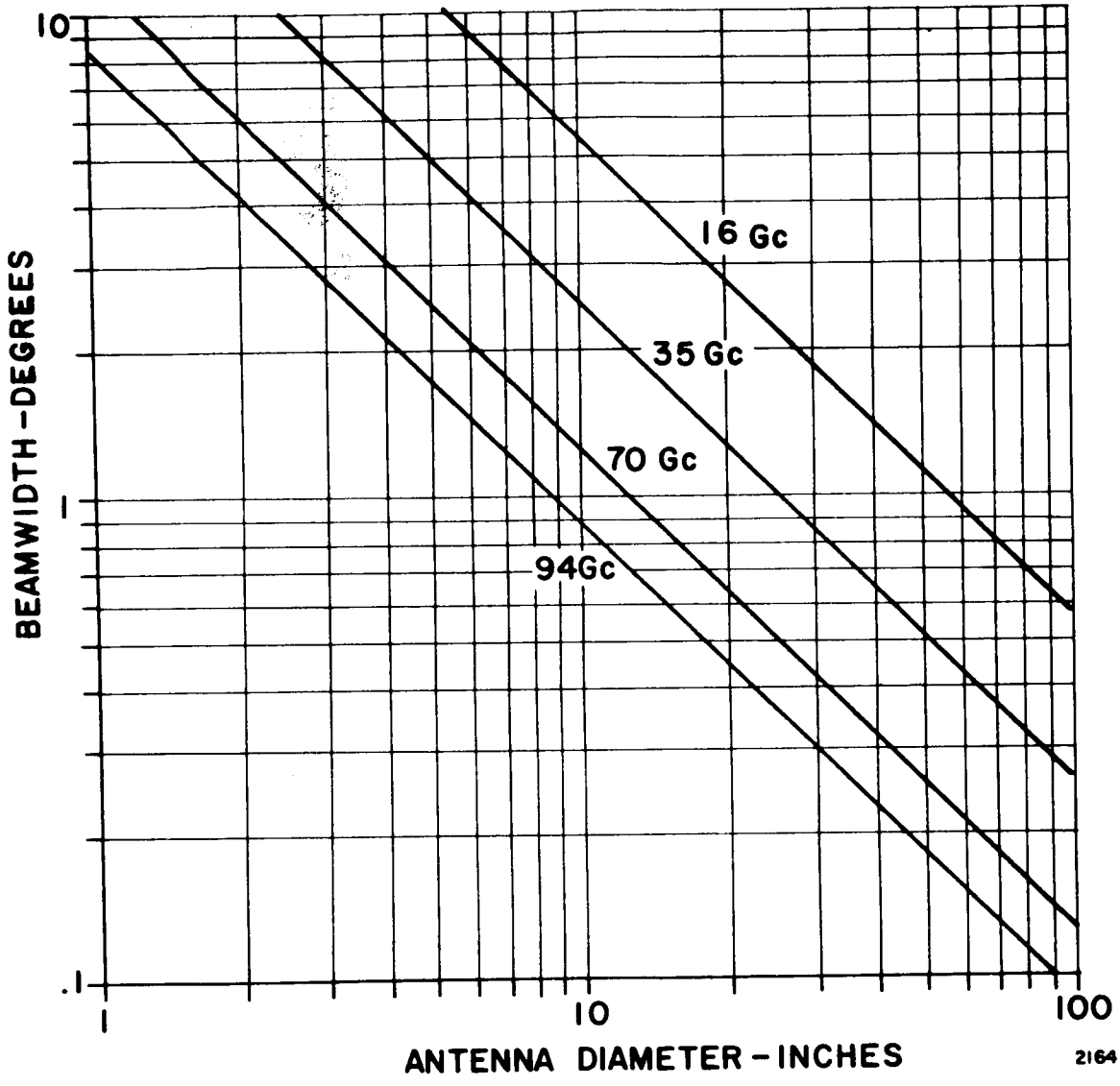

Figure IV-3 Beamwidth vs Diameter for Small MM Antennas